ВЕСТНИК ТРАНСПЛАНТОЛОГИИ И ИСКУССТВЕННЫХ ОРГАНОВ

VESTNIK TRANSPLANTOLOGII I ISKUSSTVENNYKH ORGANOV

RUSSIAN JOURNAL OF TRANSPLANTOLOGY AND ARTIFICIAL ORGANS

УЧРЕДИТЕЛИ: ОБЩЕРОССИЙСКАЯ ОБЩЕСТВЕННАЯ ОРГАНИЗАЦИЯ ТРАНСПЛАНТОЛОГОВ «РОССИЙСКОЕ ТРАНСПЛАНТОЛОГИЧЕСКОЕ ОБЩЕСТВО»

ФГБУ «НМИЦ ТИО ИМЕНИ АКАДЕМИКА В.И. ШУМАКОВА» МИНЗДРАВА РОССИИ

ФГАОУ ВО ПЕРВЫЙ МГМУ ИМЕНИ И.М. СЕЧЕНОВА МИНЗДРАВА РОССИИ (СЕЧЕНОВСКИЙ УНИВЕРСИТЕТ)

THE OFFICIAL JOURNAL OF ALL-RUSSIAN PUBLIC ORGANIZATION OF TRANSPLANTOLOGISTS "RUSSIAN TRANSPLANT SOCIETY"

SHUMAKOV NATIONAL MEDICAL RESEARCH CENTER OF TRANSPLANTOLOGY AND ARTIFICIAL ORGANS

I.M. SECHENOV FIRST MOSCOW STATE MEDICAL UNIVERSITY (SECHENOV UNIVERSITY)

2022. Том XXIV. № 4

2022. Vol. XXIV. № 4

Научно-практический журнал основан в 1999 г.
Регистр. № 018616

Scientific and Practical Journal was founded in 1999
Reg. № 018616

Журнал «Вестник трансплантологии и искусственных органов» включен ВАК РФ в перечень российских рецензируемых научных изданий, в которых должны быть опубликованы результаты диссертационных работ

Журнал «Вестник трансплантологии и искусственных органов» включен ФГБУ «НМИЦ ТИО им. ак. В.И. Шумакова» Минздрава России в перечень российских рецензируемых научных изданий, в которых должны быть опубликованы основные результаты исследований в рамках диссертаций, представляемых к защите в диссертационный совет ФГБУ «НМИЦ ТИО им. ак. В.И. Шумакова» Минздрава России

Журнал «Вестник трансплантологии и искусственных органов» индексируется в Scopus и размещен на платформе Web of Science Core Collection: Emerging Science Citation Index

"Russian Journal of Transplantology and Artificial Organs" is included in the list of leading peer-reviewed scientific publication editions, produced in the Russian Federation and is recommended for publication of primary results of dissertation research

"Russian Journal of transplantology and artificial organs" is included by the Federal State Budgetary Institution "Shumakov National Medical Research Center of Transplantology and Artificial Organs" of the Ministry of Health of Russia in the list of Russian peer-reviewed scientific publications in which the main results of research should be published within the framework of dissertations submitted for defense to the dissertation council of Shumakov National Medical Research Center of Transplantology and Artificial Organs

"Russian Journal of Transplantology and Artificial Organs" is indexed in Scopus and in the Emerging Science Citation Index of the Web of Science Core Collection

ISSN 1995-1191

Адрес для корреспонденции:

Россия, 123182, Москва, ул. Щукинская, 1
Тел./факс +7 (499) 193 87 62
E-mail: vestniktranspl@gmail.com
Интернет-сайт журнала: http://journal.transpl.ru
Научная электронная библиотека: http://elibrary.ru

Address for correspondence:

1, Shchukinskaya st., Moscow 123182, Russia
Tel./Fax +7 (499) 193 87 62
E-mail: vestniktranspl@gmail.com
Journal's web site: http://journal.transpl.ru
Scientific eLibrary: http://elibrary.ru

Подписной индекс в каталоге почты России – ПН380

СОДЕРЖАНИЕ

CONTENTS

КЛИНИЧЕСКАЯ ТРАНСПЛАНТОЛОГИЯ В РФ: ОТ ИННОВАЦИОННОЙ ФЕНОМЕНОЛОГИИ К ДОСТУПНОМУ ВИДУ МЕДИЦИНСКОЙ ПОМОЩИ

CLINICAL TRANSPLANTOLOGY IN THE RUSSIAN FEDERATION: FROM INNOVATIVE PHENOMENOLOGY TO ACCESSIBLE MEDICAL CARE

Глубокоуважаемые коллеги!

Трансплантация органов человека является выдающимся достижением медицинской науки и практики XX века, высшим проявлением гуманности в обществе, направленным на спасение жизни и здоровья пациентов с заболеваниями органов в терминальной стадии, когда иные способы лечения бессильны.

Вклад советских и российских хирургов, ученых в развитие мировой трансплантологии неоценим. В.П. Демихов в эксперименте доказал возможность проведения операций по пересадке органов. Первую в нашей стране успешную трансплантацию почки от родственного донора выполнил академик Б.В. Петровский 15 апреля 1965 года; 12 марта 1987 года первую успешную трансплантацию сердца провел выдающийся хирург и основатель отечественной трансплантологии В.И. Шумаков; в 1990 году бригадой хирургов под руководством профессора А.К. Ерамишанцева выполнена первая трансплантация печени.

К 2007 году, спустя 20 лет после первой успешной трансплантации сердца в стране, подобные операции выполнялась в трех городах – Москве, Екатеринбурге и Новосибирске, общим количеством 19 трансплантаций в год. Количество трансплантаций печени от посмертного донора было несколько больше, они выполнялись в Москве, Санкт-Петербурге, Екатеринбурге и Белгороде. Наиболее часто в стране выполнялась трансплантация почки, но во всех видах трансплантации объем операций был недостаточным.

2022 год отмечен двумя значимыми датами в истории отечественной трансплантологии – 35 лет успешной трансплантации сердца и 25 лет родственной трансплантации печени детям. Благодаря внедрению разработанных в последние годы

Dear colleagues,

Human organ transplantation is an outstanding achievement of medical science and practice in the 20th century. It is the highest manifestation of humanity in society, aimed at saving the life and health of patients with end-stage organ diseases, when other treatment methods are powerless.

The contribution by Soviet and Russian surgeons and scientists to the development of world transplantology is invaluable. Organ transplantation pioneer, Vladimir Demikhov, proved the feasibility of organ transplantation operations in his experiment. The first successful kidney transplantation in Russia was performed on April 15, 1965, by academician Boris Petrovsky. The first successful heart transplantation was performed on March 12, 1987, by Valery Shumakov, an outstanding surgeon and founder of Russian transplantology. In 1990, a surgical team, headed by Professor Alexander Yeramishantsev, carried out the first liver transplantation.

By 2007, 20 years after the first successful heart transplantation in the country, similar operations had been performed in three cities – Moscow, Yekaterinburg and Novosibirsk – with a total of 19 transplants per year. The number of deceased donor liver transplants was somewhat higher, performed in Moscow, St. Petersburg, Yekaterinburg, and Belgorod. Kidney transplantation was the most common transplant operation in Russia, but in all types of transplantation, the volume of operations was insufficient.

The year 2022 is marked by two significant dates in the history of Russian transplantology: 35 years of successful heart transplantation and 25 years of pediatric living related liver transplantation. Thanks to the implementation of scientific, technological, surgical, clinical

научно-технологических, хирургических, клинических и организационных решений удалось многократно увеличить число операций по трансплантации солидных органов.

К настоящему времени в нашей стране создана и реализована высокоэффективная программа лечения больных с приобретенными и врожденными заболеваниями органов в терминальной стадии, взрослых и детей, в том числе самого раннего возраста и с малой массой тела. В России сейчас выполняется в год около 2500 трансплантаций органов, из них порядка 300 пересадок органов детям. Благодаря организованной системе отпала необходимость в направлении за рубеж российских детей для выполнения им трансплантации органов. Достигнута выживаемость пациентов на уровне лучших мировых показателей.

Существенно расширена география трансплантологической помощи: сейчас операции по трансплантации осуществляются в 62 учреждениях в 35 регионах РФ с населением 103,4 млн человек.

Создана система региональной координации донорства органов, разработаны нормативные документы по трансплантации печени, почки, сердца, легких.

Разработаны оригинальные высокоэффективные хирургические технологии. Мировой приоритет имеют операции по лапароскопическому изъятию фрагмента печени и почки у родственного донора, первая в мировой практике успешная трансплантация печени и двух легких ребенку (от посмертного взрослого донора) и др. Разработаны технологии трансплантации печени детям от донора, не совместимого по группе крови.

Успех в области трансплантации жизненно важных органов был бы невозможен без внедрения результатов научных исследований и разработок. Раскрыты фундаментальные основы иммунной толерантности, иммуносупрессии, молекулярные механизмы взаимоотношения трансплантата с организмом реципиента. Научно обоснованы и успешно внедрены в клиническую практику новые методы персонализированной диагностики и лечения; выполнены молекулярно-генетические, иммунологические исследования биомаркеров отторжения, фиброза трансплантированных почки, печени, сердца, легкого, кардинально изменившие принципы ведения и прогноз у реципиентов. Созданы и внедрены отечественные системы вспомогательного кровообращения.

Все перечисленное позволило превратить трансплантологию в нашей стране из области престижной инновационной феноменологии в реальный, доступный для населения вид медицинской помощи.

С уважением,
главный редактор
академик РАН С.В. Готье

and organizational solutions developed in recent years, the number of solid organ transplantation operations has increased manifold.

To date, a highly effective treatment program has been created and implemented in our country for patients with acquired and congenital organ diseases in the terminal stage, adults and children, including very young age and low body weight. In Russia today, about 2,500 organ transplants are performed annually, including about 300 pediatric organ transplants. Thanks to the organized system, there is no longer the need to send Russian children abroad for organ transplants. Patient survival has reached the world's best levels.

The geographical footprint of transplant care has expanded considerably. Transplant operations are now carried out in 62 institutions spread across 35 regions of the Russian Federation with a population of 103.4 million people.

A system of regional organ donation coordination has been created, regulatory documents on liver, kidney, heart and lung transplantation have been developed.

Original highly efficient surgical techniques have been developed: laparoscopic liver and kidney resection from a related donor, etc. The world's first successful transplantation of a liver and two lungs in a child (from a deceased adult donor) was performed in Russia. Technologies for pediatric liver transplantation from a blood group incompatible donor have been developed.

Success in the field of vital organ transplantation would not have been possible without implementation of research and development results. The fundamental bases of immune tolerance, immunosuppression, molecular mechanisms of the relationship between graft and the recipient's body were revealed. New methods of personalized diagnosis and treatment were scientifically justified and successfully introduced into clinical practice; molecular-genetic, immunologic studies of rejection biomarkers, kidney, liver, heart, lung transplant fibrosis were performed, which radically changed the principles of recipient management and prognosis. Russian-made circulatory support systems have been created and implemented.

All of the above mentioned have made it possible to turn transplantology in our country from a field of prestigious innovative phenomenology into a real medical care that is accessible to everyone.

Sincerely,

S.V. Gautier
Editor-in-Chief,
Member, Russian Academy of Sciences

DOI: 10.15825/1995-1191-2022-4-7-14

RISK FACTORS IN DECEASED DONOR LIVER TRANSPLANTATION: A SINGLE CENTRE EXPERIENCE

S.I. Zubenko[1], A.R. Monakhov[1, 2], M.A. Boldyrev[1], V.R. Salimov[1], A.D. Smolyaninova[1], S.V. Gautier[1, 2]

[1] Shumakov National Medical Research Center of Transplantology and Artificial Organs, Moscow, Russian Federation

[2] Sechenov University, Moscow, Russian Federation

Deceased brain-dead donor liver transplantation (LT) is a high-risk intervention. The outcome depends on a large number of modifiable and non-modifiable factors. **Objective:** to analyze our own experience and identify preoperative and perioperative prognostic factors for poor outcomes in LT. **Materials and methods.** The study included 301 liver transplants performed between January 2016 and December 2021. Donor and recipient characteristics, intraoperative data, perioperative characteristics including laboratory test data, and the nature and frequency of complications were used for the analysis. **Results.** The 1-, 3- and 5-year recipient survival rates were 91.8%, 85.1%, and 77.9%, respectively; graft survival rates were 90.4%, 83.7%, and 76.7%, respectively. The most significant predictors of poor outcome of LT on the recipient side were biliary stents (HR 7.203, $p < 0.01$), acutely decompensated cirrhosis (HR 2.52, $p = 0.02$); in the postoperative period, non-surgical infectious complications (HR 4.592, $p < 0.01$) and number of reoperations (HR 4.063, $p < 0.01$). Donor creatinine level (HR 1.004, $p = 0.01$, one factor analysis; HR 1.004, $p = 0.016$, multivariate analysis) was the only reliable prognostic negative factor. **Conclusion.** LT taking into account established risk factors will improve surgery outcomes and help personalize the therapy for each patient.

Keywords: liver transplantation, deceased donor, expanded criteria donor, risk factors.

INTRODUCTION

LT is a high-risk operation [1]. A large number of conditions accompanying the complicated course of liver cirrhosis determine a more severe initial status of a recipient with increased early and long-term mortality [2, 3]. With the emergence of better surgical techniques, surgical contraindications to LT, such as portal vein thrombosis, are decreasing in number [4]. Progressive development of transplantation oncology also brings a large number of patients, previously considered non-transplantable, to the liver transplant waiting list [5]. Expansion of LT indications is increasing the disproportion between number of patients waiting for LT and number of donor organs available, and, as a consequence, increasing waitlist mortality [2, 6]. In an effort to maximize the use of available donor organs, many centers go beyond the traditional "ideal" donor and include expanded donor organ eligibility criteria [7]. The peculiarities of donor organs have an impact on both immediate and long-term outcomes of LT [8]. The above-mentioned peculiarities determine the continuing relevance of evaluation and reassessment of risk factors of adverse outcomes of LT in order to stratify recipients and perform the operation with optimal results for each patient.

Allocation of organs, which takes into account both donor and recipient risk factors, helps to reduce the risk of graft loss and postoperative mortality [9, 10].

MATERIALS AND METHODS

The study included deceased, brain-dead LT in adult recipients, performed at Shumakov National Medical Research Center of Transplantology and Artificial Organs Moscow (Shumakov Center) from January 2016 to December 2021.

The following recipient data were collected and analyzed: demographic characteristics, anthropometry, liver disease severity index (MELD), and concomitant characteristics affecting the severity of liver disease. In addition, we analyzed intraoperative data of LT performed, the presence of postoperative complications, the dynamics of laboratory parameters in the postoperative period, as well as recipient and graft survival rates.

To assess the quality of graft received, we used donors' anthropometric and demographic indicators, laboratory data, amount of vasopressor support, type of graft obtained, and results of histological examination (microscopy of zero-hour biopsies).

Corresponding author: Stepan Zubenko. Address: 1, Shchukinskaya str., Moscow, 123182, Russian Federation. Phone: (495) 190-35-62. E-mail: zubenko_transpl@yahoo.com

Liver harvesting technique

Our center uses a modification of the rapid liver extraction method with exclusively arterial perfusion of the liver [11]. Graft suitability was assessed on the basis of a preliminary clinical assessment of the donor, a comprehensive abdominal ultrasound examination, and visual assessment of graft. The results of "time-zero" liver allograft biopsies were retrospectively considered.

Table 1

Characteristics of liver recipients (n = 301)

Indicator	Median (min–max)
Age, years	43 (18–72)
Male, n (%)	148 (49.2)
BMI, kg/m^2	24 (15–40)
Associated conditions, n (%)	
Thrombophilia	7 (2.3)
Previous surgeries	29 (9.6)
TIPS	5 (1.7)
Biliary drains/stents	4 (1.3)
Severity of liver disease	
MELD	18 (7–40)
Fulminant liver disease, n (%)	7 (2.3)
Acutely decompensated cirrhosis, n (%)	22 (7.3)
Hepatorenal syndrome, n (%)	88 (29.2)
Waiting time, months	5 (0–48)

Table 2

Characteristics of deceased liver donors (n = 301)

Indicator	Median (min–max)
Male, n (%)	203 (67.4)
Age, years	48 (18–73)
BMI, kg/m^2	26 (17–48)
Graft type, n (%)	
Whole liver	284 (94.3)
Extended right lobe split	17 (5.6)
DRI	1.45 ± 0.28
Steatosis, n (%)	(n = 229)
Mild	181 (79)
Moderate	19 (8.3)
Severe	29 (12.7)
Fibrosis, n (%)	**(n = 229)***
F = 0	152 (66.4)
F = 1	60 (26.2)
F = 2	17 (7.4)
Laboratory indicators	
Alanine aminotransferase (ALT)	28 (1–436)
Aspartate aminotransferase (AST)	35 (8–1099)
Total bilirubin	11 (1–96)
Creatinine	101 (6–720)
Sodium	145 (124–176)

*, 229 biopsies were included in the analysis.

Liver implantation technique

The peculiarities of the surgical technique adopted in our center during deceased donor liver transplant (DDLT) are described in detail in previous works [12, 13]. The choice of caval reconstruction technique was determined by intraoperative characteristics of the recipient's hemodynamics [14].

In the postoperative period, immunosuppressive therapy was prescribed according to accepted protocols, depending on the underlying disease [15]. Patients were followed up for 1 to 3 months by transplant surgeons, with subsequent transfer to a hepatologist for long-term follow-up.

Statistical analysis

Statistical analysis was performed using the IBM SPSS Statistics 23 package. Quantitative variables were expressed as median and range values, qualitative variables as numbers and percentages. Patient and graft survival were determined by the Kaplan–Meier method. Multivariate Cox regression (proportional hazards model) was used to determine risk factors. Hazard Ratio (HR) with 95% confidence interval (CI) value was used to estimate the chances of graft loss/recipient death. The level of significance was considered significant at $p < 0.05$.

RESULTS

From January 2016 to December 2021, 304 DDLT in adult recipients were performed at Shumakov Center. Histological examination of explants in 3 cases verified tumor thrombosis of the portal vein in hepatocellular carcinoma (HCC). Patients who exceeded the UCSF criteria for LT in HCC were excluded from the study.

The general characteristics of recipients are shown in Table 1.

Donor characteristics

The main parameters used in the evaluation of brain-dead donors are shown in Table 2.

The relatively high Disease Risk Index (DRI) is noteworthy. According to the original article by Feng et al., the one-year survival of recipients with DRI from 1.4 to 1.5 is 79.7% [16].

Perioperative parameters

The time characteristics of the surgery, blood loss volume, the need for blood transfusions, and laboratory values reflecting liver function on days 1, 5, and 30 of the postoperative period were analyzed. The data are summarized in Table 3.

Complications and survival

In order to determine negative prognostic events in the postoperative period, we performed a comprehensive assessment of complications with calculation of the Comprehensive Complication Index. The data are summarized in Table 4.

The actuarial recipient and graft survival after transplantation was analyzed using the Kaplan–Meier method (Fig.).

Table 3

Perioperative characteristics of recipients

Indicator	Median (min–max)
Time, min	347 (185–805)
Cold ischemia, min	288 (105–744)
Warm ischemia, min	30 (12–80)
Biliary ischemia, min	31 (10–400)
Blood loss, ml	1000 (200–10000)
Fresh frozen plasma, doses	6 (1–28)
RBC mass, doses	2 (0–11)
Classic caval reconstruction, n (%)	283 (94)
Laboratory indicators	
Day 1 after surgery	
ALT	493 (23–6919)
AST	481 (28–21280)
Total bilirubin	46 (11–874)
Creatinine	81 (26–576)
International normalized ratio (INR)	2 (1–4)
Day 5 after surgery	
ALT	195 (29–4260)
AST	88 (6–4435)
Total bilirubin	40 (6–477)
Creatinine	82 (28–382)
INR	1 (1–2)
Day 30 after surgery	
ALT	30 (1–694)
AST	23 (3–809)
Total bilirubin	19 (2–292)
Creatinine	90 (34–537)
INR	1 (1–3)

Table 4

Postoperative complications

Indicator	n (%)
Bleeding	25 (8.3)
Arterial complications	
Obstruction	4 (1.32)
Stenosis	4 (1.32)
Thrombosis	7 (2.32)
Biliary complications	
Early stricture	13 (4.3)
Late stricture	8 (2.7)
Fistula	4 (1.32)
Wound infection	26 (8.6)
Re-interventions	60 (19.9)
Rejection	24 (8)
Non-surgical infectious complications	42 (14)
CCI (median, min–max)	0 (0–100)
Bed-day (median, min–max)	17 (1–177)
Retransplantation	5 (1.7)

Identification of risk factors

Based on the data obtained, statistical analysis was performed using single-factor and multifactor Cox regression analysis (Table 5, 6).

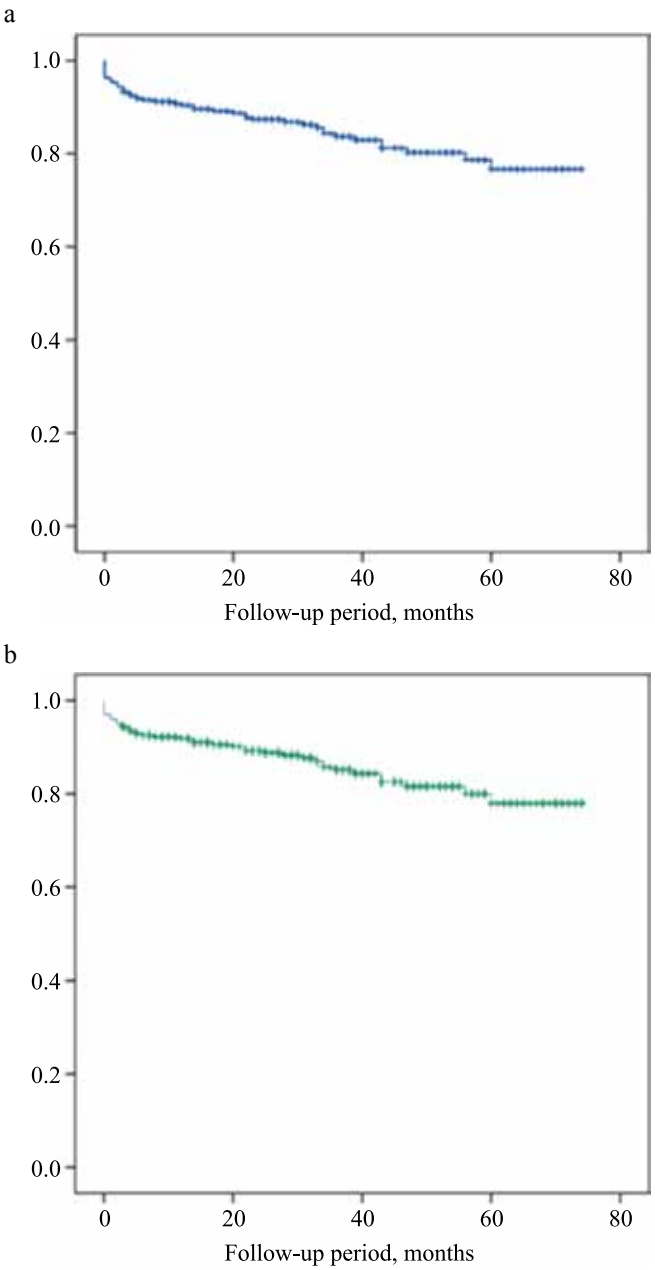

n = 301	Month 12	Month 36	Month 60
Graft survival, % (n)	90.4 (227)	83.7 (129)	76.7 (38)
Recipient survival, % (n)	91.8 (231)	85.1 (130)	77.9 (38)

Fig. Survival after liver transplantation. a, graft survival; b, recipient survival

Male gender (HR 0.55; CI 0.3–0.98; p = 0.04) reduced the risk of poor outcome. Carrying drains, intraductal stents, significantly increased recipient mortality (HR 7.203; CI 1.699–30.534; p < 0.01). Acutely decompensated cirrhosis more than doubled the risk (HR 2.52; CI 1.128–5.631; p = 0.02). Creatinine level was the only one of the assessed donor criteria that significantly influenced transplant outcome.

Time characteristics of liver transplantation, magnitude of blood loss, and greater need for transfusion media significantly reduced recipient and graft survival. In the analysis of postoperative laboratory indices, reliability was determined for almost all of the studied values. Among the identified risk factors, the INR has the greatest influence on LT outcomes. A number of postoperative complications also increased the risk of graft loss. Biliary fistulas, non-surgical infectious complications, number of repeated operations, and graft artery thrombosis had the greatest negative prognostic significance.

Based on identified risk factors, a multivariate analysis was performed using the Cox regression model.

According to multivariate analysis, liver donor creatinine levels had a significant effect on LT outcomes (HR 1.004; CI 1.002–1.007; p = 0.016).

DISCUSSION

The association between gender and mortality was shown in a recent large study by Serrano et al.

Table 5

Risk factors (univariate analysis)

Indicator	HR	95% CI	p
Recipient factors			
Age	1.025	0.99–1.05	0.06
Male	0.55	0.3–0.98	**0.04**
BMI	0.96	0.89–1.04	0.37
Thrombophilia	1.631	0.223–11.938	0.63
Portal vein thrombosis	1.424	0.723–2.792	0.31
Disseminated portal vein thrombosis	1.448	0.519–4.039	0.48
Previous surgeries	1.379	0.617–3.083	0.43
TIPS	1.452	0.2–10.554	0.71
Biliary drains/stents	7.203	1.699–30.534	**<0.01**
MELD	1.027	0.992–1.063	0.13
Fulminant liver disease	0.917	0.126–6.65	0.93
Acutely decompensated cirrhosis	2.52	1.128–5.631	**0.02**
Hepatorenal syndrome	1.589	0.885–2.854	0.12
Waiting time	0.91	0.853–0.972	**<0.01**
Donor factors			
Age	0.994	0.97–1.018	0.62
Male	0.873	0.467–1.632	0.67
BMI	1.004	0.952–1.06	0.88
Graft type	0.385	0.053–2.975	0.35
DRI	0.654	0.228–1.871	0.43
DRI >1.7	0.781	0.349–1.746	0.55
ALT	0.996	0.988–1.004	0.36
AST	1	0.997–1.003	0.91
Creatinine	1.004	1.002–1.006	**0.01**
Bilirubin	0.988	0.957–1.021	0.48
Sodium	1.002	0.971–1.034	0.91
Norepinephrine	1	1.0–1.001	0.16
Dopamine	0.941	0.788–1.123	0.5
Steatosis	0.939	0.56–1.573	0.81
Fibrosis	0.675	0.369–1.237	0.2
Intraoperative factors			
Surgery duration	1.005	1.003–1.007	**<0.01**
Preservation time	1.002	1.0–1.005	0.06
Secondary warm ischemia	1.002	0.995–1.008	0.62
Biliary ischemia	1.009	1.004–1.013	**<0.01**
Type of caval reconstruction	0.046	0–13.463	0.29
Blood loss	1	1.0–1.0	**<0.01**
Fresh frozen plasma	1.11	1.055–1.168	**<0.01**
RBC mass	1.28	1.164–1.409	**<0.01**
Postoperative indicators			
Day 1			
ALT	1	1.0–1.001	**<0.01**
AST	1	1.0–1.0	**<0.01**
Bilirubin	1.003	1.001–1.01	**<0.01**
Creatinine	1.004	1.001–1.007	**0.03**
INR	1.998	1.201–3.324	**<0.01**
Day 5			
ALT	1	1.0–1.001	0.29
AST	1	0.999–1.001	0.9
Bilirubin	1.005	1.003–1.008	**<0.01**
Creatinine	1.005	1.001–1.009	**0.01**
INR	4.228	1.392–12.838	**0.01**
Day 30			
ALT	1.001	0.999–1.004	0.28
AST	1.002	0.999–1.004	0.19
INR	4.196	1.564–11.255	**<0.01**
Creatinine	1.004	1.001–1.008	**0.02**
Bilirubin	1.012	1.008–1.017	**<0.01**
Complications			
Re-operations	4.063	2.267–7.823	**<0.01**
Non-surgical infection	4.592	2.526–8.346	**<0.01**
Wound infection	1.722	0.838–3.538	0.14
Rejection	1.04	0.416–2.603	0.93
Bleeding	3.64	1.746–7.591	**<0.01**
Arterial complications (any)	1.967	0.705–5.489	0.2
Arterial graft thrombosis	3.682	1.136–11.93	**0.03**
Biliary complications (any)	2.57	1.199–5.508	**0.015**
Biliary stricture (any duration)	2.067	0.877–4.875	0.1
Biliary fistula	5.619	1.354–23.328	**0.017**
CCI	1.04	1.03–1.049	**<0.01**

Table 6

Risk factors (multivariate analysis)

Indicator	HR	95% CI	p
Recipient factors			
Male	1.665	0.821–3.376	0.157
Biliary stents/drains	0.923	0.318–2.682	0.88
Acutely decompensated cirrhosis	0.179	0.03–1.068	0.06
Donor factors			
Donor creatinine	1.004	1.002–1.007	**0.016**
Intraoperative factors			
Surgery duration	1.001	0.997–1.005	0.61
Biliary ischemia	1.001	0.993–1.008	0.89
Blood loss	1	1.0–1.0	0.53
Fresh frozen plasma	1.037	0.938–1.147	0.47
RBC mass	1.062	0.873–1.292	0.55
Postoperative indicators			
Day 1			
ALT	1	0.999–1.001	0.9
AST	1	1.0–1.0	0.23
Bilirubin	1.001	0.996–1.006	0.65
Creatinine	0.999	0.993–1.005	0.75
INR	1.623	0.756–3.484	0.21
Day 5			
Bilirubin	1	0.994–1.007	0.95
Creatinine	1	0.992–1.008	0.94
INR	0.397	0.069–2.269	0.3
Day 30			
Bilirubin	1.003	0.995–1.011	0.48
Creatinine	1.001	0.995–1.007	0.75
INR	0.589	0.109–3.186	0.54
Complications			
Bleeding	2.067	0.715–5.972	0.18
Arterial graft thrombosis	0.522	0.112–2.429	0.41
Biliary complications (any)	0.62	0.228–1.69	0.35
Biliary fistula	2.762	0.373–20.457	0.32

Male patients are characterized by lower early mortality with higher overall and long-term mortality [17]. Prolonged wearing of conventionally sterile implants increases the risk of infectious complications [18]. Due to the high frequency of inpatient treatment, multiresistant hospital microflora predominate in such recipients [19], which, combined with post-transplant immunosuppressive therapy, causes a high risk of infectious complications with potential generalization [20]. Acute decompensation of liver cirrhosis also increased the risk of recipient death >2.5-fold. Organ dysfunction against the background of existing chronic liver disease is characterized by significant increase in patient mortality [21].

The association of donor creatinine with LT outcomes is reflected, in particular, in the SOFT prognostic scale [22]. However, the mechanism of this effect has not been reliably established. Creatinine level, according to Rogers et al., may reflect the degree of secondary ischemic damage to donor liver parenchyma. However, the authors caution against allocating organs taking into account this factor, emphasizing the need for further research [23]. The lack of influence of DRI on LT outcomes in our study is consistent with later works [24, 25]. Thus, it is possible to raise the question of switching to more modern scales for assessing the quality of organs from brain-dead donors for a more precise allocation depending on recipient's characteristics [22].

Large amount of blood loss and a need for intraoperative blood transfusion are associated with a higher incidence of infectious complications, renal dysfunction and worse survival after LT [26].

The Rostved study showed the prognostic value of MELD in the early post-transplant period to determine the risk of liver graft loss during the first year [27]. The INR value largely reflects the severity of impairment of synthetic function of the graft, which is associated with higher postoperative mortality [28]. The severity of coagulopathy indirectly reflects the degree of multiple organ dysfunction, which is most relevant for patients with septic status [29, 30]. Thus, a higher INR level can serve as a negative prognostic criterion in LT [28, 31].

CONCLUSION

We have identified prognostic risk factors for poor outcome of DDLT. Performing liver transplantation taking into account the data obtained would improve surgery outcomes and help personalize the treatment strategy for each patient.

The authors declare no conflict of interest.

REFERENCES

1. *Busuttil RW, Klintmalm G*. Transplantation of the Liver 3rd Edition. *Elsevier Health Sciences*. 2014: 1538.
2. *Montenovo M, Rahnemai-Azar A, Reyes J, Perkins J.* Clinical Impact and Risk Factors of Portal Vein Thrombosis for Patients on Wait List for Liver Transplant. *Exp Clin Transplant*. 2018 Apr; 16 (2): 166–171. doi: 10.6002/ect.2016.0277. Epub 2017 Jun 16. PMID: 286216359.
3. *Ebadi M, Montano-Loza AJ.* Sarcopenia and Frailty in the Prognosis of Patients on the Liver Transplant Waiting List. *Liver Transpl*. 2019 Jan; 25 (1): 7–9. doi: 10.1002/lt.25386. PMID: 30472786.
4. *Qi X, Dai J, Jia J, Ren W, Yang M, Li H et al.* Association between portal vein thrombosis and survival of liver transplant recipients: a systematic review and meta-analysis of observational studies. *J Gastrointestin Liver Dis*. 2015 Mar; 24 (1): 51–59, 4 p following 59. doi: 10.15403/jgld.2014.1121.qix. PMID: 25822434.
5. *Porshennikov IA, Sokolov AV, Shchekina EE, Chubukov AYu, Tret'yakova TA, Ostanina IB i dr.* Transplantatsiya pecheni pri metastaticheskom kolorektal'nom rake (klinicheskoe nablyudenie). *Annaly khirurgicheskoy gepatologii*. 2018; 23 (4): 54–67. https://doi.org/10.16931/1995-5464.2018454-67.

6. *Orman ES, Barritt AS, Wheeler SB, Hayashi PH.* Declining liver utilization for transplantation in the United States and the impact of donation after cardiac death. *Liver Transpl*. 2013; 19: 59–68.
7. *Gautier SV, Kornilov MN, Miloserdov IA i dr*. Transplantatsiya pecheni ot donorov starshe 60 let. *Vestnik transplantologii i iskusstvennykh organov*. 2018; 20 (1): 6–12.
8. *Stine JG, Argo CK, Pelletier SJ, Maluf DG, Northup PG.* Liver transplant recipients with portal vein thrombosis receiving an organ from a high-risk donor are at an increased risk for graft loss due to hepatic artery thrombosis. *Transpl Int*. 2016 Dec; 29 (12): 1286–1295. doi: 10.1111/tri.12855. Epub 2016 Oct 6. PMID: 27714853; PMCID: PMC5154764.
9. *Nacif LS, Zanini LY, Pinheiro RS, Waisberg DR, Rocha-Santos V, Andraus W et al.* Portal vein surgical treatment on non-tumoral portal vein thrombosis in liver transplantation: Systematic Review and Meta-Analysis. *Clinics (Sao Paulo)*. 2021 Jan 22; 76: e2184. doi: 10.6061/clinics/2021/e2184. PMID: 33503185; PMCID: PMC7811829.
10. *Stine JG, Northup PG.* Management of Non-tumoral Portal Vein Thrombosis in Patients with Cirrhosis. *Dig Dis Sci*. 2019 Mar; 64 (3): 619–626. doi: 10.1007/s10620-018-5427-3. PMID: 30560339.
11. *Pogrebnichenko IV.* Jeffektivnoe ispol'zovanie pecheni mul'tiorgannogo donora dlja transplantacii [Dissertation]. M.: 2014. 143.
12. *Латыпов РА*. Сплит-трансплантация печени: дис. … канд. мед. наук: 14.01.24. М., 2019. 125. *Latypov RA.* Split-transplantatsiya pecheni: dis. … kand. med. nauk: 14.01.24. M., 2019. 125.
13. *Voskanov MA.* Interventsionnye metody korrektsii sosudistykh oslozhneniy i biliodigestivnykh striktur posle transplantatsii pecheni u detey: dis. … kand. med. nauk: 14.01.24. M., 2020. 109.
14. *Gautier SV, Poptsov VN, Kornilov MN i dr*. Metodika kaval'noy rekonstruktsii pri transplantatsii pecheni ot posmertnogo donora – vybor khirurga ili anesteziologa. *Vestnik transplantologii i iskusstvennykh organov*. 2018; 20 (S1): 62.
15. Transplantatsiya pecheni: natsional'nye klinicheskie rekomendatsii / Obshcherossiyskaya obshchestvennaya organizatsiya transplantologov "Rossiyskoe transplantologicheskoe obshchestvo". M., 2016. 61.
16. *Feng S, Goodrich NP, Bragg-Gresham JL, Dykstra DM, Punch JD, DebRoy MA et al.* Characteristics associated with liver graft failure: the concept of a donor risk index. *Am J Transplant*. 2006 Apr; 6 (4): 783–790. doi: 10.1111/j.1600-6143.2006.01242.x. Erratum in: *Am J Transplant*. 2018 Dec; 18 (12): 3085. PMID: 16539636, 165.
17. *Serrano MT, Sabroso S, Esteban LM, Berenguer M, Fondevila C, Lorente S et al.* Mortality and Causes of Death After Liver Transplantation: Analysis of Sex Differences in a Large Nationwide Cohort. *Transpl Int*. 2022 May 9; 35: 10263. doi: 10.3389/ti.2022.10263. PMID: 35615539; PMCID: PMC9124758.
18. *Isik O, Kaya E, Sarkut P, Dundar HZ.* Factors Affecting Surgical Site Infection Rates in Hepatobiliary Surgery. *Surg Infect (Larchmt)*. 2015 Jun; 16 (3): 281–286. doi: 10.1089/sur.2013.195. Epub 2015 Apr 1. PMID: 25830815.
19. *Vaishnavi C, Samanta J, Kochhar R.* Characterization of biofilms in biliary stents and potential factors involved in occlusion. *World J Gastroenterol*. 2018 Jan 7; 24 (1): 112–123. doi: 10.3748/wjg.v24.i1.112. PMID: 29358888; PMCID: PMC5757116.
20. *Kim YJ, Yoon JH, Kim SI, Choi HJ, Choi JY, Yoon SK et al.* Impact of Pretransplant Infections on Clinical Course in Liver Transplant Recipients. *Transplant Proc*. 2018 May; 50 (4): 1153–1156. doi: 10.1016/j.transproceed.2018.01.036. PMID: 29731084.
21. *Sarin SK, Choudhury A, Sharma MK, Maiwall R, Al Mahtab M, Rahman S et al*. APASL ACLF Research Consortium (AARC) for APASL ACLF working Party. Acute-on-chronic liver failure: consensus recommendations of the Asian Pacific association for the study of the liver (APASL): an update. *Hepatol Int*. 2019 Jul; 13 (4): 353–390. doi: 10.1007/s12072-019-09946-3. Epub 2019 Jun 6. Erratum in: *Hepatol Int*. 2019 Nov; 13 (6): 826–828. PMID: 31172417; PMCID: PMC6728300.
22. *Torterolli F, Watanabe RK, Tabushi FI, Peixoto IL, Nassif PAN, Tefilli NL et al.* Bar, soft and dri post-hepatic transplantation: what is the best for survival analysis? *Arq Bras Cir Dig*. 2021 Jun 11; 34 (1): e1576. doi: 10.1590/0102-672020210001e1576. PMID: 34133523; PMCID: PMC8195467.
23. *Rogers ME, Delman A, Campbell K, Miethke A, Tiao G, Mullapudi B, Bondoc A.* Children undergoing early liver re-transplantation for primary non-function have improved survival. *Pediatr Transplant*. 2022 Jun 25: e14347. doi: 10.1111/petr.14347. Epub ahead of print. PMID: 35751646.
24. *Boecker J, Czigany Z, Bednarsch J, Amygdalos I, Meister F, Santana DAM et al*. Potential value and limitations of different clinical scoring systems in the assessment of short- and long-term outcome following orthotopic liver transplantation. *PLoS One*. 2019 Mar 21; 14 (3): e0214221. doi: 10.1371/journal.pone.0214221. PMID: 30897167; PMCID: PMC6428268.
25. *Rauchfuss F, Zidan A, Scheuerlein H, Dittmar Y, Bauschke A, Settmacher U.* Waiting time, not donor-risk-index, is a major determinant for beneficial outcome after liver transplantation in high-MELD patients. *Ann Transplant*. 2013 May 28; 18: 243–247. doi: 10.12659/AOT.883924. PMID: 23792527.
26. *Teofili L, Valentini CG, Aceto P, Bartolo M, Sollazzi L, Agnes S et al.* High intraoperative blood product requirements in liver transplantation: risk factors and impact on the outcome. *Eur Rev Med Pharmacol Sci*. 2022 Jan; 26 (1): 64–75. doi: 10.26355/eurrev_202201_27749. PMID: 35049021.
27. *Rostved AA, Lundgren JD, Hillingsø J, Peters L, Mocroft A, Rasmussen A.* MELD score measured day 10 after orthotopic liver transplantation predicts death and re-transplantation within the first year. *Scand J Gastroenterol*. 2016 Nov; 51 (11): 1360–1366. doi: 10.1080/00365521.2016.1196497. Epub 2016 Jun 20. PMID: 27319374.

28. *Okamura Y, Yagi S, Sato T, Hata K, Ogawa E, Yoshizawa A et al*. Coexistence of Bilirubin ≥10 mg/dL and Prothrombin Time-International Normalized Ratio ≥1.6 on Day 7: A Strong Predictor of Early Graft Loss After Living Donor Liver Transplantation. *Transplantation*. 2018 Mar; 102 (3): 440–447. doi: 10.1097/TP.0000000000001959. PMID: 28968350.
29. *Chen RX, Wu ZQ, Li ZY, Wang HZ, Ji JF*. Prognostic predictors in patients with sepsis after gastrointestinal tumor surgery: A retrospective study. *World J Gastrointest Surg*. 2021 Mar 27; 13 (3): 256–266. doi: 10.4240/wjgs.v13.i3.256. PMID: 33796214; PMCID: PMC7992996.
30. *Liu J, Bai C, Li B, Shan A, Shi F, Yao C et al*. Mortality prediction using a novel combination of biomarkers in the first day of sepsis in intensive care units. *Sci Rep*. 2021 Jan 14; 11 (1): 1275. doi: 10.1038/s41598-020-79843-5. PMID: 33446739; PMCID: PMC7809407.
31. *Ben-Ari Z, Weiss-Schmilovitz H, Sulkes J, Brown M, Bar-Nathan N, Shaharabani E et al*. Serum cholestasis markers as predictors of early outcome after liver transplantation. *Clin Transplant*. 2004 Apr; 18 (2): 130–136. doi: 10.1046/j.1399-0012.2003.00135.x. PMID: 15016125.

The article was submitted to the journal on 30.08.2022

DOI: 10.15825/1995-1191-2022-4-15-23

IVF PREGNANCY AFTER KIDNEY TRANSPLANTATION: CLINICAL CASE AND LITERATURE REVIEW

E.I. Prokopenko[1, 2], V.M. Guryeva[2], V.A. Petrukhin[2], K.V. Krasnopol'skaya[2], F.F. Burumkulova[2], D.V. Gubina[1]

[1] Vladimirsky Moscow Regional Research Clinical Institute, Moscow, Russian Federation
[2] Moscow Regional Research Institute of Obstetrics and Gynecology, Moscow, Russian Federation

Kidney transplantation (KT), the optimal treatment for stage 5 chronic kidney disease (CKD), restores impaired fertility in most women of reproductive age. However, infertility occurs in some patients after successful KT. We present our own experience of overcoming secondary tubal infertility by in vitro fertilization (IVF). The patient was a 36-year-old with a transplanted kidney, who had lost two pregnancies in the past due to severe preeclampsia (PE). After the second attempt on cryo-thawed embryo transfer against the background of hormone replacement therapy, one embryo was transferred into the uterus, resulting in pregnancy. Gestational diabetes mellitus (GDM) was diagnosed in the first trimester, and a diet was prescribed. Immunosuppression with tacrolimus, azathioprine and methylprednisolone, prophylaxis of PE with low molecular weight heparin and antiplatelet drugs were administered during pregnancy. Elective cesarean section was performed at 37–38 weeks and a healthy boy was born, weighing 2760 g (25th percentile), 48 cm tall (36th percentile). A stay in the neonatal intensive care unit was not required. The baby is growing and developing normally, the mother's renal graft function is satisfactory. So, IVF can be successfully used in post-KT patients with infertility issues, provided that the IVF program is carefully controlled, and the pregnancy is managed in a multidisciplinary manner.

Keywords: kidney transplantation, infertility, pregnancy, assisted reproductive technology, in vitro fertilization.

INTRODUCTION

KT is the most effective treatment for stage 5 CKD. Maintaining a good reproductive function is one of the medical challenges that young women with kidney transplants face. Nowadays, post-KT pregnancy is firmly established in real clinical practice. Since 1958, when a woman with a transplanted kidney first carried a pregnancy and gave birth to a healthy child, thousands of pregnancies after KT have been reported. The outcomes of such pregnancies, despite the increased risk of obstetric and perinatal complications, are generally favorable – the rate of giving birth to live and viable children is over 70%, even taking into account fetal losses in the early gestational period [1, 2].

Our country Russia has also accumulated some experience in pregnancy management in women after KT, including those after simultaneous kidney-pancreas transplant [3–6]. The key points in planning and managing pregnancy in women with a transplanted kidney are pregravid preparation, modification of immunosuppression and other types of drug therapy during planning with exclusion of teratogenic and fetotoxic drugs (mycophenolates and proliferative signal inhibitors, ACE inhibitors, angiotensin receptor blockers, statins, allopurinol, warfarin and new oral anticoagulants), diagnosis at the pregravid stage of post-transplant diabetes (new-onset diabetes mellitus after transplantation, NODAT), careful monitoring of renal function and blood calcineurin inhibitor concentrations during gestation, early detection and treatment of GDM, prevention of placenta-associated complications – PE and fetoplacental insufficiency, and preterm birth. This pregnancy should be managed by an interdisciplinary team of specialists with relevant experience: a nephrologist, obstetrician, gynecologist, in some cases, an endocrinologist, a rheumatologist, a urologist, and other specialists.

CKD is one of the causes of dysregulation in hypothalamic-pituitary-gonadal system, leading to increased levels of follicle-stimulating hormone, luteinizing hormone and prolactin, and as a result of these changes in hormonal background – to infertility [7]. After successful KT, most women of reproductive age recover their regular menstrual cycle and ability to conceive within the first postoperative year due to elimination of uremic toxins and normalization of sex hormone levels. However, hormonal changes, pelvic inflammatory processes and other causes of female infertility may persist or occur de novo in the post-transplant period. The true incidence of infertility in this cohort of patients is difficult to estimate. Apparently, due to anatomical and endocrine abnormalities, fertility disorders in women after KT occur

Corresponding author: Elena Prokopenko. Address: 61/2, Shchepkina str., Moscow, 129110, Russian Federation. Phone: (495) 681-55-85. E-mail: renalnephron@gmail.com

more frequently than in healthy women [8–10]. At the same time, such a modern method of overcoming infertility as the use of assisted reproductive technologies in patients with a transplanted kidney is rarely used in clinical practice.

The methods used to treat infertility in renal transplant recipients are generally the same as those used in the general population. The choice of method should be based on the nature of the diagnosed disorders and include ovulation induction or more advanced assisted reproductive techniques, if necessary [11]. Indications for intrauterine insemination or in vitro fertilization (IVF) are determined by existing guidelines, and the goal of IVF is to achieve a singleton pregnancy and deliver a healthy baby at term.

Data are not available on the number of the entire cohort of post-KT women who have undergone IVF, as only those cases in which a pregnancy has occurred following an IVF are routinely published. The first successful case of an IVF pregnancy in a patient with a transplanted kidney was described by Lockwood et al. in 1995 [12]. In the following years, we were able to find 11 more publications in the literature describing individual clinical cases or their small series (Table) [9, 12–22].

As shown in the table, a total of 27 kidney transplant patients who underwent IVF had 31 pregnancies and 30 live births, including 4 twins, i.e., 26 patients carried a pregnancy to the age of fetal viability. Development of PE has been described in 8 pregnancies out of 31 (26%), so the incidence of this complication is approximately 8 times higher than in the population. Gestational and chronic hypertension were present in 6 (22%) pregnant women, a rate about 2-fold higher than in the general population. GDM occurred in only 3 cases out of 31 (10%). Fetal growth restriction was observed in 8 cases (26%), which is about 5 times higher than the rate of this complication in the general population. Fifteen women (58%) delivered prematurely, with PE and impaired renal graft function being the main indications for preterm delivery. Only 3 of 26 pregnant women (11%) delivered through natural delivery routes; in the remaining cases, a C-section was performed. It should be noted that despite elevated serum creatinine levels before delivery among a significant proportion of the patients, there were

Table

Obstetric outcomes in IVF pregnancy in kidney recipients (based on 1995–2021 literature)

Authors, year of publication	Patient / pregnancy count	Living children count	Preterm birth	Gestational or chronic hypertension	PE*	FGR**	GDM***	C-section
Lockwood G.M., Ledger W.L., Barlow D.H. 1995 [12]	1/1	2 (twins)	1 (100%)	0	0	1 (100%)	–	Vaginal delivery
Furman B., Wiznitzer A., Hackmon R. et al. 1999 [13]	1/1	2 (twins)	1 (100%)	1 (100%)	1 (100%)	–	1 (100%)	1 (100%)
Khalaf Y., Elkington N., Anderson H. et al. 2000 [14]	1/1	2 (twins)	1 (100%)	–	–	–	–	Vaginal delivery
Tamaki M., Ami M., Kimata N. et al. 2003 [15]	1/1	1	1 (100%)	1 (100%)	–	–	–	1 (100%)
Rao N.N., Wilkinson C., Morton M. et al. 2011 [16]	1/1	1	1 (100%)	1 (100%)	0	0	1 (100%)	1 (100%)
Nouri K., Bader Y., Helmy S. et al. 2011 [17]	1/1	1	0	0	0	0	–	1 (100%)
Norrman E., Bergh C., Wennerholm U.B. 2015 [18]	7/8	9 (one set of twins)	3 (42.9%)	2 (26%)	1 (13%)	1 (13%)	–	8 (100%)
Pietrzak B., Mazanowska N., Kociszewska-Najman B. et al. 2015 [19]	1/1	1	1 (100%)	1	–	1 (100%)	–	1 (100%)
Warzecha D., Szymusik I., Grzechocińska B. et al. 2018 [20]	3/3	3	3 (100%)	–	3 (100%)	1 (33.3%)	1 (33.3%)	3 (100%)
Yaprak M., Dogru V., Sanhal C.Y. et al. 2019 [9]	8/11	6	3/6 (50%)	–	3/8 (37.5%)	3/8 (37.5%)	–	6 (100%)
Kosoku A., Uchida J., Maeda K., Yoshikawa Y. et al. 2019 [21]	1/1	1	0	0	0	0	0	1 (100%)
Gastañaga-Holguera T., Calvo M., Gómez-Irwin L. et al. 2021 [22]	1/1	1	0	0	0	1 (100%)	0	Vaginal delivery

Note. * PE, preeclampsia; ** FGR, fetal growth restriction; *** GDM, gestational diabetes mellitus.

no cases of renal graft loss in the outcome of pregnancy in the presented observations.

Successful pregnancy outcomes after IVF in simultaneous pancreas-kidney transplantation has also been described [23]. However, such pregnancies should be considered separately because of the additional risks associated with diabetes, especially in patients with a long history of diabetes before pancreas transplantation (it is known that long-term complications of diabetes persist for a long time after successful transplantation and complete normalization of carbohydrate metabolism, and, in some cases, are unable to completely regress).

In Russian literature, we were unable to find descriptions of IVF in patients after KT. We present our own observation of successful IVF in a woman with a transplanted kidney.

CLINICAL CASE

Patient A., born in 1985, was diagnosed with changes in urine tests as a child, but the medical records of that time were not preserved. In 2011–2012, routine check-up showed she had traces of protein in her urine, but she was not diagnosed with kidney disease. In 2013, her first pregnancy occurred spontaneously, a multiple pregnancy (twins). At 10 weeks of pregnancy, hypertension, proteinuria 1.4 g/l, microhematuria, an increase in serum creatinine to 216 μmol/l with progressive increase were detected. Clinically (without morphological verification), the patient was diagnosed with chronic glomerulonephritis, stage 3b CKD. At 16–17 weeks of gestation, the pregnancy was terminated by a small C-section. After delivery, serum creatinine level was 214 μmol/l. Subsequently, the patient received ACE inhibitor perindopril for nephroprotection, as well as a preparation of keto-analogues of amino acids. No kidney biopsy was performed.

The second pregnancy occurred spontaneously in 2017, the patient was taking oral iron (III) hydroxide polymaltose, prenatal vitamins, dipyridamole, micronized progesterone, and dopegyt on her own from early terms. At the time of registration for pregnancy at 15–16 weeks, her blood pressure (BP) was elevated to 145/90 mmHg, hemoglobin level was 97 g/l, serum creatinine level was 308 μmol/l, and urea was 17.8 mmol/l. Proteinuria was relatively low – 0.5–0.8 g/day.

The patient was explained the risks of pregnancy with CKD: risk of maternal mortality and fetal death, risk of worsening hypertension, development of early severe PE, fetal growth restriction, further deterioration in renal function during pregnancy up to the need for emergency hemodialysis, accelerated progression of CKD in the postpartum period. However, the woman strongly insisted on prolonging the pregnancy.

Amlodipine (to correct elevated BP), low molecular weight heparin, and intravenous injection of iron preparations were added to the treatment. At 19–20 weeks, renal replacement therapy (hemodialysis) had to be started due to a further increase in azotemia. Despite the treatment, the patient had a progressive increase in BP, an increase in proteinuria from 0.8 g/day to 15 g/day (her urine output remained intact after hemodialysis was initiated), platelet count decreased and was considered to be a manifestation of severe PE. At 22 weeks, a small C-section was performed due to the futility of pregnancy and high risk of maternal mortality. Subsequently, hemodialysis was discontinued due to stabilization in glomerular filtration rate (GFR) at 16–18 ml/min/1.73 m^2; the patient was put on the kidney transplant waiting list.

Deceased-donor KT was performed in April 2018, graft function was immediate, serum creatinine levels decreased rapidly to 90–95 μmol/L. Immunosuppression was induced by basiliximab according to the standard scheme, the patient received long-acting tacrolimus, mycophenolic acid and methylprednisolone orally as baseline immunosuppression. Prophylaxis for cytomegalovirus infection with valganciclovir and prophylaxis of pneumocystis with trimethoprim/sulfamethoxazole were given for 6 months after transplantation. In July 2018, a urological complication – ureteral stricture and graft kidney hydronephrosis – was diagnosed. Immediate ureteral stenting was performed, and in November 2018, reconstructive surgery – laparoscopic revision, Boari flap ureteroneocystostomy. In January 2019, the ureteral stent of the transplanted kidney was removed. A single episode of graft pyelonephritis was noted, no recurrent urinary infection thereafter. Ultrasound images of the transplanted kidney after the reconstructive surgery confirmed the absence of urodynamic disorders.

In May 2019, the patient expressed a desire to get pregnant. There were no absolute contraindications to pregnancy: her graft function was satisfactory (serum creatinine 90 μmol/l, estimated GFR 69 ml/min/1.73 m^2), daily proteinuria 0.15–0.18 g, BP was normal (120/80–110/70 mm Hg) without taking antihypertensive drugs, no recurrent urinary infection, and no obesity – body weight 56 kg at height 165 cm (BMI 20.57). In order to prepare for pregnancy, the patient was successfully converted from mycophenolic acid, a drug prohibited for use during gestation, to azathioprine. In 2019, an endometrial polyp was removed at her place of residence.

However, the patient did not become pregnant for a year despite discontinuation of contraception. Hysterosalpingography revealed blocked fallopian tubes. In 2020, a case conference consisting of a nephrologist, transplantologist, obstetrician/gynecologist physician, reproductive endocrinologist, and the head of the Moscow Regional Research Institute of Obstetrics and Gynecology, decided to use IVF in the patient with a well-functioning transplanted kidney and tubal infertility.

In October 2020, the IVF program was performed with mild stimulation according to a protocol with gonadotropin-releasing hormone antagonists, 14 oocytes

were obtained by transvaginal puncture, 3 embryos were cryopreserved on day 5 of cultivation. In December 2020, cryo-thawed embryo transfer was performed against the background of hormone replacement therapy, one embryo was transferred into the uterus, pregnancy did not occur. In January 2021, cryo-cycle IVF was repeated against the background of hormone replacement therapy, one embryo was transferred into the uterus, resulting in pregnancy.

Immunosuppressive therapy during gestation was performed with long-acting tacrolimus with gradual dose escalation due to decreasing blood concentrations, a small dose of azathioprine 50 mg/day and oral methylprednisolone 4 mg/day. The course of pregnancy from the first trimester was complicated by early GDM, which was compensated by diet, and gestational hypothyroidism, for which the patient was prescribed levothyroxine under thyroid-stimulating hormone control for continuous use. The woman had no clinical and laboratory manifestations of secondary hyperparathyroidism. An endocrinologist was involved in the management of the pregnancy, monitoring the achievement of glycemic and thyroid hormone targets.

In the first trimester, high BP values were noted during outpatient visits. However, daily BP monitoring and analysis of self-monitoring diary showed that there was no evidence of hypertension, and that episodes of BP increase were due to the patient's psycho-emotional lability. This allowed antihypertensive therapy to be discontinued. Since the first trimester, the patient received antiplatelet agents (dipyridamole) and low-molecular-weight heparin in a prophylactic dose to prevent placental-associated and thromboembolic complications, as well as for nephroprotection. At 13 weeks of gestation, dipyridamole was replaced by acetylsalicylic acid 150 mg/day, which was continued until week 36 according to a preeclampsia prevention protocol. The patient was also given recommendations on physical activity (aerobic exercise – walking 25–50 minutes daily), which were followed.

The course of GDM against the background of diet was compensated, fetal size on routine ultrasound examinations showed no abnormalities. BP in the second and third trimesters according to a self-monitoring diary remained normal, the values of the PE marker (angiogenic factor sFlt-1/PlGF), which were monitored during pregnancy, did not exceed the reference values. Gestational proteinuria was noted, which did not exceed 1 g/day in most studies. Bacteriuria was constantly monitored; fortunately, there were no episodes of pyelonephritis, and a one-week course of oral cefixime was administered for a single episode of asymptomatic bacteriuria. Mild anemia was treated with oral iron supplements.

At 37 weeks of pregnancy, the patient had her BP increasing to 145–155/90–100 mmHg, mostly against the background of psychoemotional stress (scheduled hospitalization at an obstetric hospital, preparation for delivery), which were regarded as moderate PE by doctors at the obstetric department. At the same time, there was no increase in proteinuria over time, no significant increase in serum creatinine levels, the sFlt-1/PlGF indicator was 10.0 (normal for this gestational age).

The patient delivered a baby in September 2021 at 37–38 weeks, an elective C-section was performed due to uterine scar. The baby was born male, weighing 2760 g (25th percentile), height 48 cm (36th percentile), Apgar score 7–8. The baby's condition after birth was satisfactory; he was discharged home with his mother on day 5 after surgery. Lactation in the mother was suppressed in order to quickly restore immunosuppressive therapy in full, with resumption of mycophenolate administration. Although, it is currently believed that breastfeeding in women receiving tacrolimus, small doses of corticosteroids, azathioprine, is possible [24]. The boy is growing and developing normally; renal graft function in the mother is satisfactory.

DISCUSSION

The case we presented clearly illustrates that in young women, kidney disease can be diagnosed for the first time during pregnancy, although changes in urine tests had been noted earlier (A.'s first pregnancy), and that the course of pregnancy complicated by PE can significantly accelerate the progression of renal dysfunction and rapidly lead to end-stage CKD (A.'s second pregnancy). It should be noted, however, that prior to KT, our patient had spontaneous pregnancies within a short period of time after discontinuation of contraception. After successful KT, we encountered the problem of secondary infertility, which was related to the tubal factor. Repeated abdominal surgical interventions: two small cesarean sections, the Boari operation, which uses transperitoneal access, might have been the cause of the blocked fallopian tubes. As in the general population, ovarian or tubal factors, as well as male factors may be the cause of infertility in renal transplant recipients [24].

Given the patient's age (35 years), we decided not to postpone IVF since the effectiveness of this method of overcoming infertility decreases sharply with increasing age. In patients after organ transplantation, the most important goal of IVF is not only to achieve pregnancy, but also to prevent possible complications: IVF uses mild ovarian stimulation to reduce the risk of ovarian hyperstimulation syndrome (OHSS); one embryo is typically transferred, as multifetal gestation complications can negatively affect both the gestation outcome and the transplanted organ [13].

Khalaf et al. described a patient after kidney transplantation who developed OHSS in an IVF cycle with worsening graft function – an increase in serum creatinine to a maximum of 230 μmol/L [14]. In the pathogenesis of renal dysfunction in the described case, compression

of the renal graft by the enlarged ovary and hypoperfusion of the transplanted kidney against the background of hypovolemia, typical for this complication, played a role. Conservative treatment of OHSS was effective, graft function normalized; three months later, she had two frozen–thawed embryos transferred that resulted in a twin pregnancy and subsequent birth of two living children. In the second published observation of OHSS in a patient after KT, the complication was also successfully managed, but embryo transfer was never performed subsequently [26].

In recent years, due to improvements in IVF protocols, the incidence of OHSS has been decreasing, resulting in a lower risk of IVF, including in patients with transplanted organs [27]. An important point when preparing for IVF is the withdrawal of mTOR inhibitors sirolimus and everolimus used for immunosuppression in some patients, which not only have teratogenic effects, but can also reduce the effectiveness of IVF due to their negative impact on oocyte maturation [28].

In our observation, the kidney disease was not hereditary, and IVF was used to overcome secondary infertility. But it should be remembered that assisted reproductive technology is used not only in infertility: IVF with preimplantation genetic testing and selection of healthy embryos can be successfully used in patients with monogenic renal diseases, including patients with a renal transplant, to obtain healthy offspring. This applies primarily to women with the most common monogenic renal diseases – autosomal dominant or autosomal recessive polycystic kidney disease and Alport syndrome [29, 30].

In our patient, IVF resulted in a pregnancy, but early GDM was already detected in the first trimester, which manifested as clinically significant fasting hyperglycemia. The true incidence of GDM in pregnant women after IVF with a transplanted kidney is not known; in our opinion, it should exceed the population rate by at least 2–4 times, because both the IVF procedure (estrogens, ovulation induction) and the immunosuppression drugs have a strong diabetogenic potential. In the presented observation, early GDM, in whose pathogenesis the contra-insulin effect of placental hormones is minimal, developed.

However, the literature does not allow an objective assessment of GDM incidence in this group of pregnant women, since different countries and at different times used different diagnostic criteria. Nevertheless, modern studies have shown the high importance of achieving normoglycemia in pregnant women with GDM for a good perinatal outcome, including by reducing the incidence of PE [31, 32]; so, identification and effective treatment of GDM in women with a transplanted kidney is very important.

The literature sources cited above (Table) shows a high incidence of PE, which, in this population of pregnant women, is one of the main causes of early delivery and can lead to deterioration of graft function. Effective PE prophylaxis can both reduce the incidence of PE and increase the gestational age at which PE manifests (if this complication is not completely prevented), which significantly improves pregnancy outcomes for the fetus. For this reason, PE prophylaxis in renal transplant patients (especially after IVF) should be administered as early as possible. In our opinion, the use of aspirin alone to prevent PE is not enough for pregnant women after KT; a combination of low molecular weight heparin and antiplatelet agents is necessary. It should be noted that none of the publications we cited mention any measures taken to prevent placental-associated complications. There are no studies on the effectiveness of PE prophylaxis in patients after KT. However, the results of our earlier study showed that a combined use of heparin and antiplatelet agents significantly increases the frequency of favorable pregnancy outcomes in women with reduced renal function corresponding to stage 3 CKD [33]; renal graft function in most cases corresponds to CKD stage 2–3.

The feasibility of comprehensive PE prophylaxis is partly confirmed by the presented observation. Recall that the patient's two previous pregnancies were complicated by early severe PE, which resulted not only in termination of pregnancy due to vital signs, but also in accelerated progression of CKD. In the third pregnancy, which occurred after KT and IVF, the patient received low molecular weight heparin and antiplatelet agents from the moment the pregnancy was established until it ended; as a result, symptoms that could be attributed to PE appeared only at full-term pregnancy, 2–3 days before delivery, and did not worsen the perinatal outcome. The diagnosis of PE in the case we presented is generally quite controversial because the patient had no proteinuria and the value of biomarker sFlt-1/PlGF remained normal.

Nephrologists, transplantologists, and obstetricians/gynecologists may be wary of kidney transplant rejection during pregnancy and in the postpartum period. However, the risk of rejection in pregnancy is relatively low: according to a 2019 meta-analysis that included 6,712 pregnancies in 4,174 kidney transplant recipients, the rejection rate was about 9%, which is not significantly different from this rate outside of pregnancy [1]. Apparently, with adequate control of immunosuppression, IVF is not an additional factor that increases the risk of rejection.

In our case, the favorable outcome of the IVF pregnancy in the patient with a history of obstetric complications after KT was due to a thorough IVF and pregnancy risk assessment at the planning stage, prevention of placental-associated complications (PE, fetal growth restriction), early diagnosis of GDM and achievement of normoglycemia, control of immunosuppressive therapy, and a multidisciplinary approach to pregnancy management.

CONCLUSION

Literature data and our observation suggest that in the absence of unambiguous contraindications to pregnancy, patients with infertility after KT can be successfully treated with IVF and give birth to healthy children without deterioration in graft function. However, such women have a high incidence of pregnancy complications, primarily PE, which requires prevention. Early detection and treatment of GDM, hypertension, urinary tract infection and anemia are also necessary. Observation by an interdisciplinary team of qualified specialists and optimal tactics for such a pregnancy, taking into account risk factors, can reduce the incidence of preterm birth and achieve satisfactory pregnancy outcomes for both mother and fetus.

The authors declare no conflict of interest.

REFERENCES

1. *Shah S, Venkatesan RL, Gupta A, Sanghavi MK, Welge J, Johansen R et al.* Pregnancy outcomes in women with kidney transplant: Metaanalysis and systematic review. *BMC Nephrol.* 2019; 20 (1): 24. doi: 10.1186/s12882-019-1213-5.
2. *Puthenveettil N, Mohan A, Rahman S, Paul J*. Pregnancy outcomes in renal transplant recipients. *Indian J Anaesth.* 2021; 65 (9): 695–699. doi: 10.4103/ija.ija_362_21.
3. *Murashko LE, Kandidova IE, Sukhikh GT.* Zabolevaniya pochek u beremennyh i beremennost' posle transplantacii pochki. M.: Avtorskaya akademiya, 2012; 246.
4. *Prokopenko EI, Nikolskaya IG, Vatazin AV, Novikova SV, Gurieva VM, Yankovoy AG, Shcherbakova EO.* Povtornaya uspeshnaya beremennost' i neobychnoe techenie preeklampsii u pacientki s pochechnym allotransplantatom. *Klinicheskaya nefrologiya.* 2014; 5: 36–39.
5. *Temirbulatov RR, Bezhenar VF, Reznik ON, Anan'ev AN.* Beremennost' i rody u pacientok s pochechnym allotransplantatom (klinicheskoe nablyudenie). *Uchenye zapiski SPbGMU im. akad. I.P. Pavlova.* 2017; 24 (1): 74–78.
6. *Zagajnov VE, Katkova NYu, Vasenin SA, Kukosh VM, Murtazalieva MS, Pauzina OA i dr.* Sluchaj uspeshnogo vedeniya beremennosti i rodov u pacientki posle transplantacii podzheludochnoj zhelezy i pochki. *Vestnik transplantologii i iskusstvennyh organov.* 2021; 23 (S): 90.
7. *Dumanski SM, Ahmed SB*. Fertility and reproductive care in chronic kidney disease. *J Nephrol.* 2019; 32 (1): 39–50. doi: 10.1007/s40620-018-00569-9.
8. *Sarkar M, Bramham K, Moritz MJ, Coscia L.* Reproductive health in women following abdominal organ transplant. *Am J Transplant*. 2018; 18: 1068–1076. doi: 0.1111/ajt.14697.
9. *Yaprak M, Doğru V, Sanhal CY, Özgür K, Erman M.* In vitro fertilization after renal transplantation: a single-center experience. *Transplant Proc.* 2019; 51 (4): 1089–1092. doi: 10.1016/j.transproceed.2019.01.105.
10. *Kuczera P, Więcek A, Adamczak M.* Impaired fertility in women and men with chronic kidney disease. *Adv Clin Exp Med.* 2022; 31 (2): 187–195. doi: 0.17219/acem/141188.
11. *Szymusik I, Warzecha D, Wielgoś M, Pietrzak B.* Infertility in female and male solid organ recipients – from diagnosis to treatment: an up-to-date review of the literature. *Ann Transplant.* 2020; 25: e923592. doi: 10.12659/AOT.923592.
12. *Lockwood GM, Ledger WL, Barlow DH.* Successful pregnancy outcome in a renal transplant patient following in-vitro fertilization. *Hum Reprod.* 1995; 10: 1528–1530. doi: 10.1093/humrep/10.6.1528.
13. *Furman B, Wiznitzer A, Hackmon R, Gohar J, Mazor M.* Multiple pregnancies in women after renal transplantation. Case report that rises a management dilemma. *Eur J Obstet Gynecol Reprod Biol.* 1999; 84 (1): 107–110. doi: 10.1016/s0301-2115(98)00258-9.
14. *Khalaf Y, Elkington N, Anderson H, Taylor A, Braude P.* Ovarian hyperstimulation syndrome and its effect on renal function in a renal transplant patient undergoing IVF treatment: case report. *Hum Reprod.* 2000; 15 (6): 1275–1277. doi: 10.1093/humrep/15.6.1275.
15. *Tamaki M, Ami M, Kimata N, Tsutsui T, Watanabe Y, Saito T et al*. Successful singleton pregnancy outcome resulting from in vitro fertilization after renal transplantation. *Transplantation*. 2003; 75 (7): 1082–1083. doi: 10.1097/01.TP.0000055984.84947.90.
16. *Rao NN, Wilkinson C, Morton M, Bennett GD, Russ GR, Coates PT, Jesudason S.* Successful pregnancy in a recipient of an ABO-incompatible renal allograft. *J Assist Reprod Genet.* 2011; 28: 351–353. doi: 10.1007/s10815-010-9521-5.
17. *Nouri K, Bader Y, Helmy S, Ott J, Jirecek S, Tempfer CB.* Live birth after in vitro fertilization and single embryo transfer in a kidney transplant patient: a case report and review of the literature. *J Assist Reprod Genet*. 2011; 28: 351–353. doi: 10.1007/s10815-010-9521-5.
18. *Norrman E, Bergh C, Wennerholm UB.* Pregnancy outcome and long-term follow-up after in vitro fertilization in women with renal transplantation. *Hum Reprod.* 2015; 30: 205–213. doi: 10.1093/humrep/deu293.
19. *Pietrzak B, Mazanowska N, Kociszewska-Najman B, Szymusik I, Grzechociska B, Pazik J et al.* Successful pregnancy outcome after in vitro fertilization in a kidney graft recipient: a case report and literature review. *Ann Transplant.* 2015; 20: 338–341. doi: 10.12659/AOT.893735.
20. *Warzecha D, Szymusik I, Grzechocinska B, Cyganek A, Kociszewska-Najman B, Mazanowska N et al.* In vitro fertilization and pregnancy outcomes among patients after kidney transplantation: case series and single-center experience. *Transplant Proc*. 2018; 50 (6): 1892–1895. doi: 10.1016/j.transproceed.2018.02.144.
21. *Kosoku A, Uchida J, Maeda K, Yoshikawa Y, Hamuro A, Shimada H et al.* Successful pregnancy after in vitro fertilization in an ABO-incompatible kidney transplant recipient receiving rituximab: a case report. *BMC Nephrol.* 2019; 20 (1): 206. doi: 10.1186/s12882-019-1396-9.

22. *Gastañaga-Holguera T, Calvo M, Gómez-Irwin L, Campo Gesto I, González-González V, Vidaurreta M.* Successful pregnancy and follow-up after in vitro fertilization of a kidney transplant patient with systemic lupus erythematosus, primary biliary cholangitis, and hypothyroidism. *JBRA Assisted Reproduction.* 2021; 25 (4): 657–660. doi: 10.5935/1518-0557.20210052.
23. *Mohammadi F, McDonald S, Clark E, Jesudason S.* Two pregnancies after simultaneous pancreas-kidney transplantation: A case report. *Obstet Med.* 2020; 13 (2): 92–95. doi: 10.1177/1753495X18789584.
24. *Agarwal KA, Pavlakis M.* Sexuality, contraception, and pregnancy in kidney transplantation. *Kidney Med.* 2021; 3 (5): 837–847. doi: 10.1016/j.xkme.2021.05.009.
25. *Mishra VV, Nanda SS, Mistry K, Choudhary S, Aggarwal R, Vyas BM.* An overview on fertility outcome in renal transplant recipients. *J Obstet Gynaecol India.* 2016; 66 (Suppl 1): 330–334. doi: 10.1007/s13224-016-0919-6.
26. *Zheng HH, Song Y, Wu JY.* Critical ovarian hyperstimulation syndrome after in vitro fertilization treatment in a renal transplant recipient: a case report. *Transplant Proc.* 2016; 48 (1): 267–270. doi: 10.1016/j.transproceed.2016.01.008.
27. *Schirmer DA 3rd, Kulkarni AD, Zhang Y, Kawwass JF, Boulet SL, Kissin DM.* Ovarian hyperstimulation syndrome after assisted reproductive technologies: trends, predictors, and pregnancy outcomes. *Fertil Steril.* 2020; 114 (3): 567–578. doi: 10.1016/j.fertnstert.2020.04.004.
28. *Wald K, Cakmak H, Noel M.* mTOR inhibitor sirolimus negatively impacts in vitro fertilization outcomes. *J Assist Reprod Genet.* 2019; 36 (5): 947–950. doi: 10.1007/s10815-019-01439-4.
29. *Snoek R, Stokman MF, Lichtenbelt KD, van Tilborg TC, Simcox CE, Paulussen A et al.* Preimplantation genetic testing for monogenic kidney disease. *Clin J Am Soc Nephrol.* 2020; 15 (9): 1279–1286. doi: 10.2215/CJN.03550320.
30. *Chaperon JL, Wemmer NM, McKanna TA, Clark DM, Westemeyer MA, Gauthier P et al.* Preimplantation genetic testing for kidney disease-related genes: a laboratory's experience. *Am J Nephrol.* 2021; 52: 684–690. doi: 10.1159/000518253.
31. *Jain R, Davey S, Davey A, Raghav SK, Singh JV.* Can the management of blood sugar levels in gestational diabetes mellitus cases be an indicator of maternal and fetal outcomes? The results of a prospective cohort study from India. *J Family Community Med.* 2016; 23 (2): 94–99. doi: 10.4103/2230-8229.181002.
32. *Yang Y, Wu N.* Gestational diabetes mellitus and preeclampsia: correlation and influencing factors. *Front Cardiovasc Med.* 2022; 9: 831297. doi: 10.3389/fcvm.2022.831297.
33. *Prokopenko EI, Nikolskaya IG, Vatazin AV, Novikova SV, Gurieva VM.* Impact of heparin and antiplatelet agents on pregnancy outcome in women with chronic renal failure. *Nephrology and Dialysis*. 2015; 17 (2): 185–192.

The article was submitted to the journal on 20.07.2022

DOI: 10.15825/1995-1191-2022-4-24-38

RISKS AND WAYS OF PREVENTING KIDNEY DYSFUNCTION IN DRUG-INDUCED IMMUNOSUPPRESSION IN SOLID ORGAN RECIPIENTS

Sh.R. Galeev[1], *S.V. Gautier*[1, 2]

[1] Shumakov National Medical Research Center of Transplantology and Artificial Organs, Moscow, Russian Federation

[2] Sechenov University, Moscow, Russian Federation

Immunosuppressive therapy (IMT) is the cornerstone of treatment after transplantation. The goal of immunosuppression is to prevent acute and chronic rejection while maximizing patient survival and long-term graft function. However, the expected effects of IMT must be balanced against the major adverse effects of these drugs and their toxicity. The purpose of this review is to summarize world experience on current immunosuppressive strategies and to assess their effects on renal function.

Keywords: organ transplantation, induction therapy, immunosuppressive therapy, adverse events, renal failure.

INTRODUCTION

Organ transplantation is the method of choice in the treatment of patients with irreversible loss of vital organ function. Achieving the desired results is possible with optimal use and a deep understanding of IMT that is aimed at preventing acute and chronic allograft rejection. The beginning of widespread use of calcineurin inhibitors (CNIs) was an important milestone in the evolution of IMT, significantly reducing the incidence of acute rejection [1]. This review discusses advances and techniques in IMT that have emerged over the past 50 years in the practice of clinical transplantology. The possibilities and limitations of these advances and how they affect current outcomes in post-transplant patients are also assessed.

I. IMMUNOSUPPRESSANTS AND RENAL FUNCTION IN EXTRARENAL ORGAN TRANSPLANTATION

Prolonged survival of donor organ recipients has led to greater exposure to immunosuppressants and increased adverse events associated with their use. Today, the main causes of late post-transplant mortality are largely due to long-term use of immunosuppressants [2]. Since the beginning of the decade, more than two-thirds of post-liver transplant deaths are unrelated to liver graft function, which underlines the effectiveness of modern IMT regimens [3]. However, the good survival rate of liver recipients has demonstrated the role of adverse events associated with prolonged exposure to IMT on the recipient's body. With better survival rates in solid organ recipients, reports on the detection of chronic kidney disease (CKD) in child recipients of extrarenal transplants began to appear [4, 5]. The incidence of CKD in pediatric donor heart, lung, and liver recipients ranges from 8% to 38%, depending on the definition and duration of post-transplant follow-up [4–6].

Ruebner et al analyzed data from over 16,000 children who underwent extrarenal organ transplantation between 1990 and 2010. During a median follow-up of 6.2 years, end-stage renal disease (ESRD) developed in 3% (n = 426) [4]. Choudhry et al also studied the Scientific Registry of Transplant Recipients (SRTR) and the United States Renal Data System (USRDS) databases and found that during a median follow-up of 11.8 years, ESRD developed in 4% of heart recipients [7]. The actuarial risk of developing ESRD after heart transplantation was 3% at 10 years and 16% at 20 years.

In a retrospective cohort study, Menon et al. assessed the risk of acute kidney injury (AKI) and CKD in solid organ recipients. The study included patients under 21 years of age who underwent liver (n = 112) or heart transplantation (n = 109) between July 1, 2009, and December 31, 2016. Pediatric AKI was seen in 63% (n = 69) after heart and 43% (n = 43) after liver transplant. Cumulative incidence (95% CI) of CKD stages 3–5 at 60 months post-heart transplant was 40.9% (27.9–57.1%) in patients with AKI vs 35.8% (17.1–64.8%) in those without (P = NS). Post-liver transplant, the cumulative incidence of CKD stages 3–5 at 60 months was 0% in those without perioperative AKI vs 10% (3.2–29.3%) in those with (P = 0.01). Patients with perioperative AKI

Corresponding author: Shamil Galeev. Address: 86, Generala Karbysheva str., Volzhskiy, 404120, Russian Federation. Phone: (917) 237-16-50. E-mail: namerec_taor_su@outlook.com

had lower estimated glomerular filtration (eGFR) at last follow-up [8].

Kidneys in recipients of extrarenal organs often begin to suffer at the pre-transplant stage. The use of calcineurin inhibitors (as a component of maintenance immunosuppression) and baseline renal dysfunction are traditionally considered risk factors for CKD [4, 5, 7]. Other provoking factors are infection, arterial hypertension and other nephrotoxic drugs [5, 8]. Kidney injury is a common event after extrarenal organ transplantation in adults [10–12]. Studies show that in adults after extrarenal organ transplantation, the decline in renal function is most pronounced in the first six months after transplantation, and renal dysfunction progresses more slowly or even stabilizes thereafter [13]. Even a single episode of AKI developing in the first three months after transplantation is associated with a threefold increased risk of CKD [5]. Renal failure persisting one month after liver transplantation is associated with increased risk of CKD [14]. CKD and ESRD are reported in 70% and 8.5% of patients, respectively, in the long term after liver transplantation [15]. Although kidney injury in non-renal transplant recipients is caused by multifactorial mechanisms, calcineurin inhibitor-induced renal arteriole vasoconstriction plays a leading role [16, 17]. Due to the high significance of kidney injury in clinical practice, a nephroprotection strategy is being developed, which is conventionally divided into early and late.

Early nephroprotection strategy includes induction immunosuppression with delayed administration of low-dose CNIs in combination with non-nephrotoxic immunosuppressants to safely minimize CNIs.

Induction IMT in liver transplantation is used less frequently than in other organ transplantation because of the lower risk of rejection and the often-severe clinical condition of patients with cirrhosis at the time of transplantation. In the United States, only 20–25% of liver recipients receive induction immunosuppression. Nevertheless, induction with rabbit antithymocyte globulin (rATG) appears to be reasonable in liver recipients with impaired renal function [18].

A United Network for Organ Sharing registry study [19] showed that lymphocyte-depleting agents like alemtuzumab and rATG, especially in combination with steroids, appear to be more effective in preventing renal dysfunction than agents that do not affect on liver recipients' lymphocyte counts (basiliximab and daclizumab).

Because of the existing data on the correlation between CNI levels, early renal dysfunction, and mortality, many induction immunosuppression protocols have been studied as part of a strategy to minimize CNIs in order to preserve renal function. The use of anti-CD-25 monoclonal antibodies for induction allows minimal starting doses of CNIs to be administered or delayed in liver recipients with acute kidney injury. This approach leads to a more rapid recovery of renal function with a comparable or even lower rejection rate [20]. In a more recent study by Pratima Sharma et al, the results were not as clear-cut. In a group of liver recipients with severe renal dysfunction, delayed tacrolimus (TAC) initiation combined with basiliximab induction therapy had no durable effect on long-term post-transplant outcome [21].

Standard residual tacrolimus trough levels (TAC C0) in randomized controlled trials ranged from 10 to 15 ng/mL. Combination with mycophenolate mofetil (MMF) can safely reduce TAC C0 levels to 7–10 ng/ml, with a similar incidence of acute rejection with better renal function, metabolic and cardiovascular profile [22]. The possibility of using mammalian target of rapamycin (mTOR) inhibitors, at one time caused considerable interest, due to the better safety profile in terms of renal function and high immunosuppressive efficacy. Unfortunately, the combination of TAC with rapamycin (RAP) in de novo transplanted patients showed an increased risk of hepatic artery thrombosis and acute graft rejection compared to the group on the standard IMT regimen, which required early termination of the study [23]. In another study comparing the combination of RAP with MMF versus TAC with MMF, there was a significant improvement in renal function four weeks after liver transplantation, but an increased rate of rejection in the RAP group [24]. A randomized controlled trial H2304 compared a combination of everolimus (EVE) with low-dose TAC, EVE without TAC, and a conventional TAC regimen. At month 12, 24 and 36, renal function was better in the EVE group with low-dose TAC, and the study in the EVE group without TAC was terminated early because of the high rate of acute rejection there [25].

Similar results were obtained in the PROTECT study, which compared the combination of EVE with a reduction in CNIs 8–16 weeks after liver transplantation with standard CNI doses. Better kidney function in the group of patients receiving EVE was observed for 5 years [26]. One meta-analysis of randomized controlled trials of adult recipients after de novo liver transplantation who received EVE in combination with low-dose TAC, or without TAC, found that they were associated with improved renal function at 12 months with similar efficacy in terms of rejection or mortality [27]. A number of centers have suggested the use of a combination of mTOR inhibitors with low-dose TAC starting in the immediate postoperative period. Unfortunately, there is no convincing evidence to support the effectiveness of this strategy [28]. It should be noted that IMT regimens without CNIs have also been proposed as options for therapy after induction immunosuppression with a combination of monoclonal and polyclonal antibodies. A high rejection rate has been reported for this protocol [29]. An attempt to replace nephrotoxic CNIs with belatacept (BEL), a costimulation blocker, showed an improvement in renal function one year after transplan-

tation. However, the study was prematurely terminated due to an unexplained increase in deaths in the group of patients receiving BEL [30].

Nephroprotection strategy in the late post-transplant period

Late conversion, 1 year or more after transplantation, from CNIs to RAP, showed no significant effect on renal function, with a high rate of rejection and side effects of RAP necessitating a return to CNIs [31]. Two large, but relatively old, randomized controlled trials of conversion from CNIs to a combination of EVE with low-dose TAC at one to five years showed a comparable probability of developing acute rejection with no significant effect on renal function [32, 33].

Another retrospective study examined the efficacy of conversion to EVE, in patients with impaired renal function following liver transplantation. Improvement in renal function at 12 months was achieved in the group of patients in whom conversion was performed no later than 1 year after liver transplantation [34]. The strategy of conversion to MMF monotherapy or their combination with low-dose CNIs resulted in better renal function if performed no later than 2 years after transplantation. A systematic review that summarized the switch to MMF concluded that it demonstrated beneficial effects on renal function, with an increased risk of developing rejection [35]. On the other hand, there is evidence that even with complete withdrawal of immunosuppression in liver recipients, which has been achieved in some cases [36, 37, 38], no studies have reported beneficial effects of such withdrawal in terms of renal function, hypertension, diabetes or hyperlipidemia [2].

II. MAJOR IMMUNOSUPPRESSANTS

A. Glucocorticoids (GCs)

Glucocorticoids (GCs) were used as first-line drugs in organ transplantation even before the advent of azathioprine (AZA) and cyclosporine (CsA). They were used as immunosuppressive agents as well as maintenance therapy to prevent acute rejection. GCs are anti-inflammatory agents, and their immunosuppressive effect results from several mechanisms. They act through glucocorticoid receptor (GCR) [39]. The genomic effects of GCs are realized within a few hours of drug administration [40]. GCs also produce immediate effects occurring within seconds or minutes and are referred to as nongenomic glucocorticoid effect [41]. Collectively, GCs disrupt or inhibit various cellular activities such as migration, phagocytosis, and release of inflammatory chemokines and cytokines from various cells. GCs also accelerate lymphocyte apoptosis and interrupt immune responses to foreign antigens. Clinically, these effects of GCs are associated with increased risk of bacterial, viral and fungal infections in the recipient. GCs are an integral component of induction IMT, but their use as a component of maintenance IMT is not as straightforward. Adverse effects of GCs include mineral-bone disorders, infectious complications [42], cataracts, hyperlipidemia, aseptic necrosis of the femoral head, osteoporosis, mood changes and a Cushingoid appearance; long-term use of GCs in children leads to growth retardation [43]. The frequency of arterial hypertension associated with the use of GCs is about 15%, and in almost 10% of cases, GCs are the cause of impaired glucose tolerance i.e., the so-called post-transplant diabetes mellitus (PTDM) [44]. Hence, minimizing the use of GCs may improve graft and patient survival [45].

A meta-analysis of seven studies evaluating the effects of CsA-based, steroid-free IMT protocols on graft and patient survival and incidence of acute graft rejection demonstrated that absence or withdrawal of GCs increased the risks of acute rejection but had no adverse effect on patient or graft survival. Since only one study evaluated patient and graft survival two years after transplantation, no reliable long-term conclusions on the risk of chronic rejection or graft loss could be drawn [46]. A meta-analysis of ten other studies demonstrated an increased risk of acute cellular rejection (ACR) in groups of patients in whom GCs were abolished, along with increased relative risk of graft dysfunction [47]. Because of the inconsistency of the findings and the use of AZA as a component of maintenance IMT in these studies, a third meta-analysis included only randomized controlled trials of patients receiving CNIs and MMF. This study concluded that late withdrawal of GCs was associated with a higher incidence of ACR but had no adverse effect on graft survival in the medium term [48]. Since most transplant centers today use induction IMT followed by TAC and MMF maintenance therapy, many protocols provide for either rapid withdrawal of GCs or complete rejection of their use [49].

The Kidney Disease: Improving Global Outcomes (KDIGO) guidelines state that in patients who are at low immunological risk and who receive induction IMT with lymphocyte-depleting antibodies, GCs can be discontinued within the first week of transplantation [47, 50]. These recommendations are supported by a meta-analysis of 9 studies, in 5 of which maintenance IMT was based on TAC administration, and in 4 – on CsA, in one study mTOR inhibitor was used [51]. Mortality and graft loss were similar in both patients receiving GCs and patients on steroid-free protocols [52]. These data are consistent with the observation from an analysis of US registry data showing that de novo immunosuppression without GCs did not increase the risk of adverse clinical outcomes in the medium term [53].

B. Antiproliferative drugs: azathioprine and mycophenolate mofetil

1. Azathioprine

AZA belongs to the class of antimetabolites, an imidazoline derivative of 6-mercaptopurine. AZA is a structural equivalent of adenine, hypoxanthine and guanine, which are part of nucleic acids [54]. Inhibition of purine synthesis de novo blocks lymphocyte proliferation [55]. 6-mercaptopurine is metabolized to 6-thioguanosine-5'-monophosphate, which is further metabolized by a series of kinases and reductases to form deoxy-6-thioguanosine-5'-triphosphate. Cell cycle arrest and apoptosis are triggered by incorporation of deoxy-6-thioguanosine-5'-triphosphate into the cell DNA [56]. AZA was found to block the CD28 costimulation pathway, thereby inhibiting the proliferation of activated lymphocytes [57]. AZA, along with GCs and CsA, was the immunosuppressant of choice after organ transplantation, until several randomized trials comparing it to MMF demonstrated significant advantages of the latter. [58].

2. Mycophenolate mofetil

MMF is the 2-morpholinoethyl ester of mycophenolic acid (MFA). MMF is a potent selective noncompetitive and reversible inhibitor of inosine monophosphate dehydrogenase, which inhibits de novo synthesis of guanosine nucleotides in T and B cells [59, 60]. Moreover, MMF predominantly inhibits inosine monophosphate dehydrogenase 2, whose activity is increased in activated lymphocytes, and, consequently, MMF has the greatest effect on proliferation of activated lymphocytes and reduces cytokine and antibody production induced by allergens and mitogens [61]. This selective effect is a factor that provides a better safety profile of MMF compared to azathiprine or cyclophosphamide [62]. In addition to the antiproliferative effect on lymphocytes, MPA has other mechanisms of action: due to depletion of guanosine triphosphate reserves, fucosylation and surface expression of lymphocyte and monocyte adhesion molecules are impaired [63]. MMF inhibits the surface expression of antigens responsible for differentiation and efficient presentation of allergens by dendritic cells, thus suppressing adaptive immune response [64]. Another advantage of MPA is its nephroprotective effect observed in patients with chronic graft nephropathy [65]. A review of 19 studies comparing the effectiveness of MMF and AZA in combination with CNIs demonstrated that the use of MMF provides a positive clinical effect by reducing the absolute risk of acute rejection or graft loss [66].

C. Calcineurin inhibitors

Introduction of CNIs into clinical practice has resulted in increased graft survival without rejection. However, the use of CsA or TAC requires frequent monitoring of blood levels because of their very narrow therapeutic index. Narrow therapeutic index, high individual variability, and poorly predictable and variable oral bioavailability put these drugs at risk for serious adverse effects [67]. The best-known side effect is nephrotoxicity, which has been detected almost since the beginning of clinical use [68]. Another undesirable effect of CNIs is the development of insulin resistance. Although TAC is considered less nephrotoxic than CsA, it is up to 5 times more diabetogenic, which provokes the development of PTDM. In the long term, PTDM is associated with impaired renal function and worsened patient survival [69]. Another problem with the use of CNIs is neurotoxicity, which can occur at both therapeutic and toxic levels of the drug. The main manifestation of neurotoxicity is the posterior reversible encephalopathy syndrome, whose radiological sign is a change in signal intensity reflecting vasogenic cerebral edema, localized mainly in the posterior parieto-occipital regions of the brain [70]. Today, TAC is considered to be the preferred CNI in all types of solid organ transplantation because of its ability to better control the risks of acute rejection reaction and potentially less nephrotoxicity [67].

The Efficacy Limiting Toxicity Elimination (ELITE)–Symphony study compared four groups of patients after kidney transplantation: group 1, those who received standard-dose CsA with a minimum concentration (C0) of 200–300 ng/mL; group 2, those who received low-dose CsA with C0 equal to 100–200 ng/mL; group 3, those who received low-dose TAC with C0 equal to 4–7 ng/mL; group 4, those who received low-dose sirolimus (SRL) with C0 4–8 ng/mL. All patients received induction IMT with daclizumab and received MMF and GCs as maintenance therapy. Incidence of acute rejection was lower in group 3 patients. Allograft survival differed significantly among the four groups and was highest in the low-dose TAC group. At the same time, serious adverse events were more common in the low-dose SRL group [71]. These trends were observed over a 3-year period [72]. This study provided reliable evidence of the effectiveness of maintenance IMT based on a TAC + MMF + and + GCs combination for renal transplant recipients.

D. Mammalian target of rapamycin inhibitors: Sirolimus and Everolimus

SRL or RAP, a secondary metabolite produced by S. hygroscopicus, was obtained in the 1970s [73]. EVE is a derivative of RAP, characterized by increased bioavailability when ingested and a shorter half-life [74]. mTor inhibitors significantly inhibit IL-2-stimulated T-cell proliferation and also affect B cells by inhibiting their antigen- and cytokine-dependent proliferation [75]. RAP has been shown to inhibit cytokine-dependent (IL-2, IL-6) differentiation of B cells into plasma cells, thus suppressing immunoglobulin synthesis [76]. The side

effects of mTOR inhibitors include hyperlipidemia, thrombocytopenia, mucositis, edema, and proteinuria [77]. No nephrotoxicity has been found for mTOR inhibitors [78]. The premise of using mTOR inhibitors was to avoid adverse effects – chronic nephrotoxicity inherent to CNIs. A combination of RAP or EVE with a standard-dose CsA has been associated with increased risk of nephrotoxicity [79]. Therefore, attempts have been made to use RAP instead of CNIs. A study of a combination of RAP with MPA in renal transplant recipients demonstrated increased risk of rejection [80]. Subsequent studies have explored the potential of RAP, either as a salvage therapy to replace CNIs early after transplantation [81], or in patients with a "problematic" kidney transplant [82]. Also, mTOR inhibitors were studied as a means of preserving renal function in recipients of other organs with elevated creatinine levels on the background of CsA or TAC treatment [83–85].

The potential of EVE has inspired cautious hope in heart transplantation, and its combination with TAC appears to be a safe alternative to TAC- and MMF-based maintenance therapy [86]. In heart recipients without proteinuria, EVE can be used to minimize the CsA dose. Since up to 20% of liver transplant recipients develop end-stage CKD, administration of EVE in combination with low-dose CNIs has been studied in liver transplant recipients [87]. Data from a 3-year randomized trial demonstrate long-term preservation of kidney function in liver recipients with no loss of efficacy when CNIs are withdrawn early, and EVE continued [88]. The advantages of mTOR inhibitors also include their ability to block endothelial proliferation, the ability to suppress viral replication and some types of tumor cells. In this regard, RAP and EVE are used instead of CNIs for secondary prevention of neoplasia such as skin cancer, Kaposi's sarcoma and hepatocellular carcinoma, and post-transplant lymphoproliferative disorders [89].

E. Belatacept

BEL is based on abatacept (CTLA-4 Ig), a recombinant immunoglobulin that consists of the extracellular part of the CTLA-4 molecule and the constant IgG domain [90]. It is approved for prevention of graft rejection and it excludes CNI-related nephrotoxicity after kidney transplantation [91, 92]. Studies such as BENEFIT and BENEFIT-EXT have found that the use of BEL instead of CsA preserves kidney function [93]. There was increased ACR incidence in patients who received BEL compared to those who received CsA. However, this did not affect graft function at year 3 and 5 of follow-up. This is due to the fact that BEL is less effective than CsA in preventing early, but not late rejection [94]. In addition, only a small fraction of patients on BEL-based maintenance therapy form donor-specific antibodies (3% versus 8% on CsA). Besides, BEL-based maintenance therapy, compared with CsA, provides a better cardiovascular and metabolic risk profile, and is also associated with a lower risk of PTDM [95]. In a meta-analysis in which BEL was compared with CsA, an indirect assessment of the effectiveness of BEL, CsA, and TAC on graft and patient survival, acute rejection rates, and renal function was attempted [94, 96]. The study concluded that all three drugs provided comparable graft and patient survival. In addition, BEL was associated with significantly better GFR compared with CsA. Compared with TAC, this difference was clinically but not statistically significant. [97]. BEL is not used in transplantation of organs other than the kidney, except for a phase II study in liver transplantation that was terminated early due to increased risk of death and graft loss [30].

III. INDUCTION IMMUNOSUPPRESSIVE THERAPY

Based on the idea that during donor conditioning, organ removal, warm and cold ischemia, there is increased activation of immunogenic complexes, the concept of induction IMT began to be implemented. Another justification for the use of induction immunosuppression is the fact that the risk of acute rejection reactions is maximal in the first weeks and months after transplantation [98]. To date, two different categories of immunological agents used for induction IMT are available. The first includes lymphocyte-depleting antibodies: for example, polyclonal antibodies such as equine and rabbit antithymocyte immunoglobulin (rATG) [107], the second includes genetically engineered humanized IgG1 kappa monoclonal anti-CD52 antibodies [99]. As of 2008, 82% of kidney recipients received induction IMT drugs. In recipients of other organs, induction immunosuppression was used less frequently: 57% in lung transplantation, 47% in heart and 26% in liver transplantation. In transplantation of extrarenal organs, as a rule, non-lymphocyte depleting agents were used [100]. In 2020, immunosuppression induction was already used in 91% of kidney recipients, 1% less than in 2019. The main decrease in the use of lymphocyte-depleting agents occurred at the beginning of the COVID-19 pandemic [101].

A. Rabbit antithymocyte globulin (rATG, thymoglobulin)

rATG is a polyclonal antibody produced by rabbits after immunization with infantile human thymus tissue. rATG contains antibodies not only to T cells but also to many other antigens expressed in human thymus tissues [103]. It has been shown that rATG in vitro leads to an increase in regulatory CD4+CD25+FOXP3+ T cells that suppress the immune response to allergen and participate in tolerance induction [104, 105], and also suppresses genes involved in NF-κB regulation, costimulation, apoptosis, chemoattraction and dendritic cell function [106, 107]. A number of patients produce antibodies against

rabbit immunoglobulin. Antibodies are detected in more than 50% of patients after rATG administration, but their presence does not affect the efficacy of the drug [108]. Induction IMT with thymoglobulin compared to basiliximab in kidney recipients from a postmortem donor with a high risk of delayed function or acute rejection significantly reduced the probability of developing rejection, but did not affect the duration of graft dysfunction. Patient and graft survival were comparable in both groups [109].

B. Basiliximab (anti-CD-25 monoclonal antibody)

Basiliximab is a chimeric non-lymphocyte-destroying mouse/human monoclonal antibody targeted against the α-chain of IL-2R (also known as CD25 or IL-2Rα) [99, 110]. Acting as an IL-2Rα antagonist, basiliximab competitively inhibits lymphocyte activation. The main advantage when using anti-CD25 monoclonal antibodies is its specificity and the absence of leukopenia and thrombocytopenia, which are often observed when using lymphocytopenic antibodies.

Numerous randomized controlled trials have shown that basiliximab significantly reduces the risk of acute rejection compared with placebo in renal transplant recipients receiving double (CNIs and GCs) or triple IMT (CNIs, GCs and AZA or MMF). However, graft and patient survival rates at 12 months were comparable [111–113]. The effects of basiliximab appear to be even less pronounced when used as the main component of maintenance IMT using TAC. This may be due to the lack of large studies or to the more pronounced immunosuppressive effect of TAC compared to CsA [112]. At the same time, there is little information on the long-term effects of basiliximab. As for the safety profile of basiliximab, according to this study, it is an independent risk factor for PTDM [115].

C. Alemtuzumab (Campath-1H)

Alemtuzumab is a humanized rat monoclonal antibody originally designed to treat chronic lymphocytic leukemia (rat IgG2b); it is an antibody that targets the lymphocyte-specific surface marker CD52. The CD52 antigen is present on the surface of T cells, B cells, natural killer cells, macrophages, and monocytes [114, 116]. Even small doses of the drug cause persistent profound lymphopenia, and it may take considerable time to restore the number of lymphocytes. Alemtuzumab was first used for the purpose of induction IMT by Calne et al. in 1998 [117]. They suggested that the achieved profound depletion of lymphocyte level would minimize the dose of GCs, CNIs and even contribute to the development of immune system tolerance to the transplanted kidney. However, all patients developed reversible acute graft rejection within the first month [118]. Other studies have evaluated the efficacy and safety of alemtuzumab on maintenance therapy with CNIs or its combination with MMF [119]. In one study in patients at low immunological risk, biopsy-confirmed acute graft rejection within the first year was less common with alemtuzumab compared to standard induction IMT with basiliximab or rATG, while in high immunological risk the effectiveness of all three drugs was comparable [119]. Another review, which included 1,687 kidney transplants to adult recipients performed between January 1, 2002, and December 31, 2007, compared outcomes in patients who received alemtuzumab (n = 632), basiliximab (n = 690), or thymoglobulin (n = 125) as IMT inducers. Cumulative 1, 3, and 5-year survival rates were significantly lower in the alemtuzumab group, and the incidence of antibody-mediated rejection was higher. Alemtuzumab was found to be an independent risk factor for allograft loss ($P = 0.004$), opportunistic infections ($P = 0.01$), cytomegalovirus infections ($P = 0.001$) and antibody-mediated rejection ($P = 0.002$) [120]. An analysis of the elderly population showed that alemtuzumab appeared to be associated with increased risk of death and graft loss in this group [121]. A combination of induction alemtuzumab with RAP monotherapy was another attractive hypothesis and was tested on 29 patients. Eight patients required treatment for acute rejection and one patient had graft loss [122]. Other researchers have found that a combination of RAP with MMF after induction alemtuzumab was associated with a high rate of rejection and complications in the form of leukopenia and respiratory distress syndrome [123].

D. Other agents

Rituximab is an antitumor and immunomodulatory agent. It is a chimeric mouse/human monoclonal antibody that binds specifically to the CD20 transmembrane antigen [124]. Over the past 15 years, it has mainly been used in ABO-incompatible kidney transplants and has been used with varying degrees of success in protocols for desensitization of kidney transplant recipients and treatment of antibody-mediated rejection [125–127]. Data on the use of rituximab as an IMT inducer are still limited. Its efficacy has been evaluated in a prospective double-blind, randomized, placebo-controlled study [128]. The incidence of acute rejection as well as kidney function did not differ significantly between the rituximab group and placebo group. Another randomized controlled trial comparing rituximab with daclizumab was terminated early due to increased incidence of ACR in the rituximab group [129].

CONCLUSION

Since the mere fact of taking immunosuppressants has a negative effect, the goal of treatment is to prescribe the least immunosuppressive regimen that can reliably

prevent graft rejection. However, this simple concept presents many challenges when adapted to clinical practice. There are major differences in IMT regimens between different centers, between physicians at the same center, and even between physicians treating the same patient, but at different time periods. Moreover, reduction of immunosuppression regimen is based on surrogate markers (i.e., trough blood levels) and clinical events (i.e., rejection episodes, infectious complications). Because clinical practice lacks a reliable mechanism for assessing the adequacy of immunosuppression, it is very difficult to determine the minimum level of IMT that is sufficient for each individual patient at any given time. In addition, there are relatively few up-to-date studies describing IMT strategies in the available literature, and the average period of publications cited in current reviews dates back to 2011. All this determines the relevance of the search for new principles and modes of IMT, ensuring long-term survival of solid organ recipients, with minimal negative effects. The absence of new molecules preventing the development of rejection leaves clinicians with only the possibility to search for optimal combinations of existing immunosuppressants, used both at the induction stage and in further maintenance regimen.

The authors declare no conflict of interest.

REFERENCES

1. *Metalidis C, Kuypers D.* Immunosuppressive therapy after kidney transplantation: current and new strategies. *Minerva Urol Nefrol*. 2011 Mar; 63 (1): 1–19. PMID: 21336242.
2. *Di Maira T, Little EC, Berenguer M.* Immunosuppression in liver transplant. *Best Pract Res Clin Gastroenterol*. 2020 Jun–Aug; 46–47: 101681. doi: 10.1016/j.bpg.2020.101681. Epub 2020 Sep 11. PMID: 33158467.
3. *Watt KD, Pedersen RA, Kremers WK, Heimbach JK, Charlton MR.* Evolution of causes and risk factors for mortality post-liver transplant: results of the NIDDK long-term follow-up study. *Am J Transplant*. 2010 Jun; 10 (6): 1420–1427. doi: 10.1111/j.1600-6143.2010.03126.x. Epub 2010 May 10. PMID: 20486907; PMCID: PMC2891375.
4. *Ruebner RL, Reese PP, Denburg MR, Abt PL, Furth SL.* End-stage kidney disease after pediatric nonrenal solid organ transplantation. *Pediatrics*. 2013 Nov; 132 (5): e1319–e1326. doi: 10.1542/peds.2013-0904. Epub 2013 Oct 14. PMID: 24127468; PMCID: PMC3813394.
5. *Williams C, Borges K, Banh T, Vasilevska-Ristovska J, Chanchlani R, Ng VL et al.* Patterns of kidney injury in pediatric nonkidney solid organ transplant recipients. *Am J Transplant*. 2018 Jun; 18 (6): 1481–1488. doi: 10.1111/ajt.14638. Epub 2018 Feb 6. PMID: 29286569.
6. *LaRosa C, Glah C, Baluarte HJ, Meyers KE.* Solid-organ transplantation in childhood: transitioning to adult health care. *Pediatrics*. 2011 Apr; 127 (4): 742–753. doi: 10.1542/peds.2010-1232. Epub 2011 Mar 7. PMID: 21382946.
7. *Choudhry S, Dharnidharka VR, Castleberry CD, Goss CW, Simpson KE, Schechtman KB, Canter CE.* End-stage renal disease after pediatric heart transplantation: A 25-year national cohort study. *J Heart Lung Transplant*. 2017 Oct 2: S1053–2498(17)32042-9. doi: 10.1016/j.healun.2017.09.027. Epub ahead of print. PMID: 29055603; PMCID: PMC5880747.
8. *Menon S, Pollack AH, Sullivan E, Murphy T, Smith J.* Acute kidney injury and chronic kidney disease after non-kidney solid organ transplantation. *Pediatr Transplant*. 2020 Sep; 24 (6): e13753. doi: 10.1111/petr.13753. Epub 2020 Jun 4. PMID: 32497381.
9. *Sigurjonsdottir VK, Chaturvedi S, Mammen C, Sutherland SM.* Pediatric acute kidney injury and the subsequent risk for chronic kidney disease: is there cause for alarm? *Pediatr Nephrol*. 2018 Nov; 33 (11): 2047–2055. doi: 10.1007/s00467-017-3870-6. Epub 2018 Jan 26. PMID: 29374316.
10. *Charbonney E, Saudan P, Triverio PA, Quinn K, Mentha G, Martin PY.* Prognosis of acute kidney injury requiring renal replacement therapy in solid organ transplanted patients. *Transpl Int*. 2009 Nov; 22 (11): 1058–1063. doi: 10.1111/j.1432-2277.2009.00914.x. Epub 2009 Jul 13. PMID: 19624498.
11. *Pham PT, Slavov C, Pham PC.* Acute kidney injury after liver, heart, and lung transplants: dialysis modality, predictors of renal function recovery, and impact on survival. *Adv Chronic Kidney Dis*. 2009 Jul; 16 (4): 256–267. doi: 10.1053/j.ackd.2009.04.002. PMID: 19576556.
12. *Nadkarni GN, Chauhan K, Patel A, Saha A, Poojary P, Kamat S et al.* Temporal trends of dialysis requiring acute kidney injury after orthotopic cardiac and liver transplant hospitalizations. *BMC Nephrol*. 2017 Jul 19; 18 (1): 244. doi: 10.1186/s12882-017-0657-8. PMID: 28724404; PMCID: PMC5516358.
13. *Bloom RD, Doyle AM.* Kidney disease after heart and lung transplantation. *Am J Transplant*. 2006 Apr; 6 (4): 671–679. doi: 10.1111/j.1600-6143.2006.01248.x. PMID: 16539623.
14. *Gonwa TA, Mai ML, Melton LB, Hays SR, Goldstein RM, Levy MF, Klintmalm GB.* End-stage renal disease (ESRD) after orthotopic liver transplantation (OLTX) using calcineurin-based immunotherapy: risk of development and treatment. *Transplantation*. 2001 Dec 27; 72 (12): 1934–1939. doi: 10.1097/00007890-200112270-00012. PMID: 11773892.
15. *Beckebaum S, Cicinnati VR, Radtke A, Kabar I.* Calcineurin inhibitors in liver transplantation – still champions or threatened by serious competitors? *Liver Int*. 2013 May; 33 (5): 656–665. doi: 10.1111/liv.12133. Epub 2013 Feb 27. PMID: 23442173.
16. *Ojo AO.* Renal disease in recipients of nonrenal solid organ transplantation. *Semin Nephrol*. 2007 Jul; 27 (4): 498–507. doi: 10.1016/j.semnephrol.2007.03.010. PMID: 17616280.

17. *Nowicki M, Zwiech R.* Chronic renal failure in non-renal organ transplant recipients. *Ann Transplant*. 2005; 10 (3): 54–58. PMID: 16617670.
18. *Uemura T, Schaefer E, Hollenbeak CS, Khan A, Kadry Z.* Outcome of induction immunosuppression for liver transplantation comparing anti-thymocyte globulin, daclizumab, and corticosteroid. *Transpl Int*. 2011 Jul; 24 (7): 640–650. doi: 10.1111/j.1432-2277.2011.01250.x. Epub 2011 Mar 23. PMID: 21429047.
19. *Cai J, Terasaki PI.* Induction immunosuppression improves long-term graft and patient outcome in organ transplantation: an analysis of United Network for Organ Sharing registry data. *Transplantation*. 2010 Dec 27; 90 (12): 1511–1515. doi: 10.1097/TP.0b013e3181fecfcb. PMID: 21057388.
20. *Levitsky J, O'Leary JG, Asrani S, Sharma P, Fung J, Wiseman A, Niemann CU.* Protecting the Kidney in Liver Transplant Recipients: Practice-Based Recommendations From the American Society of Transplantation Liver and Intestine Community of Practice. *Am J Transplant*. 2016 Sep; 16 (9): 2532–2544. doi: 10.1111/ajt.13765. Epub 2016 Apr 22. PMID: 26932352; PMCID: PMC5007154.
21. *Sharma P, Sun Y, Neal J, Erley J, Shen J, Tischer S et al*. Renal Outcomes of Liver Transplantation Recipients Receiving Standard Immunosuppression and Early Renal Sparing Immunosuppression: A Retrospective Single Center Study. *Transplant Direct*. 2019 Aug 8; 5 (9): e480. doi: 10.1097/TXD.0000000000000917. PMID: 31579808; PMCID: PMC6739043.
22. *Jain A, Sharma R, Ryan C, Tsoulfas G, Orloff M, Abt P et al*. Potential immunological advantage of intravenous mycophenolate mofetil with tacrolimus and steroids in primary deceased donor liver transplantation and live donor liver transplantation without antibody induction. *Liver Transpl*. 2008 Feb; 14 (2): 202–209. doi: 10.1002/lt.21348. PMID: 18236395.
23. *Asrani SK, Wiesner RH, Trotter JF, Klintmalm G, Katz E, Maller E et al*. *De novo* sirolimus and reduced-dose tacrolimus versus standard-dose tacrolimus after liver transplantation: the 2000–2003 phase II prospective randomized trial. *Am J Transplant*. 2014 Feb; 14 (2): 356–366. doi: 10.1111/ajt.12543. Epub 2014 Jan 23. PMID: 24456026.
24. *Teperman L, Moonka D, Sebastian A, Sher L, Marotta P, Marsh C et al*. Spare-the-Nephron Trial Liver Transplantation Study Group. Calcineurin inhibitor-free mycophenolate mofetil/sirolimus maintenance in liver transplantation: the randomized spare-the-nephron trial. *Liver Transpl*. 2013 Jul; 19 (7): 675–689. doi: 10.1002/lt.23658. PMID: 23775875.
25. *Fischer L, Saliba F, Kaiser GM, De Carlis L, Metselaar HJ, De Simone P et al.* H2304 Study Group. Three-year Outcomes in *De Novo* Liver Transplant Patients Receiving Everolimus With Reduced Tacrolimus: Follow-Up Results From a Randomized, Multicenter Study. *Transplantation*. 2015 Jul; 99 (7): 1455–1462. doi: 10.1097/TP.0000000000000555. PMID: 26151607.
26. *Sterneck M, Kaiser GM, Heyne N, Richter N, Rauchfuss F, Pascher A et al*. Long-term follow-up of five yr shows superior renal function with everolimus plus early calcineurin inhibitor withdrawal in the PROTECT randomized liver transplantation study. *Clin Transplant*. 2016 Jun; 30 (6): 741–748. doi: 10.1111/ctr.12744. Epub 2016 May 10. PMID: 27160359.
27. *Lin M, Mittal S, Sahebjam F, Rana A, Sood GK*. Everolimus with early withdrawal or reduced-dose calcineurin inhibitors improves renal function in liver transplant recipients: A systematic review and meta-analysis. *Clin Transplant*. 2017 Feb; 31 (2). doi: 10.1111/ctr.12872. Epub 2017 Jan 18. PMID: 27862340.
28. *Charlton M, Levitsky J, Aqel B, O'Grady J, Hemibach J, Rinella M et al*. International Liver Transplantation Society Consensus Statement on Immunosuppression in Liver Transplant Recipients. *Transplantation*. 2018 May; 102 (5): 727–743. doi: 10.1097/TP.0000000000002147. Erratum in: *Transplantation*. 2019 Jan; 103 (1): e37. PMID: 29485508.
29. *De Simone P, Carrai P, Coletti L, Ghinolfi D, Petruccelli S, Filipponi F.* Modification of immunosuppressive therapy as risk factor for complications after liver transplantation. *Best Pract Res Clin Gastroenterol*. 2017 Apr; 31 (2): 199–209. doi: 10.1016/j.bpg.2017.03.001. Epub 2017 Apr 12. PMID: 28624108.
30. *Klintmalm GB, Feng S, Lake JR, Vargas HE, Wekerle T, Agnes S et al*. Belatacept-based immunosuppression in *de novo* liver transplant recipients: 1-year experience from a phase II randomized study. *Am J Transplant*. 2014 Aug; 14 (8): 1817–1827. doi: 10.1111/ajt.12810. PMID: 25041339; PMCID: PMC4140547.
31. *Abdelmalek MF, Humar A, Stickel F, Andreone P, Pascher A, Barroso E et al.* Sirolimus Liver Conversion Trial Study Group. Sirolimus conversion regimen versus continued calcineurin inhibitors in liver allograft recipients: a randomized trial. *Am J Transplant*. 2012 Mar; 12 (3): 694–705. doi: 10.1111/j.1600-6143.2011.03919.x. Epub 2012 Jan 10. PMID: 22233522.
32. *De Simone P, Metselaar HJ, Fischer L, Dumortier J, Boudjema K, Hardwigsen J et al*. Conversion from a calcineurin inhibitor to everolimus therapy in maintenance liver transplant recipients: a prospective, randomized, multicenter trial. *Liver Transpl*. 2009 Oct; 15 (10): 1262–1269. doi: 10.1002/lt.21827. PMID: 19790150.
33. *Saliba F, Dharancy S, Lorho R, Conti F, Radenne S, Neau-Cransac M et al*. Conversion to everolimus in maintenance liver transplant patients: a multicenter, retrospective analysis. *Liver Transpl*. 2011 Aug; 17 (8): 905–913. doi: 10.1002/lt.22292. PMID: 21384525.
34. *Bilbao I, Salcedo M, Gómez MA, Jimenez C, Castroagudín J, Fabregat J et al.* EVEROLIVER study group. Renal function improvement in liver transplant recipients after early everolimus conversion: A clinical practice cohort study in Spain. *Liver Transpl*. 2015 Aug; 21 (8): 1056–1065. doi: 10.1002/lt.24172. PMID: 25990257.
35. *Goralczyk AD, Bari N, Abu-Ajaj W, Lorf T, Ramadori G, Friede T, Obed A.* Calcineurin inhibitor sparing with mycophenolate mofetil in liver transplantion:

a systematic review of randomized controlled trials. *Am J Transplant*. 2012 Oct; 12 (10): 2601–2607. doi: 10.1111/j.1600-6143.2012.04157.x. Epub 2012 Jul 19. PMID: 22813081.

36. *Feng S, Ekong UD, Lobritto SJ, Demetris AJ, Roberts JP, Rosenthal P et al*. Complete immunosuppression withdrawal and subsequent allograft function among pediatric recipients of parental living donor liver transplants. *JAMA*. 2012 Jan 18; 307 (3): 283–293. doi: 10.1001/jama.2011.2014. PMID: 22253395.
37. *Benítez C, Londoño MC, Miquel R, Manzia TM, Abraldes JG, Lozano JJ et al*. Prospective multicenter clinical trial of immunosuppressive drug withdrawal in stable adult liver transplant recipients. *Hepatology*. 2013 Nov; 58 (5): 1824–1835. doi: 10.1002/hep.26426. Epub 2013 Sep 19. PMID: 23532679.
38. *Shaked A, DesMarais MR, Kopetskie H, Feng S, Punch JD, Levitsky J et al*. Outcomes of immunosuppression minimization and withdrawal early after liver transplantation. *Am J Transplant*. 2019 May; 19 (5): 1397–1409. doi: 10.1111/ajt.15205. Epub 2018 Dec 31. Erratum in: *Am J Transplant*. 2019 Aug; 19 (8): 2393. PMID: 30506630; PMCID: PMC6482056.
39. *Griekspoor A, Zwart W, Neefjes J, Michalides R*. Visualizing the action of steroid hormone receptors in living cells. *Nucl Recept Signal*. 2007 Mar 9; 5: e003. doi: 10.1621/nrs.05003. PMID: 17464358; PMCID: PMC1853070.
40. *Hayashi R, Wada H, Ito K, Adcock IM*. Effects of glucocorticoids on gene transcription. *Eur J Pharmacol*. 2004 Oct 1; 500 (1–3): 51–62. doi: 10.1016/j.ejphar.2004.07.011. PMID: 15464020.
41. *Stellato C*. Post-transcriptional and nongenomic effects of glucocorticoids. *Proc Am Thorac Soc*. 2004; 1 (3): 255–263. doi: 10.1513/pats.200402-015MS. PMID: 16113443.
42. *Gheith OA, Nematalla AH, Bakr MA, Refaie A, Shokeir AA, Ghoneim MA*. Steroid avoidance reduce the cost of morbidities after live-donor renal allotransplants: a prospective, randomized, controlled study. *Exp Clin Transplant*. 2011 Apr; 9 (2): 121–127. PMID: 21453230.
43. *Citterio F*. Steroid side effects and their impact on transplantation outcome. *Transplantation*. 2001 Dec 27; 72 (12 Suppl): S75–80. PMID: 11833145.
44. *Veenstra DL, Best JH, Hornberger J, Sullivan SD, Hricik DE*. Incidence and long-term cost of steroid-related side effects after renal transplantation. *Am J Kidney Dis*. 1999 May; 33 (5): 829–839. doi: 10.1016/s0272-6386(99)70414-2. PMID: 10213637.
45. *Opelz G, Döhler B, Laux G*. Collaborative Transplant Study. Long-term prospective study of steroid withdrawal in kidney and heart transplant recipients. *Am J Transplant*. 2005 Apr; 5 (4 Pt 1): 720–728. doi: 10.1111/j.1600-6143.2004.00765.x. PMID: 15760395.
46. *Hricik DE, O'Toole MA, Schulak JA, Herson J*. Steroid-free immunosuppression in cyclosporine-treated renal transplant recipients: a meta-analysis. *J Am Soc Nephrol*. 1993 Dec; 4 (6): 1300–1305. doi: 10.1681/ASN.V461300. PMID: 8130356.
47. *Kasiske BL, Zeier MG, Chapman JR, Craig JC, Ekberg H, Garvey CA et al*. Kidney Disease: Improving Global Outcomes. KDIGO clinical practice guideline for the care of kidney transplant recipients: a summary. *Kidney Int*. 2010 Feb; 77 (4): 299–311. doi: 10.1038/ki.2009.377. Epub 2009 Oct 21. PMID: 19847156.
48. *Pascual J, Quereda C, Zamora J, Hernández D*. Spanish Group for Evidence-Based Medicine in Renal Transplantation. Updated metaanalysis of steroid withdrawal in renal transplant patients on calcineurin inhibitor and mycophenolate mofetil. *Transplant Proc*. 2005 Nov; 37 (9): 3746–3748. doi: 10.1016/j.transproceed.2005.09.177. PMID: 16386525.
49. *Welberry Smith MP, Cherukuri A, Newstead CG, Lewington AJ, Ahmad N, Menon K et al*. Alemtuzumab induction in renal transplantation permits safe steroid avoidance with tacrolimus monotherapy: a randomized controlled trial. *Transplantation*. 2013 Dec 27; 96 (12): 1082–1088. doi: 10.1097/TP.0b013e3182a64db9. PMID: 24056618.
50. *Heemann U, Abramowicz D, Spasovski G, Vanholder R*. European Renal Best Practice Work Group on Kidney Transplantation. Endorsement of the Kidney Disease Improving Global Outcomes (KDIGO) guidelines on kidney transplantation: a European Renal Best Practice (ERBP) position statement. Nephrol Dial Transplant. 2011 Jul; 26 (7): 2099–2106. doi: 10.1093/ndt/gfr169. Epub 2011 May 9. PMID: 21555392.
51. *Pascual J*. Steroid avoidance or withdrawal in kidney transplantation. *Curr Opin Organ Transplant*. 2011 Dec; 16 (6): 600–605. doi: 10.1097/MOT.0b013e32834c23fa. PMID: 21971514.
52. *Pascual J, Royuela A, Galeano C, Crespo M, Zamora J*. Very early steroid withdrawal or complete avoidance for kidney transplant recipients: a systematic review. *Nephrol Dial Transplant*. 2012 Feb; 27 (2): 825–832. doi: 10.1093/ndt/gfr374. Epub 2011 Jul 22. PMID: 21785040.
53. *Luan FL, Steffick DE, Gadegbeku C, Norman SP, Wolfe R, Ojo AO*. Graft and patient survival in kidney transplant recipients selected for *de novo* steroid-free maintenance immunosuppression. *Am J Transplant*. 2009 Jan; 9 (1): 160–168. doi: 10.1111/j.1600-6143.2008.02442.x. Epub 2008 Oct 24. PMID: 18976304; PMCID: PMC2626128.
54. Azathioprine: instruction [Internet]. Vidal: Spravochnik lekarstvennyh sredstv; s2020-09 [Updated 2022 July 11]. Available from: https://www.vidal.ru/.
55. *Elion GB*. The purine path to chemotherapy. *Science*. 1989 Apr 7; 244 (4900): 41–47. doi: 10.1126/science.2649979. PMID: 2649979.
56. *Swann PF, Waters TR, Moulton DC, Xu YZ, Zheng Q, Edwards M, Mace R*. Role of postreplicative DNA mismatch repair in the cytotoxic action of thioguanine. *Science*. 1996 Aug 23; 273 (5278): 1109–1111. doi: 10.1126/science.273.5278.1109. PMID: 8688098.
57. *Karam S, Wali RK*. Current State of Immunosuppression: Past, Present, and Future. *Crit Rev Eukaryot Gene Expr*. 2015; 25 (2): 113–134. doi: 10.1615/critreveukaryotgeneexpr.2015011421. PMID: 26080606.

58. *Sollinger HW.* Mycophenolate mofetil for the prevention of acute rejection in primary cadaveric renal allograft recipients. U.S. Renal Transplant Mycophenolate Mofetil Study Group. *Transplantation*. 1995 Aug 15; 60 (3): 225–232. doi: 10.1097/00007890-199508000-00003. PMID: 7645033.
59. *Sievers TM, Rossi SJ, Ghobrial RM, Arriola E, Nishimura P, Kawano M, Holt CD.* Mycophenolate mofetil. *Pharmacotherapy*. 1997 Nov-Dec; 17 (6): 1178–1197. PMID: 9399601.
60. Mycophenolate mofetil [Internet]. Vidal: Spravochnik lekarstvennyh sredstv; s2020-09 [Updated 2022 July 11]. Available from: https://www.vidal.ru/.
61. *Carr SF, Papp E, Wu JC, Natsumeda Y.* Characterization of human type I and type II IMP dehydrogenases. *J Biol Chem*. 1993 Dec 25; 268 (36): 27286–27290. PMID: 7903306.
62. *Eugui EM, Almquist SJ, Muller CD, Allison AC.* Lymphocyte-selective cytostatic and immunosuppressive effects of mycophenolic acid *in vitro*: role of deoxyguanosine nucleotide depletion. *Scand J Immunol*. 1991 Feb; 33 (2): 161–173. doi: 10.1111/j.1365-3083.1991.tb03746.x. PMID: 1826793.
63. *Blaheta RA, Leckel K, Wittig B, Zenker D, Oppermann E, Harder S et al*. Mycophenolate mofetil impairs transendothelial migration of allogeneic CD4 and CD8 T-cells. *Transplant Proc*. 1999 Feb-Mar; 31 (1–2): 1250–1252. doi: 10.1016/s0041-1345(98)01984-8. PMID: 10083559.
64. *Colic M, Stojic-Vukanic Z, Pavlovic B, Jandric D, Stefanoska I.* Mycophenolate mofetil inhibits differentiation, maturation and allostimulatory function of human monocyte-derived dendritic cells. *Clin Exp Immunol*. 2003 Oct; 134 (1): 63–69. doi: 10.1046/j.1365-2249.2003.02269.x. PMID: 12974756; PMCID: PMC1808848.
65. *Gonzalez Molina M, Seron D, Garcia del Moral R, Carrera M, Sola E, Jesus Alferez M et al*. Mycophenolate mofetil reduces deterioration of renal function in patients with chronic allograft nephropathy. A follow-up study by the Spanish Cooperative Study Group of Chronic Allograft Nephropathy. *Transplantation*. 2004 Jan 27; 77 (2): 215–220. doi: 10.1097/01.TP.0000100684.59784.FF. PMID: 14742984.
66. *Knight SR, Russell NK, Barcena L, Morris PJ.* Mycophenolate mofetil decreases acute rejection and may improve graft survival in renal transplant recipients when compared with azathioprine: a systematic review. *Transplantation*. 2009 Mar 27; 87 (6): 785–794. doi: 10.1097/TP.0b013e3181952623. PMID: 19300178.
67. *Provenzani A, Santeusanio A, Mathis E, Notarbartolo M, Labbozzetta M, Poma P et al*. Pharmacogenetic considerations for optimizing tacrolimus dosing in liver and kidney transplant patients. *World J Gastroenterol*. 2013 Dec 28; 19 (48): 9156–9173. doi: 10.3748/wjg.v19.i48.9156. PMID: 24409044; PMCID: PMC3882390.
68. *Calne RY, White DJ, Thiru S, Evans DB, McMaster P, Dunn DC et al*. Cyclosporin A in patients receiving renal allografts from cadaver donors. *Lancet*. 1978 Dec 23–30; 2 (8104-5): 1323–1327. doi: 10.1016/s0140-6736(78)91970-0. PMID: 82836.
69. *Kasiske BL, Snyder JJ, Gilbertson D, Matas AJ.* Diabetes mellitus after kidney transplantation in the United States. *Am J Transplant*. 2003 Feb; 3 (2): 178–185. doi: 10.1034/j.1600-6143.2003.00010.x. PMID: 12603213.
70. *Gudkova VV, Kimel'fel'd EI, Stakhovskaya LV.* Maloizvestnyy sindrom zadney obratimoy entsefalopatii, trebuyushchiy neotlozhnoy pomoshchi. *Consilium Medicum*. 2018; 20 (2): 84–89. doi: 10.26442/2075-1753_2018.2.84-89.
71. *Ekberg H, Tedesco-Silva H, Demirbas A, Vítko S, Nashan B, Gürkan A et al.* ELITE-Symphony Study. Reduced exposure to calcineurin inhibitors in renal transplantation. *N Engl J Med*. 2007 Dec 20; 357 (25): 2562–2575. doi: 10.1056/NEJMoa067411. PMID: 18094377.
72. *Ekberg H, Bernasconi C, Tedesco-Silva H, Vítko S, Hugo C, Demirbas A et al*. Calcineurin inhibitor minimization in the Symphony study: observational results 3 years after transplantation. *Am J Transplant*. 2009 Aug; 9 (8): 1876–1885. doi: 10.1111/j.1600-6143.2009.02726.x. Epub 2009 Jun 26. PMID: 19563339.
73. *Vézina C, Kudelski A, Sehgal SN.* Rapmycin (AY-22,989), a new antifungal antibiotic. I. Taxonomy of the producing streptomycete and isolation of the active principle. *J Antibiot* (Tokyo). 1975 Oct; 28 (10): 721–726. doi: 10.7164/antibiotics.28.721. PMID: 1102508.
74. *Kirchner GI, Meier-Wiedenbach I, Manns MP.* Clinical pharmacokinetics of everolimus. *Clin Pharmacokinet*. 2004; 43 (2): 83–95. doi: 10.2165/00003088-200443020-00002. PMID: 14748618.
75. *Aagaard-Tillery KM, Jelinek DF.* Inhibition of human B lymphocyte cell cycle progression and differentiation by Rapmycin. *Cell Immunol*. 1994 Jul; 156 (2): 493–507. doi: 10.1006/cimm.1994.1193. PMID: 7517796.
76. *Kim HS, Raskova J, Degiannis D, Raska K Jr.* Effects of cyclosporine and Rapmycin on immunoglobulin production by preactivated human B cells. *Clin Exp Immunol*. 1994 Jun; 96 (3): 508–512. doi: 10.1111/j.1365-2249.1994.tb06058.x. PMID: 8004821; PMCID: PMC1534564.
77. *Ponticelli C.* The pros and the cons of mTOR inhibitors in kidney transplantation. *Expert Rev Clin Immunol*. 2014 Feb; 10 (2): 295–305. doi: 10.1586/1744666X.2014.872562. Epub 2013 Dec 30. PMID: 24377908.
78. *Viklický O, Zou H, Müller V, Lacha J, Szabó A, Heemann U.* SDZ-RAD predotvrashchaet proyavlenie khronicheskogo ottorzheniya u pochechnykh allotransplantatov krys. *Peresadka*. 2000 Fev 27; 69 (4): 497–502. doi: 10.1097/00007890-200002270-00006. PMID: 10708101.
79. *Kahan BD.* Efficacy of sirolimus compared with azathioprine for reduction of acute renal allograft rejection: a randomised multicentre study. The Rapmune US Study Group. *Lancet*. 2000 Jul 15; 356 (9225): 194–202. doi: 10.1016/s0140-6736(00)02480-6. PMID: 10963197.

80. *Garcia R, Machado PG, Felipe CR, Park SI, Spinelli GA, Franco MF et al*. Exploratory calcineurin inhibitor-free regimens in living-related kidney transplant recipients. *Braz J Med Biol Res*. 2007 Apr; 40 (4): 457–465. doi: 10.1590/s0100-879x2007000400003. PMID: 17401488.
81. *Weir MR, Mulgaonkar S, Chan L, Shidban H, Waid TH, Preston D et al*. Mycophenolate mofetil-based immunosuppression with sirolimus in renal transplantation: a randomized, controlled Spare-the-Nephron trial. *Kidney Int*. 2011 Apr; 79 (8): 897–907. doi: 10.1038/ki.2010.492. Epub 2010 Dec 29. PMID: 21191361.
82. *Schena FP, Pascoe MD, Alberu J, del Carmen Rial M, Oberbauer R, Brennan DC et al.* Sirolimus CONVERT Trial Study Group. Conversion from calcineurin inhibitors to sirolimus maintenance therapy in renal allograft recipients: 24-month efficacy and safety results from the CONVERT trial. *Transplantation*. 2009 Jan 27; 87 (2): 233–242. doi: 10.1097/TP.0b013e3181927a41. PMID: 19155978.
83. *Roman A, Ussetti P, Zurbano F, Borro JM, Solé A, Carreño MC, Santos F.* A retrospective 12-month study of conversion to everolimus in lung transplant recipients. *Transplant Proc*. 2011 Sep; 43 (7): 2693–2698. doi: 10.1016/j.transproceed.2011.06.028. PMID: 21911148.
84. *De Simone P, Nevens F, De Carlis L, Metselaar HJ, Beckebaum S, Saliba F et al.* H2304 Study Group. Everolimus with reduced tacrolimus improves renal function in *de novo* liver transplant recipients: a randomized controlled trial. *Am J Transplant*. 2012 Nov; 12 (11): 3008–3020. doi: 10.1111/j.1600-6143.2012.04212.x. Epub 2012 Aug 6. PMID: 22882750; PMCID: PMC3533764.
85. *Eisen HJ, Kobashigawa J, Starling RC, Pauly DF, Kfoury A, Ross H et al*. Everolimus versus mycophenolate mofetil in heart transplantation: a randomized, multicenter trial. *Am J Transplant*. 2013 May; 13 (5): 1203–1216. doi: 10.1111/ajt.12181. Epub 2013 Feb 22. PMID: 23433101.
86. *Wang SS, Chou NK, Chi NH, Huang SC, Wu IH, Wang CH et al*. Clinical experience of tacrolimus with everolimus in heart transplantation. *Transplant Proc*. 2012 May; 44 (4): 907–909. doi: 10.1016/j.transproceed.2012.01.094. PMID: 22564581.
87. *LaMattina JC, Mezrich JD, Fernandez LA, D'Alessandro AM, Djamali A, Musat AI et al*. Native kidney function following liver transplantation using calcineurin inhibitors: single-center analysis with 20 years of follow-up. *Clin Transplant*. 2013 Mar-Apr; 27 (2): 193–202. doi: 10.1111/ctr.12063. Epub 2013 Jan 7. PMID: 23294013; PMCID: PMC3622762.
88. *Sterneck M, Kaiser GM, Heyne N, Richter N, Rauchfuss F, Pascher A et al*. Everolimus and early calcineurin inhibitor withdrawal: 3-year results from a randomized trial in liver transplantation. *Am J Transplant*. 2014 Mar; 14 (3): 701–710. doi: 10.1111/ajt.12615. Epub 2014 Feb 6. PMID: 24502384; PMCID: PMC4285226.
89. *Finn RS.* Current and Future Treatment Strategies for Patients with Advanced Hepatocellular Carcinoma: Role of mTOR Inhibition. *Liver Cancer*. 2012 Nov; 1 (3–4): 247–256. doi: 10.1159/000343839. PMID: 24159589; PMCID: PMC3760459.
90. *Sushkov AI, Moysyuk YaG.* Belatatsept pri transplantatsii pochki. *Vestnik transplantologii i iskusstvennykh organov*. 2013; 15 (1): 96–105. https://doi.org/10.15825/1995-1191-2013-1-96-105.
91. Belatacept: description [Internet]. Vidal: Spravochnik lekarstvennyh sredstv; s2020-09 [Updated 2022 July 11]. Available from: https://www.vidal.ru/.
92. *Su VC, Harrison J, Rogers C, Ensom MH.* Belatacept: a new biologic and its role in kidney transplantation. *Ann Pharmacother*. 2012 Jan; 46 (1): 57–67. doi: 10.1345/aph.1Q537. Epub 2012 Jan 3. PMID: 22215686.
93. *Florman S, Vincenti F, Durrbach A, Abouljoud M, Bresnahan B, Garcia VD et al*. Outcomes at 7 years post-transplant in black vs nonblack kidney transplant recipients administered belatacept or cyclosporine in BENEFIT and BENEFIT-EXT. *Clin Transplant*. 2018 Apr; 32 (4): e13225. doi: 10.1111/ctr.13225. Epub 2018 Mar 14. PMID: 29461660.
94. *Vincenti F, Charpentier B, Vanrenterghem Y, Rostaing L, Bresnahan B, Darji P et al*. A phase III study of belatacept-based immunosuppression regimens versus cyclosporine in renal transplant recipients (BENEFIT study). *Am J Transplant*. 2010 Mar; 10 (3): 535–546. doi: 10.1111/j.1600-6143.2009.03005.x. PMID: 20415897.
95. *Vanrenterghem Y, Bresnahan B, Campistol J, Durrbach A, Grinyó J, Neumayer HH et al*. Belatacept-based regimens are associated with improved cardiovascular and metabolic risk factors compared with cyclosporine in kidney transplant recipients (BENEFIT and BENEFIT-EXT studies). *Transplantation*. 2011 May 15; 91 (9): 976–983. doi: 10.1097/TP.0b013e31820c10eb. PMID: 21372756.
96. *Durrbach A, Pestana JM, Pearson T, Vincenti F, Garcia VD, Campistol J et al*. A phase III study of belatacept versus cyclosporine in kidney transplants from extended criteria donors (BENEFIT-EXT study). *Am J Transplant*. 2010 Mar; 10 (3): 547–557. doi: 10.1111/j.1600-6143.2010.03016.x. PMID: 20415898.
97. *Goring SM, Levy AR, Ghement I, Kalsekar A, Eyawo O, L'Italien GJ, Kasiske B.* A network meta-analysis of the efficacy of belatacept, cyclosporine and tacrolimus for immunosuppression therapy in adult renal transplant recipients. *Curr Med Res Opin*. 2014 Aug; 30 (8): 1473–1487. doi: 10.1185/03007995.2014.898140. Epub 2014 Apr 3. PMID: 24628478.
98. *Cai J, Terasaki PI.* Induction immunosuppression improves long-term graft and patient outcome in organ transplantation: an analysis of United Network for Organ Sharing registry data. *Transplantation*. 2010 Dec 27; 90 (12): 1511–1515. doi: 10.1097/TP.0b013e3181fecfcb. PMID: 21057388.
99. Basiliximab [Internet]. Vidal: Spravochnik lekarstvennyh sredstv; s2020-09 [Updated 2022 April 11]. Available from: https://www.vidal.ru/.
100. 2009 OPTN/SRTR annual report: transplant data 1999–2008 [report on the Internet]. Bethesda, MD: Health Resources and Services Administration, US De-

partment of Health & Human Services; 2009 [cited 20 April 2015].
101. *Lentine KL, Smith JM, Hart A, Miller J, Skeans MA, Larkin L et al*. OPTN/SRTR 2020 Annual Data Report: Kidney. *Am J Transplant*. 2022 Mar; 22 Suppl 2: 21–136. doi: 10.1111/ajt.16982. PMID: 35266618.
102. *Wagner SJ, Brennan DC*. Induction therapy in renal transplant recipients: how convincing is the current evidence? *Drugs*. 2012 Mar 26; 72 (5): 671–683. doi: 10.2165/11631300-000000000-00000. PMID: 22439670.
103. *Michallet MC, Preville X, Flacher M, Fournel S, Genestier L, Revillard JP*. Functional antibodies to leukocyte adhesion molecules in antithymocyte globulins. *Transplantation*. 2003 Mar 15; 75 (5): 657–662. doi: 10.1097/01.TP.0000053198.99206.E6. PMID: 12640305.
104. *Feng X, Kajigaya S, Solomou EE, Keyvanfar K, Xu X, Raghavachari N et al*. Rabbit ATG but not horse ATG promotes expansion of functional CD4+CD25highFOXP3+ regulatory T cells *in vitro*. *Blood*. 2008 Apr 1; 111 (7): 3675–3683. doi: 10.1182/blood-2008-01-130146. Epub 2008 Feb 4. PMID: 18250226; PMCID: PMC2275026.
105. *Zhulay GA, Oleynik EK*. Regulyatornye T-limfotsity CD4+CD25+FOXP3+. Perspektivy primeneniya v immunoterapii. *Trudy Karel'skogo nauchnogo tsentra RAN*. 2012; 2: 3–17.
106. *Urbanova M, Brabcova I, Girmanova E, Zelezny F, Viklicky O*. Differential regulation of the nuclear factor-κB pathway by rabbit antithymocyte globulins in kidney transplantation. *Transplantation*. 2012 Mar 27; 93 (6): 589–596. doi: 10.1097/TP.0b013e31824491aa. PMID: 22334040.
107. Thymoglobulin: instruction [Internet]. Vidal: Spravochnik lekarstvennyh sredstv; s2020-09 [Updated 2022 July 11]. Available from: https://www.vidal.ru/.
108. *Deeks ED, Keating GM*. Rabbit antithymocyte globulin (thymoglobulin): a review of its use in the prevention and treatment of acute renal allograft rejection. *Drugs*. 2009 Jul 30; 69 (11): 1483–1512. doi: 10.2165/00003495-200969110-00007. PMID: 19634926.
109. *Brennan DC, Daller JA, Lake KD, Cibrik D, Del Castillo D*. Thymoglobulin Induction Study Group. Rabbit antithymocyte globulin versus basiliximab in renal transplantation. *N Engl J Med*. 2006 Nov 9; 355 (19): 1967–1977. doi: 10.1056/NEJMoa060068. PMID: 17093248.
110. *Boggi U, Danesi R, Vistoli F, Del Chiaro M, Signori S, Marchetti P et al*. A benefit-risk assessment of basiliximab in renal transplantation. *Drug Saf*. 2004; 27 (2): 91–106. doi: 10.2165/00002018-200427020-00002. PMID: 14717621.
111. *Lawen JG, Davies EA, Mourad G, Oppenheimer F, Molina MG, Rostaing L et al*. Simulect International Study Group. Randomized double-blind study of immunoprophylaxis with basiliximab, a chimeric anti-interleukin-2 receptor monoclonal antibody, in combination with mycophenolate mofetil-containing triple therapy in renal transplantation. *Transplantation*. 2003 Jan 15; 75 (1): 37–43. doi: 10.1097/00007890-200301150-00007. PMID: 12544868.
112. *Sugiyama K, Isogai K, Horisawa S, Toyama A, Satoh H, Saito K et al*. Comparative study of the cellular pharmacodynamics of tacrolimus in renal transplant recipients treated with and without basiliximab. *Cell Transplant*. 2012; 21 (2–3): 565–570. doi: 10.3727/096368911X605493. PMID: 22793066.
113. *Beniaminovitz A, Itescu S, Lietz K, Donovan M, Burke EM, Groff BD et al*. Prevention of rejection in cardiac transplantation by blockade of the interleukin-2 receptor with a monoclonal antibody. *N Engl J Med*. 2000 Mar 2; 342 (9): 613–619. doi: 10.1056/NEJM200003023420902. PMID: 10699160.
114. Alemtuzumab [Internet]. Vidal: Spravochnik lekarstvennyh sredstv; s2020-09 [Updated 2022 April 11]. Available from: https://www.vidal.ru/.
115. *Prasad N, Gurjer D, Bhadauria D, Gupta A, Srivastava A, Kaul A et al*. Is basiliximab induction, a novel risk factor for new onset diabetes after transplantation for living donor renal allograft recipients? *Nephrology* (Carlton). 2014 Apr; 19 (4): 244–250. doi: 10.1111/nep.12209. PMID: 24447227.
116. *Morris PJ, Russell NK*. Alemtuzumab (Campath-1H): a systematic review in organ transplantation. *Transplantation*. 2006 May 27; 81 (10): 1361–1367. doi: 10.1097/01.tp.0000219235.97036.9c. PMID: 16732169.
117. *Calne R, Friend P, Moffatt S, Bradley A, Hale G, Firth J et al*. Prope tolerance, perioperative campath 1H, and low-dose cyclosporin monotherapy in renal allograft recipients. *Lancet*. 1998 Jun 6; 351 (9117): 1701–1702. doi: 10.1016/S0140-6736(05)77739-4. Erratum in: *Lancet* 1998 Aug 1; 352 (9125): 408. PMID: 9734890.
118. *Kirk AD, Hale DA, Mannon RB, Kleiner DE, Hoffmann SC, Kampen RL et al*. Results from a human renal allograft tolerance trial evaluating the humanized CD52-specific monoclonal antibody alemtuzumab (CAMPATH-1H). *Transplantation*. 2003 Jul 15; 76 (1): 120–129. doi: 10.1097/01.TP.0000071362.99021.D9. PMID: 12865797.
119. *Hanaway MJ, Woodle ES, Mulgaonkar S, Peddi VR, Kaufman DB, First MR et al*. INTAC Study Group. Alemtuzumab induction in renal transplantation. *N Engl J Med*. 2011 May 19; 364 (20): 1909–1919. doi: 10.1056/NEJMoa1009546. PMID: 21591943.
120. *LaMattina JC, Mezrich JD, Hofmann RM, Foley DP, D'Alessandro AM, Sollinger HW, Pirsch JD*. Alemtuzumab as compared to alternative contemporary induction regimens. *Transpl Int*. 2012 May; 25 (5): 518–526. doi: 10.1111/j.1432-2277.2012.01448.x. Epub 2012 Mar 6. PMID: 22394259; PMCID: PMC3665410.
121. *Hurst FP, Altieri M, Nee R, Agodoa LY, Abbott KC, Jindal RM*. Poor outcomes in elderly kidney transplant recipients receiving alemtuzumab induction. *Am J Nephrol*. 2011; 34 (6): 534–541. doi: 10.1159/000334092. Epub 2011 Nov 18. PMID: 22104284; PMCID: PMC3237278.

122. *Knechtle SJ, Pirsch JD, H Fechner J Jr, Becker BN, Friedl A, Colvin RB et al*. Campath-1H induction plus Rapmycin monotherapy for renal transplantation: results of a pilot study. *Am J Transplant*. 2003 Jun; 3 (6): 722–730. doi: 10.1034/j.1600-6143.2003.00120.x. PMID: 12780564.
123. *Flechner SM, Friend PJ, Brockmann J, Ismail HR, Zilvetti M, Goldfarb D et al*. Alemtuzumab induction and sirolimus plus mycophenolate mofetil maintenance for CNI and steroid-free kidney transplant immunosuppression. *Am J Transplant*. 2005 Dec; 5 (12): 3009–3014. doi: 10.1111/j.1600-6143.2005.01123.x. PMID: 16303017.
124. Rituximab [Internet]. Vidal: Spravochnik lekarstvennyh sredstv; s2020-09 [Updated 2022 July 11]. Available from: https://www.vidal.ru/.
125. *Vo AA, Lukovsky M, Toyoda M, Wang J, Reinsmoen NL, Lai CH et al*. Rituximab and intravenous immune globulin for desensitization during renal transplantation. *N Engl J Med*. 2008 Jul 17; 359 (3): 242–251. doi: 10.1056/NEJMoa0707894. PMID: 18635429.
126. *Fuchinoue S, Ishii Y, Sawada T, Murakami T, Iwadoh K, Sannomiya A et al*. The 5-year outcome of AB0-incompatible kidney transplantation with rituximab induction. *Transplantation*. 2011 Apr 27; 91 (8): 853–857. doi: 10.1097/TP.0b013e31820f08e8. PMID: 21297552.
127. *Stolyarevich ES, Artyukhina LYu, Ivanova ES, Tomilina NA*. Ispol'zovanie kombinirovannoy terapii plazmaferezom, vnutrivennym chelovecheskim immunoglobulinom i rituksimabom dlya lecheniya khronicheskogo ottorzheniya transplantirovannoy pochki. *Nefrologiya*. 2016; 20 (6): 67–74.
128. *Tydén G, Genberg H, Tollemar J, Ekberg H, Persson NH, Tufveson G et al*. A randomized, doubleblind, placebo-controlled, study of single-dose rituximab as induction in renal transplantation. *Transplantation*. 2009 May 15; 87 (9): 1325–1329. doi: 10.1097/TP.0b013e3181a235fd. PMID: 19424032.
129. *Clatworthy MR, Watson CJ, Plotnek G, Bardsley V, Chaudhry AN, Bradley JA, Smith KG*. B-cell-depleting induction therapy and acute cellular rejection. *N Engl J Med*. 2009 Jun 18; 360 (25): 2683–2685. doi: 10.1056/NEJMc0808481. PMID: 19535812; PMCID: PMC4143588.

The article was submitted to the journal on 12.09.2022

DOI: 10.15825/1995-1191-2022-4-39-45

CURRENT VIEW ON RADIATION-INDUCED HEART DISEASE AND METHODS OF ITS DIAGNOSIS

R.M. Muratov, S.I. Babenko, M.N. Sorkomov

Bakulev Scientific Center of Cardiovascular Surgery, Moscow, Russian Federation

In recent years, cardiologists and cardiovascular surgeons are increasingly encountering radiation-induced heart disease (RIHD) in their practice. This complication is described in literature but is poorly understood and clinically challenging. Radiation therapy (RT) is widely used in the treatment of many cancers. Despite the considerable risk of RT complications, it is used in 20–55% of cancer patients. Radiation-associated cardiotoxicity appears to be delayed, typically 10 to 30 years following treatment. Mediastinal irradiation significantly increases the risk of non-ischemic cardiomyopathy. Recent reviews estimate the prevalence of radiation-induced cardiomyopathy at more than 10%. Therefore, it is important to understand the pathophysiology of RIHD, consider risk factors associated with radiation injury, and detect the condition early.

Keywords: mediastinal tumors, radiation therapy, radiation-induced cardiomyopathy.

In recent years, cardiologists and cardiovascular surgeons are increasingly encountering radiation-induced heart disease (RIHD) in their practice. This complication is described in literature but is poorly understood and clinically challenging. Radiation therapy (RT) is widely used in the treatment of many cancers. Despite the considerable risk of complications, this method is used in 20–55% of cancer patients. Its basic principle consists of inhibiting proliferation or inducing apoptosis of cancer cells [4].

When using high doses of mediastinal irradiation, almost any component of the heart – myocardium, pericardium, valves, coronaries or conduction system – can be damaged. Basically, the cardiotoxic effect is caused by irradiation in such diseases as mediastinal lymphoma, esophageal cancer, thymoma, lung cancer (especially left-sided), and breast cancer (especially left-sided). The cumulative dose of mediastinal irradiation is a major risk factor for subsequent heart disease. Although complications can occur at any dose, there is a linear increase in the risk of valvular disorders at doses above 30 Gy/m^2 [1]. Radiation-induced cardiotoxicity is delayed, usually occurring 10 to 30 years after treatment. For example, in patients with a history of Hodgkin's lymphoma who have undergone RT, the average time from diagnosis of malignancy to onset of cardiac complications is about 19 years [2]. Hodgkin's lymphoma is one of the most common cancers in young adults, with an estimated incidence of 3 cases per 100,000 population. The cumulative long-term incidence of RIHD is nearly 60% in Hodgkin's lymphoma survivors 40 years after exposure with a relative risk of 3.2 times that of the general population, and 51.4% of patients develop 2 or more cardiovascular events [13]. Many studies have confirmed that cardiovascular risk factors such as hypertension, diabetes mellitus, dyslipidemia, and obesity significantly increase the risk of heart disease and related complications of RT [3]. Risks also increase after chemotherapy and/or when two or more cardiovascular risk factors are present.

Mediastinal irradiation significantly increases the risk of non-ischemic cardiomyopathy; these include direct myocardial fibrosis, myocardial hypertrophy secondary to valvular disorders, and diastolic dysfunction due to constrictive pericarditis. Reviews of the problem estimate the prevalence of radiation-induced cardiomyopathy at >10%. Therefore, it is important to understand the pathophysiology of RIHD, to consider risk factors associated with radiation injury, and to diagnose the condition early enough.

The walls of the heart are composed of three layers: endocardium, myocardium and epicardium. The myocardium is a highly vascularized tissue with capillary density approaching 2,800 capillaries per square millimeter. In comparison, the capillary density of skeletal muscle is much lower, approximately 350 capillaries per square millimeter. The myocardial subunit consists of cardiac myocytes, capillaries, and stromal tissue. Each myocardial subunit has a network of capillaries and depends on diffusion for nutrient metabolism because there are no arterioles in the tissue. Capillaries completely surround individual myocytes and are normally always open to perfusion. Myocardial blood supply is crucial for cardiac muscle function and depends on the degree of development of the capillary system.

Radiation injury is characterized by both acute and chronic changes in cardiac tissue [11]. Within minutes after exposure to ionizing radiation, cellular damage causes vasodilation and increased vascular permeability.

Corresponding author: Maxim Sorkomov. Address: 135, Rublevskoe Shosse, Moscow, 121552, Russian Federation. Phone: (495) 414-78-49. E-mail: sorcommn@gmail.com

Cardiomyocytes themselves are known to be resistant to radiation. However, when combined radiation/chemotherapy treatment is used, the risk of complications increases significantly. According to Suter and Ewer classification, all cytostatics are divided according to the nature of their damaging effect on the cardiovascular system. There are two types of cardiotoxicity: type I cardiotoxicity (irreversible myocardial dysfunction due to cardiomyocyte death; anthracyclines have such an effect; the degree of myocardial damage in this case depends on the cumulative dose) and type II cardiotoxicity (reversible cardiomyocyte dysfunction due to mitochondrial and protein damage; this type is most typical for trastuzumab and does not depend on the cumulative dose). High cumulative dose, intravenous bolus administration of drug, high single dose, co-administration of other cardiotoxic drugs (cyclophosphamide, trastuzumab, paclitaxel, etc.), previous RT, female gender, <15 years old and >65 years old, existing heart disease (especially hypertension and coronary heart disease), obesity, elevated biomarker levels (troponin) during or after anthracycline treatment are all risk factors for type I cardiotoxicity. Risk factors for type II cardiotoxicity are previous or concurrent anthracycline therapy, left ventricular (LV) ejection fraction <55%, existing cardiovascular disease (especially hypertension and ischemic heart disease), >50 years old, and body mass index >25 kg/m^2.

One of the most understood pathophysiological mechanisms of radiation exposure is macrovascular damage. Radiation burn of coronary artery endothelium causes an inflammatory response in the vessel wall, resulting in the release of a large number of cytokines responsible for macrophage activation and, consequently, lipoprotein deposition. Plaques may crack and cause thrombosis. This process reduces the arterial lumen to varying degrees, leading to the clinical manifestations of coronary heart disease: stable and unstable angina, myocardial infarction. The mechanism is essentially similar to the formation of atherosclerotic plaques, which we observe in traditional coronary heart disease, but with radiation damage the event occurs at an accelerated rate.

From 1998 to 2001, 114 patients were enrolled onto an IRB-approved prospective clinical study to assess changes in regional and global cardiac function after RT for left-sided breast cancer. Perfusion imaging by technetium-99m myocardial scintigraphy were performed before and after RT. The incidence of new perfusion defects 6, 12, 18, and 24 months after RT was 27%, 29%, 38%, and 42%, respectively. There was also a significant difference in myocardial perfusion between patients whose LV radiation lesion volume was less or more than 5%. New defects occurred in approximately 10% to 20% and 50% to 60% of patients with less than 5%, and greater than 5%, of their left ventricle included within the RT fields, respectively. The rates of wall motion abnormalities in patients with and without perfusion defects were 12% to 40% versus 0% to 9%, respectively [5].

In addition to large vessel damage, microvascular myocardial damage occurs. Radiation-induced endothelial cell damage is considered the primary and major cause of myocardial damage [8]. It is characterized by both acute and chronic changes in cardiac tissue. Within minutes of exposure to ionizing radiation, cell damage causes vasodilation and increased vascular permeability. Damaged endothelial cells trigger an acute inflammatory response. Inflammatory cytokines include monocyte chemotactic factor, tumor necrosis factor and interleukins including IL-1, IL-6 and IL-8. The predominant cells in the acute phase are neutrophils, which appear in all layers of the heart in areas exposed to RT. There is proliferation, damage, edema and degeneration of capillaries, and their number is significantly reduced. Although endothelial cells can regenerate, capillary network damage is irreversible, and this naturally leads to a significant reduction in myocardial blood supply.

Radiation exposure to the heart not only causes endothelial cell damage and reduction of capillaries, but also alters coagulation function and platelet activity, leading to immediate fibrin deposition. Deposition and release of von Willebrand factor in endothelial cells increases. This eventually leads to increased platelet adhesion and capillary thrombosis [9]. The acute phase takes place within a few days after RT. After this acute infiltration, there is a quiescent period when there are no obvious microscopic changes in the tissue. The acute proinflammatory environment is a powerful initiator of fibrosis [10]. Fibroblasts are recruited from a variety of sources: from mesenchymal cells, from bone marrow, or from transitional epithelial-mesenchymal cells.

However, radiation alters the biology of pro-fibrotic cells. It turned out that ionizing radiation induces premature differentiation of fibroblasts. Normal fibroblast differentiation requires 25–35 cell division cycles. After ionizing radiation, progenitor fibroblasts differentiate into post-mitotic fibroblasts within 2–3 weeks, which is only 3–4 cell cycles. The lifespan of these terminally differentiated radiation-induced fibrocytes is nearly 40–45% shorter than that of naturally differentiated cells. These post-mitotic cells are shown to be five to eight times more active in the production of interstitial collagens I, III, and IV compared to progenitor fibroblasts. Myofibroblasts are permanently activated in these tissues [12]. Chronic deposition of collagen and other components of other extracellular matrix components can produce a fibrotic scar, reducing the functionality of the affected tissue. Pathologic examination of these lesions show elevated inflammatory cells, fibroblasts, and excessive extracellular matrix, such as collagens, proteoglycans, and fibronectin. Extracellular matrix deposition by fibroblasts results in late pathologic dysfunction of myocytes, vascular endothelial cells, and the pericardium

[11]. Progressive myocardial fibrosis eventually leads to decreased tissue elasticity and extensibility.

The cardiovascular system responds differently to RT-related myocardial damage compared with ischemia-related heart failure. In RT-unrelated myocardial damage, the body activates the sympathetic nervous system continuously, while simultaneously down-regulating β-adrenergic receptors. In contrast, RT-related myocardial damage results in no augmentation of the sympathetic nervous system in the adrenal glands, but β-receptors initially are upregulated in the heart. This upregulation of the receptors may allow the heart to stabilize cardiac output despite damage. Eventually, as damage progresses, further reductions in cardiac output occur near the onset of congestive heart failure [11].

Restrictive cardiomyopathy is a late stage of myocardial damage due to fibrosis with severe diastolic dysfunction and symptoms of heart failure. Most radiation-induced myocardial lesions have no clinical symptoms for a long time; therefore, the rate of early diagnosis of the disease is low, only about 10% [6]. Transthoracic echocardiography is the optimal imaging modality for the diagnosis of LV systolic and diastolic dysfunction. The most common echocardiographic features are regional wall motion abnormalities (usually lower LV wall), moderate LV hypertrophy, and diastolic dysfunction, which can manifest as severe congestive heart failure [7].

In a study by Paul A Heidenreich et al. [14], the prevalence of LV wall motion abnormalities was 13% (12/89) for individuals with a latency period of 2 to 10 years, 18% (24/132) for a latency period of 11 to 20 years, and 29% (21/73) for a latency period greater than 20 years post-RT (at least 35 Gy) for mediastinal Hodgkin lymphoma. Regional wall motion abnormalities were independently associated with a greater biologically equivalent dose (odds ratio 1.07 per one-unit increase, 95% CI 1.02–1.13) and older age (odds ratio 1.7 per 10-year increase, 95% CI 1.2–2.4) in addition to time following irradiation.

The authors investigated the effect of irradiation on LV myocardial mass. The LV mass was lower for irradiated patients than for those of similar sex and age in the general population (Framingham Heart study [15]). LV hypertrophy (defined as more than 163 g/m for men and 121 g/m for women) was present in 6% (7/121) of female and 2% (2/104) of male patients compared with 19% of women and 16% of men in the Framingham Heart Study. The difference in myocardial mass was due to lower LV diastolic volume in patients after irradiation, as systolic volume and wall thickness were similar to the Framingham cohort.

It was also found that the age-adjusted ventricular mass remained constant or slightly decreased over time following irradiation. This is in contrast to the usual increase in LV myocardial mass that occurs with aging [16]. When the authors stratified changes in LV myocardial mass by age, there was a clear trend toward lower mass with greater latency period . In multivariate analysis, ventricular mass decreased by 0.6 g/m ($p = 0.001$) for each year following exposure, but increased by 0.8 g/m ($p < 0.0001$) for each year increase in age. Similar findings were observed for interventricular septal and LV posterior wall thickness, which decreased by 0.05 mm ($p = 0.08$) for each year following irradiation but increased by 0.1 mm ($p < 0.001$) for each year increase in age.

Modern imaging techniques for examining myocardial deformation have shown that they may be more sensitive to detect early subclinical LV dysfunction than standard measures such as ejection fraction measurement. Strain is a dimensionless value reflecting the change in length relative to the initial state [17]. Longitudinal strain reflects the change in length of a section of myocardium along the long axis. Short-axis circular strain shows the contraction of circularly arranged myocardial fibers. Transverse (radial) strain describes the processes of thickening/thinning of myocardial fibers in different phases of the cycle, which occurs due to the principle of incompressibility of cardiac muscle.

Global longitudinal strain (GLS) and strain rate assessed using automated 2D spectral echocardiography reveal minimal changes in LV systolic function. The prospective BACCARAT study was designed to examine the association between cardiac radiation doses and subclinical LV dysfunction based on reduced GLS. The study included 79 breast cancer (BC) patients (64 left-sided BC, 15 right-sided BC) treated with RT without chemotherapy. Echocardiographic parameters including GLS were measured before RT and 6 months after.

The association between subclinical LV dysfunction, defined as GLS decrease >10%, and cardiac radiation doses, was performed using logistic regression. Non-radiation associated with subclinical LV dysfunction included age, body mass index, hypertension, hypercholesterolemia, and endocrine pathology. These were also considered in the multivariate analysis but were found not to be significant. The authors conclude that subclinical LV dysfunction can be detected early after RT for BC with GLS measurement based on 2D speckle-tracking echocardiography.

Reduction in longitudinal deformity in a period of a few days to 14 months after RT has also been observed by other authors in patients with left-sided BC [18, 20]. Suvi Sirkku Tuohinen et al. also draw attention to RT-induced regional changes. The study showed that the changes corresponded to the RT fields. Patients with left-sided BC showed apical changes, whereas patients with right-sided BC showed basal changes in the anterior and anteroposterior regions, which corresponds to the area most vulnerable to RT [18].

AF Yu et al. also conducted a study to determine whether RT leads to early changes in LV function. The study was based on 2D echocardiographic assessment of such

parameters as LV ejection fraction, myocardial strain indicators including longitudinal (GLS), radial (GRS) and circular deformation (GCS), LV diastolic indices and high-sensitivity troponin. There appeared to be no predictors of changes in LV ejection fraction or changes in longitudinal strain indicators during the immediate period of RT. Similarly, age, hypertension, baseline systolic blood pressure, and intake of cardiac medications were not predictors of changes in LV function [19].

Electrocardiography rarely has specific changes [14]. However, resting heart rate is higher in patients with longer latency after RT (70 ± 13 beats/min for a period ≤10 years, 74 ± 12 for 11 to 20 years, and 81 ± 10 for >20 years). In multivariate analyses controlling for age, gender, diabetes, hypertension, and dose of irradiation, a 10-year increase in latency period was independently predictive of a higher resting heart rate (increase of 3.7 beats/min, 95% CI 1.3 to 6.1), right bundle branch block (odds ratio 7.3, 95% CI 1.2 to 45), and abnormal Q-waves (odds ratio 4.9, 95% CI 1.7 to 14).

Magnetic resonance imaging of the heart, detecting both functional and structural changes simultaneously, allows the diagnosis of radiation-induced coronary, valve, myocardial, and pericardial disease. Features of the method include myocardial tissue characterization based on various tissue relaxation properties such as fat, muscle, and areas of inflammation. The use of gadolinium has significantly improved the diagnosis of altered myocardium of non-ischemic genesis. Images obtained 5–20 minutes after gadolinium injection at a dose of 0.1–0.2 mmol/kg allow to describe nonischemic cardiomyopathic processes and provide valuable diagnostic and pathophysiological information with unprecedented resolution and highly specific images of fibrosis and myocardial scarring [21].

Development of modern imaging methods allows for early identification of patients with potential risk of cardiotoxicity who require further cardiovascular monitoring or cardioprotective therapy. Evaluation of parameters using echocardiography and magnetic resonance imaging over time can contribute to early diagnosis of heart damage before overt heart failure develops.

Evaluation and early treatment of traditional cardiovascular risk factors is the first step towards preventing cardiotoxicity. Finally, in patients with high-risk heart disease, primary prophylaxis, including cardioprotectors and/or drugs commonly used to treat cardiovascular disease, should be used. According to recent studies [22], early initiation of ACE inhibitors and β-blockers and modification of anti-cancer therapy can prevent cardiac fibrosis and decrease in LV ejection fraction in the terminal stage of a disease. However, further multicenter studies are needed to establish prevention and treatment protocols.

Due to the direct toxic effects of RT, myocardial fibrosis and vasculopathy lead to ventricular remodeling, which, in turn, may increase the risk of developing valvular dysfunction [23]. Although the precise pathophysiologic mechanisms of radiation-induced valvulopathy are not completely understood, irradiation is thought to have a direct effect on the pathologic fibrosis and calcification of the valvular apparatus. Due to the avascular nature of valve tissue, the mechanism of injury is believed to be distinct from radiation-induced damage to the myocardium and vasculature. There is a lack of histological markers of chronic inflammation or neovascularization on tissue specimens removed during surgery [24]. Interestingly, there are histopathological differences noted in the affected valves. Thus, patients who have undergone RT for BC show a degenerative calcific process as opposed to a predominantly fibrotic process in lymphoma patients who have received RT. This difference is probably due to the young age at which irradiation for Hodgkin's lymphoma was performed.

Risk stratification of surgical treatment for valvular pathology using modern scales does not take into account side effects and complications associated with previous RT and may underestimate the true risk. A retrospective analysis by Wu et al. [25] on the surgical outcomes of 173 patients (75% women; age, 63 ± 14 years, mean EuroSCORE 7.8 ± 3) with RIHD, compared with 305 operated patients matched on the basis of age, sex, and procedure type, revealed a higher mortality rate in the RIHD group than in the comparison group (55% vs 28%; $p < 0.001$) over a mean follow-up of 7.6 ± 3 years, despite comparable EuroSCORE scores. Analysis of the results of surgical treatment of valvular pathology in 60 patients with previous RT in the Handa et al study showed an increased rate of early mortality in patients with constrictive pericarditis (40% vs. 6%, $p = 0.011$). In the same cohort, lower preoperative LV ejection fraction and longer aortic constriction time were also associated with early mortality [26].

Among 230 patients in a study by Chang ASY et al. [27] who underwent cardiac surgery after thoracic irradiation, the proportion of perioperative complications, in-hospital and long-term mortality was significantly higher in patients who received extensive radiation exposure. Therefore, an understanding of the nature of radiation exposure to the heart and its structure is primarily necessary to determine the degree of surgical risk prior to cardiothoracic surgery, which will determine the most appropriate treatment tactics, emphasizing the need for interdisciplinary collaboration between the radiation oncologist, cardiologist, cardiac surgeon, and other specialists.

The authors declare no conflict of interest.

REFERENCES

1. *Cutter DJ, Schaapveld M, Darby SC, Hauptmann M, van Nimwegen FA, Krol AD et al*. Risk of valvular heart

disease after treatment for Hodgkin lymphoma. *J Natl Cancer Inst*. 2015; 107 (4): djv008. doi: 10.1093/jnci/djv008.
2. *Aleman BMP, van den Belt-Dusebout AW, De Bruin ML, van't Veer MB, Baaijens MHA, Boer JPD et al.* Late cardiotoxicity after treatment for Hodgkin lymphoma. *Blood*. 2007; 109: 1878–1886. doi: 10.1182/blood-2006-07-034405.
3. *Armstrong GT, Oeffinger KC, Chen Y et al.* Modifiable risk factors and major cardiac events among adult survivors of childhood cancer. *J Clin Oncol*. 2013; 31: 3673–80.
4. *Quintero-Martinez JA, Cordova-Madera SN, Villarraga HR.* Radiation-Induced Heart Disease. *J Clin Med*. 2022 Jan; 11 (1): 146. doi: 10.3390/jcm11010146.
5. *Marks LB, Yu X, Prosnitz RG, Zhou SM, Hardenbergh PH, Blazing M et al*. The incidence and functional consequences of RT-associated cardiac perfusion defects. *Int J Radiat Oncol Biol Phys*. 2005 Sep 1; 63 (1): 214–223. doi: 10.1016/j.ijrobp.2005.01.029.
6. *Chang HM, Okwuosa TM, Scarabelli T, Moudgil R, Yeh ETH*. Cardiovascular Complications of Cancer Therapy: Best Practices in Diagnosis, Prevention, and Management: Part 2. *J Am Coll Cardiol*. 2017; 70: 2552–2565.
7. *Filopei J, Frishman W*. Radiation-induced heart disease. *Cardiol Rev*. 2012; 20: 184–188.
8. *Boerma M, Sridharan V, Mao XW, Nelson GA, Cheema AK, Koturbash I et al.* Effects of ionizing radiation on the heart. *Mutat Res*. 2016; 770: 319–327.
9. *Boerma M, Kruse JJ, van Loenen M, Klein HR, Bart CI, Zurcher C et al.* Increased deposition of von Willebrand factor in the rat heart after local ionizing irradiation. *Strahlenther Onkol*. 2004; 180: 109–116.
10. *Yarnold J, Vozenin Brotons M-C.* Pathogenetic mechanisms in radiation fibrosis. *Radiother Oncol*. 2010; 97 (1): 149–161. doi: 10.1016/j.radonc.2010.09.002.
11. *Taunk NK, Haffty BG, Kostis JB, Goyal S*. Radiation-Induced Heart Disease: Pathologic Abnormalities and Putative Mechanisms. *Front Oncol*. 2015; 5: 39. doi: 10.3389/fonc.2015.00039.
12. *Weigel C, Schmezer P, Plass C, Popanda O*. Epigenetics in radiation-induced fibrosis. *Oncogene.* 2014; 55 (12): 1237–1239. doi: 10.1038/onc.2014.145.
13. *Van Nimwegen FA, Schaapveld M, Janus CP et al.* Cardiovascular disease after Hodgkin lymphoma treatment: 40-year disease risk. *JAMA Intern Med.* 2015; 175: 1007–1017.
14. *Heidenreich PA, Hancock SL, Lee BK, Mariscal CS, Schnittger I*. Asymptomatic cardiac disease following mediastinal irradiation. *J Am Coll Cardiol*. 2003 Aug 20; 42 (4): 743–749.
15. *Levy D, Savage DD, Garrison RJ, Anderson KM, Kannel WB, Castelli WP*. Echocardiographic criteria for left ventricular hypertrophy: The Framingham heart study. *Am J Cardiol*. 1987 April 15; 59 (9): 956–960.
16. *Fleg JL.* Alterations in cardiovascular structure and function with advancing age. *Am J Cardiol*. 1986; 57: 33–44.
17. *Snegovoy AV, Vitsenya MV, Kopp MV, Larionova VB*. Prakticheskie rekomendatsii po korrektsii kardiovaskulyarnoy toksichnosti, indutsirovannoy khimioterapiey i targetnymi preparatami. *Zlokachestvennye opukholi*. 2016; 4 (S2): 418–427. doi: 10.18027/2224-5057-2016-4s2-418-427.
18. *Tuohinen SS, Skyttä T, Poutanen T, Huhtala H, Virtanen V, Kellokumpu-Lehtinen PL, Raatikainen P*. Radiotherapy-induced global and regional differences in early-stage left-sided versus right-sided breast cancer patients: speckle tracking echocardiography study. *Int J Cardiovasc Imaging*. 2017 Apr; 33 (4): 463–472. doi: 10.1007/s10554-016-1021.
19. *Yu AF, Ho AY, Braunstein LZ, Thor ME, Lee Chuy K, Eaton A et al.* Assessment of early radiation-induced changes in left ventricular function by myocardial strain imaging after breast radiation therapy. *J Am Soc Echocardiogr*. 2019; 32: 521–528. doi: 10.1016/j.echo.2018.12.009.
20. *Lo Q, Hee L, Batumalai V, Allman C, MacDonald P, Lonergan D et al.* Strain Imaging Detects Dose-Dependent Segmental Cardiac Dysfunction in the Acute Phase After Breast Irradiation. *Int J Radiat Oncol Biol Phys.* 2017; 99: 182–190.
21. *Karamitsos TD, Francis JM, Myerson S, Selvanayagam JB, Neubauer S.* The role of cardiovascular magnetic resonance imaging in heart failure. *J Am Coll Cardiol*. 2009 Oct 6; 54 (15): 1407–1424. doi: 10.1016/j.jacc.2009.04.094.
22. *Mavrogeni SI, Sfendouraki E, Markousis-Mavrogenis G, Rigopoulos A, Noutsias M, Kolovou G et al*. Cardio-oncology, the myth of Sisyphus, and cardiovascular disease in breast cancer survivors. *Heart Fail Rev*. 2019 Nov; 24 (6): 977–987. doi: 10.1007/s10741-019-09805-1.
23. *Patil S, Pingle SR, Shalaby K, Kim AS*. Mediastinal irradiation and valvular heart disease. *Cardiooncology*. 2022 Apr 8; 8 (1): 7.
24. *Van Rijswijk JW, Farag ES, Bouten CVC, de Boer OJ, van der Wal A, de Mol BAJM, Kluin J.* Fibrotic aortic valve disease after radiotherapy: an immunohistochemical study in breast cancer and lymphoma patients. *Cardiovasc Pathol*. 2020; 45: 107176. https://doi.org/10.1016/j.carpath.2019.107176.
25. *Wu W, Masri A, Popovic ZB et al.* Long-term survival of patients with radiation heart disease undergoing cardiac surgery: a cohort study. *Circulation*. 2013; 127 (14): 1476–1484.
26. *Handa N, McGregor CGA, Danielson GK et al.* Valvular heart operation in patients with previous mediastinal radiation therapy. *Ann Thorac Surg*. 2001; 71 (6): 1880–1884.
27. *Chang AS, Smedira NG, Chang CL, Benavides MM, Myhre U, Feng J et al.* Cardiac surgery after mediastinal radiation: extent of exposure influences outcome. *J Thorac Cardiovasc Surg*. 2007; 133 (2): 404–413.

The article was submitted to the journal on 14.07.2022

DOI: 10.15825/1995-1191-2022-4-46-53

DEVELOPMENT OF A CANNULA DEVICE FOR GAS FRACTION REMOVAL IN SURGICAL DRAINS

A.P. Kuleshov[1], *A.S. Buchnev*[1], *A.A. Drobyshev*[1], *O.Yu. Esipova*[1], *G.P. Itkin*[1, 2]

[1] Shumakov National Medical Research Center of Transplantology and Artificial Organs, Moscow, Russian Federation

[2] Moscow Institute of Physics and Technology, Moscow, Russian Federation

The development of low-traumatic surgical drains aimed at maximum possible separation of blood and air, is an important trend in modern medicine. The objective of this work is to create an inexpensive, user-friendly and low-traumatic dynamic blood aspiration system (DBAS). The system allows effective separation of blood and air when drawing blood from a wound under vacuum conditions required for blood aspiration. The operating principle of the system is to separate liquid and gas fractions of the blood-air mixture by modifying the blood intake cannula. The effect is achieved by applying the principles of centrifugal forces of a rotating blood-air flow combined with Archimedes lift forces.

Keywords: aspiration, CPB, cannula, blood drainage.

INTRODUCTION

Venous blood drainage is used in most surgical procedures [1, 2]. It was not generally used until the recent development of invasive cardiac surgery, along with the spread of open-heart surgeries that do not require blood transfusion [3]. Patients undergoing cardiac surgery with cardiopulmonary bypass (CPB) require large quantities of donor red blood cells [4]. Considerable evidence suggests that transfusions during cardiac surgery increase infectious and noninfectious risks [5–7]. Venous drainage is an acceptable method for patients to preserve their own blood. During the procedure, blood is aspirated from the wound cavities using a suction cannula connected to a blood suction system (roller or vacuum pump). In turn, the blood further enters the recirculation system represented by the collection reservoir and connecting tubes (Fig. 1).

According to experts, blood aspiration is the main factor traumatizing the blood and, along with the effect of air microbubbles getting into the blood circulation circuit, increases the patient's rehabilitation time after surgical intervention. In reviewing literature sources, it was noted that 79% (n = 15) of the authors believe that the vacuum drainage technique benefits the assisted circulation procedure and/or the patient. Reducing the number of transfusions helps to prevent blood bank overload [8–14]. The reduction is due to improved biochemical parameters and, therefore, there is no need to increase the volume of the venous reservoir to maintain the level of protection against air ingress into the system.

Reduced use of blood products helps to reduce postoperative complications, and the technique provides a reduction in total blood count, reducing hemodilution [3, 8–15] and maintaining hematocrit and hemoglobin at acceptable levels.

However, along with increased use of venous drainage, specific side effects of the procedure have been reported. Willcox et al., LaPietra et al., Davila et al., Burch and Locke have separately reported cases in in vitro studies where the venous drainage system returns air-laden blood to the patient [16–19]. This results in systematic microemboli. Microemboli often cause significant cerebral morbidity, usually manifesting as postoperative cognitive deficit or stroke [16].

Air embolism has been reported in other studies [10, 11, 20, 21]. It has been shown that venous vacuum drainage caused almost 10 times more embolisms in the arterial line compared to passive drainage, despite the use of appropriate equipment. The above-mentioned embolism is a consequence of microbubble formation in the liquid due to turbulence caused by high-pressure passage through a narrow tube. The same studies show that just by comparing the lengths of the vacuum and gravity methods, in the situation of air supply to the venous circuit through the venous line, the vacuum allows more air to enter the system.

There has been disagreement about the presence of high levels of hemolysis when using a vacuum. Most authors believe that hemolysis caused by negative pressure procedures was similar to hemolysis with passive drainage [3, 10, 11, 22]. However, comparing vacuum

Corresponding author: Arkadiy Kuleshov. Address: 1, Shchukinskaya str., Moscow, 123182, Russian Federation. Phone: (915) 292-47-98. E-mail: ilovemylene@yandex.ru

drainage with centrifugal pump drainage, Cirri et al. [23] showed that vacuum drainage causes a higher degree of hemolysis, which were also confirmed by Gregoretti et al. [24]. However, Lau et al. disagree, showing similar levels of hemolysis [25].

In the last decade, the efforts of many specialists working in the field of artificial blood circulation were aimed at developing new pumps, membrane oxygenators, which would reduce blood trauma during such operations. Nevertheless, despite certain successes in this direction, blood trauma is still a great danger, and this is mainly due to the traumatic effect of the blood aspiration system. This problem has become especially urgent recently when the age of patients undergoing open cavity surgery has significantly changed and the length of rehabilitation has increased. As a result, efficiency of blood drainage systems is an important part of the surgical process.

MATERIALS AND METHODS

The main causes of blood injury when using the existing blood aspiration systems include:

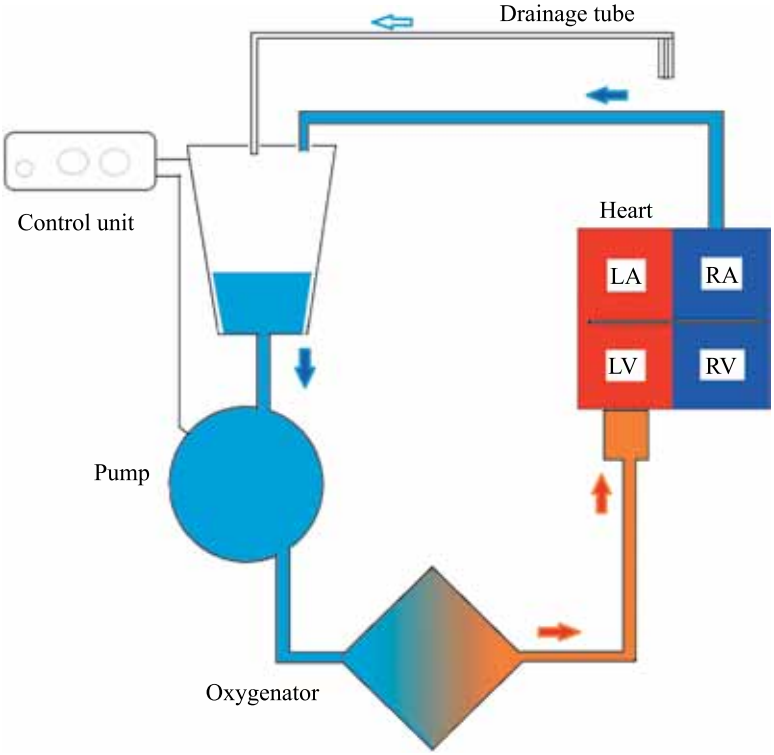

Fig. 1. Vacuum-assisted venous drainage. LA, left atrium; RA, right atrium; LV, left ventricle; RV, right ventricle

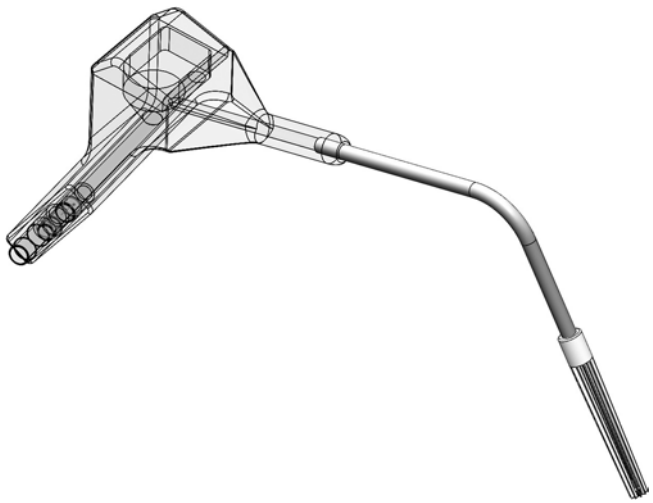

Fig. 2. Schematic representation of the modified separation cannula

– massive mixing of blood with air in the cannula, connecting tubes, and pump;
– high vacuum produced by the pump.

To reduce the influence of the above factors, an ergonomic and practical DBAS was developed. The appearance of the modified cannula is shown in Fig. 2. The system includes a mixture intake tube bearing a special nozzle and a cannula separation unit.

The separation unit, shown in Fig. 3, has a narrow part A, in which the mixture feed tube 1 is located. The wide part C, follows the narrow part through a smooth transition B. From the blood sampling nozzle through the tube, a liquid-air mixture enters the inlet tube of the separation unit, which is an extension of it. The mixture feed channel is directed to the thickened part C, in which a conical cavity 2, an air filtration zone 3 and two tubes

of blood and air fraction withdrawal 4 and 5, located inside the handle of cannula D, are cut out.

One of the tubes 4 is a continuation of the conical part, and the liquid phase is discharged through it with a minimal air residue. The second tube 5 is parallel to the first one, but is connected to the filtration zone, which is vertically above the conical part. Through this tube, the air separated during flow through the conical part is removed. A bio-inert exchangeable sponge is installed in the filtration zone to optimize the separation process. The sponge is replaced by opening the top cover.

The conical part is located vertically with a narrowing downwards. With respect to the cross section of the cone, the inlet channel to it is located at an angle.

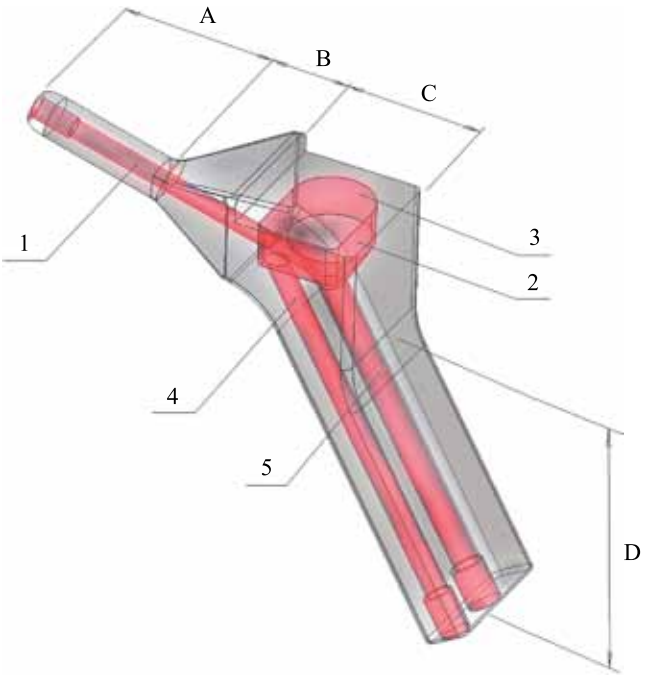

Fig. 3. Schematic representation of the separation unit

At the junction, the inlet channel is positioned such that the flow enters the conical part in a tangential line at the maximum radius of the cone cross section at the inlet. The wide section transitions into a handle designed to hold the system comfortably. The handle has slotted channels for the liquid and gas phases mentioned earlier. The channels end with outlet fittings, and are connected to a vacuum generation system. A sketch of the complete DBAS is shown in Fig. 4. Since the separation of blood and air must be performed as close to the wound as possible, the working chamber of the device is built into the handle of the drainage cannula (Fig. 3, D). Thus, after the separation process, blood is collected at the lower end of the working cyclone chamber and aspirated through a separate channel (Fig. 3, 5) using a roller pump (Fig. 4, 4).

In turn, air is collected in the upper part of the chamber and aspirated through another channel (Fig. 3, 4) by a vacuum roller pump (Fig. 4, 5). Blood and air are then fed separately into the cardiotomy tank (6).

How the device works

The blood-air mixture, under vacuum, is captured through the tip of the cannula from the wound and flows through the channel (Fig. 4). The mixture then enters the inlet of the cyclonic conical chamber at an angle to the vertical axis (Fig. 3). Rotation of the blood-air mixture is achieved, which is maintained by the conical expansion of the cyclone chamber. Blood is collected in the lower part of the nozzle, while air, due to centrifugal and Archimedes forces, is collected in the center of the rotating flow and rushes to the highest point. The forces acting on the air bubble can be considered in the coordinate system as shown in Fig. 5.

It can be seen from the figure that when an air bubble enters the cyclone chamber, its motion in the vertical direction along the axis is due to the applied vacuum P_1

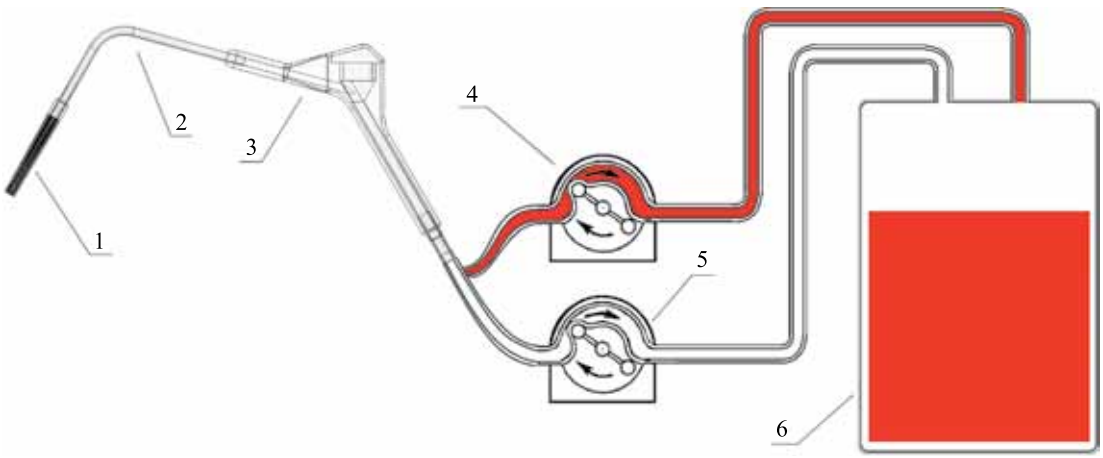

Fig. 4. Schematic representation of the dynamic blood aspiration system. 1, suction cannula; 2, liquid-air mixture supply tube; 3, separator; 4, roller blood pump; 5, roller air pump; 6, cardiotomy tank

from the liquid channel, the vacuum from the air channel P_2, the Archimedes force F_A, and viscous friction force F_T. It was decided to neglect the weight of the bubble due to the weak influence of this parameter in these conditions. Since the mixture intake channel enters the cyclone chamber at a tangent and vertical angle α, the vacuum in the *xy* plane can be considered as the projection of the flow force F_P on the *y* axis. In the *xy* plane, viscous friction force F_{Ty} will act on the bubble as a counterbalance to the motion of the bubble. We obtain the basic steady-state equation of bubble rising (1):

$$F_A - F_{Py} - F_{Ty} + F_2 = 0. \quad (1)$$

In the case of absence or weak influence of vacuum P_2 and a decrease in force F_2, a solution of the system of equations gives the bubble ascent velocity and initial rotation velocity in the cyclone chamber (2):

$$\upsilon_y = \frac{1}{18}\frac{\rho g D_b^2}{\eta} - \frac{32}{3}\frac{LQ}{\pi d^2 D_b}\cdot \sin\alpha, \quad (2)$$

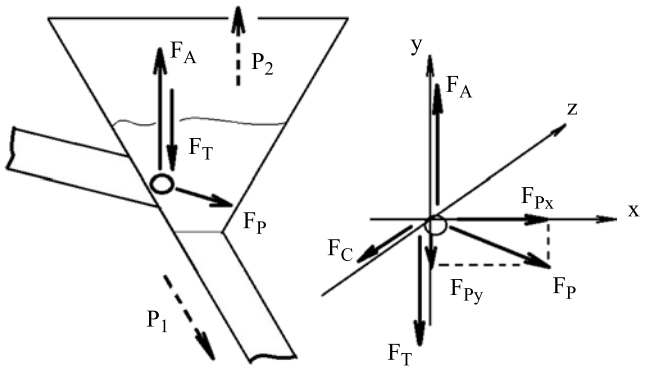

Fig. 5. The position of forces acting on air bubble

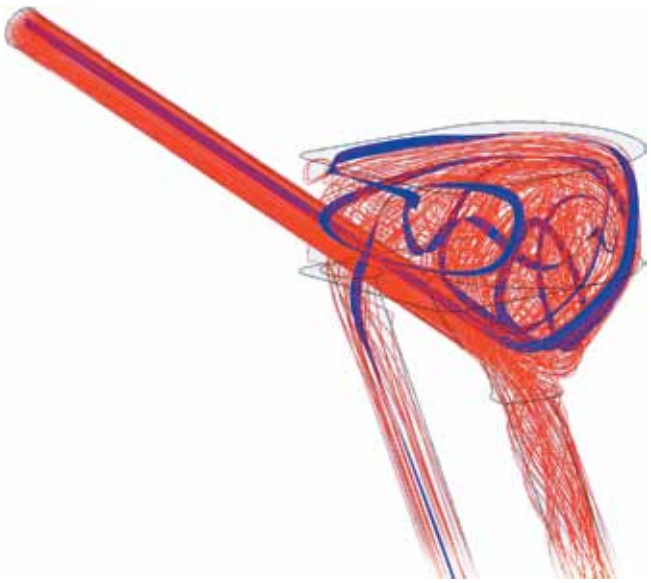

Fig. 6. An example of simulation of fraction flow in a 20 mm Hg vacuum with 4 mm air bubble diameter

where υ_y is the air bubble rising velocity, ρ is blood density, *g* is free fall acceleration, η is blood viscosity, α is the angle of blood intake channel entry into the cyclone chamber, *L* is the blood intake channel length, D_b is the diameter of the air bubble under study, and *Q* is the blood flow rate.

The rising rate, as follows from analysis of the equation, depends to a greater extent on the amount of blood flow that the pump produces and the angle α. Evaluating the relationship between vacuum and separation efficiency is part of the initial DBAS design process.

Computer model of the device

We developed a three-dimensional DBAS mathematical model of viscous liquid flow with the presence of liquid bubbles of different diameters using the COMSOL Multiphysics software. As a result of the studies, a picture of liquid and gas fraction motion was obtained, an example of which is shown in Fig. 6. The calculation boundary conditions included a vacuum value of up to 50 mm Hg. We applied a multiphase modeling mode of blood and air flow.

The criterion of amount of air fraction separated from liquid after flowing in the cyclone chamber was introduced as the required parameter. Convergence criterion 10^{-4} by pressure was defined as the convergence criterion. A k-ε turbulence model was used to simulate the flow field. A sufficiently fine grid consisting of tetrahedral cells consisting of 80,000 elements, was obtained.

The calculation example shows the mechanics of fraction movement, assuming a 0.5 l/min liquid flow rate. One can observe blue lines of trajectories of air bubbles up to 4 mm in diameter in the blood flow, shown by red lines. Calculation is made under the condition that air volume in the blood is equal to 10% of the total flow.

Most of the air flow with some amount of blood (not more than 0.05 l/min) is separated into the air channel. Volumetric flow was created under a 20 mm Hg vacuum condition. Thus, air and vacuum reduce the influence on further blood advancement into the cardiotomy tank. In the air channel, the blood is strongly affected by all thrombosis factors, but the volume of this fraction is reduced to a minimum.

Hydrodynamic bench

Initially, the efficiency of DBAS was assessed visually on a hydrodynamic bench by the nature of the air-bubble concentration zone and by the change in the composition of the air-liquid mixture after the intake tube (Fig. 7). However, in practice, due to the impossibility to observe air bubbles in a fairly wide range of changes, electronic microbubble counting devices were used.

The vacuum system is represented by two pumps – a roller pump, capable of developing the required vacuum for liquid and gas outlet channels, and a vacuum suction system.

The bench includes a roller pump (9), which sets the vacuum required for study and the liquid flow rate, measured by a flow sensor (6). Air is withdrawn into the vacuum suction tank (8) through a channel (3), and blood outlet through a channel (4). Bubbles of different diameters are injected into the cardiotomy tank (2) through a syringe (5) connected to the injection device, on which the volume of the supplied gas fraction is regulated. A cannula (1) is placed in the reservoir, which simulates the patient's wound.

Flow rate was measured using an ultrasonic flow sensor (Transonic Systems Inc., USA) (6), and pressure was measured using transducers (Edwards Lifesciences, USA) (7). To record hemodynamic parameters, we used multichannel module ANGIOTON (Biosoft-M, Russia) with recording on a personal computer using the Pumpax software program (Biosoft-M, Russia). Initially, water was used as the working fluid.

Standard 3/8″ silicone tubing was used to connect the various elements of the bench. During the study, the roller pump was operated on standard configurations for clinical use, to achieve flow rates ranging from 0 to 1 L/min.

RESULTS

The amount of vacuum required to drain the gas-liquid mixture was determined on the bench under pump flow conditions up to 1 L/min. Vacuum was measured

Fig. 7. Hydrodynamic bench. 1, cannula; 2, cardiotomy tank; 3, air channel; 4, liquid channel; 5, air supply device; 6, flow measurement / microbubble counting sensor; 7, vacuum measurement sensor; 8, vacuum suction tank; 9, roller pump

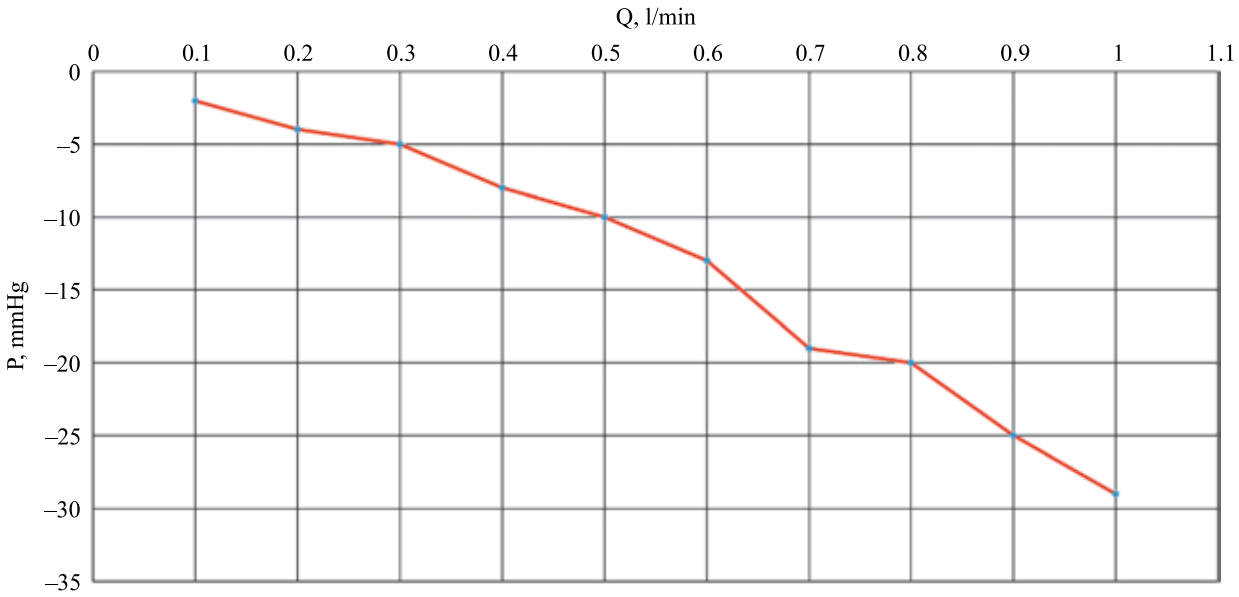

Fig. 8. A graph of flow rate versus applied vacuum

at the inlet of the roller pump. In this case, the variable was the percentage of air in the mixture from 0 to 50%. Fig. 8 shows the dependence of the required vacuum for drainage of various blood flow rates (at a constant roller pump flow rate).

As can be seen from Fig. 8, the vacuum changes from a weakly negative pressure, determined by the difference of the differential between the suction point and the pump inlet to a value of –29 mm Hg at a flow rate of 1 L/min. The picture of bubble separation at the calculated vacuum is shown in Fig. 9.

The obtained results confirm that in the process of gas-liquid mixture separation, efficiency simultaneously decreases both with increasing vacuum, which is known to significantly affect the injury by blood-forming elements, and with increasing volume of supplied air. The operating flow rate range used in surgical operations is up to 0.5 L/min with separation efficiency averaging more than 50% and under vacuum conditions not more than 10–15 mm Hg.

Given that blood viscosity (even in conditions of dilution during extracorporeal circulation) is 2–3 times higher than water ($\mu = 4.2 \times 10^{-3}$ kg/(m·s) and density $\rho = 1054$ kg/m^3), the required vacuum should be higher than in our measurements.

In the developed blood drainage device with pre-separation, it is necessary to choose capacities in blood and air suction lines. In basic drainage mode, the amount of air can be several times higher than the amount of blood. In this case, some of the air will enter the blood channel, flowing into the rotary pump, which constitutes the most dangerous mode in terms of hemolysis. To address the consequences of this mode, the air channel capacity can be increased several times relative to the blood suction channel capacity. Under airless blood drainage, blood will be drained through both channels. Under drainage with simple cannula use, air will also be drained through both channels.

CONCLUSION

We have proposed an alternative method that is based on the physical principles of centrifugal influence and Archimedes forces on air microbubbles for their effective removal from the blood suction system in surgical operations involving users of heart–lung machines. A dynamic blood aspiration system was developed to minimize gas fraction for blood return systems in the heart–lung machine circuit.

The authors declare no conflict of interest.

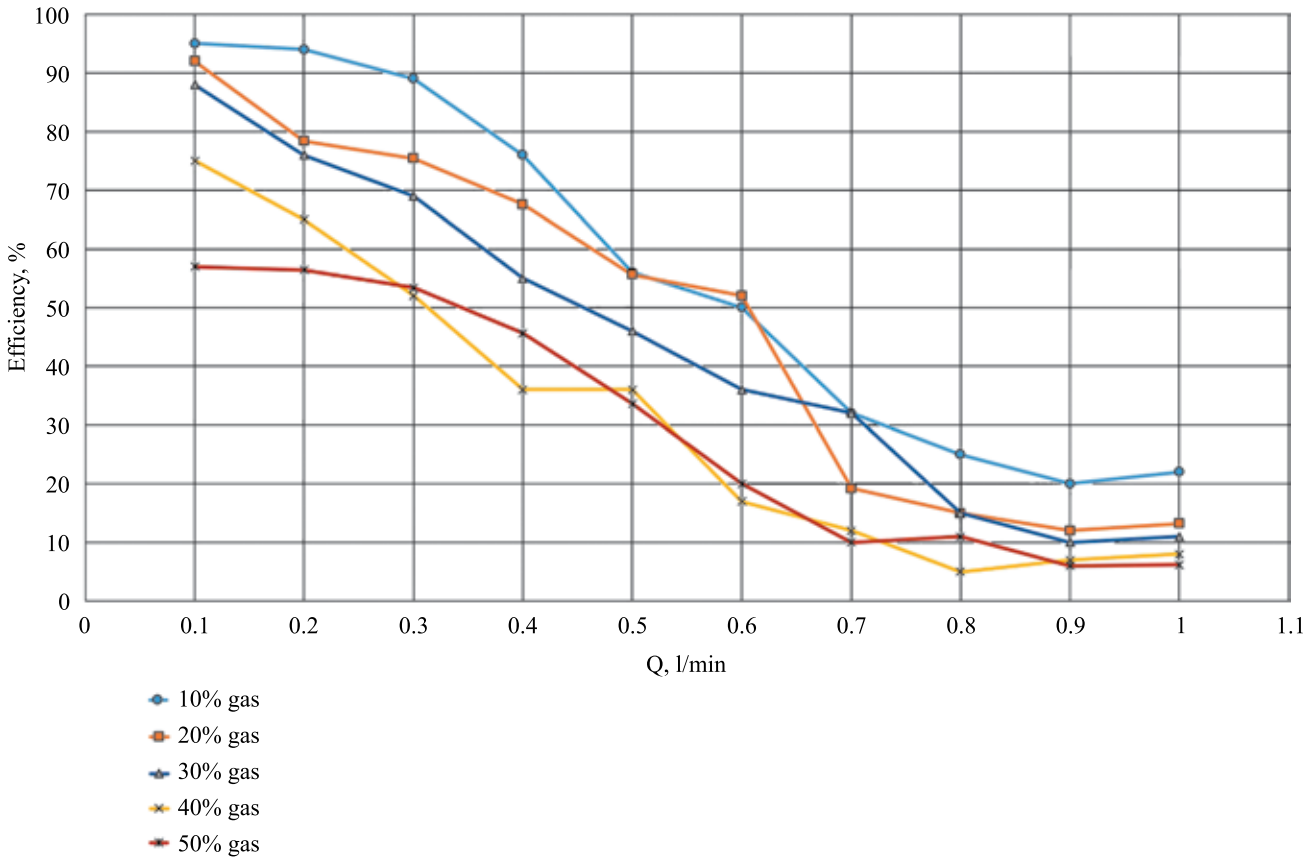

Fig. 9. Separation efficiency

REFERENCES

1. *Jones RE, Donald DE, Swan HJ, Harshbarger HG, Kirklin JW, Wood EH*. Apparatus of the Gibbon type for mechanical bypass of the heart and lungs; preliminary report. *Proc Staff Meet Mayo Clinic.* 1955; 30: 105–113.
2. *Miller BJ.* Laboratory work preceding the first clinical application of cardiopulmonary bypass. *Perfusion*. 2003; 18: 145–154.
3. *Hayashi Y, Kagisaki K, Yamaguchi T, Sakaguchi T, Naka Y, Sawa Y et al.* Clinical application of vacuum-assisted cardiopulmonary bypass with a pressure relief valve. *Eur J Cardiothorac Surg*. 2001; 20: 621–626.
4. *Mazer CD, Whitlock RP, Fergusson DA, Hall J, Belley-Cote E, Connolly K et al.* Restrictive or liberal red-cell transfusion for cardiac surgery. *N Engl J Med.* 2017; 377: 2133–2144.
5. *Vamvakas EC, Carven JH.* Transfusion and postoperative pneumonia in coronary artery bypass graft surgery: effect of the length of storage of transfused red cells. *Transfusion.* 1999; 39: 701–710.
6. *Karamlou T, Schultz JM, Silliman C, Sandquist C, You J, Shen I et al.* Using a miniaturized circuit and an asanguineous prime to reduce neutrophil-mediated organ dysfunction following infant cardiopulmonary bypass. *Ann Thorac Surg*. 2005; 80: 6–13; discussion 13–14.
7. *Vlaar AP, Juffermans NP.* Transfusion-related acute lung injury: a clinical review. *Lancet.* 2013; 382: 984–994.
8. *Taketani S, Sawa Y, Masai T, Ichikawa H, Kagisaki K, Yamaguchi T et al.* A novel technique for cardiopulmonary bypass using vacuum system for venous drainage with pressure relief valve: an experimental study. *Artif Organs*. 1998; 22 (4): 337–341.
9. *Chalegre ST, Salerno PR, Salerno LMVO, Melo ARS, Pinheiro AC, Frazão CS et al.* Drenagem venosa assistida a vácuo na circulação extracorpórea e necessidade de hemotransfusão: experiência de serviço. *Rev Bras Cir Cardiovasc*. 2011; 26 (1): 122–127.
10. *Zangrillo A, Garozzo FA, Biondi-Zoccai G, Pappalardo F, Monaco F, Crivellari M et al.* Miniaturized cardiopulmonary bypass improves short-term outcome in cardiac surgery: a meta-analysis of randomized controlled studies. *J Thorac Cardiovasc Surg*. 2010; 139 (5): 1162–1169.
11. *Nasso G, Costantini C, Petralia A, Del Prete A, Lopriore V, Fattouch K et al.* A new extracorporeal vacuum-assited device to optimize cardiopulmonary bypass. Comparison with the conventional system. *Interact Cardiovasc Thorac Surg*. 2011; 12 (4): 591–595.
12. *Banbury MK, White JA, Blackstone EH, Cosgrove 3rd DM.* Vacuum-assisted venous return reduces blood usage. *J Thorac Cardiovasc Surg*. 2003; 126 (3): 680–687.
13. *Bevilacqua S, Matteucci S, Ferrarini M, Kacila M, Ripoli A, Baroni A et al.* Biochemical evaluation of vacuum-assisted venous drainage: a randomized, prospective study. *Perfusion*. 2002; 17 (1): 57–61.
14. *Nakanishi K, Shichijo T, Shinkawa Y, Takeuchi S, Nakai M, Kato G et al.* Usefulness of vacuum-assisted cardiopulmonary bypass circuit for pediatric open-heart surgery in reducing homologous blood transfusion. *Eur J Cardiothorac Surg*. 2001; 20 (2): 233–238.
15. *Pappalardo F, Corno C, Franco A, Giardina, Scandroglio AM, Landoni G et al.* Reduction of hemodilution in small adults undergoing open heart surgery: a prospective randomized trial. *Perfusion*. 2007; 22 (5): 317–322.
16. *Willcox TW, Mitchell SJ, Gorman DF.* Venous air in the bypass circuit: a source of arterial line emboli exacerbated by vacuum-assisted drainage. *Ann Thorac Surg*. 1999; 68: 1285–1289.
17. *LaPietra A, Grossi EA, Pua BB, Esposito RA, Galloway AC, Derivaux CC et al.* Assisted venous drainage presents the risk of undetected air microembolism. *J Thorac Cardiovasc Surg*. 2000; 120: 856–863.
18. *Davila RM, Rawles T, Mack MJ.* Venoarterial air embolus: a complication of vacuum-assisted venous drainage. *Ann Thorac Surg*. 2001; 71: 1369–1371.
19. *Burch TM, Locke AQ.* Air lock and embolism upon attempted initiation of cardiopulmonary bypass while using vacuum-assisted venous drainage. *J Cardiothorac Vasc Anesth* 2012; 26: 468–470.
20. *Colangelo N, Torracca L, Lapenna E, Moriggia S, Crescenzi G, Alfieri O.* Vacuum-assisted venous drainage in extrathoracic cardiopulmonary bypass management during minimally invasive cardiac surgery. *Perfusion*. 2006; 21 (6): 361–365.
21. *Kiyama H, Imazeki T, Katayama Y, Murai N, Mukouyama M, Yamauti N.* Vacuum-assisted venous drainage in single-access minimally invasive cardiac surgery. *J Artif Organs*. 2003; 6 (1): 20–24.
22. *Murai N, Cho M, Okada S, Chiba T, Saito M, Shioguchi S et al.* Venous drainage method for cardiopulmonary bypass in single-access minimally invasive cardiac surgery: siphon and vacuum-assisted drainage. *J Artif Organs*. 2005; 8 (2): 91–94.
23. *Cirri S, Negri L, Babbini M, Latis G, Khlat B, Tarelli G et al.* Haemolysis due to active venous drainage during cardiopulmonary bypass: comparison of two different techniques. *Perfusion*. 2001; 16 (4): 313–318.
24. *Gregoretti S.* Suction-induced hemolysis at various vacuum pressures: implications for intraoperative blood salvage. *Transfusion*. 1996; 36 (1): 57–60.
25. *Lau CL, Posther KE, Stephenson GR, Lodge A, Lawson JH, Darling EM et al.* Mini-circuit cardiopulmonary bypass with vacuum assisted venous drainage. Feasibility of an asanguineous prime in the neonate. *Perfusion*. 1999; 14 (5): 389–396.

The article was submitted to the journal on 13.07.2022

DOI: 10.15825/1995-1191-2022-4-54-59

MECHANIZED LYMPHATIC DRAINAGE IN ACUTE DECOMPENSATED HEART FAILURE. A STUDY ON A HYDRODYNAMIC TEST BENCH

A.S. Buchnev[1], *G.P. Itkin*[1, 2], *A.A. Drobyshev*[1], *A.P. Kuleshov*[1], *O.Yu. Esipova*[1], *A.I. Syrbu*[1]

[1] Shumakov National Medical Research Center of Transplantology and Artificial Organs, Moscow, Russian Federation

[2] Moscow Institute of Physics and Technology, Moscow, Russian Federation

Objective: to investigate the effectiveness of a new mechanized lymphatic drainage method in acute decompensated heart failure (ADHF) modeling through local reduction in venous pressure in the site of lymphatic drainage from the thoracic duct. **Materials and methods.** Main components of the device are a catheter with built-in inlet and outlet mechanical valves designed for insertion into the left brachiocephalic vein through the left internal jugular vein. It comes with an extracorporeal drive system made as a valveless pulsator pump with a 10 ml shock discharge and a controller ensuring preset frequency and pressure/rarefaction duty cycle. The operating principle of the device is based on local reduction of venous pressure in the site of lymphatic drainage from the thoracic duct (in the junction of the left internal jugular and subclavian veins). **Results.** When modeling hydrodynamics under ADHF conditions on a hydrodynamic test bench, the upper venous flow through the left brachiocephalic vein was 0.4 l/min, the pressure in the site of lymphatic drainage from the thoracic duct, was decreased from 20–25 mmHg to 0–5 mmHg due to operation of the mechanized drainage device with suction/injection phase duration ratio 0.2/0.8 and pulsator pump operating frequency from 30 to 60 beats/min.

Keywords: lymphatic system, thoracic duct, heart failure, local decrease in venous pressure, catheter, pulsator pump.

INTRODUCTION

As we know, ADHF remains the most common cause of emergency hospitalization requiring intensive care and is accompanied by high patient mortality. Approximately half of patients with ADHF are discharged from the hospital not fully recovered and about 25% of patients require rehospitalization within one month, and over 50% are rehospitalized after 6 months and almost 66% of the total number die [1–4].

One of the main symptoms of ADHF disease is the phenomena of organ and tissue edema associated with difficulties in the lymph discharges into the venous system due to increased central venous pressure (CVP) [5–10]. At the same time, pharmacotherapeutic agents based on loop diuretics have limited progress in improving the condition of these patients, many of whom become resistant to such therapy [11–14].

It is known that under physiological normal conditions, $^{3}/_{4}$ of the lymph drains into the left subclavian vein through the left thoracic duct (TD) and $^{1}/_{4}$ of the lymph flows through the right lymphatic duct into the right subclavian vein. In ADHF, increased CVP makes it difficult for lymph to drain into the venous system. Lack of progress in pharmacotherapy of patients with ADHF, based on the use of loop diuretics, have limited progress in improving the condition of these patients, with resistance to their administration in many cases [15, 16]. This has stimulated the development of a number of new methods aimed at normalizing lymph circulation in these patients. In separate early works, it was shown that in patients with ADHF, external TD decompression can improve such symptoms of the disease as dyspnea, orthopnea, and anorexia [17]. External TD drainage can lead to significant metabolic, immunological and fluid imbalance. TD shunting into the pulmonary vein has also been described, but it requires complex surgical procedures [18, 19]. Therefore, the problem of creating conditions for local reduction in venous pressure in the site of lymphatic drainage from the TD, remains rather acute.

One of the first developments of such system proposed by WhiteSwell is based on the use of an axial pump built into an intravenous venous catheter inserted into the left internal jugular vein with blood intake from the site of lymphatic drainage from the TD, and blood discharge into the left brachiocephalic vein (Fig. 1) [20, 21].

The device for local reduction of venous pressure in the site of lymphatic drainage from the thoracic duct is

Corresponding author: Alexander Buchnev. Address: 1, Shchukinskaya str., Moscow, 123182, Russian Federation. Phone: (926) 470-09-88. E-mail: labbts@mail.ru

based on the use of an intravenous catheter (1) with a mechanically driven axial pump (2) installed in it using a shaft from an external drive (3). The catheter (1) is inserted into the left internal jugular vein (5) before entering the left brachiocephalic vein (6), with heparin continuously injected between the pump drive cable and the catheter to reduce the possibility of thrombosis [22], potentially causing bleeding during this procedure.

Local reduction of venous pressure in the site of lymphatic drainage from the thoracic duct (7), is performed by drawing blood through the drainage orifice (8) located in the area of confluence of the left internal jugular (5) and subclavian (9) veins, and releasing blood into the brachiocephalic vein (6) at the axial pump outlet (2). To increase the efficiency of the system, there is an inflatable balloon (4) at the exit of the catheter (1) partially or completely blocking blood flow through the left brachiocephalic vein.

More than 20 patents were obtained for this system from 2016 to 2021. However, to date, there have been no publications on the implementation of these projects in experiment and clinical practice. Preliminary calculations show that for effective local reduction of venous pressure in the site of lymphatic drainage from the TD, in such a system, it is necessary to create a 0.8–1 l/min flow. As simple calculations show, in ADHF conditions with 50% reduction in cardiac output, the total venous flow in the upper parts of the circulatory system also decreases by 50% and is 0.8 l/min (0.4 l/min each for the left and right parts). Therefore, the flow of 0.8–1 l/min required to reduce local pressure in the site of lymphatic drainage from the TD, may result in venous stasis in the right upper veins. To solve this problem, we proposed a method and device based on pulse blood flow formation in the site of lymphatic drainage from the TD (Fig. 2) [23].

The device contains a catheter (1) introduced through the left internal jugular vein (5), connected to a valveless pump (2) with a pneumatic drive (3). Thus, reduction of local pressure in the lymphatic drainage site (7) is realized by displacement of blood volume from a given space through inlet valve (8) in the venous catheter into the chamber of the valveless pump (2). Thus, conditions of local pressure reduction in the site of lymphatic drainage from the TD (by analogy with WhiteSwell system operation mode) are created during the suction phase. During the injection phase of the valveless pump (2), blood volume returns to the venous circulation system through the exit valve (9) of the catheter. Thus, the average flow through the left brachiocephalic vein is maintained at the initial flow level (0.4 l/min).

MATERIALS AND METHODS

A hydrodynamic test bench (HTB) simulating upper left brachial venous system (Fig. 3) was developed to assess the effective performance of the mechanized lymphatic drainage system. The HTB includes: Rotaflow pump (Maquet Inc., Germany) (1) providing venous circulation under ADHF conditions at 0.4 l/min, venous reservoir (2) simulating right atrium entrance at 20–25 mmHg CVP, left superior venous system including left internal jugular vein simulator (3), left subclavian vein (4), and left brachiocephalic vein (7) with a thoracic duct simulator (5).

A catheter (6) with 5 mm internal diameter was inserted into the internal jugular vein simulator (3) up to the entrance to the left brachiocephalic vein (7) with an inlet valve (8) located at the level of the confluence of the left internal jugular vein (3) and left subclavian vein (4) (i.e., in the site of lymphatic drainage from the TD (5)) and an outlet mechanical valve (9) at the distal end of the catheter. The catheter is hermetically connected to

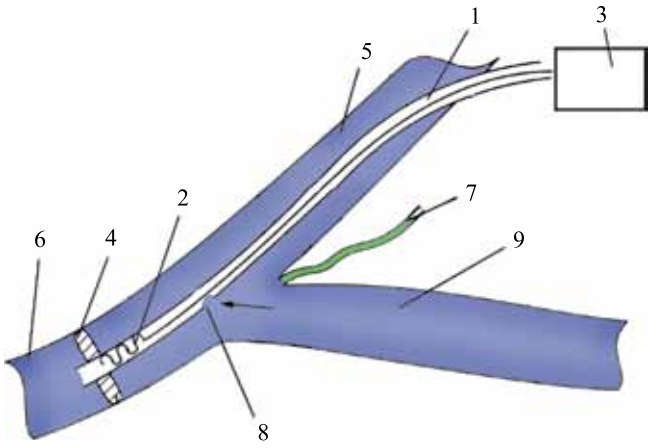

Fig. 1. Schematic diagram of the device for local reduction of venous pressure in the site of lymphatic drainage from the thoracic duct. WhiteSwell. 1, intravenous catheter; 2, axial pump; 3, external pump drive; 4, inflatable balloon catheter; 5, internal jugular vein; 6, brachiocephalic vein; 7, thoracic duct; 8, distal suction branch pipe; 9, left subclavian vein

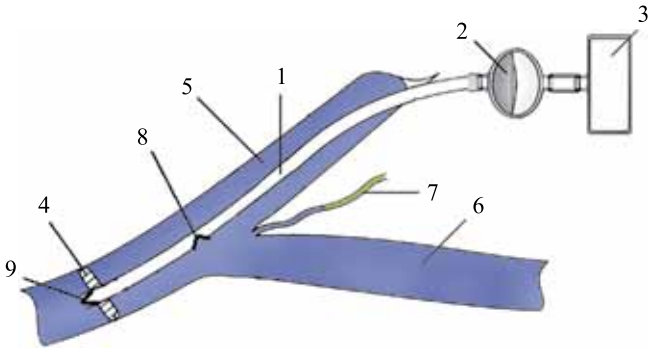

Fig. 2. A new method and device for local reduction of venous pressure in the site of lymphatic drainage from the TD. 1, intravenous catheter; 2, valveless pump; 3, external drive of the valveless pump; 4, inflatable balloon catheter; 5, left internal jugular vein; 6, left brachiocephalic vein; 7, thoracic duct; 8, inlet valve; 9, outlet valve

external valveless pump (10) with a flexible 20 ml diaphragm, driven by a pneumatic drive Sinus IS (MZEMA, Russia) (11) with a given frequency and pressure/rarefaction duty cycle. To increase the efficiency of the device, there is an inflatable balloon (12) behind the inlet valve (8) on the outer wall of the catheter, connected through a port to a separate channel (13) of the catheter to fill the balloon (12) with gas or liquid, providing partial/full blockage of the lumen between the left brachiocephalic vein (7) and the outer diameter of the balloon.

Fluid flow rate was recorded using a TS420 ultrasonic sensor (Transonic Systems, Inc, USA) (14, 15).

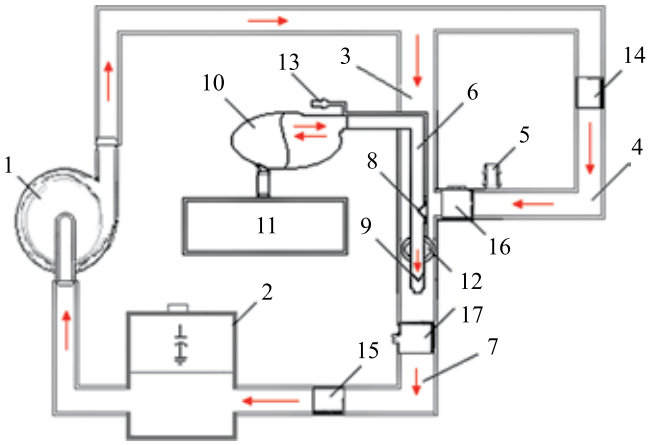

Fig. 3. Schematic diagram of hydrodynamic test bench. 1, Rotaflow centrifugal pump; 2, venous reservoir; 3, left internal jugular vein; 4, left subclavian vein; 5, thoracic duct; 6, intravenous catheter; 7, brachiocephalic vein; 8, inlet catheter valve; 9, outlet catheter valve; 10, valveless pump; 11, valveless pump drive; 12, inflatable balloon catheter; 13, balloon filling catheter; 14, fluid flow sensors in the left subclavian vein; 15, fluid flow sensors in the circuit; 16, pressure sensor located in the thoracic duct site; 17, pressure sensor in right atrium site

The pressure in the system was set at 20 ± 5 mmHg and recorded using pressure transducers (Edwards, USA) (16, 17) with the Angioton (Biosoft-M, Russia) multichannel hydrodynamic measurement module with data output to a personal computer for data recording and processing.

The system operation is determined by frequency of valveless pump and ratio of suction/injection phase durations. In the mode of fluid suctioning by the valveless pump (10) through catheter inlet valve (8), the pressure in the area of the junction of the left internal jugular and left subclavian veins will decrease, creating conditions for lymph drainage from TD into the venous system. In the injection mode, the valveless pump (10) ejects the withdrawn blood through the exit valve (9) of the catheter (6) into the left brachiocephalic vein (7). To maintain a given average blood flow through the left brachiocephalic vein at 0.4 L/min (in accordance with the conditions of venous circulation in ADHF), in this work, we chose 50 beats/min as the frequency of the valveless pump at a suction/injection phase duration ratio of 0.2/0.8.

RESULTS

A mechanized lymphatic drainage device with its valveless pump having changing frequency parameters, was tested on a hydrodynamic test bench. Based on the obtained data, a specialist can set the appropriate operating mode for the device for the greatest unloading (reduction of venous pressure in the site of lymphatic drainage from the thoracic duct). The data obtained are summarized in Table.

The effect of the mechanized lymphatic drainage device is shown in Fig. 4, which shows the dynamics of venous pressure obtained on the hydrodynamic test bench in ADHF (a) and in the operation of the device (b) in the site of lymphatic drainage from the thoracic duct.

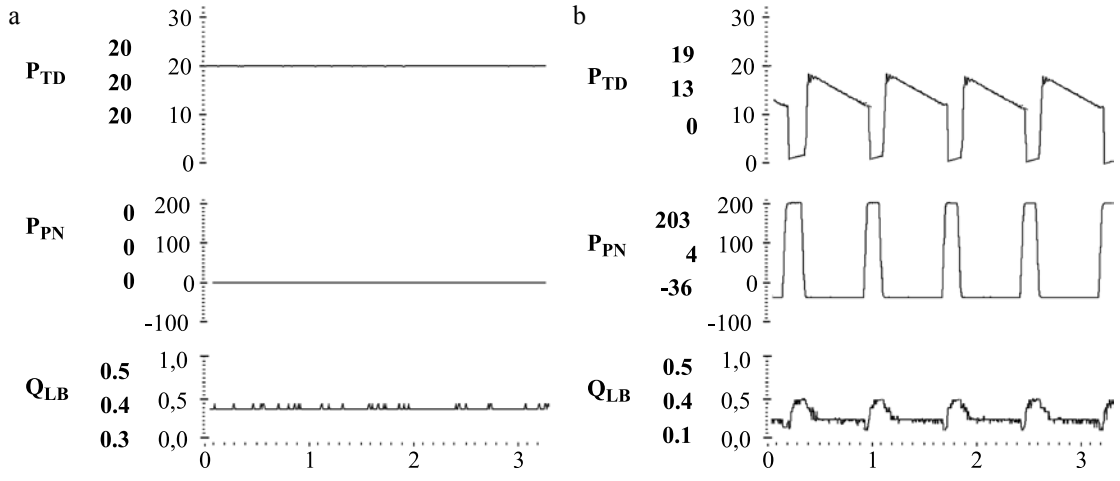

Fig. 4. Circulatory hemodynamics obtained in ADHF simulation conditions (a) and during operation of the mechanized lymphatic drainage device (b) (P_{TD}, pressure in the site of lymphatic drainage from the thoracic duct; P_{PN}, pneumatic pressure of the valveless pump drive; Q_{LB}, flow in the left brachiocephalic vein simulator)

Table

Hemodynamic variables in ADHF simulation condition when a valveless pump is operated at different frequencies

F (bpm)	P_{TD} (mmHg)	P_{CVP} (mmHg)	tc/td
20	–2 ± 1	20 ± 2	1/4
30	0 ± 1	20 ± 2	1/4
40	2 ± 1	20 ± 2	1/4
50	4 ± 1	20 ± 2	1/4
60	5 ± 1	20 ± 2	1/4

Note. F, valveless pump frequency; P_{TD}, venous pressure in the site of lymphatic drainage from the thoracic duct; P_{CVD}, central venous pressure; tc/td, systole/diastole duration ratio of the valveless pump.

As a result of the valveless pump operation at a 10 ml shock discharge in the suction phase, the venous pressure decreased from 20 ± 5 mmHg to 0 ± 3 mmHg with 30 beats/min pump frequency and a suction/injection duty cycle of 0.2/0.8. Thus, conditions are created during the longer period of the work cycle of the mechanized lymphatic drainage device to ensure normalization of lymph drainage from the thoracic duct. Average blood flow through the left brachiocephalic vein is maintained – 0.4 ± 0.1 L/min.

CONCLUSION

This study presents the design and preliminary characteristics of a proposed mechanized lymphatic drainage device designed to alleviate the symptoms of lymphedema in patients with ADHF. Tests on a hydrodynamic bench confirm the possibility of using this device to normalize lymphatic circulation from the thoracic duct to the venous bed by locally reducing the venous pressure to 0 mmHg in ADHF conditions within the general target criteria. This device can be considered as one of the options to restore lymph circulation in patients with ADHF to effectively treat a sufficiently large group of patients with ADHF with minimal drug therapy using diuretics or hemodialysis and relieve symptoms of organ and tissue edema to normal levels with minimal antithrombotic therapy. In addition, this device can be further used to normalize lymphatic circulation in the pulmonary circuit to relieve pulmonary edema symptoms [24].

The authors declare no conflict of interest.

REFERENCES

1. *Ambrosy AP, Fonarow GC, Butler J, Chioncel O, Greene SJ, Vaduganathan M et al*. The global health and economic burden of hospitalizations for heart failure: lessons learned from hospitalized heart failure registries. *J Am Coll Cardiol*. 2014; 63 (12): 1123–1133.
2. *Jencks SF, Williams MV, Coleman EA*. Rehospitalizations among patients in the Medicare fee-for-service program. *N Engl J Med*. 2009; 360 (14): 1418–1428.
3. *Setoguchi S, Stevenson LW, Schneeweiss S.* Repeated hospitalizations predict mortality in the community population with heart failure. *Am Heart J*. 2007; 154 (2): 260–266.
4. *Chang PP, Wruck LM, Shahar E, Rossi JS, Loehr LR, Russell SD.* Trends in hospitalizations and survival of acute decompensated heart failure in four US communities (2005–2014): ARIC Study Community Surveillance. *Circulation*. 2018; 138 (1): 12–24.
5. *Fallick C, Sobotka PA, Dunlap ME.* Sympathetically mediated changes in capacitance: redistribution of the venous reservoir as a cause of decompensation. *Circ Heart Fail*. 2011; 4 (5): 669–675.
6. *Burkhoff D, Tyberg JV.* Why does pulmonary venous pressure rise after onset of LV dysfunction: a theoretical analysis. *Am J Physiol*. 1993; 265 (5 Pt 2): H1819–H1828.
7. *Itkin M, Rockson SG, Burkhoff D.* Pathophysiology of the Lymphatic System in Patients With Heart Failure: JACC State-of-the-Art Review. *J Am Coll Cardiol.* 2021; 78 (3): 278–290.
8. *Szabo G, Magyar Z.* Effect of increased systemic venous pressure on lymph pressure and flow. *Am J Physiol*. 1967; 212 (6): 1469–1474.
9. *Brace RA, Valenzuela GJ.* Effects of outflow pressure and vascular volume loading on thoracic duct lymph flow in adult sheep. *Am J Physiol*. 1990; 258 (1 Pt 2): R240–244.
10. *Laine GA, Allen SJ, Katz J, Gabel JC, Drake RE*. Outflow pressure reduces lymph flow rate from various tissues. *Microvasc Res*. 1987; 33 (1): 135–142.
11. *Lucas C, Johnson W, Hamilton MA, Fonarow GC, Woo MA, Flavell CM et al*. Freedom from congestion predicts good survival despite previous class IV symptoms of heart failure. *Am Heart J*. 2000; 140 (6): 840–847.
12. *Mullens W, Verbrugge FH, Nijst P, Tang WHW*. Renal sodium avidity in heart failure: from pathophysiology to treatment strategies. *Eur Heart J*. 2017; 38 (24): 1872–1882.
13. *Voors AA, Greenberg BH, Pang PS, Levin B, Hua TA et al.* Diuretic response in patients with acute decompensated heart failure: char-acteristics and clinical outcome – an analysis from RELAX-AHF. *Eur J Heart Fail*. 2014; 16 (11): 1230–1240.
14. *Valente MA, Voors AA, Damman K, Van Veldhuisen DJ, Massie BM, O'Connor CM et al*. Diuretic response in acute heart failure: clinical characteristics and prognostic significance. *Eur Heart J*. 2014; 35 (19): 1284–1293.
15. *Rouvière H, Tobias MJ.* Anatomy of the Human Lymphatic System. 1938. *BJS (British Journal of Surgery)*. 1939; 27 (Issue 105): 194–195.

16. *Scallan JP, Zawieja SD, Castorena-Gonzalez JA, Davis MJ*. Lymphatic pumping: mechanics, mechanisms and malfunction. *J Physiol*. 2016; 594 (20): 5749–5768.
17. *Witte MH, Dumont AE, Clauss RH, Rader B, Levine N, Breed ES*. Lymph Circulation in Congestive Heart Failure: Effect of External Thoracic Duct Drainage. *Circulation.* 1969; 39 (6): 723–733.
18. *Drake RE, Teague RA, Gabel JC*. Lymphatic drainage reduces intestinal edema and fluid loss. *Lymphology*. 1998; 31 (2): 68–73.
19. *Cole WR, Witte MH, Kash SL, Rodger M, Bleisch VR, Muelheims GH*. Thoracic Duct-to-Pulmonary Vein Shunt in the Treatment of Experimental Right Heart Failure. *Circulation*. 1967; 36 (4): 539–543.
20. US 2016/0331378 A1 System and methods for reduction pressure at an outflow of duct Nitzan Y., Yacjby M., Feld T. 2016.
21. US 2018/0250456 A1 System and methods for reduction pressure at an outflow of duct Nitzan Y., Yacjby M., Rar S., Chen S., Inbar O., 2018.
22. US 2020/0397963 A1. Intravascular catheters. Nitzan Y. 2020.
23. RU 2021107668 A. Заявка: 2021107668 от 23.03.2021.
24. *Uhley HN, Leeds SE, Sampson JJ, Freadman M*. Role of pulmonary lymphatics in chronic pulmonary edema. *Circ Res.* 1962; 11: 966–970.

The article was submitted to the journal on 15.09.2022

DOI: 10.15825/1995-1191-2022-4-60-72

TREATMENT OF CHRONIC LIVER DISEASE USING CELL-ENGINEERED CONSTRUCTS: MORPHOFUNCTIONAL CHARACTERISTICS

M.Yu. Shagidulin[1, 2], N.A. Onishchenko[1], A.V. Grechina[2], M.E. Krasheninnikov[4], A.O. Nikolskaya[1], E.A. Volkova[1], N.P. Mogeiko[1], N.A. Boiarinova[2], A.V. Lyundup[4], G.A. Piavchenko[2], L.I. Davydova[3], A.Yu. Arhipova[5, 6], V.G. Bogush[3], S.V. Gautier[1, 2]

[1] Shumakov National Medical Research Center of Transplantology and Artificial Organs, Moscow, Russian Federation
[2] Sechenov University, Moscow, Russian Federation
[3] Kurchatov Institute, Moscow, Russian Federation
[4] RUDN University, Moscow, Russian Federation
[5] Moscow State University, Moscow, Russian Federation
[6] Shenzhen MSU-BIT University, Shenzhen, China

Objective: to study the effectiveness of correcting the morphofunctional characteristics of the liver in an experimental model of chronic liver disease (CLD), using implanted cell-engineered constructs (CECs). **Materials and methods.** Experiments were carried out on male Wistar rats (n = 80) aged 6–8 months with an initial weight of 230–250 g. CLD was modeled by inoculating the rats with 60% CCl_4 oil solution for 42 days based on a modified scheme. Microgel based on recombinant spidroin rS1/9 was used as a matrix for CECs fabrication. Allogeneic liver cells (LCs) and multipotent bone marrow-derived mesenchymal stem cells (BM-MSCs) from a healthy donor were used as the cellular component of the CECs. The effectiveness of the corrective effect of the implanted CECs was assessed in an experimental CLD model (n = 60) in two groups of rats: Group 1 (control, n = 20, 1 mL of saline solution was injected into the damaged liver parenchyma) and Group 2 (experimental, n = 40, CECs containing allogenic LCs and BM-MSCs in a 5 : 1 ratio in a volume of 1 mL were implanted into the damaged liver parenchyma). For long-term monitoring of the CEC state, the CECs were labeled by additional inclusion in Cytodex-3. The effectiveness of the regulatory effect of CECs on regenerative processes in the liver was evaluated using biochemical, morphological and morphometric techniques, as well as by flow cytometry at 90 days after implantation. **Results.** In the control group, the mortality rate in CLD was 25%. There was no death in the experimental group with CLD after CEC implantation. The CECs were found to have a corrective effect on the biochemical and morphological parameters of the liver in CLD during 90 days of follow-up, with concomitant preservation of structural cellular homeostasis in the implanted CECs. **Conclusion.** Implantation of CECs in the liver facilitates effective correction of CLD by activating regenerative processes in the damaged liver, which is due to long-term preservation of structural cellular homeostasis in the CECs.

Keywords: regenerative medicine, chronic liver disease treatment, matrix, microgel, liver cells, bone marrow-derived mesenchymal stem cells, cell-engineered constructs.

INTRODUCTION

Over the past decades, Russia and the world at large have witnessed a significant increase in the number of severe chronic liver disease (CLD), leading to decompensated CLD. The disease is progressive in nature, which requires continuous corrective actions. Among the treatment options, liver transplantation is the most effective and the only radical treatment for end-stage CLD with respect to long-term survival of patients [1, 2].

The main goal of the current stage of transplantology is to ensure that all patients in need have access to organ transplantation. The need for liver transplantation is 20 per million population [1]. However, the progressively growing shortage of donor organs limits the use of this high-tech form of care, so the number of patients on the waiting list continues to grow steadily [2–5]. The steady growth of chronic liver diseases [3], leading to irreversible damage, requires new effective methods of treatment.

Analysis of works carried out in the field of transplantology and artificial organs testifies to the emergence of a fundamentally new approach to the regenerative treatment of damaged vital organs, based on tissue engineering and regenerative medicine (TERM) [6].

Corresponding author: Murat Shagidulin. Address: 1, Shchukinskaya str., Moscow, 123182, Russian Federation. Phone: (499) 196-87-90. E-mail: dr.shagidulin@mail.ru

In connection with the above, developing biomedical technologies to support liver functions in patients with decompensated CLD and especially in patients on the liver transplant waitlist, is an urgent task for modern medicine [5].

One of the leading directions of TERM is the development of techniques for correction of affected liver functions in CLD by creating a new functionally active liver tissue that is capable of eliminating the deficiency in damaged liver functions for a certain period of time, especially in the pre-transplant period.

To date, a number of studies on the use of CECs, which included biopolymer-based scaffolds, LCs and multipotent BM-MSCs have been conducted [7, 8]. However, we did not find any studies on the application of recombinant spidroin microgel for the production of CECs for CLD correction and treatment.

Recombinant spidroin rS1/9 used in this work was created based on a protein whose gene was previously developed, synthesized and cloned in the Saccharomyces cerevisiae yeast cells [9]. rS1/9 is an analog of natural spidroin 1, one of the two proteins of dragline silk of the orb weaver spider *Nephila clavipes*, and characterized by molecular weight of 94 kDa and isoelectric point of pI = 10.3, i.e. it is positively charged at all pH values. In in vitro and in vivo experiments, rS1/9-based 2D and 3D materials/products have been shown to be characterized by absence of toxicity and allergenicity, slow resorption in the animal body, and ability to support adhesion and proliferation of different cell types [10]. A hydrogel was formed from a solution of recombinant spidroin rS1/9, from which a microgel was obtained by mechanical crushing, which is a suspension of microgel particles ranging from 100 to 300 μm in size, having a pronounced regenerative effect [11].

Objective: to, on an experimental CLD model, investigate the possibility of long-term correction and restoration of liver function by implantation of a CEC that is based on rS1/9 microgel containing allogenic LCs and BM-MSCs.

MATERIALS AND METHODS

To solve the tasks, experimental studies were carried out on male Wistar rats (n = 80) aged 6–8 months with an initial weight of 230–250 g. The animals were kept in a vivarium at a temperature of 18–20 °C on a mixed diet with free access to water. Experiments on animals were carried out from 9 am to 7 pm at room temperature (t = 22–24 °C), which excluded daily fluctuations in the mitotic activity in the liver cells; the relative humidity was 50–65%, the lighting cycle was twelve hours, and the change in room air volume per hour was tenfold. The diet at the vivarium for rats was standard: animals were fed a combined diet for laboratory animals (microbiological status complied with GOST R 51849-2001 "Veterinary and sanitary standards and requirements for the quality of feed for nonproductive 55 animals"), *ad libitum* filtered tap water was delivered in standard drinking bottles (microbiological status of water complied with SanPiN 2.1.4.1074-01 "Hygienic requirements for water quality in centralized drinking water supply systems"). Experiments and all manipulations with animals were performed according to the rules adopted in the European Convention for the Protection of Vertebrate Animals Used for Experimental and other Scientific Purposes (ETS 123), Strasbourg, 1986).

CLD was simulated by prolonged inoculation of male Wistar rats with carbon tetrachloride for 42 days according to the modified scheme [8].

The donors of allogenic LCs and BM-MSCs were male Wistar rats aged 5–6 months, weighing 150–230 g.

The cells were isolated and cultured in accordance with the general principles of culture studies. BM-MSCs were prepared according to the generally accepted procedure [8].

LCs were also prepared and used according to a known technique [12].

In the manufacture of CECs, isolated LCs ($2.5–4.0 \times 10^6$ cells/cm^3) and BM-MSCs ($0.5–0.8 \times 10^6$ cells/cm^3) were first co-cultured for 3 days using a certain ratio of these cells (LCs : BM-MSCs = 5 : 1). An additional 150 μL of rS1/9-based microgel suspension was added to the culture of co-cultured cells for their adhesion, and Cytodex-3 (150 μl volume) was added to enable assessment of the status of the cellular material in the CEC composition for long periods after implantation into the liver.

On day 7 after inoculation, the rats that survived CLD modeling (n = 60) were divided into 2 groups. Group 1 (control, n = 20, saline (CLD + 1.0 mL of saline solution) saline was injected into liver parenchyma). Group 2 (experimental, n = 40, CECs consisting of rS1/9 microgel, allogeneic LCs and BM-MSCs = 5 : 1, and 1 ml Cytodex-3 were injected into the liver parenchyma by chipping.

Yeast cultivation, isolation and purification of recombinant rS1/9 spidroin, preparation of hydrogel and microgel based on it were performed as previously described in accordance with a previously published protocol [11].

The morphology of the hydrogel surface was analyzed using a CamscanS2 microscope (Cambridge Instruments, UK). Images were obtained using MicroCapture software (SMA, Russia).

Adequacy control of the created CLD models and efficacy of correction of morphofunctional disorders in the liver using CECs was estimated according to mortality and survival of animals, morphological and morphometric characteristics of the liver, as well as CECs themselves. The functional efficacy of CECs was assessed based on biochemical blood parameters. After modeling CLD and the therapy used, the surviving animals were removed from the experiment at day 90 by

intraperitoneal injection of sodium thiopental in a dose causing respiratory arrest. At autopsy, liver biopsies were subjected to morphological and morphometric studies. Immunosuppression was not used.

Live blood sampling from rats for biochemical studies was performed under ether anesthesia by notching the tip of the tail. Liver function – alanine aminotransferase (ALT), aspartate aminotransferase (AST), alkaline phosphatase (ALP) – was studied on a Reflotron™ biochemical analyzer (Roche, Switzerland) using special Reflotron test strips.

For morphological studies, we used liver from groups 1 and 2 animals. We studied the state of regenerative processes in the liver both inside and outside the CEC implantation areas. We evaluated light microscopy data by staining the sections with hematoxylin and eosin, Mallory and Van Gieson (Leica DM 6000 B microscope with Leica LTDCH 9435 camera, Germany).

Morphometric analysis was performed using morphometric software ImageScopeM (Systems for microscopy and analysis, Russia) using a Leica DM 1000 microscope and a Leica LTDCH 9435 DFC 295 camera (LeicaCamera AG, Germany). We determined morphometrically the following: the presence of cirrhosis (counting the number of false lobules); specific area of connective tissue (in % of the total area of liver section) [13, 14]; we counted the number of binuclear hepatocytes (per 10 fields of view at 400× magnification), hepatocytes with signs of fatty A distinctly positive trend in the recovery of hepatic parenchyma was noted. Liver architectonics was almost completely restored, regression in fatty degeneration and its transition to a fine-droopy form was noted; liver lobule structure was restored. Preserved hepatocytes without signs of dystrophy around the veins appeared; beam architectonics was restored, formation of false lobules was not determined (Fig. 3, g), whereas in the control, there were appearance of false lobules and expressed protein degeneration of hepatocytes, sclerosis and fibrosis of liver parenchyma, hepatocytes with degenerating nuclei and intranuclear lipid inclusions; area of blood vessels and bile ducts (in ‰).

For verification and structural analysis of liver tissue slices, images were processed using artificial intelligence (AI) analysis. This method is an effective way to analyze and present results obtained [15, 16] and allows to clearly differentiate structures in the tissue based on tinctorial properties.

MATLAB program (MATLAB Corporation, USA) was used to transform images of liver histological sections into three-dimensional space. The following types of structures were distinguished: “oxyphilic hepatocyte cytoplasm”, “basophilic hepatocyte nuclei”, “fibrous connective tissue”, “intercellular substance” and “empty spaces (vascular lumen, adipocytes)”. The initial image was converted to grayscale. After that, a 3D model was built taking into account the added constants for each grayscale image. Constructed models and pseudocoloring were individualized for each image [17].

Methylene blue staining was used for assessing cell viability in the primary culture [18].

The blood levels of CD4+CD25+Foxp3+ Tregs, which reflects the degree of immune tolerance to allogeneic cells in CECs, was also measured using flow cytometry (BeckmanCoulter, USA). For this purpose, blood lymphocytes were labeled with rat $CD4^{+}CD25^{+}Foxp3^{+}$ antibodies from eBioscience (USA).

Results obtained were statistically processed using the computer statistical package Biostat; the significance of differences was assessed by Student’s t-test with Bonferroni correction taken into account. Differences were considered significant at $p < 0.05$ (statistical package recommended by WHO, EpiInfo 5.0). Actuarial survival of animals within one year after CLD modeling (control) and against its correction by CECs implantation was calculated according to Kaplan–Meier using statistical software package Statistica for Windows, v.12.

RESULTS

The viability of the primary culture of BM-MSCs was 94 ± 2%. Cell suspension prepared from donor liver contained ~95–98% hepatocytes and ~5–2% non-parenchymal cells; they had 76 ± 4% viability. The cells were not separated into parenchymal and non-parenchymal.

The structure of the microgel surface was analyzed by scanning electron microscopy (SEM). The microgel represents microparticles with an average size of 100 to 300 μm and a pronounced relief surface; the surface elements of the hydrogel include nanostructures of 100 to 300 nm in diameter and microstructures of 10 to 30 μm in size (Fig. 1).

After obtaining the primary cell culture, we considered it necessary to pre-culture them to eliminate stress damage during isolation and activate their cellular functions. For this purpose, BM-MSCs were cultured for 7 days and then co-cultured with LCs introduced into the culture for subsequent 3 days. The cells were co-cultured not only in a stationary mode but also in a rotational mode (1.5–2.0 rpm) to simulate mass exchange provided by blood circulation, because only under these conditions can there be long-term viability and proliferative activity of LCs when co-cultured with BM-MSCs. To determine the suitability of rS1/9 for LCs adhesion, studies were performed that confirmed active LCs adhesion on the rS1/9 surface.

Mortality was 25% during CLD modeling. Further, after inoculation in the control group (group 1), animals continued to die: 5 rats died out of 20 (25%), which, in our opinion, confirms the adequacy of the chosen CLD model. In the experimental group (group 2), there was no mortality at this time point (day 90). Actuarial survival at the inoculation stage and during treatment is shown in Fig. 2, a and b.

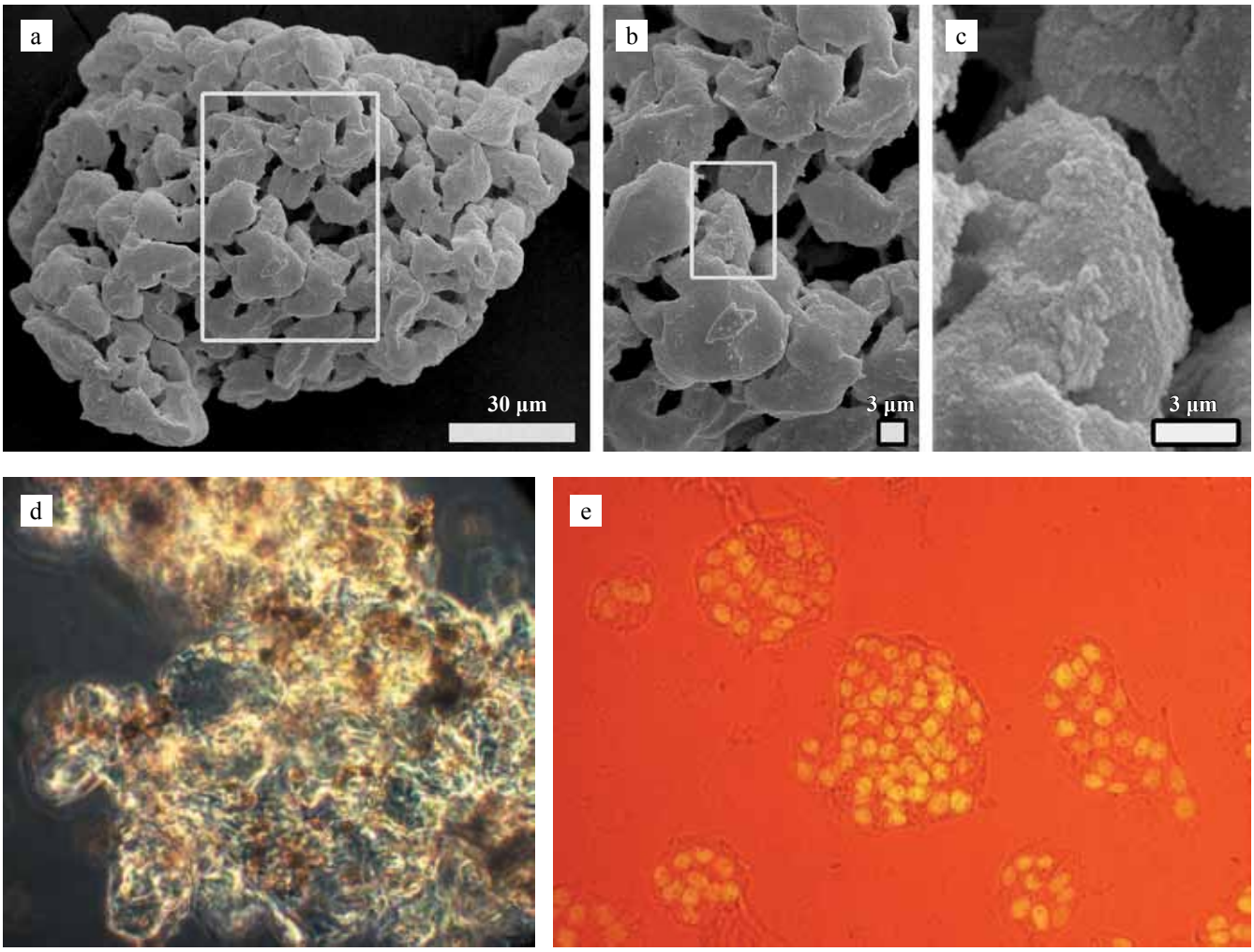

Fig. 1. Structure of rS1/9-based microgel: a, SEM image of microgel particle (scale bar = 30 µm); b and c, enlarged image of the area in a white frame (scale bar = 3 µm); d, Co-cultivation of LCs and BM-MSCs on rS1/9, phase contrast microscopy images (400× magnification); e, Staining for specific hepatocyte nuclear antigen 4 (HNF-4), fluorescence microscopy + phase contrast (200× magnification)

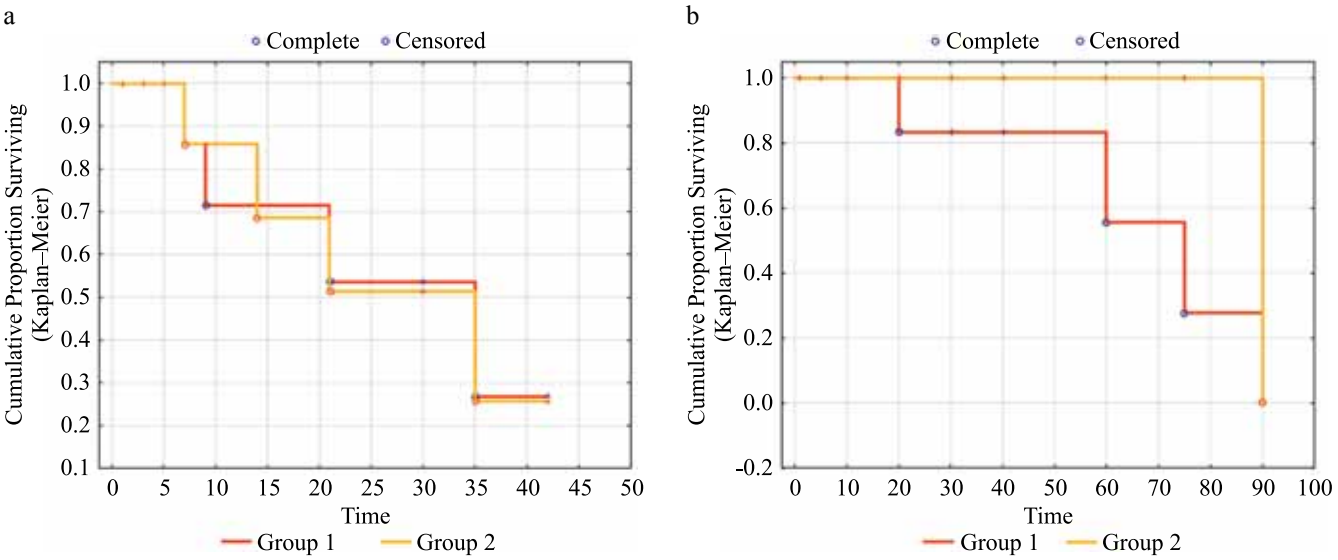

Fig. 2. Actuarial survival (according to Kaplan–Meier estimate): a, during CLD modeling: Gehan's Wilcoxon Test (Spreadsheet1) WW = –1,000 Sum = 670.00 Var = 76.32 Test statistic = –0.037655 p = 0.96996, and b, during CLD treatment: Gehan's Wilcoxon Test (Spreadsheet1) WW = –11.00 Sum = 238.00 Var = 62.632 Test statistic = –1.32676 p = 0.18459

At the initial stage of the study, the normal structure of the liver tissue was studied. Homogeneous liver parenchyma formed by hepatic cord of hepatocytes (D), with sinusoidal capillaries located between them in the form of slit-like spaces was revealed; the presence of endothelium and capillary and vein lumen was detected (Fig. 3, a–c).

After inoculation (42 days), on day 7 the following was revealed: changes in the beam structure of liver lobules, pronounced polymorphism of parenchymal cells, fatty degeneration in hepatocytes, karyorrhexis, karyolisis, hepatocyte necrosis. Massive fatty degeneration in hepatocytes and formation of false lobules were detected (Fig. 3, d–f).

By day 90 after CLD modeling, the control group witnessed subtotal restructuring of liver histoarchitectonics with replacement of normal parenchyma by false lobules. Sclerotic changes (fibrosis) were manifested by the formation of collagen fibers along the portal tracts and formation of porto-portal and porto-central septa with the formation of false lobules. Focal hepatocyte necroses, enlargement and plethora of sinusoids and plethora of central veins were revealed. Rare lymphoid-cell infiltration, proliferation of histioblasts and histocytes were noted in the liver parenchyma. In the experimental group, by day 90, we observed significantly less severity of toxic liver damage compared with the control. A distinctly positive trend in the recovery of hepatic parenchyma was

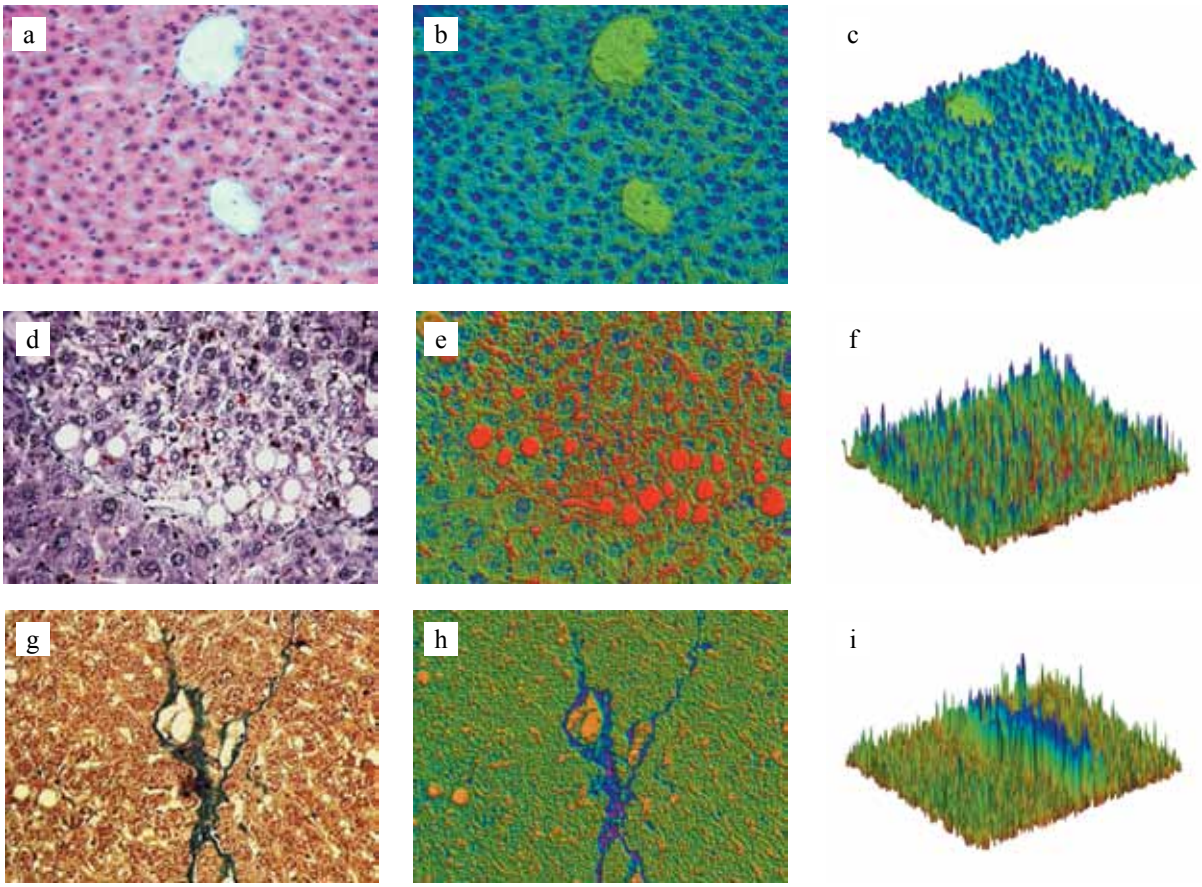

Fig. 3. Histological and pseudostained 2D and 3D liver preparations: a, Tissue specimens of healthy liver: Central part of the lobule with preserved structures with the presence of two central veins. Balloon structure is not disturbed, granular hepatocyte dystrophy, slight expansion of sinusoids. H&E staining (200× magnification). b, c, Pseudo-stained 2D and 3D images revealed the general structure of organ parenchyma without pathological changes. Hepatocytes with oxyphilic staining of cytoplasm and basophilic nuclei and a normal nuclear-cytoplasmic ratio, sinusoidal capillaries were not dilated. Hepatocyte cytoplasm is pseudostained in blue, nuclei are blue, sinusoidal spaces and vascular lumen are green, basophilic hepatocyte nuclei are lilac. d, Liver tissue specimen on day 7 after the end of CLD modeling: initial formation of fibrous tissue, focal proteinaceous granular degeneration of hepatocytes, significant group of cells in a state of ballooning degeneration and necrosis. Focal large- and small-drop fatty degeneration in hepatocytes. Sinusoidal dilatation and plethora. Rare lymphoid-cell infiltration in the parenchyma. Van Gieson's staining (400× magnification; e, f, Fatty degeneration of hepatocytes with a shift in nuclear-cytoplasmic ratio: hepatocytes with increased volume of cytoplasm. Areas of fibrosis are identified. On pseudo-stained 2D and 3D (e, f) images, hepatocyte cytoplasm is green, hepatocyte nuclei are blue and purple for pronounced hyperchromic tinctorial properties. Red color for empty spaces, predominantly in hepatocytes with fatty degeneration. g, Liver tissue specimen at day 90: CLD + CEC implantation with LCs and BM-MSCs (group 2). Central part of the lobule with preserved structures. Van Gieson's staining (200× magnification). In Fig. 3, h and i, hepatocyte cytoplasm is green, their nuclei are blue and purple with pronounced tinctorial properties, the prevailing empty spaces in hepatocytes with fatty degeneration are red

noted. Liver architectonics was almost completely restored, regression in fatty degeneration and its transition to a fine-droopy form was noted; liver lobule structure was restored. Preserved hepatocytes without signs of dystrophy around the veins appeared; beam architectonics was restored, formation of false lobules was not determined (Fig. 3, g), whereas in the control, there were appearance of false lobules and expressed protein degeneration of hepatocytes, sclerosis and fibrosis of liver parenchyma.

To objectify the results obtained, we performed quantitative and semi-quantitative assessment of structural changes occurring in the liver tissue in CLD without treatment and with the use of CECs. We performed morphometric studies of liver parenchyma cells (counting the number of hepatocytes with signs of fatty degeneration, with degenerating nuclei, with intranuclear lipid inclusions and counting the number of binucleated hepatocytes); as well as non-parenchymal structures (determination of the connective tissue specific area and the number of false lobules in liver), including blood vessels and bile ducts area in the liver tissue at day 90 after CLD modeling (Fig. 4, a, b).

A morphometric study of the state of non-parenchymal structures (determination of the specific area of the connective tissue and the number of false lobules in the liver) for a period of 90 days showed that under the influence of CECs, liver parenchyma was restored, the specific area of the liver connective tissue reduced (Fig. 4, a) and the number of false lobules in it also reduced (Fig. 4, b). At the same time, the control group showed an increase in these indicators – 8.2% and 2.8%, respectively.

It was also found that treatment with CECs (experimental group 2) resulted in a rapid and significant decrease in the number of hepatocytes with signs of fatty degeneration, with degenerating nuclei, with intranuclear lipid inclusions and a more pronounced significant increase in the number of binuclear hepatocytes. Moreover, the above changes were combined with a pronounced positive clinical effect. At day 90, blood vessel and bile duct area in the liver tissue normalized in comparison with the control group (Fig. 4, c–h).

The above studies suggest that regenerative processes in both non-parenchymal and parenchymal structures of liver tissue in CLD are intensified only when CECs are used with allogeneic LCs and BM-MSCs.

The identified features of liver regeneration when CECs are used with allogeneic LCs and BM-MSCs made it necessary to study the histological state of the CECs themselves and the surrounding liver tissue at day 90 after implantation.

Obtained results indicate that allogeneic LCs in CECs implanted into the recipient liver retain their viability and proliferative activity for a long time (90 days), with no signs of rejection, despite the absence of immunosuppression (Fig. 5, a–f).

Histological and model three-dimensional analysis of the state of hepatocytes in CECs implanted into the liver parenchyma in CLD showed that structural changes in hepatocytes in CECs are well distinguishable in tissue specimens. They are clearly identified by different color staining, which allows different structures to be distinguished. Thus, implantation of CECs containing rS1/9-based microgel and allogeneic LCs and BM-MSCs leads to positive structural changes in the liver parenchyma on the background of long-term preservation, development and maintenance of normal structural homeostasis in hepatocytes within the CECs.

It can be assumed that the long-term absence of distinct signs of immune rejection of CECs containing allogeneic cells (LCs and BM-MSCs) is a consequence of local implementation of immunomodulatory and tolerogenic properties inherent in BM-MSCs, which protect CECs against immune rejection and allow them to function for long and efficiently.

A blood test for Tregs levels by flow cytometry confirmed that rats with CLD that are treated by implantation of CECs containing allogeneic LCs and BM-MSCs, as well as the healthy controls, maintained the initial blood level of $CD4^+CD25^+Foxp3^+$ Tregs after 90 days (Fig. 6, a–c).

At the same time, there was a significant increase in the content of this pool of Regulatory T cells in the experimental group by day 90 as compared to the control group. Results of the conducted studies suggest that maintenance of the viability of the transplanted allogeneic LCs and BM-MSCs in CECs for a long time is due to immunological tolerance in the body induced and maintained by BM-MSCs.

Parallel studies of the functional state of the liver by means of dynamic measurement of serum biochemical indicators confirmed the development of sustained toxic damage to the liver immediately after CLD modeling. Development of CLD was accompanied by severe impairment of liver functional indicators: ALT, AST and ALP – they sharply increased in groups 1 and 2 animals immediately within the first 7 days after inoculation. However, in the experimental group (with CECs implantation), during the first 30 days, the studied biochemical parameters (ALT, AST, ALP) normalized rapidly and recovered completely by the end of the observation period.

Upon further follow-up in the group with implanted CECs, biochemical parameters characterizing a cytolytic syndrome remained within normal limits; in the control group (group 1), these parameters remained elevated for 90 days. This explains 25% mortality in the control group in the study period.

Thus, rapid normalization of cytolytic syndrome enzymes, the histological structure of the damaged liver tissue, a more pronounced decrease in the specific area of connective tissue, as well as reduced number of hepatocytes with fatty regeneration and degenerating nuclei

in the rat liver tissue, at day 90 after the end of CLD modeling and use of CECs in the experimental group, allows us to state that the implanted rS1/9-based CECs, which include allogenic LCs and BM-MSCs in a 5 : 1 ratio, effectively modulate regenerative processes in the damaged liver tissue. This is obviously due to the long-term preserved morphofunctional homeostasis in the newly formed hepatitis-like structure of the CECs

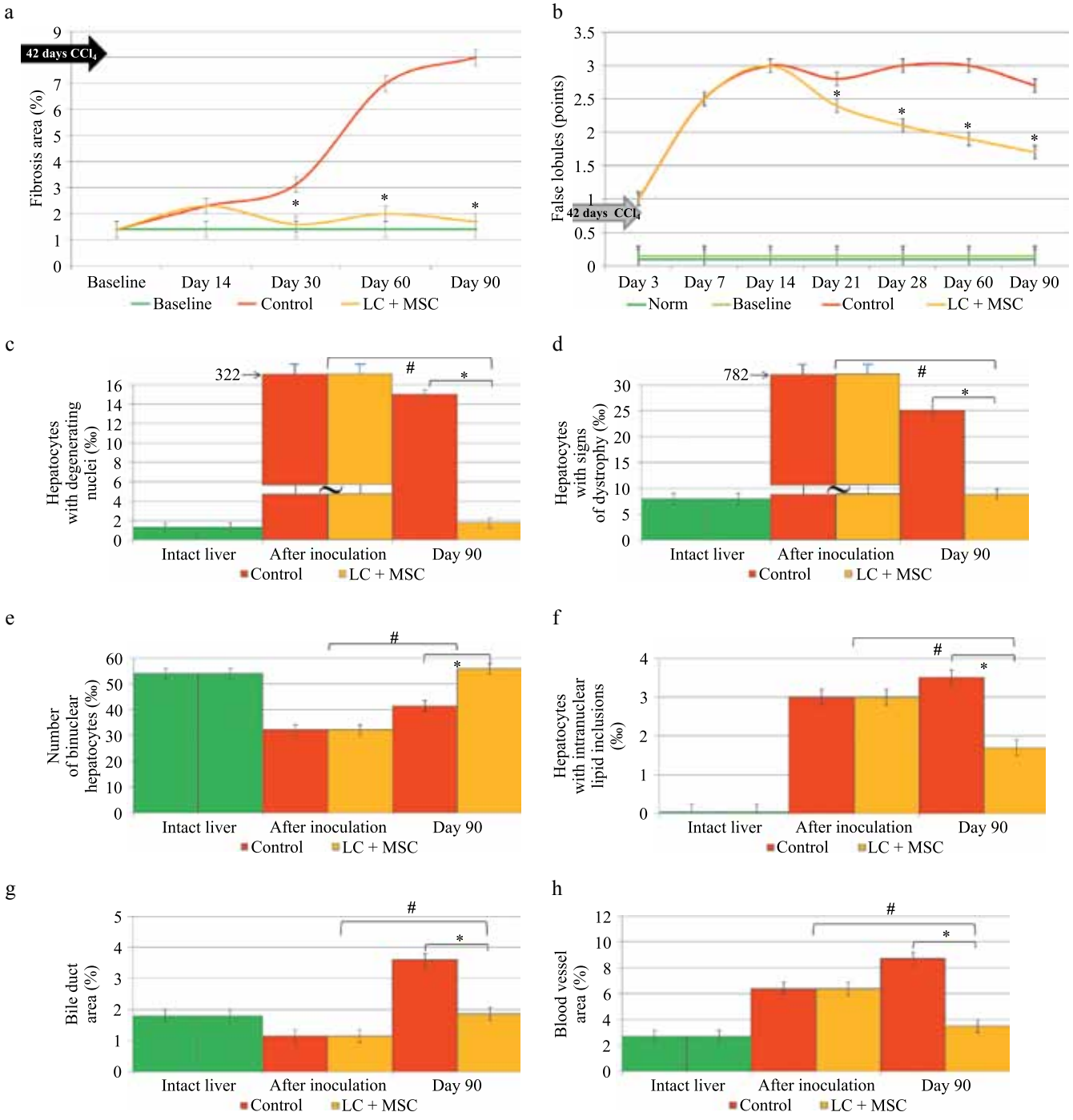

Fig. 4. Dynamic morphometric assessment of the state of nonparenchymal structures in CLD simulation without and with CEC implantation at day 90. a, Change in the specific area of the connective tissue (%). *In intact animals, the average value of the specific area of the connective tissue was 1.4%.* b, Change in the number of false lobules in the liver. *, The difference is significant compared to the level of this indicator in the liver of control rats (group 1); $p < 0.05$. c–h: dynamic morphometric assessment of the characteristics of rat liver hepatocytes, bile ducts and blood vessels in CLD simulation without and with CEC implantation at day 90: c, hepatocytes with degenerating nuclei; d, hepatocytes with fatty degeneration; e, binuclear hepatocytes; f, hepatocytes with intranuclear lipid inclusions; g, bile duct area; h, blood vessel area. group 1, control (saline); group 2, CEC with allogeneic LCs : BM-MSCs = 5 : 1. *, The difference is significant compared to the level of this indicator in the liver of control rats (group 1); $p < 0.05$. #, The difference is significant in comparison with the level of this indicator in the liver of rats after inoculation, $p < 0.05$

themselves, which is formed and maintained after CECs implantation by factors produced by the damaged liver into the body.

CONCLUSION

The study of the possibility of effective correction of morphofunctional disorders in the liver during CLD modeling using CECs implanted into the liver tissue showed that CECs made on the basis of rS1/9 microgel and containing allogeneic LCs and BM-MSCs in a 5 : 1 ratio, promote activation of regenerative processes in the damaged liver and restoration of its functional and morphological state: rapid normalization of the level of cytolytic enzymes in the blood, hepatocyte proliferation and reduction of connective tissue area in the liver. It was also found that throughout the entire period of observation in the structures of the implanted CECs, there was preservation of morphofunctional homeostasis of LCs included in their composition. The results of studies suggest that the cells included into the CECs become the centers of formation of newly formed and long-term functioning hematopoietic tissue which, by producing bioregulatory factors, activates and supports the repair processes in the damaged liver. Results obtained suggest that the long-term survival and functioning of allogeneic LCs in implanted CECs is due to the involvement of

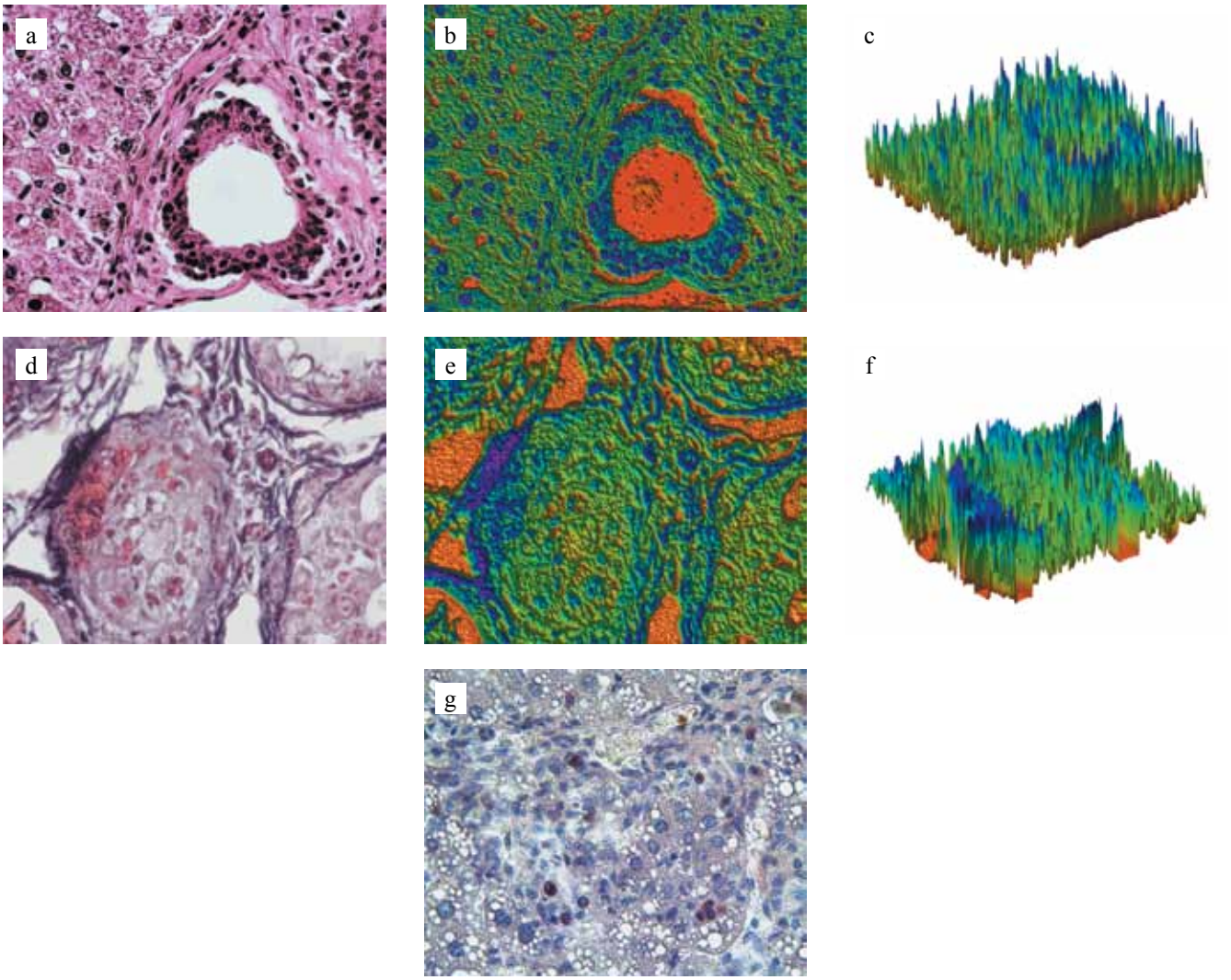

Fig. 5. Histological structure of hepatic CECs with allogeneic LCs and BM-MSCs (group 2) at day 90. a, transplanted hepatocytes as a part of CECs. H&E staining (400× magnification). b, c, there are structurally developing normal hepatocytes, hypertrophic hepatocytes, limited by fibrous connective tissue capsule, the shape and nuclear-cytoplasmic shifted to normal hepatocyte parameters. On the images after pseudo-coloring, the cell cytoplasm is green, nuclei are blue with purple inclusions, hepatocyte nuclei are in darker tones in a cell-engineered construct, the lumen is pseudo-stained red. d, transplanted hepatocytes as part of CECs. H&E staining (400× magnification; e, f, after destruction of the connective-tissue capsule, normal hepatocytes spread to neighboring areas and replace dystrophic hepatocytes. The fibrous connective tissue capsule disintegrates, and normal hepatocytes are located near its primary border. Images after pseudo-staining (e, f) show normal hepatocytes: cell cytoplasm is green, nuclei are blue, darker nuclei are purple in the cell-engineered construct, lumen is red. g, specifically PCNA-positive cells – light brown with dark brown nuclei, hepatocytes – oxyphilic cytoplasm and basophilic nuclei, PCNA staining by standard protocols with additional H&E staining (100× magnification)

BM-MSCs and rS1/9, contained in their composition, in maintaining the body's immune tolerance, due to which CECs are integrated into the damaged liver and symbiotically support each other.

Our studies have shown that implantation of CECs into the damaged liver creates numerous new centers for activation of repair processes. These centers were identified histologically and by three-dimensional analysis

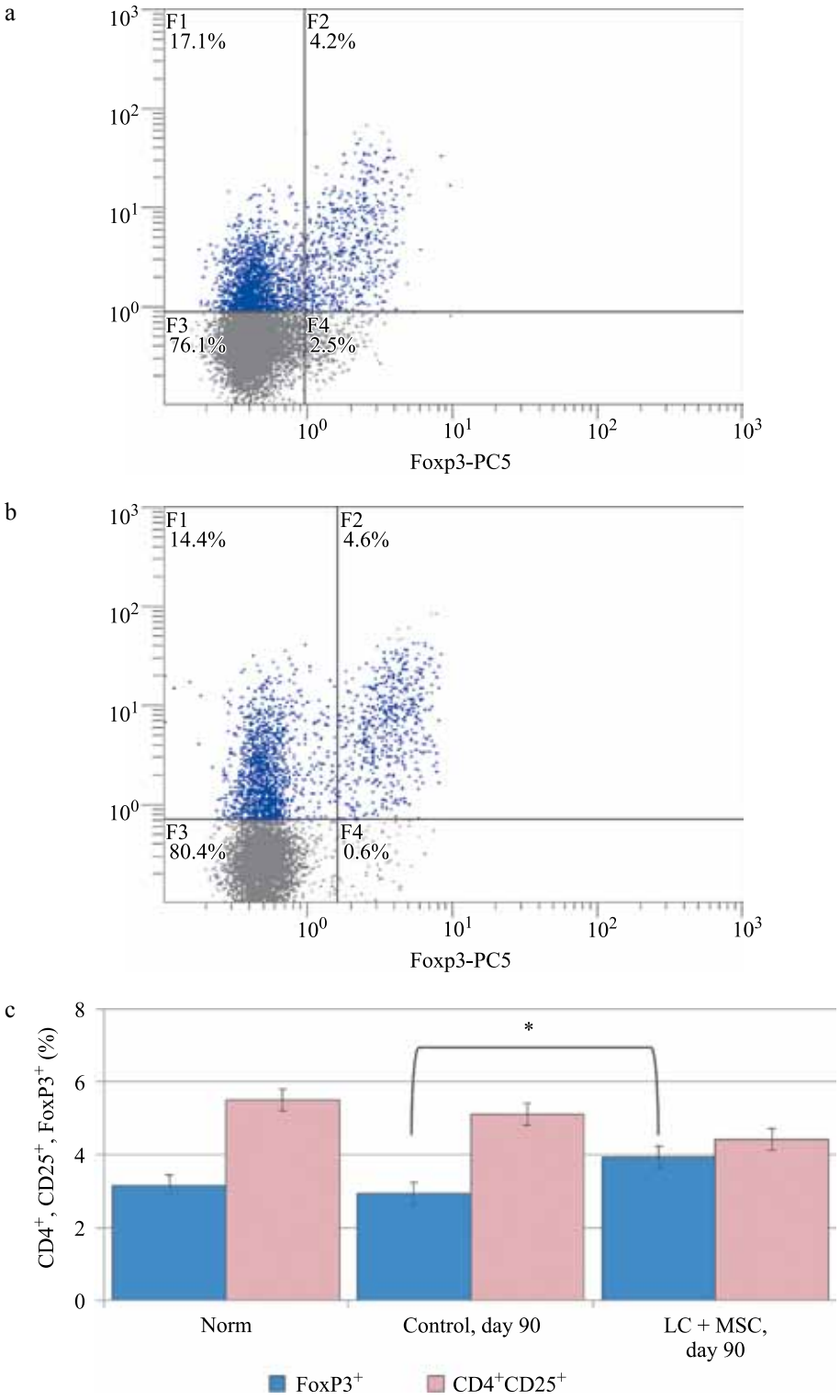

Fig. 6. Levels of $CD4^+CD25^+Foxp3^+$ Treg cells in the peripheral blood of rats: a, normal. b, day 90 after CLD modeling and implantation of CECs containing allogeneic LCs and BM-MSCs, experiments without immunosuppression. Flow cytometry. c, Graphical representation of levels of T lymphocytes containing CD4+, CD25+, Foxp3+ markers in peripheral blood of healthy, control rats after CLD modeling and implantation of CECs containing allogeneic LCs and BM-MSCs, in experiments at day 90 without immunosuppression (%). Flow cytometry. * $p < 0.05$ versus norm

of structural changes in the liver tissue and in CECs; the revealed positive structural changes in the liver were clearly visible in tissue specimens and were also identified by different color staining of structural elements of the liver in 2D and 3D images.

Implantation of CECs created on the basis of rS1/9 microgel and containing allogeneic LCs and BM-MSCs can become an effective method for correcting and treating CLD, and supporting damaged liver function in patients waitlisted for liver transplantation.

This work was supported financially by the Ministry of Science and Higher Education of the Russian Federation under Agreement No. 075-15-2021-1357.

The authors declare no conflict of interest.

REFERENCES

1. Transplantologija i iskusstvennye organy: uchebnik / Pod red. akad. RAN S.V. Gautier. M.: Laboratorija znanij, 2018; 319.
2. *Gautier SV, Konstantinov BA, Cirul'nikova OM.* Transplantacija pecheni. M.: MIA, 2008; 246.
3. *Mokdad A, Lopez A, Shahraz S, Lozano R, Mokdad A, Stanaway J et al*. Liver cirrhosis mortality in 187 countries between 1980 and 2010: a systematic analysis. *BMC. Med*. 2014; 12: 145. doi: 10.1186/s12916-014-0145-y.
4. World health statistics 2021: monitoring health for the SDGs, sustainable development goals World Health Organization, https: apps.who.int/iris/handle/10665/342703.
5. www.eurotransplant.nl/files/statistics.
6. *Atala A.* Building Organs for the Future. *Transplantation*. 2016; 100: 1595–15956. doi: 10.1097/TP.0000000000001301.
7. Metodicheskie rekomendacii po provedeniju doklinicheskih issledovanij biomedicinskih kletochnyh produktov / Pod red. akad. V.A. Tkachuka. M.: Moskovskij gosudarstvennyj universitet imeni M.V. Lomonosova, 2017; 256.
8. *Shagidulin MJu.* Razrabotka i jeksperimental'noe issledovanie kletochno-inzhenernyh konstrukcij pecheni dlja lechenija pechjonochnoj nedostatochnosti. [Dissertation]. M., 2015; 257.
9. *Bogush VG, Sokolova OS, Davydova LI et al.* A novel model system for design of biomaterials based on recombinant analogs of spider silk proteins. *J Neuroimmune Pharmacol*. 2009; 4 (1): 17–27. doi: 10.1016/j.biomaterials.2012.02.013.
10. *Debabov V, Bogush V*. Recombinant Spidroins as the Basis for New Materials. *ACS Biomater Sci Eng*. 2020; 6: 3745–3761. https: doi.org/10.1021/acsbiomaterials.0c00109.
11. *Nosenko MA, Moysenovich AM, Zvartsev RV, Arkhipova AY, Zhdanova AS, Agapov II et al*. Novel Biodegradable Polymeric Microparticles Facilitate Scarless Wound Healing by Promoting Re-epithelialization and Inhibiting Fibrosis. *Front Immunol*. 2018; 9: 2851. doi: 10.3389/fimmu.2018.02851. eCollection 2018.
12. *Gautier SV, Shagidulin MJu, Onishhenko NA, Krasheninnikov ME, Sevast'janov VI.* Sposob i transplantat dlja lechenija pechenochnoj nedostatochnosti. Patent № 2010110063/14(014141). 03.03.2011.
13. *Avtandilov GG*. Medicinskaja morfometrija: rukovodstvo. M.: Medicina, 1990; 384.
14. *Ishak K et al.* Gistologicheskaja ocenka stadii i stepeni hronicheskogo gepatita. *Klinicheskaja gepatologija*. 2010; 2: 8–11.
15. *Pradhan P, Guo S, Ryabchykov O, Popp J, Bocklitz TW.* Deep learning a boon for biophotonics? *J Biophotonics*. 2020; 13: e201960186. https://doi.org/10.1002/jbio.201960186.
16. *Rivenson Y, Wang H, Wei Z et al*. Virtual histological staining of unlabelled tissue-autofluorescence images via deep learning. *Nat Biomed Eng*. 2019; 3: 466–477. https://doi.org/10.1038/s41551-019-0362-y.
17. *Macenko M, Niethammer M, Marron JS, Borland D, Woosley JT, Guan X et al*. A method for normalizing histology slides for quantitative analysis. *2009 IEEE International Symposium on Biomedical Imaging: From Nano to Macro*. 2009: 1107–1110. doi: 10.1109/ISBI.2009.5193250.
18. *Godoy P, Hewitt NJ, Albrecht U, Andersen ME et al*. Recent advances in 2D and 3D in vitro systems using primary hepatocytes, alternative hepatocyte sources and non-parenchymal liver cells and their use in investigating mechanisms of hepatotoxicity, cell signaling and ADME. *Arch Toxicol*. 2013; 87 (8): 1315–1530. doi: 10.1007/s00204-013-1078-5.

The article was submitted to the journal on 17.05.2022

DOI: 10.15825/1995-1191-2022-4-73-84

BIOCOMPATIBLE AND FUNCTIONAL PROPERTIES OF A MICRODISPERSED TISSUE-SPECIFIC 3D MATRIX FROM DECELLULARIZED PORCINE CARTILAGE

E.A. Nemets[1], A.E. Lazhko[3], A.M. Grigoriev[1], Yu.B. Basok[1], A.D. Kirillova[1], V.I. Sevastianov[1, 2]

[1] Shumakov National Medical Research Center of Transplantology and Artificial Organs, Moscow, Russian Federation

[2] Institute of Biomedical Research and Technology, Moscow, Russian Federation

[3] Moscow State University, Moscow, Russian Federation

In contrast to decellularization of soft tissues for use as tissue-specific matrices in the creation of tissue-engineered constructs, decellularization of cartilage tissue requires several processing techniques, which can negatively affect the biocompatibility and functional properties of the native extracellular matrix (ECM). **Objective:** to study the biocompatible and functional properties of microdispersed tissue-specific 3D matrix from a porcine cartilage that is decellularized by sequential use of chemical, physical and enzymatic techniques. **Materials and methods.** For decellularization, microdispersed cartilage particles (MCPs), obtained by cryomilling, were incubated in detergent solutions (sodium dodecyl sulfate and Triton X-100), then treated with supercritical carbon dioxide ($scCO_2$) with 10% ethanol and DNase I. The Ames test (*Salmonella typhimurium* reverse mutation assay) was used to determine the genotoxicity of decellularized microdispersed cartilage particles (dMCPs). Local and general toxic effects, as well as resorption of dMCPs were studied *in vivo* on sexually mature outbred rats. Decellularized MCP specimens (10 mg) were implanted into the thigh muscle tissue. Viability of human adipose-derived mesenchymal stem/stromal cells (hAdMSCs), when cultured on dMCPs, was analyzed by *in vivo* microscopy, stained with fluorescent Calcein AM dye. Cell metabolic activity was assessed using PrestoBlue™ Cell Viability Reagent. **Results.** It has been proven that porcine dMCPs implanted in rat muscle after treatment with $scCO_2$ do not exhibit local and general toxic effects, and do not show genotoxicity and negative effects on the reproductive system of animals. After 6 months of *in vivo* experiment, most (87%) of the implanted decellularized cartilage was resorbed. It was shown that the resulting matrices are able to support adhesion and proliferation of hAdMSCs. **Conclusion.** Porcine dMCP specimens are suitable for biocompatible medical products in terms of local and general toxic effects, genotoxicity and reproductive toxicity, and can be used as a matrix for creating cell- and tissue-engineered cartilage constructs.

Keywords: articular cartilage, decellularization, 3D matrix, resorption, biocompatibility, adipose-derived MSCs, adhesion, proliferation, tissue-engineered construct.

INTRODUCTION

A number of biocompatible 3D matrices (also called scaffolds or carriers) made of resorbable synthetic [1, 2] and natural polymers [1, 3, 4], which more or less simulate the properties of native ECM, have been developed to create biomedical products for tissue engineering and regenerative medicine. However, 3D matrices made of polymeric materials do not possess tissue-specific properties characteristic of ECM, which can perform not only scaffold functions but also selectively support adhesion, proliferation and differentiation of cells of a particular tissue or organ [5]. In this regard, there is great interest in 3D matrices from decellularized allogenic or xenogeneic tissues [6–8]. The main problem of decellularization is the need for the most complete removal of cellular material with the highest possible degree of preservation of morphology, composition, biochemical and mechanical properties of native ECM. Due to the fact that the completeness of decellularization is influenced by many factors, such as donor type, organ size and integrity, tissue type, its structure and density, etc., there cannot be a universal decellularization protocol [9, 10]. To date, a wide range of decellularization protocols have been developed, using physical, chemical, enzymatic treatment methods and their combination [11–13].

Among the physical methods, the use of supercritical fluids that have zero surface tension, low viscosity, increased solubility and can penetrate deeply into the bulk of materials seems promising [14–16]. The most interesting is $scCO_2$ [17] – it reaches its critical point

Corresponding author: Evgenij Nemets. Address: 1, Shchukinskaya str., Moscow, 123182, Russian Federation. Phone: (903) 579-23-79. E-mail: evgnemets@yandex.ru

at a sufficiently low temperature (31.1 °C), it can be easily removed by simple pressure relief after treatment and it is non-toxic. At the same time, extraction of toxic compounds soluble in $scCO_2$ can occur, which leads to increased biocompatibility of the obtained materials decellularized using cytotoxic detergents [18]. Since $scCO_2$ is a non-polar compound, treatment is carried out in the presence of a polar agent, such as ethanol, to improve efficiency. Addition of ethanol increases both the efficiency of high-density tissue decellularization [19, 20] and the preservation of such important ECM components as collagens, glycosaminoglycans, adhesive proteins (fibronectin, laminin and others) and angiogenic factors [21].

The high density of cartilage makes it difficult to achieve complete decellularization, making it hard to diffuse surfactants and remove cellular detritus. Previous studies have shown that to achieve complete cartilage decellularization, it is necessary to use a protocol that includes both chemical (treatment with surfactants) and physical (supercritical fluids, cyclic freeze-thaw) treatment methods or enzymatic (DNase, RNase) methods of tissue exposure [22, 23].

The objective of this work was to investigate the biocompatibility and matrix properties of a microdispersed 3D matrix from porcine cartilage decellularized by sequential treatment with chemical, physical, and enzymatic methods.

MATERIALS AND METHODS

Porcine thigh and knee joints were obtained at slaughterhouse Promagro in Stary Oskol, Russia, after the slaughter of healthy animals (weighing about 120 kg) in accordance with the European Directive 64/433/EEC. After transportation in a refrigerated form, the cartilage was cut off from the articular surfaces with a scalpel, cut into 0.5 × 0.5 × 0.1 cm fragments, frozen at –80 °C and stored at this temperature until cryomilling began.

MCPs were obtained in a CryoMill (Retch GmBH, Germany). Grinding was done with the milling pot constantly contacting liquid nitrogen, at 25 Hz frequency for 4 minutes. The fraction of 30–100 μm particles was isolated using sieves with the appropriate mesh size.

MCPs were decellularized according to the previously developed technique [22]. The MCPs were treated at room temperature and periodically stirred on a magnetic stirrer (3 times per day, 1 hour, 200 rpm) in three changes of phosphate-buffered saline (PBS) (pH = 7.4) containing sodium dodecyl sulfate (SDS) and an increasing concentration of Triton X-100 (1, 2, and 3%, respectively).

The MCPs were then thoroughly washed of residual detergents in three changes of PBS containing an antibiotic (ampicillin, 20 μg/ml) and an antimycotic (amphotericin B, 2 μg/ml) for 72 hours at room temperature.

In the second stage, MCPs were treated in an $scCO_2$ atmosphere on a Speed SFE unit (Applied Separations, USA) at 300 bar, +35 °C, and $scCO_2$ flow rate of 2.5 ± 0.5 mL/min for 8–24 hours. 10% ethanol was used as a polarity modifier.

DNase I (New England Biolabs Inc., USA) at a concentration of 50 U/ml in 10 mM Tris-HCl buffer solution (pH 7.6) containing 2.5 mM $MgCl_2$, 0.5 mMol $CaCl_2$ was used to enhance DNA removal from porcine MCPs. The treatment time at 37 °C was 48 hours.

Specimens of decellularized MCPs (dMCPs) were sterilized by radiation at a dose of 1.5 Mrad.

Before the study, dMCP specimens were stored at –20 °C.

Determining DNA content

DNA extraction from MCPs (n = 3) and dMCPs (n = 3) specimens weighing 25 mg was performed using the DNeasy Blood & Tissue Kit (QIAGEN, Germany) according to the manufacturer's instructions. A bacteriophage λ DNA calibration curve (Invitrogen, USA) (0 ng/mL to 1000 ng/mL) was used to determine the absolute amount of DNA.

Scanning electron microscopy of specimen surfaces

MCPs and dMCP specimens were dehydrated in ethanol solutions of increasing concentrations according to the following scheme: 50% alcohol for 3 minutes, 50% alcohol for 3 minutes, 70% alcohol for 3 minutes, 90% alcohol for 6 minutes, and 96% alcohol for 6 minutes; they were air-dried and adhered to electron microscopy tables using double-sided adhesive tape.

Conductive coating was obtained by gold ion sputtering for 40 seconds at a constant current of 5–7 mA on JFC-1600 device (JEOL, Japan). The morphology of MCPs was studied using a JSM-6360LA scanning electron microscope (JEOL, Japan) at an accelerating voltage of 5 kV.

METHODS OF STUDYING THE BIOCOMPATIBLE PROPERTIES OF DMCPS

A. In vitro studies

Genotoxicity

Since the decellularization process uses potentially genotoxic substances (detergents) and fails to completely remove DNA from MCPs, it is possible that the decellularized cartilage may affect the patient's genetic material when clinically used as part of it.

The genotoxicity of dMCP specimens was assessed by the Ames test (*Salmonella typhimurium* reverse mutation assay), which is a bacterial test system for recording mutations to prototrophic histidine by the action of tested samples and (or) their metabolites inducing base replacement or frameshift type mutations in the genome of that organism.

We used a set of indicator strains of *Salmonella typhimurium* obtained from the Russian National Collection of Industrial Microorganisms under state research institute Genetika, having the appropriate certificates.

To prepare the extract, 25 mg of dMCPs were incubated for 3 days at 37 °C in 1 mL of sterile 0.9% sodium chloride solution (NaCl). Five concentrations of the extract were tested: stock solution and four successive 5-fold dilutions in 0.9% NaCl. The experiment was accompanied by positive controls, which were substances inducing mutations in the corresponding test strains.

For metabolic activation, we used the liver S9 fraction of male Wistar rats, which, 5 days before slaughter, were injected with microsomal enzyme inducer Sovol, 300 mg/kg, once intraperitoneally.

After incubation for 48 hours, the number of reverted colonies was counted in the groups of indicator strains. The mean number of revertant colonies for the drug-treated groups were compared simultaneously with the corresponding negative control groups.

If the substance and/or its metabolites have mutagenic activity, they will induce reverse mutations from auxotrophy to histidine prototrophy in histidine-dependent strains of *Salmonella typhimurium*. According to generally accepted approaches, the mutagenic effect was considered to be significant if the average number of revertant colonies per plate in the experimental variant exceeded that in the control variant by 2 or more times.

B. In vivo studies of reproductive toxicity, local and general toxic effects

The experiments were carried out on sexually mature outbred rats. Maintenance and all manipulations with the animals were performed according to the rules adopted in the European Convention for the Protection of Vertebrate Animals Used for Experimental and other Scientific Purposes (ETS 123), Strasbourg, 1986), and in accordance with GOST 33216-2014 Interstate Standard "Guidelines for the Maintenance and Care of Laboratory Animals".

Reproductive toxicity

When genotoxic effects act not only on somatic cells but also on germ cells, changes can become hereditary. To study the effects on generative function and embryotoxic effects in the antenatal and postnatal periods of development of the genotoxic effect on germ cells, the reproductive toxicity of dMCPs was studied.

The animals were divided into groups of 6 males and 12 females per group: control males, control females, males with dMCP specimens, and females with dMCP specimens. Sham-operated rats served as controls.

Fourteen days after implantation, males and females were paired in a 1 : 2 ratio (one male and two females) for 14 days. Every morning, vaginal swabs were taken from females and the presence of spermatozoa in them was determined. If spermatozoa were detected, the rat was weighed, placed in a separate cage, and the gestation period was counted, taking the day of spermatozoa detection as the first day of pregnancy.

During the study, general clinical observation was performed, body weight, feed and water consumption were determined.

Some pregnant females were euthanized on day 20 of pregnancy; fetuses were examined, weighed, and the cranio-caudal size was measured. The number of corpus luteum in the ovaries, implantation sites, and the number of live and dead fetuses were counted. Pre- and post-implantation fetal mortality rates were determined based on the data obtained. The other half of the females were left until delivery to monitor the development of the offspring for 5 days. At the end of the study, adult animals were euthanized. After death, the ovaries were removed from the females and the testes and testicular appendages from the males. These reproductive organs were examined macroscopically for abnormal or pathological changes and weighed on VIBRA AJ-1200CE scale (ShinkoDenshiCo., Ltd., Japan), with further calculation of their relative weight (percentage ratio of organ weight to animal body weight). The ovaries and testes were fixed in 10–15% neutral formalin. After fixation on histoprocessor TLP-144 (MedTechnikaPoint LLC, Russia), histological processing was performed. After that, paraffin blocks were prepared on an ESD-2800 pouring station (MedTechPoint, Russia). Then, using rotary microtome RMD-4000 (MedTechnicaPoint, Russia), we obtained 3–4 nm thick sections that were glued to a slide, deparaffinized, and stained with hematoxylin and eosin. Histological specimens were examined by light microscopy using biological microscope Leica DM1000 (Leica Microsystems GmbH, Germany).

Local and general toxic effects

The specimen (10 mg weight) was implanted into the thigh muscle tissue under sterile conditions under the anesthetic Zoletil 100 (Virbak, France) at a dose of 15 mg/kg. Sham-operated animals (underwent surgery without specimen implantation) served as controls.

To study local effects, the animals were euthanized by carbon dioxide inhalation at day 28, months 2, 3, and 6 after dMCP specimens had been implanted. The results were evaluated macroscopically and by histological methods. According to semi-quantitative assessment results [24], the reactivity class of the studied material in comparison with the control sample was determined (in points): no response or minimal response (0.0 to 2.9); mild response (3.0 to 8.9); moderate response (9.0 to 15.0); severe response (≥15.1).

General toxic effects were investigated at up to 2 months of implantation simultaneously with assessment of their local effects. Analysis of animal condition

included: survival and appearance, animal weight, behavior (excitability, aggressiveness), reaction to external stimuli, pain response, feed and water consumption. At month 2, blood was collected from the animals for clinical (hematological analyzer Mindray BC-2800-vet (Mindray, China) and biochemical (biochemical photometer Stat Fax 4500+ (Awareness Technology Inc., USA) studies and urine (URISCAN Optima, YD Diagnostics Corporation, Korea). The following organs were taken and weighed: heart, lungs, thymus, liver, spleen, kidneys, and brain. These organs were weighed using Shinko scales, AJ-1200CE (Shinko Denshi Co., Ltd., Japan). H&E-stained histological preparations of the heart, lungs, thymus, liver, spleen, intestines, kidney, brain, and regional lymph nodes were examined using biological microscope LeicaDM 1000 (Leica Microsystems GmbH, Germany).

The degree of resorption of the implanted specimens was determined morphometrically using LAS Interactive Measurement Module, a computer morphometric program.

The excised sections of organs and tissues were fixed in 10–15% neutral formalin solution with subsequent embedding in paraffin. 5–7μm-thick sections were prepared. Histological preparations were examined by light microscopy using biological microscope LeicaDM 1000 (Leica Microsystems GmbH, Germany).

Investigation of the ability of dMCPs to support cell adhesion and proliferation (functional properties)

Third-passage hAdMSCs were isolated and cultured in complete cell culture medium (CCCM) according to the standard technique [25].

Adhesion and proliferation experiments were performed using a hAdMSCs culture. These cells are capable of differentiating in the chondrogenic direction with subsequent formation of cartilage tissue. To prevent cell growth outside the matrix surface, the experiment was performed in polypropylene tubes. 5 mg of dMCPs were placed in sterile tubes under aseptic conditions, CCCM was added and incubated for 24 hours at +37 °C to saturate the medium. A day later, hAdMSC suspension was prepared with a concentration of 500,000 cells/mL; excess medium was removed from the tubes, and 1 mL of cell suspension was added to each tube. The tubes were placed in a rack and shaken on laboratory shaker MultiBio 3D (Biosan, Latvia) for 2 hours at room temperature, after which the tubes were placed in a CO_2 incubator and cultured at +37 °C in a humid atmosphere containing (5 ± 1)% CO_2.

To assess the interaction between cells and dMCP specimens using in vivo microscopy, we used fluorescent Calcein AM dye (Thermo Fisher Scientific, USA).

The metabolic activity of cells was determined using reagent test PrestoBlue™ (Invitrogen, USA) according to the manufacturer's instructions. Spectrophotometric analysis was carried out on plate reader Tecan Spark 10M (Tecan Trading AG, Switzerland). Cell count was measured according to the calibration curve constructed.

Statistical data analysis

The obtained data were statistically processed using Microsoft Office Excel 2010 software. The group arithmetic mean (M) and standard error of the mean (m) were calculated. Statistical significance of differences was assessed by Student's t-test. Differences between the groups were considered significant at $p < 0.05$.

RESULTS AND DISCUSSION

Decellularization reduced the amount of DNA from 367 ± 53 ng/mg to 7 ± 1 ng/mg of tissue, which is less than 2% of the initial value and shows the decellularization process to be highly efficient [26]. At the same time, there are significant differences in the surface morphology of native and decellularized cartilage (Fig. 1).

The surface structure of the original cartilage tissue is smooth (Fig. 1). Cell lacunae characteristic of articular cartilage tissue, in which cell outlines were visualized, are detected. For decellularized cartilage, there were no cells in the lacunae on the surface of the microparticles, which also shows the treatment to be effective.

Genotoxicity

The number of revertant colonies in the control (solvent) was within the spontaneous variation for these strains. Strain response to standard mutagens was within normal.

Decellularized tissue-specific matrices from porcine MCPs at concentrations of 0.1, 0.5, 1, 5, and 25 mg/ml did not induce gene mutations in *Salmonella typhimurium* test strains TA 100, TA 98, and TA 97 with and without metabolic activation. In all variants of the experiment, the multiplicity of excess of the average number of revertant colonies per cup in the experiments over that in the control was less than 2-fold.

Thus, experimental samples of porcine dMCPs obtained by sequential treatment with detergents and $scCO_2$ are not genotoxic.

Local effect

Healing of surgical wounds in animals of the experimental and control groups occurred by primary intention. None of the animals showed symptoms of implant rejection, suppuration, suture divergence, and other postoperative complications. There were no necroses, hemorrhages, granulomas and severe edema around all specimens along the periphery in the surrounding muscle tissue. There were no signs of inflammation in the matrix

implantation area. Macroscopic examination revealed no signs of tissue irritation and inflammation, no scar tissue was detected.

Tissue response to surgical intervention and subsequent implantation of porcine decellularized cartilage specimens followed the usual pattern that is characteristic of the wound process and reaction to a foreign body, including traumatic inflammation and connective tissue formation stages.

The microscopic picture on day 28 of dMCPs implantation (Fig. 2) was characterized by the presence of a thin capsule around the implant consisting of dense fibrous connective tissue. No infiltration of the connective tissue into the implants was observed. No necrosis, hemorrhages, lymphohistiocytic infiltration and edema were observed in the surrounding fibrous and muscular tissue. Lymphomacrophage infiltration was noted in the capsule and surrounding tissues, as well as the presence of single giant cells, indicating the initial stages of resorption. Among connective tissue cells, fibroblastic cells prevailed: mesenchymal cells, fibroblasts and fibrocytes. A small number of neutrophils was detected in the surrounding tissues. A scanty vascular pattern was noted.

On day 28 after implantation, there was mild resorption of dMCP specimens. The average area of one implanted dMCPs particle per group of animals was 13867 ± 964 μm^2. The central part of the implant not populated with cells was clearly distinguished. Active infiltration by macrophages was observed at the periphery.

After 2 months (Fig. 2), the implantation site was covered with hair and was not visually identified. Signs of regeneration in the form of muscle-joint tissue were observed. The regenerate was in the form of thin bundles of collagen fibers infiltrated by fibroblasts and fibrocytes. In the stroma, there were small vessels, myocytes forming growth buds and strands of newly formed thin muscle fibers.

At month 3 (Fig. 2), the implant was an oval, with no capsule around it. There was intensive resorption of the matrix by macrophages in the periphery. Compared to 30 days of implantation, the material was resorbed by ~44%. The average implant area was 7644 ± 155 μm^2. The structure of the non-resorbed dMCPs was not altered. There was a macrophage reaction at the periphery of the implant with the presence of lymphocytes.

At month 6 of implantation (Fig. 2), a thin capsule of collagen fibers was formed around the dMCP specimens, which is an indicator of high biocompatibility. At the same time, the number of active macrophages in the tissues surrounding the implants still remained high. At the periphery of the implanted particles resorbed by ~87% (average implant area was 1759 ± 1482 μm^2), we observed formation of mature connective tissue in the form of collagen fiber bundles and surrounding fibrocytes.

The slow resorption may be due to the high density of cartilage tissue, making it difficult for cells to penetrate and substances to diffuse into the dMCPs. Data obtained indicate the possibility of using dMCPs as a matrix for in vitro and in vivo formation of cartilage tissue equivalent.

Fig. 3 shows the results of a semi-quantitative assessment of the biological effect of the implanted specimens.

From the data presented in Fig. 3, we can see that the local effect of dMCPs on the surrounding tissues decreases during the six months of implantation from "mild tissue response" (3.0 to 8.9 points) to "no reaction or minimal response" (0.0 to 2.9 points). Note that the change in the nature of the tissue response to dMCPs occurs during the time of resorption of the main mass of implanted particles.

Thus, microdispersed particles of decellularized porcine cartilage and their resorption products show no

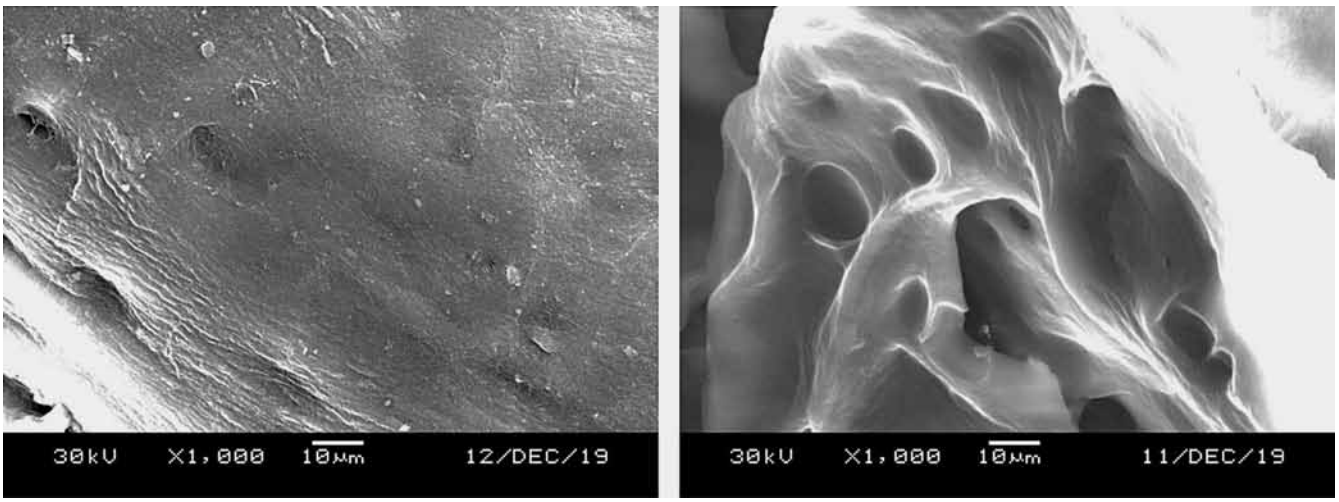

The original cartilage **Decellularized cartilage**

Fig. 1. Changes in the structure of porcine cartilage microparticles as a result of decellularization

negative biological effect on the tissues surrounding the implant.

General toxic effect

The animals in the control and experimental groups were healthy for 2 months of the experiment. No changes in the appearance and behavior toward oppression or agitation were observed in any of the rats. The body weight of the rats during the experiment had positive dynamics and did not differ between the groups.

Implantation of dMCP specimens did not affect hematopoiesis in the rats. There were no significant differences in the average values of clinical blood analysis between the control and experimental rats.

To identify the possible damaging effects of the test specimens on the liver, heart, and bone tissue, the activity of alkaline phosphatase, aspartate and alanine aminotransferases was determined in the blood serum. Analysis of data obtained did not reveal any differences in the activity of the studied enzymes and the content of total bilirubin, as well as in the indicators of protein metabolism in the body between the groups.

Introduction of the studied specimens in rats did not affect the urine parameters in comparison with the control group. Protein, glucose, bilirubin, urobilinogen, nitrites, ketone bodies, leukocytes and ascorbic acid were absent in the urine of animals or were below the first value determined by the Uriscan Optima device as positive.

Macroscopic study did not establish any clear effect of the studied specimens on the state of the internal organs of the rats. No differences between the control and experimental groups were found.

Histological examination did not reveal any distinct effect of the studied specimens on the state of the internal organs of the rats. No differences between the control and experimental groups were found.

Consequently, specimens of tissue-specific matrices of decellularized porcine cartilage do not exhibit systemic toxic effects on the body of the animals.

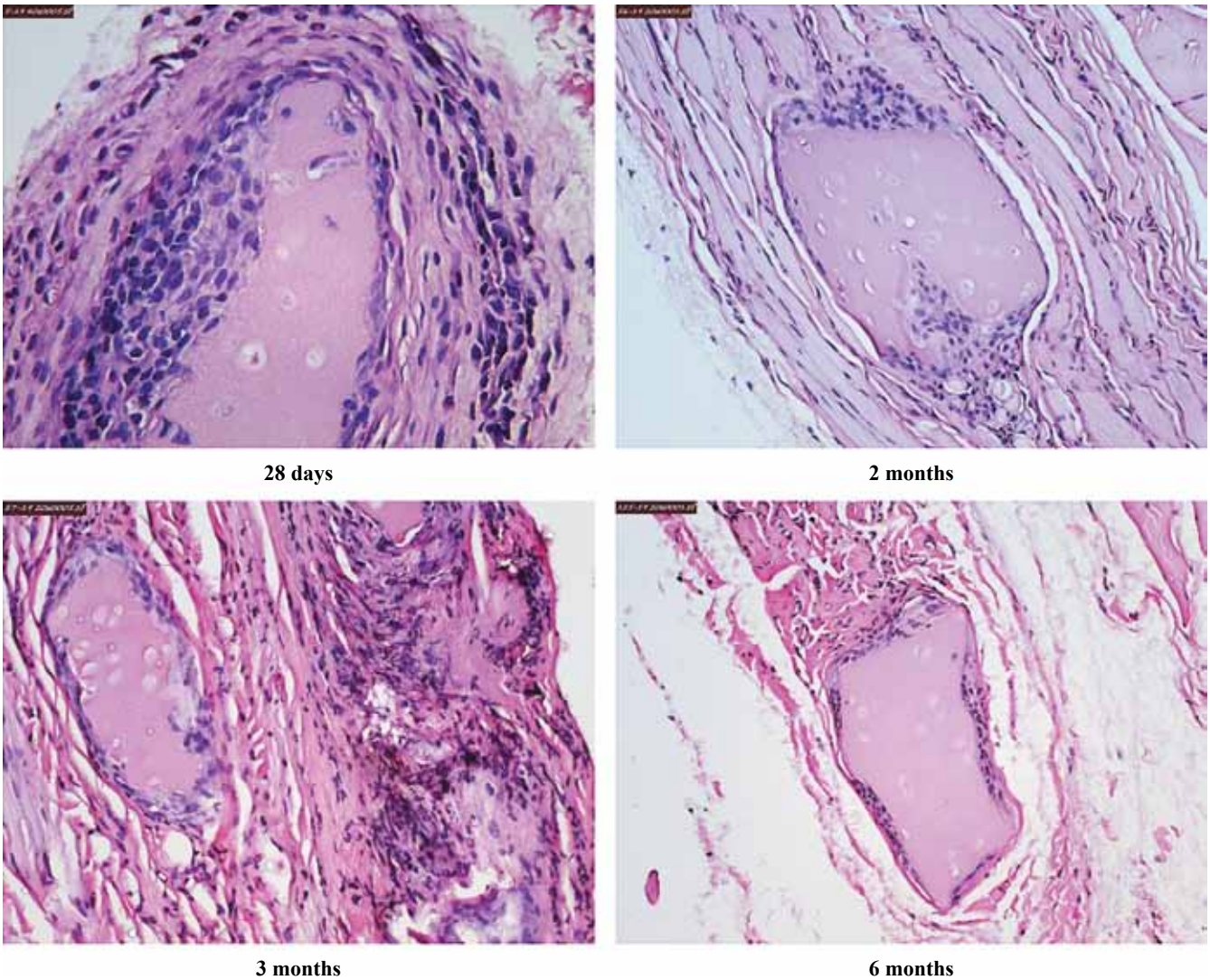

Fig. 2. Tissue response to implantation of decellularized porcine cartilage particles. H&E staining. ×400 magnification

Reproductive toxicity

When observing the sexual behavior of animals after pairing, it was noted that the latent period and duration of sexual activity in experimental males (with implanted dMCP specimens) corresponded to the control males (sham-operated).

During gestation, the behavior of female experimental groups was similar to that of control ones. During gestation, the weight gain of pregnant rats in the experimental groups did not differ from that of the control group.

Some pregnant females were euthanized on day 20 of pregnancy. At autopsy, the number of corpus luteum in the ovaries, implantation sites in the uterus, the number of live and dead fetuses, and the number of resorptions were counted. External examination revealed no developmental abnormalities in any embryo.

Some of the pregnant females were left until delivery to monitor the survival and development of the offspring for 5 days. Duration of pregnancy, number of born rats, their weight and cranio-caudal size did not statistically differ between the experimental and control

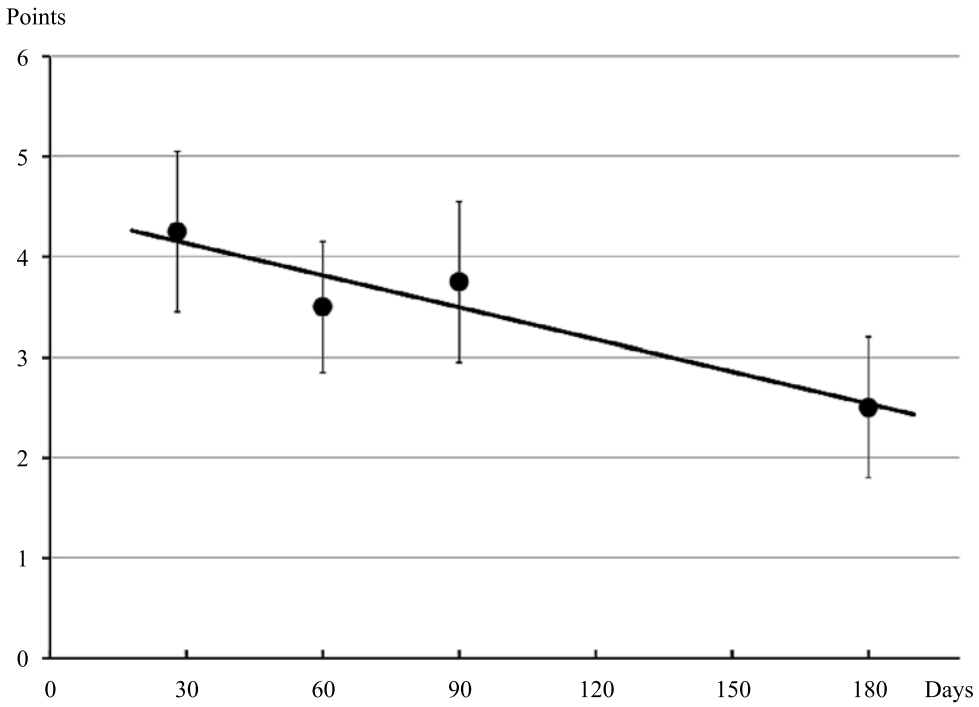

Fig. 3. Semi-quantitative assessment of tissue response to implantation of porcine decellularized cartilage particles

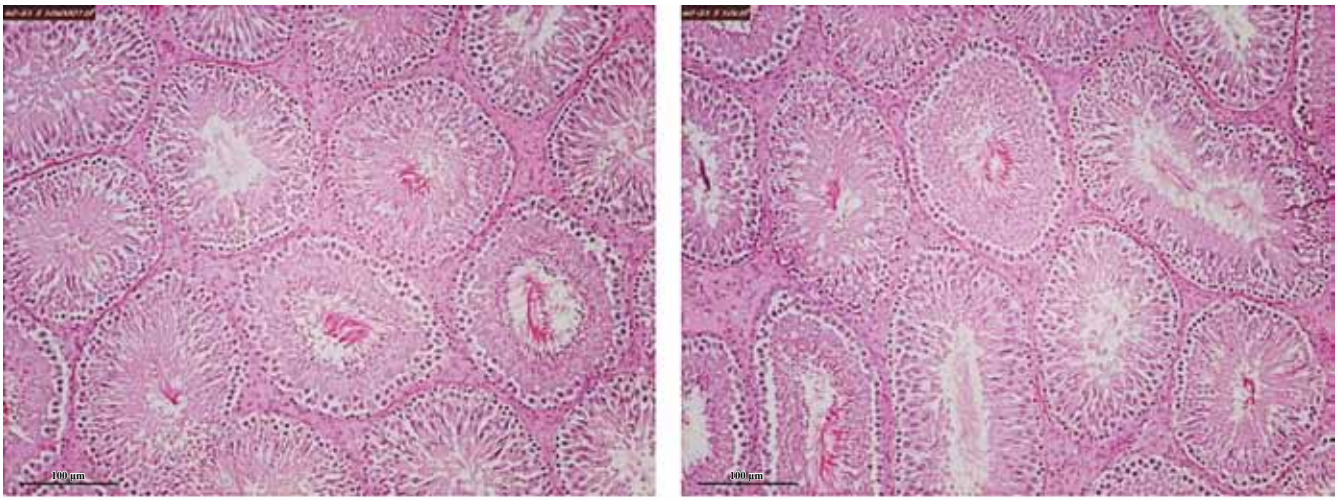

Control group **Decellularized cartilage group**

Fig. 4. Histological section of rat testis. H&E staining. ×100 magnification

groups. There were no stillbirths in any of the females. After delivery, all females exhibited maternal instinct. Five-day offspring survival was 100% in all groups. In this period, the rats developed without abnormalities.

Histological examination of testes (Fig. 4) showed no changes in the morphological structure of the organ and no damage to the spermatogenic epithelium in any case. A similar study of rat ovaries showed no morphological changes in the organ (Fig. 5).

It follows from the results obtained that the dMCP specimens implanted in the muscle tissue, both before mating the animals and during gestation, do not have negative effects on the reproductive system of the animals.

Interaction of tissue-specific matrix obtained from decellularized porcine cartilage with cells

By day 3 of the experiment, the number of proliferating adherent hAdMSCs was $112 \pm 10 \times 10^3$ cells/mm^2; by day 7 of the experiment, the number had doubled.

The study of cell viability using Calcein AM dye showed that by day 3 of the experiment, proliferation of cells, evenly distributed over the matrix surface, was visualized (Fig. 6).

Cell morphology is normal and fibroblast-like. By day 7, the number of cells increased, the attached cells were evenly distributed over the surface of dMCP matrices, had a flattened fibroblast-like morphology, maintained viability and normal morphology.

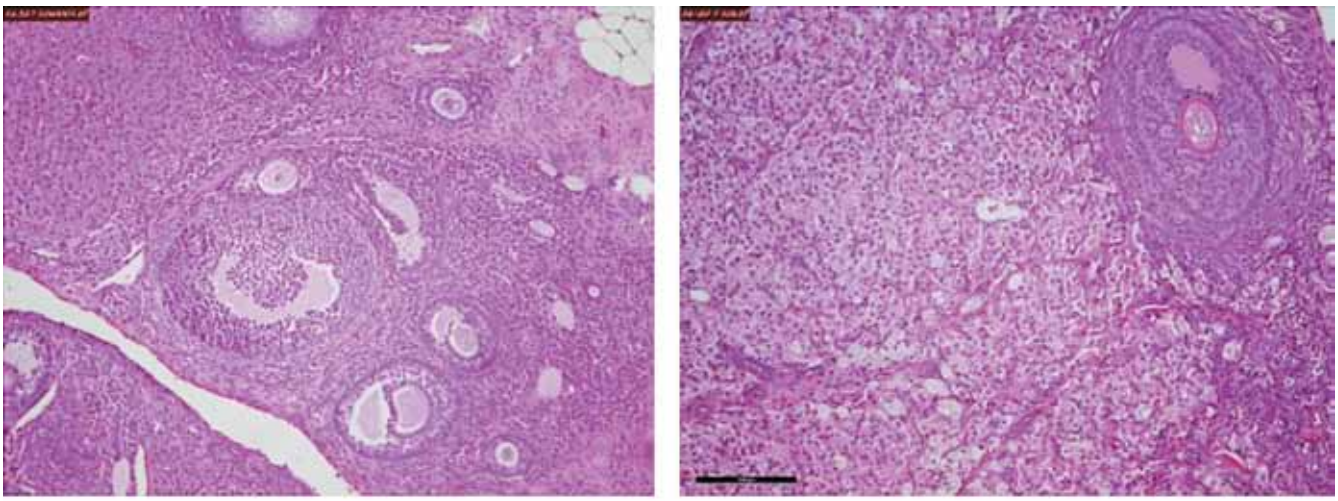

Control group **Decellularized cartilage group**

Fig. 5. Histological section of rat ovary. H&E staining. ×100 magnification

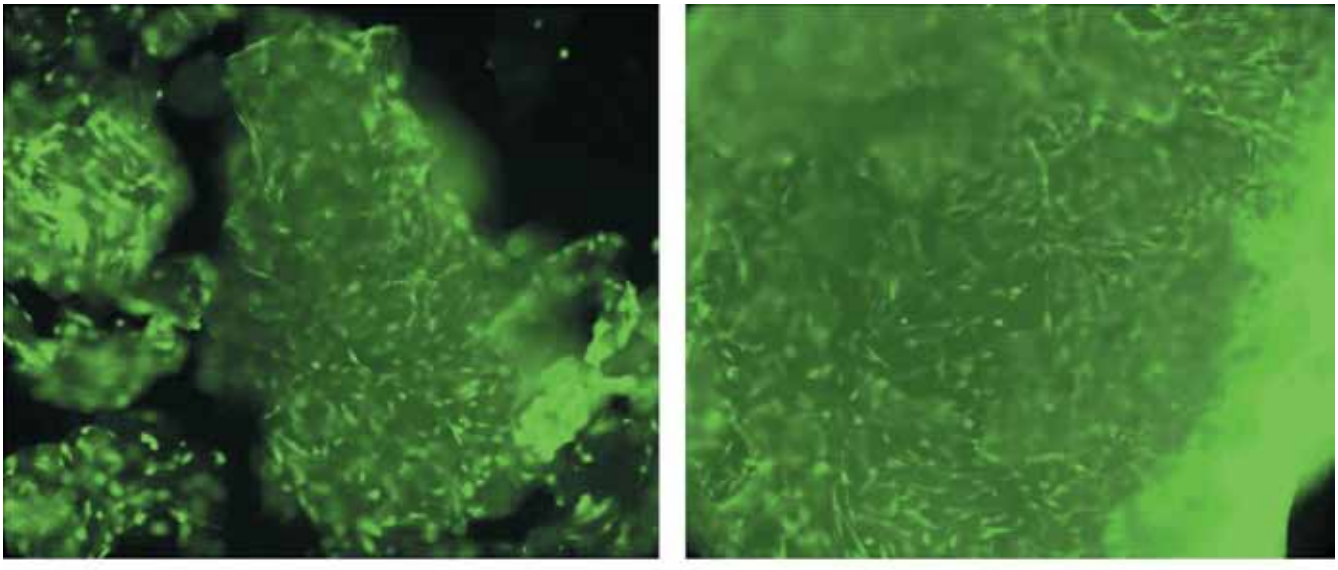

3 days **7 days**

Fig. 6. hAdMSCs cultured on decellularized microdispersed porcine cartilage particles. Calcein AM staining. ×100 magnification

CONCLUSION

The effectiveness of sequential treatment with surfactants, $scCO_2$ and DNase to obtain a biocompatible tissue-specific matrix from xenogeneic material, decellularized porcine articular cartilage, has been proven.

The experiments showed that the specimens of microdispersed decellularized porcine cartilage tissue do not exhibit adverse biological effects in terms of local and general toxicity, genotoxicity and reproductive toxicity. The specimens are capable of maintaining hAdMSC adhesion and proliferation.

So, the obtained xenogeneic tissue-specific microdispersed matrix can be recommended for the creation of tissue equivalents of human cartilage tissue.

The study was supported by a grant from the Russian Science Foundation (Project No. 21-15-00251).

The authors declare no conflict of interest.

REFERENCES

1. *Reddy MSB, Ponnamma D, Choudhary R, Sadasivuni KK*. A comparative review of natural and synthetic biopolymer composite scaffolds. *Polymers (Basel)*. 2021; 13 (7): 1105. doi: 10.3390/polym13071105.
2. *Jafari M, Paknejad Z, Rad MR, Motamedian SR, Eghbal MJ, Nadjmi N et al.* Polymeric scaffolds in tissue engineering: a literature review. *J Biomed Mater Res B Appl Biomater*. 2017; 105 (2): 431–459. doi: 10.1002/jbm.b.33547.
3. *Song R, Murphy M, Li C, Ting K, Soo C, Zheng Z.* Current development of biodegradable polymeric materials for biomedical applications. *Drug Des Devel Ther*. 2018; 12: 3117–3145. doi: 10.2147/DDDT.S165440.
4. *Vasilets VN, Surguchenko VA, Ponomareva AS, Nemetz EA, Sevastianov VI, Bae JW et al.* Effects of surface properties of bacterial poly(3-hydroxybutyrate-co-3-hydroxyvalerate) on adhesion and proliferation of mouse fibroblasts. *Macromolecular Research*. 2015; 23: 205–213. doi 10.1007/s13233-015-3025-1.
5. *Gattazzo F, Urciuolo A, Bonaldo P.* Extracellular matrix: a dynamic microenvironment for stem cell niche. *Biochim Biophys Acta*. 2014; 1840 (8): 2506–2519. doi: 10.1016/j.bbagen.2014.01.010.
6. *Paulo Zambon J, Atala A, Yoo JJ.* Methods to generate tissue-derived constructs for regenerative medicine applications. *Methods*. 2020; 171: 3–10. doi: 10.1016/j.ymeth.2019.09.016.
7. *Gupta SK, Mishra NC, Dhasmana A*. Decellularization methods for scaffold fabrication. *Methods Mol Biol*. 2018; 1577: 1–10. doi: 10.1007/7651_2017_34.
8. *Cramer MC, Badylak SF.* Extracellular matrix-based biomaterials and their influence upon cell behavior. *Ann Biomed Eng*. 2020; 48 (7): 2132–2153. doi: 10.1007/s10439-019-02408-9.
9. *Philips C, Campos F, Roosens A, Sánchez-Quevedo MDC, Declercq H, Carriel V.* Qualitative and quantitative evaluation of a novel detergent-based method for decellularization of peripheral nerves. *Ann Biomed Eng*. 2018; 46 (11): 1921–1937. doi: 10.1007/s10439-018-2082-y.
10. *Mendibil U, Ruiz-Hernandez R, Retegi-Carrion S, Garcia-Urquia N, Olalde-Graells B, Abarrategi A*. Tissue-specific decellularization methods: rationale and strategies to achieve regenerative compounds. *Int J Mol Sci*. 2020; 21 (15): 5447. doi: 10.3390/ijms21155447.
11. *Gilpin A, Yang Y.* Decellularization strategies for regenerative medicine: from processing techniques to applications. *Biomed Res Int*. 2017; 2017: 9831534. doi: 10.1155/2017/9831534.
12. *Porzionato A, Stocco E, Barbon S, Grandi F, Macchi V, De Caro R.* Tissue-engineered grafts from human decellularized extracellular matrices: a systematic review and future perspectives. *Int J Mol Sci*. 2018; 19 (12): 4117. doi: 10.3390/ijms19124117.
13. *Sevastianov VI, Basok YB, Kirsanova LA, Grigoriev AM, Kirillova AD, Nemets EA et al.* A comparison of the capacity of mesenchymal stromal cells for cartilage regeneration depending on collagen-based injectable biomimetic scaffold type. *Life*. 2021; 11 (8): 756. doi: 10.3390/life11080756.
14. *Song C, Luo Y, Liu Y, Li S, Xi Z, Zhao L et al.* Fabrication of PCL scaffolds by supercritical CO_2 foaming based on the combined effects of rheological and crystallization properties. *Polymers (Basel)*. 2020; 12 (4): 780. doi: 10.3390/polym12040780.
15. *Gil-Ramírez A, Rosmark O, Spégel P, Swärd K, Westergren-Thorsson G, Larsson-Callerfelt A.K et al.* Pressurized carbon dioxide as a potential tool for decellularization of pulmonary arteries for transplant purposes. *Sci Reports*. 2020; 10 (1): 4031. doi: 10.1038/s41598-020-60827-4.
16. *Alekseev ES, Alentiev AYu, Belova AS, Bogdan VI, Bogdan TV, Bystrova AV et al.* Supercritical fluids in chemistry. *Russ Chem Rev*. 2020; 89 (12); 1337–1427. [In Russ]. doi: 10.1070/RCR4932.
17. *Razgonova MP, Zakharenko AM, Sergievich AA, Kalenik TK, Golokhvast KS.* Sverxkriticheskie flyuidy': teoriya, e'tapy' stanovleniya, sovremennoe primenenie: uchebnoe posobie. SPb.: Lan', 2019; 192.
18. *Nemets EA, Malkova AP, Dukhina GA, Lazhko AE, Basok YB, Kirillova AD et al.* Effect of supercritical carbon dioxide on the in vivo biocompatible and resorptive properties of tissue-specific scaffolds from decellularized pig liver fragments. *Inorganic Materials: Applied Research*. 2022; 13: 413–420. doi: 10.1134/S2075113322020319.
19. *Ingrosso F, Ruiz-López MF.* Modeling solvation in supercritical CO_2. *Chemphyschem*. 2017; 18: 2560–2572. doi: 10.1002/cphc.201700434.
20. *Sevastianov VI, Nemets EA, Lazhko AE, Basok YuB, Kirsanova LA, Kirillova AD.* Application of supercritical fluids for complete decellularization of porcine cartilage. *Journal of Physics: Conference Series*. XV International Russian Chinese Symposium "New Materials and Technologies". 2019; 1347 (1): 012081. doi: 10.1088/1742-6596/1347/1/012081.
21. *Seo Y, Jung Y, Kim SH.* Decellularized heart ECM hydrogel using supercritical carbon dioxide for improved

angiogenesis. *Acta Biomater*. 2018; 67: 270–281. doi: 10.1016/j.actbio.2017.11.046.

22. *Nemets EA, Lazhko AE, Basok YuB, Kirsanova LA, Kirillova AD, Sevastianov VI.* Preparation of tissue-specific matrix from decellularized porcine cartilage. *Russian Journal of Physical Chemistry B*. 2020; 14: 1245–1251. doi: 10.1134/S1990793120080059.
23. *Huang Z, Godkin O, Schulze-Tanzil G.* The challenge in using mesenchymal stromal cells for recellularization of decellularized cartilage. *Stem Cell Rev Rep*. 2017 Feb; 13 (1): 50–67. doi: 10.1007/s12015-016-9699-8.
24. GOST ISO 10993-6. Izdeliya medicinskie. Ocenka biologicheskogo dejstviya medicinskix izdelij. Chast' 6. Issledovanie mestnogo dejstviya posle implantacii.
25. *Basok YB, Kirillova AD, Grigoryev AM, Kirsanova LA, Nemets EA, Sevastianov VI.* Fabrication of microdispersed tissue-specific decellularized matrix from porcine articular cartilage. *Inorganic Materials: Applied Research*. 2020; 11 (5): 1153–1159. doi: 10.1134/S2075113320050044.
26. *Crapo PM, Gilbert TW, Badylak SF.* An overview of tissue and whole organ decellularization processes. *Biomaterials*. 2011; 32: 3233–3243. doi: 10.1016/j.biomaterials.2011.01.057.

The article was submitted to the journal on 20.07.2022

DOI: 10.15825/1995-1191-2022-4-85-93

APOPTOTIC BONE MARROW-DERIVED MONONUCLEAR CELLS ACCELERATE LIVER REGENERATION AFTER EXTENDED RESECTION

N.A. Onishchenko[1], A.O. Nikolskaya[1], Z.Z. Gonikova[1], L.A. Kirsanova[1], M.Yu. Shagidulin[1, 2], V.I. Sevastianov[1]

[1] Shumakov National Medical Research Center of Transplantology and Artificial Organs, Moscow, Russian Federation

[2] Sechenov University, Moscow, Russian Federation

Objective: to compare the efficiency of regenerative processes in the liver using apoptotic bone marrow-derived mononuclear cells (BMMCs) and intact BMMCs from healthy animals on an extended liver resection (ELR) model. **Materials and methods.** Male Wistar rats (n = 77) with an ELR model (70–75%) were divided into 3 groups: group 1 (control with a single intraperitoneal injection of saline), group 2 (single intraperitoneal injection of unsorted intact BMMCs at a dose of 30–35 × 10^6, and group 3 (single intraperitoneal injection of apoptotic BMMCs at the same dose). Restoration of biochemical parameters of liver function and mass, as well as the emerging microstructural changes in hepatocytes in histological preparations, were monitored by assessing hepatocyte mitotic activity (MA) during the first 7–10 days after ELR. **Results.** It was found that in groups 2 and 3, as compared with group 1, there was no death after ELR modeling, and that the biochemical parameters of liver function normalized more rapidly (at days 10–14). Hepatocyte MA in group 3 sharply increased as early as on day 1, and mitotic index (MI) averaged 14‰, reaching 20.9‰ in some experiments; MI in the control group remained at the baseline by this time, while in group 2, MI was only 3.2‰. In group 3, liver mass recovered more rapidly after ELR to baseline values already at days 8–10, whereas the recovery was at day 12–14 and day 17–20 in group 2 and group 1, respectively. It was suggested that the more pronounced increase in the efficiency of regenerative processes in the liver after ELR in group 3 after using apoptotic BMMCs was due to the release from these cells of a large spectrum of formed paracrine factors, including various classes of RNA molecules involved in the regeneration process. **Conclusion.** Apoptotic BMMNCs have a more effective adaptive and regulatory potential than intact BMMCs because reorganizations are rapidly formed in the damaged liver cells, providing an early and more powerful activation of the targeted regenerative program.

Keywords: apoptotic bone marrow cells, regeneration, liver resection.

INTRODUCTION

It is known that damage to the liver and to other organs, triggers adaptive processes in them, which, in turn, activates evolutionarily programmed reparative regeneration mechanisms. Meanwhile, under severe chronic or extensive acute liver injury (under conditions when a significant mass of cells perishes), the remaining cells are forced to perform their functions with an increased load, which exceeds the evolutionarily programmed norm of cellular energy expenditure for these processes.

Under the created conditions, due to the developing energy deficit in liver cells, activation of the reparative regeneration mechanisms is sharply inhibited, which is believed to be a consequence of insufficient efficiency of adaptation processes, energetically supporting the regenerative process.

According to modern concepts, adaptive restructuring of metabolism in tissues begins with the development of cell autophagy processes in them [1–3]. Therefore, the initially reduced level of cell autophagy activity in an organ predetermines the low regenerative potential of the remaining cells and insufficient efficiency of regenerative processes [4–6]. To activate regenerative processes in the damaged organs, it was proposed to use hematopoietic and stromal cells derived from the bone marrow, which are known to have the highest regenerative potential in the body. However, the experience in clinical application of bone marrow-derived cells (BMDCs) turned out to be not so convincing and not always reproducible [7, 8], which forced researchers to start directly studying the mechanisms of induction of regenerative processes caused by BMDCs to increase the therapeutic efficiency of their use. A hypothesis on the determining regulatory role of apoptotic BMDCs producing paracrine factors in the state of apoptosis has been put forward [9]. The validity of this hypothesis has been subsequently proven [10] and repeatedly confirmed [11, 12]. By now, it has been established that it is the apoptotic cells that release

Corresponding author: Zalina Gonikova. Address: 1, Shchukinskaya str., Moscow, 123182, Russian Federation. Phone: (966) 188-33-33. E-mail: zalina3393@gmail.com

growth-stimulating signals in the form of nanovesicles [13], lipids [14], exosomes, various miRNAs, proteins [15] and other components called secretomes into the body. The result is not only an acceleration of regenerative processes in the body, but also an increase in their efficiency through immunomodulatory effects and blocking of inflammatory reactions [16, 17].

Existing ideas about the mechanisms of induction of regenerative processes suggest that in order to produce an effective regenerative response in cells in a damaged organ, the impact force of the adaptive stress signal should be high enough to enhance the severity of autophagy process and even reach the state of reversible apoptosis by cells, but should not exceed the evolutionarily programmed response, i.e. be physiological. Apoptotic BMDCs, which, as it has already been shown [11], support renewal and replenishment of the blood and immune system cell composition in the body, obviously possess such properties – adequate and physiological adaptogen.

The objective of this study is to investigate the possibility of increasing the regenerative activity of liver cells after extended resection by using apoptotic BMMCs of a healthy donor as an adaptive and regulatory stress signal.

MATERIALS AND METHODS

Work was carried out on male Wistar rats weighing 250–300 g (n = 77). The animals were kept in the vivarium at 18–20 °C on a mixed diet with free access to water. Experiments on animals were performed in the morning hours at room temperature (t = 22–24 °C), which excluded the influence of diurnal fluctuations in MA of liver cells. Relative humidity was 50–65%, lighting cycle was 12 hours; room air volume was changed ten times per hour. The animals were fed with standard compound feed for laboratory animals (microbiological status corresponded to GOST R 51849-2001 "Veterinary and sanitary standards and quality requirements for nonproductive animals"). Filtered tap water ad libitum was delivered in standard drinking bottles (microbiological status of water corresponded to SanPiN 2.1.4.1074-01 "Hygienic requirements for water quality in centralized drinking water supply systems"). Experiments and all manipulations with animals were performed according to the rules adopted by the European Convention for the Protection of Vertebrate Animals used for Experimental and other Scientific Purposes (ETS 123), Strasbourg, 1986).

The ability of apoptotic BMMCs to amplify regenerative signals and ensure their targeted delivery to the damaged liver tissue was studied in an ELR model (70–75%) in rats, which is accompanied by activation of hypertrophic regeneration mechanisms with marked hepatocyte MA in the remaining part of the organ [18].

Before the ELR modeling, the operated rats (n = 65) were anesthetized by diethyl ether inhalation, then the abdominal cavity was opened in compliance with aseptic and antiseptic rules, the liver was removed into the wound and ligatures were sequentially applied to the bases of medial, left lateral and right upper lobe of the liver, after which they were removed (70–75% of total liver mass). Surgery and subsequent studies were always performed between 10 and 12 hours, when the diurnal rhythm of MA in liver cells was minimal. In the early postoperative period, the operated animals always developed a clinical picture of acute liver failure.

To prove the possibility of enhancing the regenerative activity of cells in the damaged liver using apoptotic BMMCs, healthy rats without ELR were used as donors (n = 12). An unsorted mononuclear (hematopoietic) cell fraction was obtained from the bone marrow of these rats for subsequent administration to ELR rats at a dose of $30–35 \times 10^6$ cells. All animals after ELR were divided into 3 groups: Group 1 (control, n = 25, rats were injected once intraperitoneally with 1.0–1.5 ml of saline), Group 2 (n = 25, experimental, 1.5 ml of $30–35 \times 10^6$ freshly isolated intact BMMCs were injected intraperitoneally 3–5 hours after ELR modeling), and Group 3 (n = 25, experimental, 1.5 ml of $30–35 \times 10^6$ apoptotic BMMCs were injected intraperitoneally 3–5 hours after ELR modeling). Apoptotic BMMCs were obtained by incubating freshly isolated BMMCs in Custodiol ion-balanced preservative solution (Bretschneider's HTK-solution) at a temperature of 4–6 °C for 48 hours, because according to our studies [19], under the specified storage regimes, the content of apoptotic BMMCs – (cell secretomes) in the state of early reversible apoptosis was significantly expressed and reached 44.8 ± 0.9%, while the content of apoptotic BMMCs in the state of late irreversible apoptosis in the cell pool did not exceed 2–8% ($p < 0.02$).

The dynamics of restoration of hepatic homeostasis in rats after injection of ELR and BMMCs (intact and apoptotic) were studied using standard methods on biochemistry analyzer Arik-test (Germany) according to the content of total protein and bilirubin in the blood serum in the early postoperative period (within 14 days). We also measured the activity of hepatic cytolysis enzymes: alanine aminotransferase (ALT), aspartate aminotransferase (AST) and alkaline phosphatase (ALP). We evaluated the rate of overcoming the critical mass of the liver residue and its recovery to baseline values after ELR within 20–22 days. For this purpose, we weighed the resected part of the liver in each operated animal immediately after ELR, which was taken as 70% of the total liver mass, and then the initial liver mass was calculated for each animal on the basis of the weighing results. Then, the remaining liver was explanted at each study period, its mass was determined by weighing, and the values obtained were compared with the calculated initial liver mass for the given animal.

The degree of severity of ELR induction effect on regenerative processes in the liver during modeling of critical injury (group 1), as well as changes in the nature

of regenerative processes in the liver after ELR against the background of introduction of intact BMMCs (group 2) and apoptotic BMMCs (group 3) were determined quantitatively by degree of changes in the microstructural state of liver cells in histological preparations. For this purpose, in groups 1, 2 and 3, we studied hepatocyte MA in the liver remnant at 24, 36, 48 and 72 hours, as well as on day 5, 7 and 10 after ELR. The liver was dissected on these time points and histological specimens stained with hematoxylin and eosin. We performed histological analysis of the preparations (Leica DM microscope, Germany), and measured the number of dividing hepatocytes in 30 fields of view, followed by calculation of MI in ppm (‰).

Significance of difference between the studied parameters in the compared groups was assessed using the parametric Student's t-test at $p < 0.05$.

RESULTS

A comparative study of the recovery of liver homeostasis in the 3 groups showed that in the control group 1, 5 out of 25 rats died within the first 5 days after liver resection (20% mortality). In experimental groups 2 and 3 (administration of intact BMMCs (n = 25) and apoptotic BMMCs (n = 15), respectively), there were no dead animals during the entire follow-up period. The absence of mortality in these groups was accompanied by a higher rate of recovery of hepatic homeostasis in the body, which was expressed in an early normalization of total protein and cytolytic enzymes (ALT, AST and ALP) in the blood serum compared with group 1.

Cytolysis indicators in groups 2 and 3 rats, as in group 1, increased during the first 3 days, but then in group 3, they stabilized more sharply than in group 2 and recovered by day 10–14. The reduced level of total protein after ELR in these groups also recovered by the end of the follow-up period (14 days), while in the control group, normalization of all studied parameters did not occur by the end of the observation period. The higher rate of recovery of hepatic homeostasis in groups 2 and 3 compared with the control can be down to the higher activity of restorative and proliferative processes in the cells of the remaining part of the liver, which was due to the introduction of intact BMMCs and apoptotic BMMCs. Indeed, a comparative study of hepatocyte MA in the liver after ELR in all three studied groups revealed a rapid increase in hepatocyte MA in comparison with the initial level (MI was 0.2–0.3‰ before ELR). At the same time, the rate of development and the severity of the rise of MA in groups 2 and 3 were higher than in the control group (Fig. 1).

So, in group 1 (control), MI reached a maximum of 5.378‰ (36 mitoses per 6,653 cells) at 48 hours after ELR. In group 2, MI at 48 hours was 6.11‰ (60 mitoses per 8,448 cells) with a maximum of 10.5‰ at 72 hours (93 mitoses per 8,858 cells). In group 3, MI reached a maximum as early as 24 hours after ELR modeling. On average, it was 14‰ (135 mitoses per 9,762 cells), but in some experiments, MI reached 20.9‰. Thus, it follows from the maximum MI values in the three studied groups that apoptotic BMMCs increase hepatocyte MA almost 1.5-fold in comparison with intact BMMCs administration and almost 3-fold increase in hepatocyte MA in comparison with the control. It is important to note that apoptotic BMMCs not only intensify, but also accelerate the realization of their regulatory effect (as early as 24 hours after ELR modeling) compared to the control and the use of freshly isolated BMMCs. This fact may be due to the fact that immediately after introduction of apoptotic BMMCs into the body, they facilitate delivery and production of a complex of numerous growth-stimulating signal molecules and regulatory factors already formed in apoptotic cells [20], which provide early intensive activation of regenerative and proliferative processes in the lesion site. The maximal high and early activation of hepatocyte MA in liver tissue after ELR modeling and application of apoptotic BMMCs is also demonstrated in Fig. 2.

It can be seen (see Fig. 2) that at 24 hours, only in group 3 with apoptotic BMMCs (Fig. 2, d) that early and maximum activation of hepatocyte MA occurred, whereas in experiments with freshly isolated intact BMMCs (see Fig. 2, c), MA was just beginning to intensify. In the control with saline (Fig. 2, b), MA was totally absent at this time point, but maximally intensified only at 48 hours. Moreover, in the liver cells of groups 2 and 3 rats, signs of diffuse fine vacuolar degeneration of hepatocytes appeared 24 hours after ELR modeling, which is known [21] to be a morphological marker of the developing cellular autophagy. At the same time, the greatest expression of hepatic cell autophagy (Fig. 3) was

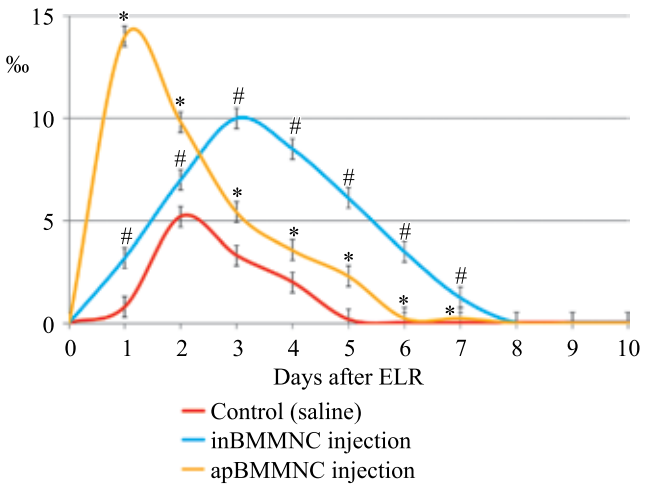

Fig. 1. Changes in mitotic index in hepatocytes in the liver of rats after ELR (‰) in 3 experimental groups. *, $p < 0.05$ compared to control; #, $p < 0.05$ compared to injection of apoptotic BMMCs

observed at 48 hours in group 3 (apoptotic BMMCs). See Fig. 3, d.

Morphological study of the liver confirms a more pronounced ability of apoptotic BMMCs compared to intact BMMCs to stimulate adaptive changes in cells at the initial stages after damage for optimal energy restructuring of metabolism in cells and early start of repair and mitotic processes in the damaged organ [2].

Another confirmation of a more pronounced inductive effect of apoptotic BMMCs on regenerative processes in the liver as compared to intact BMMCs is the dynamics of liver mass recovery in the three studied groups of animals with ELR modeling (Fig. 4).

The most accelerated rate of liver mass recovery (see Fig. 4) was observed in group 3, where apoptotic BMMCs were injected intraperitoneally in a dose of 30–35 × 10^6 cells 3–5 hours after ELR. Liver mass in this group was restored on days 8–10. Injection of intact BMMCs in the same dose in group 2 also accelerated reparative processes in the resected liver remnant, liver mass restoration to the initial values in this group occurred on day 12–14, i.e. the recovery occurred at a slower pace. In group 1 (control), restoration of liver mass after injection of saline occurred on day 17–20. Earlier we showed [22] that intraperitoneal administration of total RNA, obtained from freshly isolated intact BMMCs at 30 μg/100 g mass, also intensified the regenerative activity of rat liver cells after ELR modeling. The regenerative response of the liver to administration of total RNA from intact BMMCs was higher than that to the administration of freshly isolated intact BMMCs. So, when total RNA from intact BMMCs was injected, the MI at 48 hours was 23.4‰, and when intact BMMCs were injected, MI at 48 hours was 6.96‰, and liver mass recovery occurred on days 10–12 and 14–18 respectively. Similarity in the direction and higher efficiency of regulation of recovery processes at administration of total RNA from both freshly isolated intact BMMCs and apoptotic BMMCs as compared to freshly isolated intact BMMCs suggests the following mechanism. In the process of isolation of total

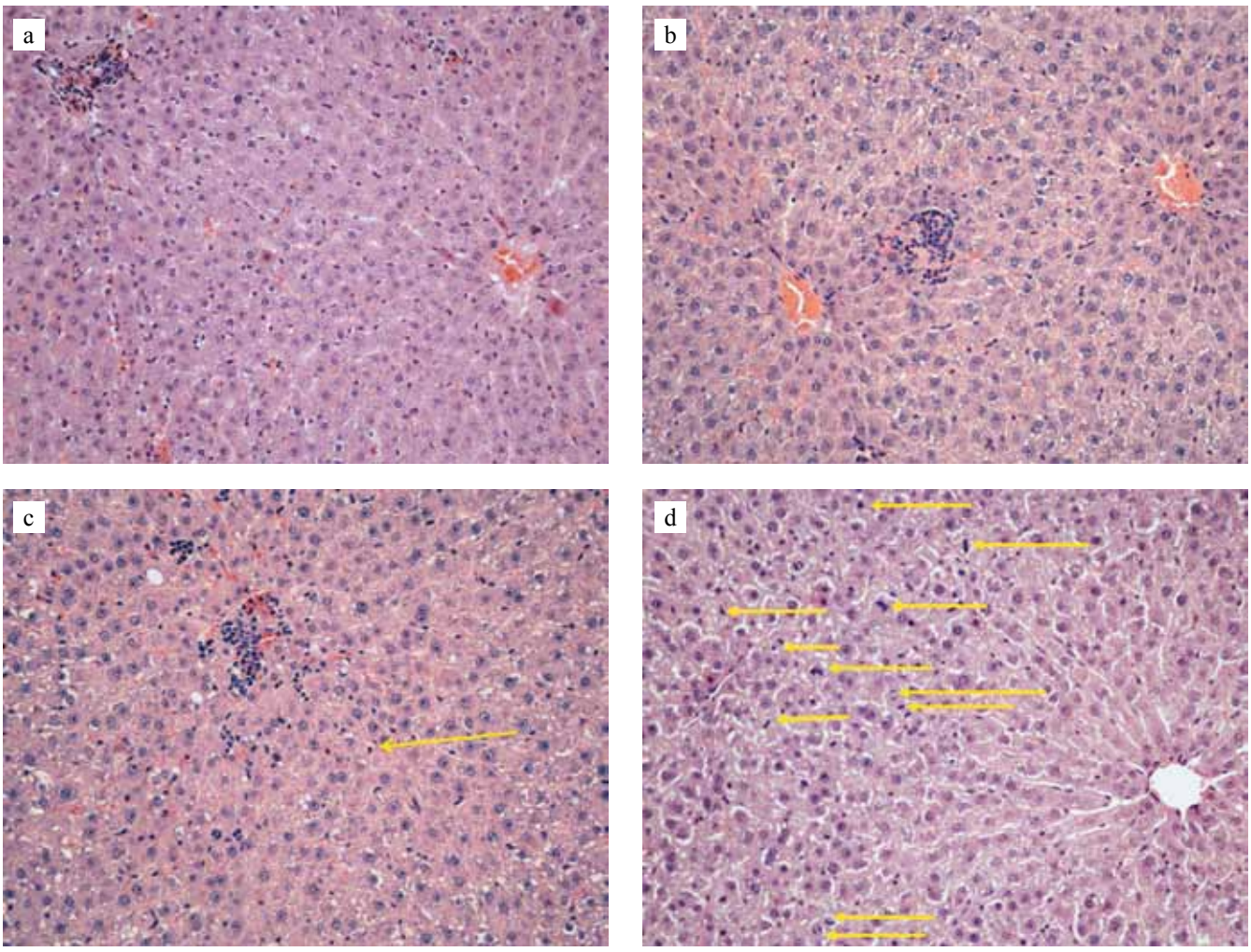

Fig. 2. Hepatocyte mitotic activity in rat liver before and 24 hours after ELR and injection of BMMCs: a, baseline (before ELR); b, group 1 (control), saline injection; c, group 2, injection of intact BMMCs; d, group 3, injection of apoptotic BMMCs. Arrows indicate hepatocytes at different stages of mitosis. H&E stain, 200× magnification

RNA from intact BMMCs, these cells are also exposed to apoptosis. Cell apoptosis is known to promote the ability of such cells to produce numerous and diverse paracrine factors, including various types of RNA and microRNA [9, 15]. The accumulating paracrine factors of apoptotic cells additionally exert a powerful stress-regulatory effect on repair processes in the damaged organs.

The results obtained, in our opinion, suggest that apoptotic BMMCs, introduced into the body against the background of ELR, act as an adequate evolutionarily engineered adaptogen within a non-specific adaptation syndrome of cellular systems. This adaptogen is designed to incorporate and optimize the survival reserves of cells in the damaged organ, by abrupt and accelerated switching of evolutionarily programmed mechanisms of cell death (such as autophagy and reversible apoptosis) to cell proliferation. The possibility of existence of such switching mechanisms in cells in a co-activated state has been discussed [23, 24].

CONCLUSION

In the early stages after ELR modeling, apoptotic BMMCs and freshly isolated intact BMMCs enhance mitotic activity in liver cells in comparison with the control (administration of saline). However, the severity of enhancement of the activation effect on liver cell proliferation when using apoptotic BMMCs is significantly higher than when using intact BMMCs. With intraperitoneal injection of apoptotic BMMCs, MI reaches its maximum values at 24 hours, whereas with intact BMMCs – only at 72 hours.

Early vacuolization of hepatocyte cytoplasm in the liver after ELR modeling, which is a morphological marker of cell autophagy and reflects activation of the evolutionarily programmed process of their adaptation to damage, develops in all groups of experiments at 24 hours, but more intensively at 48 hours. Early vacuolization was more pronounced in group 3 (apoptotic BMMCs) than in group 2 (intact BMMCs) and group 1

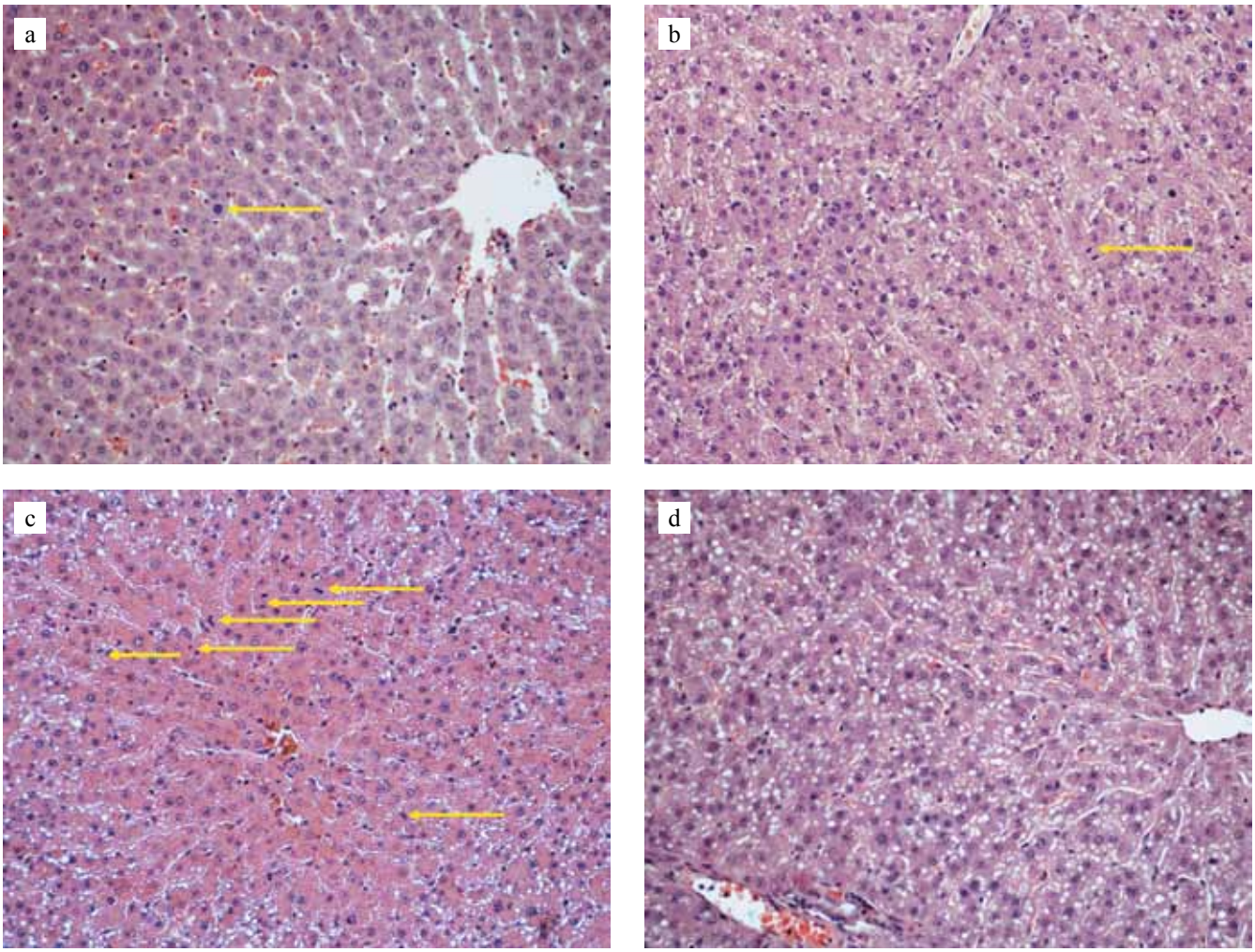

Fig. 3. Histological structure of the rat liver before and 48 hours after ELR modeling and BMMNC injection. Changes in hepatocyte morphology: a, baseline (before ELR), b, group 1 (control), saline injection; c, group 2, injection of intact BMMCs; d, group 3, injection of apoptotic BMMCs. Arrows indicate hepatocytes at different stages of mitosis. H&E stain, 200× magnification

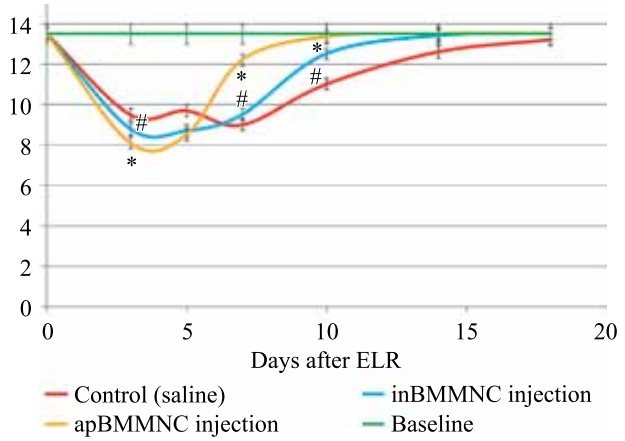

Fig. 4. Recovery of rat liver mass after extended resection in 3 experimental groups: with saline injection, with injection of intact BMMCs and with injection of apoptotic BMMCs (in grams). *, $p < 0.05$ compared to control; #, $p < 0.05$ compared to injection of apoptotic BMMCs

(saline), indicating the higher regulatory capabilities of apoptotic BMMCs.

Apoptotic and intact BMMCs provide targeted transmission of regenerative signals to the resected liver and accelerate its regenerative process. However, the rate of acceleration of reparative processes and the timing of restoration of the liver mass to its initial values for apoptotic BMMCs were higher (day 8–10) than for intact BMMCs (day 12–14) and saline (day 18–20).

All of the above suggests that apoptotic BMMCs, due to their acquisition of a more powerful regulatory stress-induced potential, unlike intact BMMCs, have more pronounced adaptive and regulatory properties that create a stronger foundation in the body for implementation of a targeted and more effective regeneration program. Higher intensity of the adaptive effect of apoptotic BMMCs due to the release of numerous and diverse paracrine factors (including various types of RNA) promotes early and more effective activation of autophagy processes in liver cells after ELR. This induces distinct increase in regenerative activity and increases the rate of recovery of resected liver mass to initial values.

The authors declare no conflict of interest.

REFERENCES

1. *Lin CW, Chen YS, Lin CC, Chen YJ, Lee PH, Kuo PL et al.* Amiodarone as an autophagy promoter reduces liver injury and enhances liver regeneration and survival in mice after partial hepatectomy. *Sci Rep.* 2015 Oct 30; 5: 15807. doi: 10.1038/srep15807.
2. *Cheng Y, Wang B, Zhou H, Dang S, Jin M, Shi Y et al.* Autophagy is required for maintenance of liver progenitor cell functionality. *Cell Physiol Biochem*. 2015; 36 (3): 1163–1174. https://doi.org/10.1159/000430287.
3. *Lv H, Fan X, Wang L, Feng H, Ci X.* Daphnetin alleviates lipopolysaccharide/d-galactosamine-induced acute liver failure via the inhibition of NLRP3, MAPK and NF-κB, and the induction of autophagy. *Int J Biol Macromol*. 2018 Nov; 119: 240–248. doi: 10.1016/j.ijbiomac.2018.07.101.
4. *Oami T, Watanabe E, Hatano M, Teratake Y, Fujimura L, Sakamoto A et al.* Blocking liver autophagy accelerates apoptosis and mitochondrial injury in hepatocytes and reduces time to mortality in a murine sepsis model. *Shock*. 2018 Oct; 50 (4): 427–434. https://doi.org/10.1097/shk.0000000000001040.
5. *Shen Y, Malik SA, Amir M, Kumar P, Cingolani F, Wen J et al.* Decreased Hepatocyte Autophagy Leads to Synergistic IL-1β and TNF Mouse Liver Injury and Inflammation. *Hepatology*. 2020 Aug; 72 (2): 595–608. doi: 10.1002/hep.31209.
6. *Ruart M, Chavarria L, Campreciós G, Suárez-Herrera N, Montironi C, Sergi Guixé-Muntet et al.* Impaired endothelial autophagy promotes liver fibrosis by aggravating the oxidative stress response during acute liver injury. *J Hepatol*. 2019 Mar; 70 (3): 458–469. doi: 10.1016/j.jhep.2018.10.015.
7. *Carvalho AB, Quintannilha LF, Dias AS et al.* Bone marrow multipotent mesenchymal stem cells do not reduce fibrosis or improve function in a rat model of severe chronic liver injury. *Stem Cells*. 2008; 26: 1307–1314. https://doi.org/10.1126/science.284.5411.143.
8. *Dai LJ, Li HY et al.* The therapeutic potential of bone marrow-derived mesenchymal stem cells on hepatic cirrhosis. *Stem Cell Res*. 2009; 2 (1): 16–25. https://doi.org/10.1016/j.clinbiochem.2007.04.017.
9. *Thum T, Bauersachs J, Poole-Wilson PA, Volk HD, Anker SD.* The dying stem cell hypothesis: immune odulation as a novel mechanism for progenitor cell therapy in cardiac muscle. *J Am Coll Cardiol*. 2005; 46: 1799–1802. https://doi.org/10.1016/j.jacc.2005.07.053.
10. *Ankersmit HJ, Hoetzenecker K, Dietl W et al.* Irradiated cultured apoptotic peripheral blood mononuclear cells regenerate infarcted myocardium. *Eur J Clin Invest*. 2009; 39: 445–456. https://doi.org/10.1111/j.1365-2362.2009.02111.x.
11. *Beer L, Mildner M, Gyöngyösi M, Ankersmit HJ.* Peripheral blood mononuclear cell secretome for tissue repair. *Apoptosis*. 2016; 21: 1336–1353. doi 10.1007/s10495-016-1292-8.
12. *Gnecchi M, Danieli P, Malpasso G, Ciuffreda MC.* Paracrine mechanisms of mesenchymal stem cells in tissue repair. *Methods Mol Biol*. 2016; 1416: 123–146. https://doi.org/10.1007/978-1-4939-3584-0_7.
13. *Sirois I, Raymond MA, Brassard N et al.* Caspase-3-dependent export of TCTP: a novel pathway for antiapoptotic intercellular communication. *Cell Death Differ*. 2011; 18: 549–562. https://doi.org/10.1038/cdd.2010.126.
14. *Huang Q, Li F, Liu X et al.* Caspase 3-mediated stimulation of tumor cell repopulation during cancer radiotherapy. *Nat Med*. 2011; 17: 860–866. https://doi.org/10.1038/nm.2385.

15. *Beer L, Zimmermann M, Mitterbauer A et al.* Analysis of the secretome of apoptotic peripheral blood mononuclear cells: impact of released proteins and exosomes for tissue regeneration. *Sci Rep*. 2015; 5: 16662. https://doi.org/10.1038/srep16662.
16. *Gray M, Miles K, Salter D, Gray D, Savill J.* Apoptotic cells protect mice from autoimmune inflammation by the induction of regulatory B cells. *Proc Natl Acad Sci USA*. 2007; 104: 14080–14085. https://doi.org/10.1073/pnas.0700326104.
17. *Zhang M, Xu S, Han Y, Cao X.* Apoptotic cells attenuate fulminant hepatitis by priming Kupffer cells to produce interleukin-10 through membrane-bound TGF-β. *Hepatology*. 2011; 53: 306–316. https://doi.org/10.1002/hep.24029.
18. *Yel'chaninov AV, Fatkhudinov TKh*. Regeneratsiya pecheni mlekopitayushchikh: Mezhkletochnyye vzaimodeystviya. M.: Nauka, 2020; 126.
19. *Onishchenko NA, Fomenko EV, Nikolskaya AO, Gonikova ZZ, Shagidulin MYu, Balyasin MV et al.* Activation of regenerative processes in the liver when using cell-bone marrow total RNA. *Russian Journal of Transplantology and Artificial Organs*. 2020; 22 (3): 134–142. https://doi.org/10.15825/1995-1191-2020-3-134-142.
20. *Korf-Klingebiel M, Kempf T, Sauer T et al.* Bone marrow cells are a rich source of growth factors and cytokines: implications for cell therapy trials after myocardial infarction. *Eur Heart J*. 2008; 29: 2851–2858. https://doi.org/10.1093/eurheartj/ehn456.
21. *Potapnev MP.* Autophagia, apoptosis, cell necrosis and immune recognition of their and someone else's. *Immunology*. 2014; 2: 95–102.
22. *Gonikova ZZ, Nikolskaya AO, Kirsanova LA, Shagidulin MYu, Onishchenko NA, Sevastianov VI.* The comparative analysis of the effectiveness of stimulation of liver regeneration by bone marrow cells and total RNA of these cells. *Russian Journal of Transplantology and Artificial Organs*. 2019; 21 (1): 113–121. (In Russ.) https://doi.org/10.15825/1995-1191-2019-1-113-121.
23. *Gazizov IM, Gumerova AA, Kiyasov AP.* Apoptosis in regenerative histogenesis of the liver after partial hepatectomy in rats. *Genes and cells*. 2015; 10 (3): 22–26. eLIBRARY ID: 26280345.
24. *Budd RC*. Death receptors coupe to both cell proliferations and apoptosis. *J Clin Jnvest.* 2002 Fev 15; 109 (4): 437–442. doi: 10.1172/JCI15077.

The article was submitted to the journal on 08.07.2022

DOI: 10.15825/1995-1191-2022-4-94-108

TISSUE-ENGINEERED VASCULAR PATCHES: COMPARATIVE CHARACTERISTICS AND PRECLINICAL TEST RESULTS IN A SHEEP MODEL

L.V. Antonova[1], A.V. Mironov[1], A.R. Shabaev[1], V.N. Silnikov[2], E.O. Krivkina[1], V.G. Matveeva[1], E.A. Velikanova[1], E.A. Senokosova[1], M.Yu. Khanova[1], V.V. Sevostyanova[1], T.V. Glushkova[1], R.A. Mukhamadiyarov[1], L.S. Barbarash[1]

[1] Research Institute for Complex Issues of Cardiovascular Diseases, Kemerovo, Russian Federation
[2] Institute of Chemical Biology and Fundamental Medicine, Novosibirsk, Russian Federation

Carotid endarterectomy (CEA) with patch angioplasty is the most effective treatment for carotid artery stenosis. However, the use of existing vascular patches is often associated with thrombosis, restenosis, calcification and other complications. **Objective:** to develop biodegradable patches for arterial reconstruction, containing vascular endothelial growth factor (VEGF) or arginyl-glycyl-aspartic acid (RGD), and comparatively evaluate their biocompatibility and efficacy in in vitro experiments and during preclinical trials in large laboratory animal models. **Materials and methods.** Biodegradable patches, made from a mixture of poly(3-hydroxybutyrate-co-3-hydroxyvalerate (PHBV) and poly(ε-caprolactone) (PCL), were fabricated by electrospinning and modified with VEGF or the peptide sequence RGD in different configurations. In in vitro experiments, the surface structure, physicomechanical and hemocompatibility properties were evaluated. In in vivo experiments, we evaluated the effectiveness of the developed vascular patches for 6 months after implantation into the carotid artery of 12 sheep. The quality of remodeling was assessed using histological and immunofluorescence studies of explanted specimens. **Results.** The PHBV/PCL/VEGF patches had physicomechanical characteristics closer to those of native vessels and their biofunctionalization method resulted in the smallest drop in strength characteristics compared with their unmodified PHBV/PCL counterparts. Modification with RGD peptides reduced the strength of the polymer patches by a factor of 2 without affecting their stress-strain behavior. Incorporation of VEGF into polymer fibers reduced platelet aggregation upon contact with the surface of the PHBV/PCL/VEGF patches and did not increase erythrocyte hemolysis. At month 6 of implantation into the carotid artery of sheep, the PHBV/PCL/VEGF patches formed a complete newly formed vascular tissue without signs of associated inflammation and calcification. This indicates the high efficiency of the VEGF incorporated into the patch. In contrast, the patches modified with different configurations of RGD peptides combined the presence of neointimal hyperplasia and chronic granulomatous inflammation present in the patch wall and developed during bioresorption of the polymer scaffold. **Conclusion.** PHBV/PCL/VEGF patches have better biocompatibility and are more suitable for vascular wall reconstruction than PHBV/PCL/RGD patches.

Keywords: vascular patch, tissue engineering, poly(3-hydroxybutyrate-co-3-hydroxyvalerate, poly(ε-caprolactone), vascular endothelial growth factor, RGD peptides, biodegradable polymers, endothelization.

INTRODUCTION

Cardiovascular diseases are the major cause of death and disability globally. Atherosclerosis remains the leading cause, which results in the formation and enlargement of atheromatous plaque, disrupting blood flow to the tissues. Atherosclerotic internal carotid artery (ICA), leading to carotid stenosis, causes 10–15% of all strokes [1].

CEA and carotid stenting are the main surgical treatments for carotid stenosis [2]. In turn, CEA is the gold standard for surgical treatment and prevention of acute stroke, demonstrating significant advantage in asymptomatic and symptomatic patients with high degree of ICA stenosis [2]. However, the presence of prolonged plaques makes it difficult to perform this procedure by the standard and most frequently used method – eversion carotid endarterectomy (eCEA). Therefore, surgeons are forced to resort to closure of the arteriotomy access using a patch [3, 4].

To date, a large number of papers with comparative results of carotid artery reconstruction using biological and synthetic patches have been published. Ren S. and colleagues found no difference in mortality, stroke and restenosis rates in CEA with venous patch versus

Corresponding author: Larisa Antonova. Address: 6, Sosnovy Boulevard, Kemerovo, 650002, Russian Federation. Phone: (905) 906-04-51. E-mail: antonova.la@mail.ru

synthetic patch material, or in CEA with Dacron patch versus polytetrafluoroethylene (PTFE) patch [5]. However, mean operative time was significantly longer with PTFE or Dacron patch due to prolonged hemostasis for suture line bleeding, whereas in the case of carotid angioplasty with biological material (xeno-pericardial), a significant reduction in suture line bleeding was noted. At the same time, the use of synthetic patches is associated with infection and thrombosis, while xeno-pericardial patch is associated with a high risk of calcification [5].

A recent meta-analysis of eight randomized control trials assessing the effectiveness of PTFE, Dacron and bovine pericardium patches, found no significant differences in a wide range of complications, including stenosis in the long-term period [6].

According to Russian authors, the incidence of perioperative strokes in the group with arterial plasty by xenopericardium was 1.5%, and ischemic strokes in the early postoperative period was 0.26%; these complications were not identified in the group with PTFE patches [7]. In the long-term follow-up, the incidence of hemodynamically significant ICA restenosis over 70% was higher when PTFE patches were used (31.2%) than when xeno-pericardial flaps were used (9.8%).

Tissue-engineered vascular patches can help avoid the problems encountered with existing materials by restoring the implant site's own tissues. To achieve such a result, the biodegradable matrix should have high biocompatibility, ensure migration of cells into the thickness of the material, their proliferation and differentiation. At the same time, the need for rapid formation of endothelial monolayer from autologous cells on the inner surface of the patches required finding ways to stimulate this process. A number of works have shown that VEGF has a great potential in stimulating endothelialization and vascular regeneration based on tissue-engineered matrices [8, 9]. Being the main angiogenic growth factor, VEGF stimulates migration and survival of endothelial cells as well as recruitment of progenitor cells from the bloodstream [10, 11].

Peptides with the RGD sequence are present in most extracellular matrix proteins. The RGD sequence can be considered a common integrin-binding motif [12]. Nevertheless, the affinity for endothelial cells makes RGDs ideal agents for modifying tissue-engineered constructs contacting with blood and requiring early surface endothelialization. Both peptide sequences obtained during extraction from natural material and artificially synthesized ones can be used for modification. The latter have a number of advantages: the risk of immune response and infection that can be associated with an insufficient degree of purification of the natural material, is reduced. When comparing the functional properties of natural RGD-containing proteins and their artificial counterparts, the latter proved to be more effective [13].

Thus, the currently used patches cannot fully meet the needs of vascular surgery, due to, among other reasons, the lack of functional activity in terms of formation of new vascular tissue on their base. Therefore, the issue of selecting a patch that would meet all the requirements necessary to reduce the risk of complications in the early and late postoperative periods remains relevant.

The **objective** of the study is to develop biodegradable patches for arterial reconstruction containing VEGF or RGD, and comparatively evaluate their biocompatibility and efficacy in in vitro experiments and in preclinical trials in large laboratory animal models.

MATERIALS AND METHODS

1. Fabrication of biodegradable patches with VEGF

Polymeric matrices were fabricated by emulsion electrospinning on a Nanon-01A machine (MECC CO, Japan) according to the protocol described earlier [14]. A mixture of 5% PHBV (Sigma-Aldrich, USA) and 10% PCL (Sigma-Aldrich, USA) in trichloromethane in a 1 : 2 ratio was prepared. Then, VEGF (Sigma-Aldrich, USA) diluted in a saline solution to a 10 μg/mL concentration was added to the polymer solution in a 20 : 1 ratio. Emulsion electrospinning was performed under the following parameters: 20 kV voltage, 0.5 mL/h feed rate, 200 rpm manifold rotation speed, 15 cm distance to the collector, and 22G needle. A metal pin with a diameter of 8.0 mm was used as the manifold. Before removal from the pin, the matrix was cut lengthwise and removed with peeling movements.

Unmodified patches, made by electrospinning from PHBV/PCL polymer mixture in trichloromethane in a 1 : 2 ratio, were used as the control group. Used as the comparison group was xeno-pericardial flap KemPeriplas-Neo (NeoCor, Russia), which is currently actively used in the clinic as a vascular patch during carotid endarterectomy.

2. Assessment of VEGF distribution during incorporation into biodegradable PHBV/PCL patches

To assess the expected distribution pattern of VEGF injected into the polymer solution in a liquid phase, an analog technique was used to incorporate fluorochrome-labeled bovine serum albumin (BSA) into the PHBV/PCL matrix. For this purpose, PHBV/PCL solution in chloroform was mixed with a BSA-Texas Red® solution (Invitrogen, USA) in phosphate-buffered saline (10 μg/mL) in a 20 : 1 ratio. Electrospinning was performed at 20 kV, a feed rate of 0.5 mL/h, and a microscopy slide was used as the manifold. The obtained specimens were examined on an Axio Imager A1 microscope (Carl Zeiss, Germany) using a BP 546/12 – FT 580 – LP 590 light filter.

3. Fabrication of biodegradable patches with RGD and detection of arginine-rich peptides on the patch surface

Polymer matrices were fabricated by electrospinning on a Nanon-01A machine (MECC CO, Japan) according to the protocol described previously [15].

Before modification with RGD peptides, oil and dust residues were removed from the surface of PHBV/PCL matrices using a 1 : 1 mixture of 2-propanol and water with further washing with deionized water. To activate the polymer surfaces, the matrices were treated with 10% ethylenediamine (EDA) dissolved in 2-propanol at 37 °C for 1 hour. The matrices were then washed thoroughly with 0.3% Tween-20 solution in deionized water and air dried.

Then, in accordance with the previously described technique, primary modification of the patch surface with amino groups was performed using 4,7,10-trioxa-1,13-tridecanediamine (Sigma-Aldrich, USA) as a linker group [16]. The PHBV/PCL patch surface was further modified using RGD containing peptides produced by NanoTech-S (Russia): RGDK (P1), AhRGD (P2), c[RGDFK] (P3) [16]. Thus, 3 varieties of RGD-modified patches were obtained: PHBV/PCL/P1, PHBV/PCL/P2, and PHBV/PCL/P3.

The method for determining the presence of arginine-rich peptides was performed according to the Saccucci method [17]. Arginine/aspartic acid solution (1 mg/mL in deionized water) was used as the positive control. The reference values were taken from Sedaghati et al. [18]. Orange-red staining of the sample indicated the presence of the guanidinium group characteristic of arginine.

4. Assessment of the surface structure of vascular patches before and after implantation into the carotid artery of sheep

Before implantation, specimens of PHBV/PCL, PHBV/PCL/VEGF, PHBV/PCL/RGD, and KemPeriplas-Neo patches 0.5 × 0.5 cm in size were subjected to gold-palladium sputtering to obtain a 15 nm coating using an EM ACE200 sputtering system (Leica Mikrosysteme GmbH, Austria) and studied on a scanning electron microscope S-3400N (Hitachi, Japan) under high vacuum conditions at an accelerating voltage of 10 kV.

5. Physical and mechanical testing of vascular patches

Specimens of unmodified and modified patches (n = 6 in each group) were cut longitudinally. The mechanical properties of the PHBV/PCL/VEGF and PHBV/PCL/RGD vascular patches were evaluated under uniaxial tension conditions on a universal testing machine (Zwick/Roell, Germany) according to the procedure described earlier [14]. Strength and stress-strain properties were evaluated using a transducer with a nominal force of 50 N and a crosshead travel speed of 10 mm/min during the test. The strength of the material was evaluated by the maximum tensile stress (MPa). Elasticity and stiffness of the material were evaluated by relative elongation corrected for specimen fracture behavior (%) and Young's modulus (MPa). To measure the thickness of the specimens, a thickness gauge with a ±0.01 mm error limit (measuring force not more than 1.5 N) was used. The carotid artery of a sheep and the human internal thoracic artery (A. mammaria) were used as controls. Human A. mammaria segments were taken during coronary artery bypass surgery from patients who signed an informed consent for the material to be taken. Xeno-pericardial flap KemPeriplas-Neo (NeoCor, Russia) and unmodified PHBV/PCL specimens were used as comparison groups. The specimens were cut out longitudinally.

6. Assessment of hemocompatibility of the patches

To assess the hemocompatibility of the developed patches, we studied erythrocyte hemolysis and platelet aggregation after fresh citrate blood and platelet-rich plasma had come in contact with the patch surfaces. The studies were performed according to the methods described in [19].

7. Implantation of biodegradable vascular patches into the carotid artery of sheep

A series of experiments was carried out on Edilbay sheep, weighing 42–45 kg. All the animals were non-pregnant females. The animals were operated on sequentially. When performing experimental studies, we were guided by the requirements of order No. 1179 of the USSR Ministry of Health, dated October 10, 1983, and order No. 267 of the Russian Ministry of Health dated June 19, 2003 "Rules for handling experimental animals", principles of the European Convention (Strasburg, 1986) and the World Medical Association Declaration of Helsinki about humane treatment of animals (1996). The work was approved by the local ethics committee of the Research Institute for Complex Issues of Cardiovascular Diseases (protocol No. of September 11, 2018).

Biodegradable vascular patches PHBV/PCL/VEGF (n = 3), PHBV/PCL/P1 (n = 3), PHBV/PCL/P2 (n = 3), and PHBV/PCL/P1 (n = 3) were implanted into the carotid artery of sheep. Patch size was 40.0 × 4.0 mm. Follow-up after implantation lasted for 6 months.

Anesthesia: Premedication: Xylazine (Xylanit) 0.05–0.25 mL per 10 kg of animal weight + atropine 1 mg IM. Induction anesthesia: 5–7 mg of propofol per 1 kg of animal weight; within 90 seconds after that, atracurium besylate (Ridelat) is administered at IV dose of 0.5–0.6 mg/kg. Tracheal intubation with a 9.0 endotracheal tube. Anesthesia maintenance: Sevoran 2–4 vol%,

Ridelat was administered by continuous infusion at a rate of 0.3–0.6 mg/kg/h.

Monitoring: blood pressure (BP), heart rate (HR), blood oxygen saturation (SpO_2). Artificial ventilation: Respiratory rate (RR) 12–15/min, PEEP 7–9 mbar, tidal volume (TV) 6–8 ml/kg, FiO_2 – 40–60%.

Main stage: Carotid artery access; systemic heparinization – 5000 IU IV; carotid artery clamping, longitudinal carotid incision 40 mm long, implantation of 40 × 4 mm vascular patches with separate knotty sutures using Prolene 6/0 thread (Ethicon, USA). Standard protocol for prevention of air embolism and triggering of blood flow; wound closure with Vicril 2.0 suture (Ethicon, USA); suture treatment with BF glue, enoxaparin sodium subcutaneously 4000 anti-Ha IU/0.4 ml; extubation.

Intraoperative drug administration: infusion of 0.9% NaCl 500 ml – IV drip; Axetine (cefuroxime) 1.5 g – IV drip.

Postoperative medical management: antibiotic therapy (Axetine (cefuroxime) 1.5 g – IM/m twice daily + enoxaparin sodium subcutaneously 4000 anti-Ha IU/0.4 ml for 5 days. With proven vascular patency with implanted patches: clopidogrel 75 mg orally once daily + sodium heparin 5000 IU subcutaneously twice daily).

Postoperative ultrasound screening of the patched vessels patency was performed after 1 and 5 days, then once every 3 months up to the expected date of animal withdrawal from experiment.

8. Histological study of explanted specimens of biodegradable vascular patches

The explanted vascular patch specimens with surrounding carotid artery sections were divided into 2 parts. One part was frozen at –140 °C for subsequent immunofluorescence study. The second part was used for histological study using H&E, Van Gieson and Alizarin red S stains, which were described earlier [14].

After each type of staining, all specimens were examined by light microscopy using an AXIO Imager A1 microscope (Carl Zeiss, Germany) at 50×, 100×, and 200× magnifications.

9. Immunofluorescence study of explanted specimens of biodegradable vascular patches

From frozen sections of explanted vascular patches, serial 8 μm thick cryosections were made using a cryotome (Thermo Scientific, USA). The preparations were fixed in 4% paraformaldehyde solution for 10 minutes. Before staining for intracellular markers, the sections were permeabilized with Triton-X100 solution (Sigma-Aldrich, USA) for 15 minutes. They were then stained with primary antibodies in the following combinations: rabbit anti-CD31 antibodies (Abcam, UK) and mouse anti-alpha smooth muscle actin antibody (α-SMA, Abcam, UK); rabbit anti-von Willebrand factor (vWF, Abcam, UK); rabbit anti-collagen type IV antibody (Abcam, UK) and mouse anti-collagen type I antibody (Abcam, UK); rabbit anti-collagen type III antibody (Novus Biologicals, USA).

The sections were incubated with antibodies overnight at 4 °C, then with goat secondary antibodies to rabbit IgG conjugated with Alexa Fluor 488-conjugated (Thermo Fisher, USA), and goat antibodies to mouse IgG conjugated with Alexa Fluor 555-conjugated (Thermo Fisher Scientific, USA) for 1 hour at room temperature. At all stages of staining, phosphate-buffered saline with the addition of 0.1% Tween (Sigma-Aldrich, USA) was used for intermediate washing of the sections.

To remove autofluorescence, the sections were treated with Autofluorescence Eliminator Reagent (Millipore, USA) according to the manufacturer's procedure. Nuclei were contrasted using DAPI staining (10 μg/mL, Sigma-Aldrich, USA) for 30 minutes. Stained preparations were incubated under a coverslip using ProLong mounting medium (Thermo Fisher, USA). The preparations were analyzed using a scanning laser microscope LSM 700 confocal microscope (Carl Zeiss, Germany).

10. Statistical data processing

Data were analyzed using Prism (Graph Pad Software). Normality of distribution was assessed by Kolmogorov–Smirnov test. Mann–Whitney U test was used to compare two independent groups. When comparing three or more independent groups, the nonparametric Kruskal–Wallis H test was used; when the groups were compared in pairs, the Dunn's test was used. Differences were considered significant at significance level $p < 0.05$. Data are presented as median and 25th and 75th percentiles of Me (25%; 75%).

RESULTS

To manufacture biodegradable vascular patches with VEGF, emulsion electrospinning was used, which can be used to introduce bioactive molecules into a polymer fiber composition, which can then be controlled and stably released from the matrix in the process of its resorption [20–22].

To assess the expected distribution pattern of VEGF injected into the polymer solution in a liquid phase, we performed an analog experiment with BSA labeled with Texas Red and incorporated into the PHBV/PCL matrix. Fig. 1 (a, b) shows that aqueous domains with BSA-Texas Red are evenly distributed in the thickness of polymer fiber along its entire length. At the same time, the fiber structure was not violated.

Modification of PHBV/PCL biodegradable patches made by electrospinning with RGD peptides was performed to biofunctionalize the inner surface of patches in order to attract and fully adhere mature and progenitor

endothelial cells and form an endothelial monolayer. Tripeptide RGD was chosen as a modifying agent because it is a cell adhesion site and is present in the structure of most natural extracellular matrix proteins. Three configurations of RGD were obtained by chemical synthesis: RGDK (linear configuration of the molecule, Arg-Gly-Asp-Lys sequence), AhRGD (linear configuration of the molecule, Ah-Arg-Gly-Asp sequence and c[RGDFK] (cyclic configuration of the molecule, c[Arg-Gly-Asp-Phe-Lys] sequence).

L-lysine, which contains two amino groups (-NH_2) and one carboxyl group (-COOH), and is used for surface modification of various materials to improve their adhesive properties and biocompatibility, was used in synthesis of linear RGDK molecule [23]. During the synthesis of linear molecule AhRGD, a synthetic analogue of L-lysine, aminocaproic acid (Ah), was added to the basic adhesive tripeptide RGD. Aminocaproic acid is used in medical practice as an antifibrinolytic drug because of its ability to inhibit fibrinolysis. Cyclic configurations of RGD with constant geometry of the molecule, according to literature data, are able to demonstrate maximum affinity to cellular receptors in comparison with their linear analogues [24]. Therefore, the cyclic RGD peptide c[RGDFK] was the third type of RGD used for surface modification of vascular patches.

Previously, we proved that the linker length significantly affects the availability of RGD peptides for cellular receptors; therefore, in this work, extended hydrophilic linker 4,7,10-trioxa-1,13-tridecanediamine [16] was used for aminolysis of the PHBV/PCL matrix surface. RGD peptide was injected using a cross-linking reagent. The presence of peptides on the polymer surface was confirmed using the Sakaguchi test for the presence of arginine (Fig. 1, c) [17]. After covalent attachment of RGD peptide, the light-yellow staining did not disappear after washing the PHBV/PCL/RGD polymer patch specimens. The light-yellow staining of unmodified PHBV/PCL patches that did not contain RGD on their surface disappeared when washed (Fig. 1, c).

Structural features of patches

Scanning electron microscopy (SEM) of the surface of biodegradable vascular patches was compared with xeno-pericardial patch KemPeriplas-Neo (Neocor, Kemerovo), which is actively used in the clinic during endarterectomy of internal carotid arteries. The preservation of the native architectonics of the xeno-pericardial flap, which consisted in relief due to the tortuosity of collagen fibers, was shown. High density of collagen fibers caused the absence of pores.

SEM of polymer patch surface before implantation into the vascular bed showed that all biodegradable specimens, both unmodified and those containing VEGF or RGD, had a highly porous structure and consisted

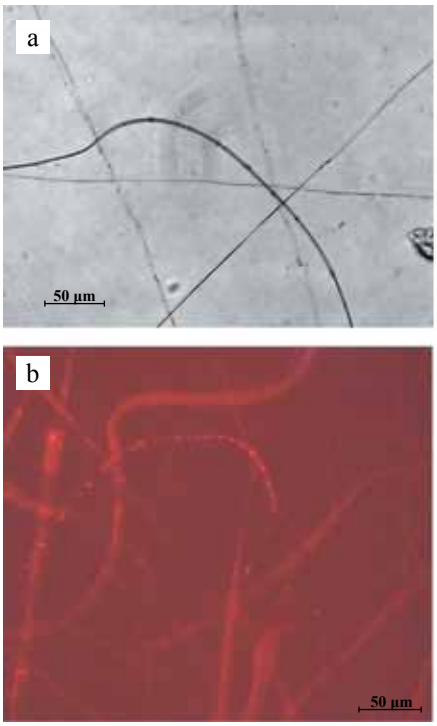

c

RGD type	Scaffold – PHBV/PCL Linker – 4,7,10-trioxa-1,13-tridecanediamine
RGDK	
AhRGD	
c[RGDFK]	
PHBV/PCL without RGD	

Fig. 1. Test results confirming the incorporation/attachment of bioactive peptides into the structure/to the matrix surface. a, b, incorporation of fluorescein-labeled BSA into the PHBV/PCL scaffold during emulsion electrospinning: a, light microscopy (400× magnification); b, fluorescence microscopy (400× magnification); c, results of RGD peptide detection on the surface of PHBV/PCL scaffold obtained using Sakaguchi test

of micro-sized multidirectional fibers (Fig. 2). The PHBV/PCL/VEGF fibers were 1.47 ± 0.67 μm in diameter, which was 1.8-fold smaller than for PHBV/PCL/RGD and unmodified PHBV/PCL (2.64 ± 1.14 μm; $p < 0.05$), which is associated with the use of emulsion electrospinning to make patches with VEGF.

Additional modification using RGD did not change the architectonics of the patch surface (Fig. 2).

Mechanical properties of patches

Mechanical test results demonstrate that the strength of the PHBV/PCL/VEGF patches was 1.7-fold lower than that of the PHBV/PCL patches that did not contain VEGF ($p < 0.05$) (Table 1). However, the strength of PHBV/PCL/VEGF patches was fully consistent with that of the human internal thoracic artery and 1.9-fold greater than that of sheep carotid artery. The force applied to the

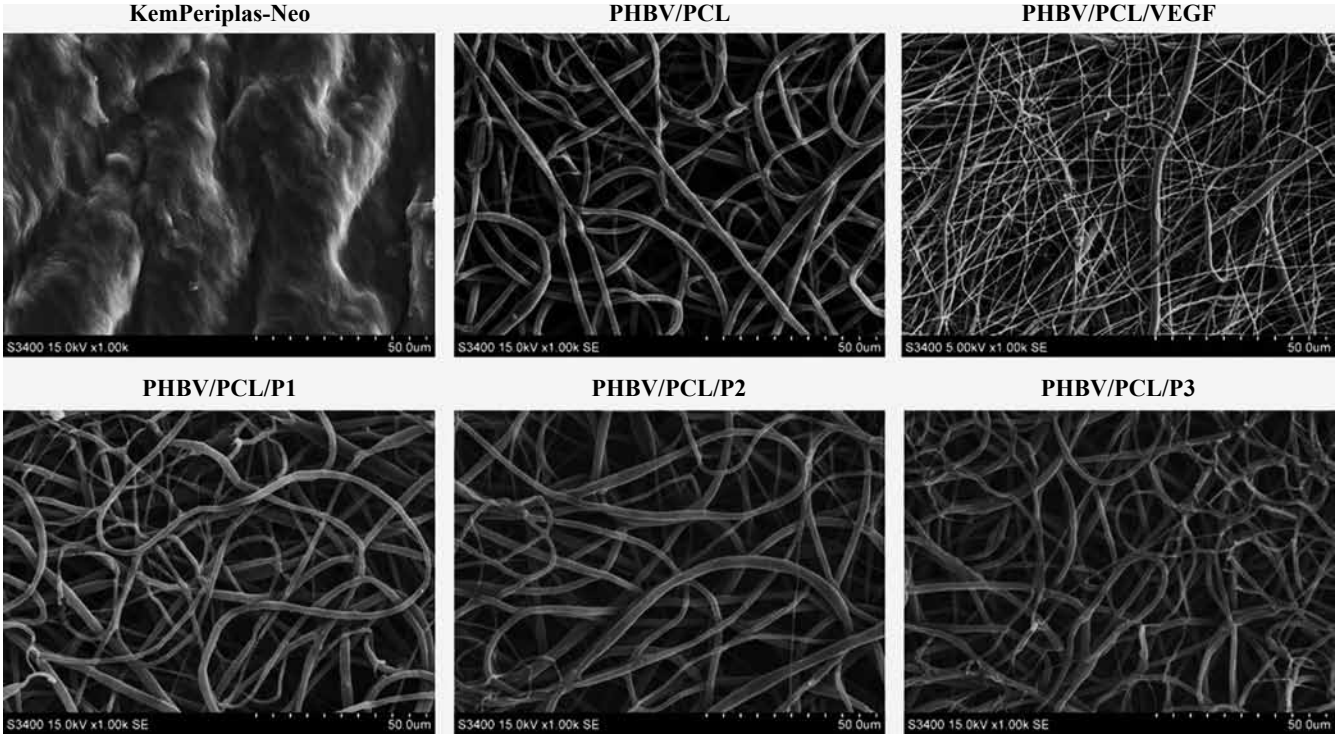

Fig. 2. Morphology of the inner surface of vascular patches PHBV/PCL, PHBV/PCL/VEGF, PHBV/PCL/RGD and xeno-pericardial patch KemPeriplas-Neo. Scanning electron microscopy, 1000× magnification

Table 1

Physicomechanical properties of PHBV/PCL polymer patches before and after VEGF incorporation or RGD modification in comparison with the KemPeriplas-Neo flap and a. mammaria. Data are presented as Me (25–75%)

	Voltage (MPa)	F_{max} (N)	Relative elongation (%)	Young's modulus (MPa)	Sample thickness (mm)
PHBV/PCL	3.9 (2.88–4.5)*/**▪	3.0 (2.59–3.3)*/**▪	102.7 (79.37–106.3)*/**▪	21.8 (19.2–25.2)*/**▪	0.4 (0.35–0.5)*
PHBV/PCL/VEGF	2.25 (2.14–2.6)**#▪	1.97 (1.82–2.3)*#▪	81.83 (77.0–103.4)*/**	16.9 (15.5–17.5)*/**▪	0.43 (0.4–0.5)*
PHBV/PCL /RGD	1.2 (1.12–1.3)*# ▪	1.3 (1.2–1.4)#•	102.6 (80.38–144.1)*/**▪	21.8 (20.15–23.9)*/**▪	0.5 (0.49–0.5)*
Sheep carotid artery	1.2 (1.06–1.9)*	1.01 (0.88–1.42)	158.5* (126.0–169.5)	0.49* (0.39–0.66)	0.25 (0.23–0.3)
Human a. mammaria	2.48 (1.36–3.25)**	0.92 (0.59–1.72)	29.72 (23.51–39.62)**	2.42 (1.87–3.19)**	0.27▪ (0.24–0.3)
KemPeriplas-Neo	10.06 (9.12–21.38)*/**#	15.4 (12.6–26.2)*/**#	64.96 (61.08–72.6)*/**#	1.11 (1.02–1.34)#	0.69 (0.63–0.7)*

*, $p < 0.05$ versus A. mammaria; **, $p < 0.05$ versus sheep carotid artery; #, $p < 0.05$ versus PHBV/PCL; ▪, $p < 0.05$ versus KemPeriplas-Neo.

specimen before it began to break was 2.1-fold higher in the PHBV/PCL/VEGF patches than in a. mammaria, 1.9-fold higher than in the sheep carotid artery, and 1.5-fold lower than in the PHBV/PCL specimens ($p < 0.05$). The differences in performance between PHBV/PCL/VEGF and PHBV/PCL may be related to the fact that aqueous domains with the growth factor within the fiber create additional points that are unable to withstand load. These are points where polymer filament is more likely to damage, leading to reduced strength and less force required to break.

We also did not observe a significant change in relative elongation in polymer patches after injection of the growth factor compared to unmodified counterparts (Table 1). Introduction of VEGF reduced the stiffness of the polymer matrix by 1.3-fold ($p < 0.05$).

A preliminary study of the physical and mechanical properties of biodegradable patches, whose surface was modified with various RGD-containing peptides, found no significant intergroup differences. Therefore, to further compare the physical and mechanical parameters of modified patches with unmodified ones, xeno-pericardial flap and native human and sheep vessels, all specimens of patches modified with RGD peptides were combined into one group – PHBCV/PCL/RGD.

It was found that the strength of PHBV/PCL/RGD was identical to that of sheep carotid, but was 2-fold lower than that of a. mammaria ($p < 0.05$). The force exerted on the specimen before destruction in PHBV/PCL/RGD patches did not differ from that of native vessels but was 1.5-fold lower than in PHBV/PCL/VEGF patches and 2.3-fold lower than in unmodified PHBV/PCL, ($p < 0.05$), (Table 1). The relative elongation of all biodegradable patches did not differ among themselves but was, on average, 3.2-fold higher than that of a. mammaria, 1.5-fold higher than that of xeno-pericardial patches, and 1.7-fold lower than that of sheep carotid, ($p < 0.05$). The Young's modulus of unmodified patches and PHBV/PCL/RGD patches was 44-fold higher than that of sheep carotid artery, 9-fold higher than that of a. mammaria, 19.6-fold higher than that of xeno-pericardial flap, and 1.3-fold higher than that of the PHBV/PCL/VEGF specimens ($p < 0.05$).

All biodegradable vascular patches, regardless of the modification method, were significantly less strong and stiffer than the xeno-pericardial flap, as indicated by such indicators as stress, force and Young's modulus (Table 1). However, KemPeriplas-Neo differed significantly in its physical and mechanical characteristics from a. mammaria and sheep carotid artery as well (Table 1). Thus, the stress and force applied to the specimen before its destruction was 4-fold and 16.7-fold higher in xenopericardium than in a. mammaria, and 8.4-fold and 15.2-fold higher than in sheep carotid artery ($p < 0.05$). At the same time, the Young's modulus of KemPeriplas-Neo was 2.6-fold lower than that of internal thoracic artery and 2.3-fold lower than that of the sheep carotid artery, although the xeno-pericardial flap was 2.6-fold thicker than the wall thickness of the native vessels ($p < 0.05$).

Thus, the PHBV/PCL/VEGF patches had physicomechanical characteristics closer to those of native vessels; their biofunctionalization technique resulted in the least drop in strength characteristics relative to the unmodified PHBV/PCL counterparts. Modification of RGD reduced the strength of polymer patches without affecting their stress-strain behavior.

Table 2

Degree of hemolysis and maximum aggregation of human blood platelets after contact with PHBV/PCL polymer patches before and after VEGF incorporation or RGD modification in comparison with xeno-pericardial flap KemPeriplas-Neo

Sample type	Degree of RBC hemolysis (%)	Maximum platelet aggregation (%)
	Me (25–75%)	Me (25–75%)
PHBV/PCL	0.5 (0–1.01)*	87.23 (83.95–89.84)*▪
PHBV/PCL/VEGF	0.5 (0–1.01)*	81.35 (81.01–88.51)*
PHBV/PCL/RGD	0.72 (0–0.72)*	86.15 (82.24–87.43)*▪
KemPeriplas-Neo	**2.12 (0.9–3.95)**	**93.32 (84.24–96.42)▪**
Intact platelet-rich plasma	–	**74.65 (72.45–75.31)**

*, $p < 0.05$ versus KemPeriplas-Neo flap; ▪, $p < 0.05$ versus intact platelet-rich plasma.

Outcomes of hemolysis

The degree of hemolysis after contact with the VEGF-, RGD- modified patch, and unmodified PHBV/PCL patches was 0.5%, 0.72%, and 0.5%, respectively, without statistically significant differences (Table 2), thus confirming them to be highly hemocompatible [25].

The level of hemolysis after contact with the surface of the KemPeriplas-Neo flap was 3-fold higher than that after contact of red blood cells with the surface of biodegradable patches, but did not go beyond the acceptable values [25].

Outcomes of platelet aggregation

The results of the study showed that platelet aggregation activity upon contact with the surface of the PHBV/PCL and PHBV/PCL/RGD patches was 1.2-fold greater than that of intact platelet-rich plasma (PRP), ($p < 0.05$), (Table 2). Maximum platelet aggregation after contact with PHBV/PCL/VEGF specimens was the lowest among all biodegradable specimens.

The contact of platelets with the surface of the KemPeriplas-Neo flap revealed the most significant increase in the maximum aggregation up to 93.32 (84.24; 96.42) %, which was 1.3-fold higher than the maximum aggregation of platelets from intact PRP, ($p < 0.05$). There was no significant difference between the xenogeneic pericardial flap and PHBV/PCL patches before and after VEGF or RGD modification (Table 2).

Therefore, the PHBV/PCL/VEGF and PHBV/PCL/RGD polymer patches caused a lower degree of hemolysis and platelet aggregation than the KemPeriplas-Neo flap.

Outcomes of implantation of biodegradable vascular patches into sheep carotid artery

We previously studied the biocompatibility and efficacy of patches with VEGF and various RGD configurations in a comparative aspect with unmodified PHBV/PCL patches and KemPeriplas-Neo xeno-pericardial flaps in a rat model [14, 16]. Biodegradable patches demonstrated ease of implantation. Throughout the experiment, no bleeding and or violation of the integrity of the implants were noted. It was proved that after 12 months of implantation, vessels that were prosthetized with PHBV/PCL/VEGF had 100% patency and no neointimal hyperplasia. A mature endothelial monolayer on the inner surface of PHBV/PCL/VEGF patches was fully formed after 3 months, whereas on the unmodified PHBV/PCL patches, only after 12 months. Remodeling of the patches was accompanied by repopulation by cells with the formation of an extracellular matrix.

With long-term implantation of PHBV/PCL/RGD patches into the aorta of rats, it has been proven that elements of new vascular tissue can be formed on their basis: both migration of cellular elements into the thickness of the patch and formation of neointimal lining with an endothelial layer from the side of vessel lumen occur, especially when patches are modified with peptides P3 and P1 [16].

PHBV/PCL polymer patches modified with VEGF or RGD experienced slight calcinosis at 12 months of implantation in rat aorta. At the same time, PHBV/PCL/VEGF and PHBV/PCL/P1 patches demonstrated maximum resistance to calcification.

KemPeriplas-Neo xeno-pericardial flaps, on their basis, were unable to support the development of new vascular tissue and endothelial layer, and were prone to calcification already after one month of implantation into rat aorta. After 12 months of implantation of KemPeriplas-Neo flaps, massive deposition of crystalline calcium in 100% of the implanted flaps and delamination of their wall, which led to shape deformation, were detected. Also after 12 months of implantation, 50% of the xeno-pericardial flaps showed neointimal hyperplasia, whose thickness was almost 3-fold greater than that of rat aortic wall [14, 16].

Tests on the rat model confirmed the low efficiency and biocompatibility of xeno-pericardial flaps and insufficient ability of unmodified PHBV/PCL to form a new vascular tissue on its base. Therefore, only PHBV/PCL/VEGF, PHBV/PCL/P1, PHBV/PCL/P2, and PHBV/PCL/P3 patches were included in the protocol of preclinical trials in sheep.

The sheep model was used to implant the developed vascular patches, which is optimal for in vivo testing of cardiovascular implants, as it is suitable for worst-case modeling due to the increased tendency of their vessels to calcification and blood to hypercoagulation. Therefore, the use of the sheep model allows for the most rigorous testing of vascular prostheses, including their degeneration in vivo [26–30]. In addition, sheep are considered an optimal animal model for assessment of growth, permeability, endothelialization, thromboresistance and post-implant imaging of products for cardiovascular surgery.

It is known that the high porosity of tissue-engineered matrix and nanosized fibers in its structure can provide cell migration inside the matrix and early endothelization of its surface due to the similarity of the surface structure to that of natural extracellular matrix and a larger area of interaction between cells and artificial matrix [31–33]. In its turn, effective infiltration of cells into the thickness of the porous material promotes its better integration with native tissues at the implantation site.

Two sheep (with implanted PHBV/PCL/P1 and PHBV/PCL/P2 patches) did not survive to the expected date of withdrawal from experiment, dying at 14 days due to formation of massive paravasal hematomas around the operated vessels. Most likely, this was due to microdamage in the patch wall in response to pulse wave after implantation, since no bleeding from the suture areas was detected immediately after implantation and hemostasis was achieved within 2 minutes.

All sheep with implanted PHBV/PCL/VEGF and PHBV/PCL/P3 patches survived to the expected withdrawal date. During six months of follow-up, the vessels with implanted patches maintained their patency. No aneurysmal dilatation of the vessels in the implanted patch site was detected. However, all vessels with RGD patches showed increased blood flow velocity, which may be an indirect reflection of vessel lumen narrowing.

According to the results of morphological examination (histological study and scanning electron microscopy) of the patches with vascular endothelial growth factor, we can see that after 6 months of implantation into sheep carotid artery, a complete three-layer newly-formed vascular tissue was formed on the basis of these patches (Fig. 3).

Thin neointima, covered by a layer of endothelium-like cells on the vessel lumen side, lined the entire inner surface of the patches. The bulk of the neointima consisted of smooth muscle cells. Next came the patch itself. There were processes of visible biodegradation of the

polymer matrix accompanied by disruption in its integrity, visible only by specimen microscopy. The PHBV/PCL/VEGF patch was filled with cellular elements (macrophages, fibroblast-like and smooth muscle cells, few foreign-body giant cells), permeated with bundles of collagen fibers. There were vasa vasorum in the patch

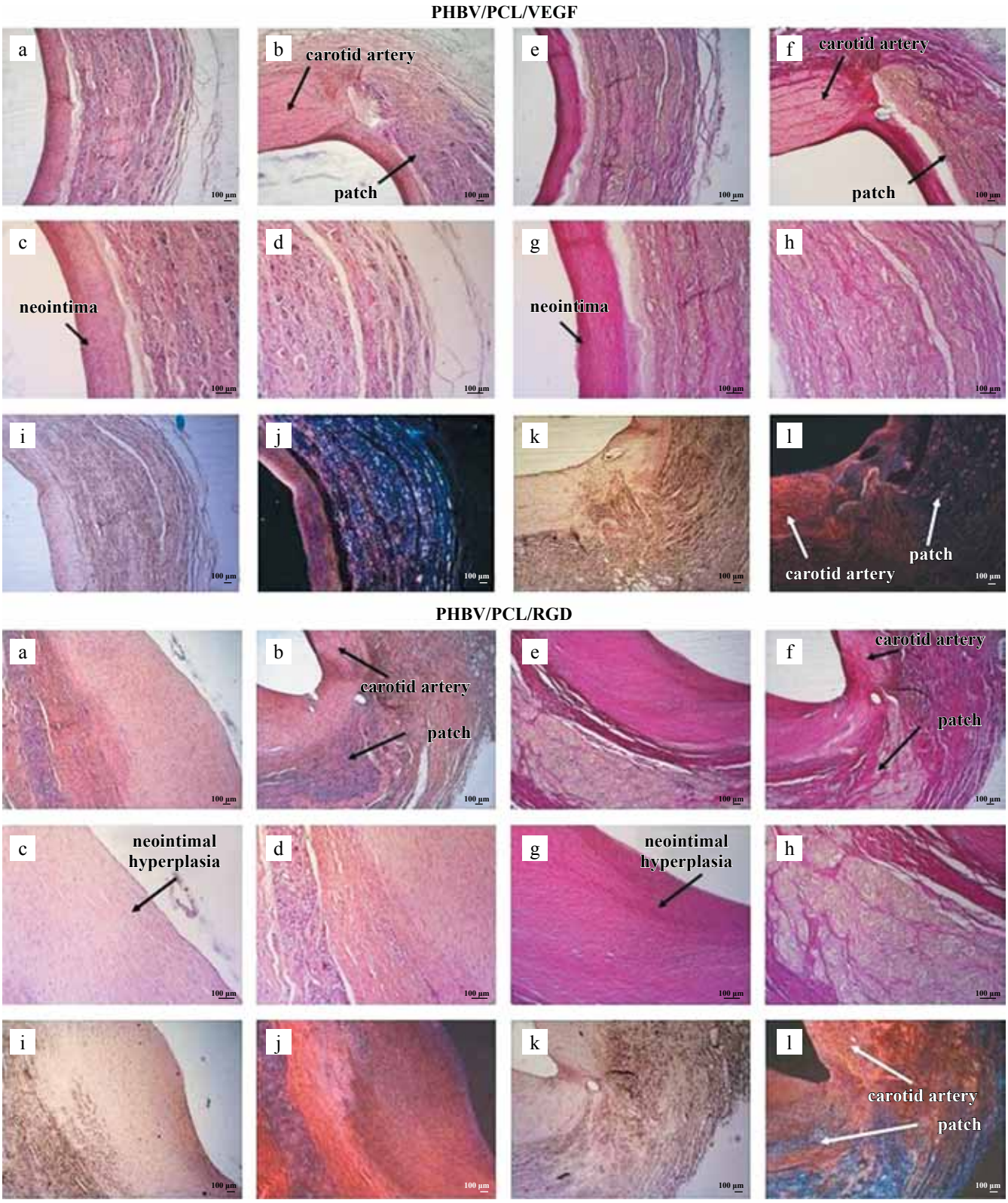

Fig. 3. Results of histological examination of PHBV/PCL/VEGF and PHBV/PCL/RGD vascular patches at month 6 of implantation into sheep carotid artery: a–d, H&E stain; e–h, Van Gieson's stain; i–l, Alizarin Red S stain (i, k, light microscopy; j, l, fluorescent microscopy); a, e, i, j, central part of the patch; b, f, k, l, junction of the patch and carotid artery in the anastomosis zone; c, e, inner and middle layer of the patch wall; d, h, middle and outer layer of the patch wall. a, b, e, f, i–l, 50× magnification; c, d, g, h, 100× magnification

thickness. External layer of the patches contained all structural elements characteristic of natural adventitial layer: collagen fibers, fibroblasts and fibrocytes, single foreign-body giant cells, lymphoid follicles and vasa vasorum. There were no signs of calcification (Fig. 3).

When studying the histological pattern of explanted specimens of PHBV/PCL/RGD patches, we obtained a similar picture – all the specimens had neointimal hyperplasia (Fig. 3). The neointima thickness corresponded to the thickness of the wall of the patch itself. The neointima surface facing the vessel lumen was covered by a cell monolayer. The walls of the patches were partially resorbed and contained a moderate number of foreign-body multinucleated giant cells. Macrophages, smooth muscle and fibroblast-like cells, and bundles of collagen fibers were also present in the patch walls; vasa vasorum were formed (Fig. 3).

Histological examination (Alizarin Red S staining) showed that there was no calcium deposition in the explanted PHBV/PCL/RGD patches (Fig. 3).

The large extent of the implanted patches made it possible to perform slices during immunofluorescence study such that the carotid artery wall, into which the patch was implanted, was opposite the patch (Fig. 4). This arrangement led to better visualization of the similarity of the new vascular tissue formed on the basis of the patches within 6 months of their implantation with the native sheep carotid artery. The neointima formed on the inner surface of the PHBV/PCL/VEGF patches was proved to consist of smooth muscle cells, as evidenced by the presence of alpha actin in the cells (Fig. 4). On the vessel lumen side, the neointima was lined by mature CD31+ endothelial cells secreting von Willebrand factor vWF+ throughout its entire length (Fig. 4). Type IV collagen formed a basal membrane on which endothelial cells were located and was detected in large numbers both in the patch wall thickness and in the sheep carotid artery wall. Type III collagen was formed throughout the patch thickness with a predominant concentration at the basal membrane and in the neointima (Fig. 4).

Thus, on the basis of the biodegradable VEGF patch, after 6 months of its implantation into sheep carotid arteries, a complete new vascular tissue was formed. The exception was elastin, which was not detected either after patch implantation into the rat aorta or after patch implantation into sheep carotid arteries. Nevertheless, incorporated VEGF promoted harmonization of tissue formation processes in situ without signs of chronic granulomatous inflammation, neointimal hyperplasia, and calcification.

Immunofluorescence study of the explanted PHBV/PCL/RGD patches revealed the same structural ele-

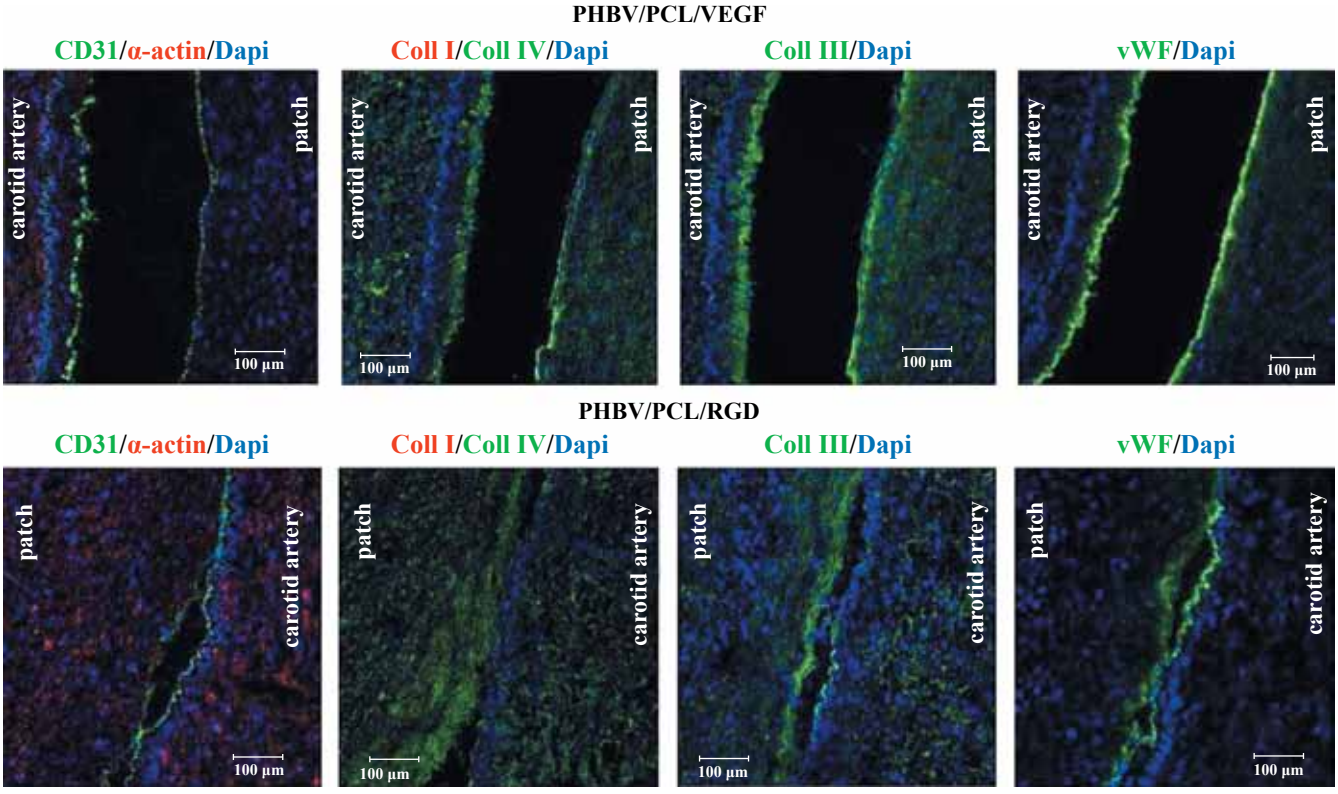

Fig. 4. Results of immunofluorescence study of explanted PHBV/PCL/VEGF and PHBV/PCL/RGD patches with surrounding sections of the sheep carotid artery: CD31/alpha actin/Dapi panel: mature endothelial cells (green glow), smooth muscle and other cells containing alpha actin (red glow); panel Coll I/Coll IV/Dapi: collagen type I (red glow), collagen type IV (green glow); Coll III/Dapi panel: collagen type III (green glow); vWF/Dapi panel: von Willebrand factor (green glow). The nuclei of all cells were stained with Dapi nuclear dye (blue glow). 100× magnification

ments of the new vascular tissue as in the PHBV/PCL/VEGF patches: endothelial monolayer consisting of CD31+vWF+ mature endothelial cells; type I, III and IV collagen (Figure 4). However, what draws attention is the higher number of smooth muscle cells in the neointima and high total cellularity of the patch wall due to the presence of chronic granulomatous inflammation, as well as the lower number of type III collagen relative to PHBV/PCL/VEGF patches (Fig. 4).

CONCLUSION

The efficacy of using pro-angiogenic growth factor VEGF and various configurations of RGD peptides, as well as different approaches to modifying the product, was evaluated in a comparative aspect in vitro and in preclinical tests on a sheep model.

The identified advantage of PHBV/PCL/VEGF biodegradable patches was that incorporation of VEGF into the patch during manufacturing by emulsion electrospinning and the absence of subsequent surface modification manipulations with aggressive surfactants resulted in preservation of physical and mechanical characteristics of the patches, without reducing strength and or increasing rigidity of the final product, as observed after modifying the surface of the biodegradable patches with RGD peptides. The hemocompatibility of PHBV/PCL/VEGF patches proved to be the highest even in comparison with the xeno-pericardial flap that is actively used in the clinic.

In the sheep model, patches with RGD, regardless of the peptide configuration, promoted endothelialization, but provoked neointimal hyperplasia and granulomatous inflammation, whereas the PHBV/PCL/VEGF patches in the sheep model demonstrated optimal ability to form a healthy new vascular tissue on their basis, with the formation of thin neointima lined with endothelium, middle smooth muscle layer and adventitia containing all the basic structural elements characteristic of this layer: bundles of collagen fibers, fibroblast-like cells and vasa vasorum. All this testifies to the high efficiency of the vascular endothelial growth factor incorporated into patches.

The research was carried out within the framework of the fundamental theme No. 0419-2022-0001 of the Research Institute for Complex Issues of Cardiovascular Diseases "Molecular, cellular and biomechanical mechanisms of pathogenesis of cardiovascular diseases in the development of new methods of treatment of cardiovascular diseases based on personalized pharmacotherapy, introduction of minimally invasive medical devices, biomaterials and tissue-engineered implants".

The authors declare no conflict of interest.

REFERENCES

1. *Bonati LH, Dobson J, Featherstone RL, Ederle J, van der Worp HB, de Borst GJ, Mali et al.* Long-term outcomes after stenting versus endarterectomy for treatment of symptomatic carotid stenosis: the international carotid stenting study (ICSS) randomised trial. *Lancet.* 2015; 385: 529–38. doi: 10.1016/S0140-6736(14)61184-3. PMID: 25453443.
2. *Abbott AL, Paraskevas KI, Kakkos SK, Golledge J, Eckstein HH, Diaz-Sandoval LJ et al.* Systematic review of guidelines for the management of asymptomatic and symptomatic carotid stenosis. *Stroke.* 2015; 46: 3288–3301. doi: 10.1161/strokeaha.115.003390. PMID: 26451020.
3. *Gavrilenko AV, Kuklin AV, Fomina VV.* Conventional and eversion carotid endarterectomy for internal carotid artery stenosis. *Pirogov Russian Journal of Surgery = Khirurgiya. Zurnal im. N.I. Pirogova.* 2018; (2): 87–92. [In Russ]. doi: 10.17116/hirurgia2018287-92.
4. *Zannetti S, Cao P, De Rango P, Giordano G, Parlani G, Lenti M et al.* Intraoperative assessment of technical perfection in carotid endarterectomy: a prospective analysis of 1305 completion procedures. Collaborators of the EVEREST study group. Eversion versus standard carotid endartectomy. *Eur J Vasc Endovasc Surg.* 1999; 18 (1): 52–8. doi: 10.1053/ejvs.1999.0856. PMID: 10388640.
5. *Ren S, Li X, Wen J, Zhang W, Liu P.* Systematic review of randomized controlled trials of different types of patch materials during carotid endarterectomy. *PLoS one.* 2013; 8 (1): e55050. PMID: 23383053. doi: 10.1371/journal.pone.0055050.
6. *Texakalidis P, Giannopoulos S, Charisis N, Giannopoulos S, Karasavvidis T, Koullias G et al.* A meta-analysis of randomized trials comparing bovine pericardium and other patch materials for carotid endarterectomy. *J Vasc Surg.* 2018; 68 (4): 1241–1256. doi: 10.1016/j.jvs.2018.07.023. PMID: 30244928.
7. *Karpenko AA, Kuzhuget RA, Starodubtsev VB, Ignatenko PV, Kim IN, Gorbatykh VN.* Immediate and long-term outcomes of carotid bifurcation remodeling. *Patologiya krovoobrashcheniya i kardiokhirurgiya.* 2013; 17 (1): 21–24. [In Russ]. doi: 10.21688/1681-3472-2013-1-21-24.
8. *Antonova LV, Sevostyanova VV, Mironov AV, Krivkina EO, Velikanova EA, Matveeva VG et al. In situ* vascular tissue remodeling using biodegradable tubular scaffolds with incorporated growth factors and chemoattractant molecules. *Complex Issues of Cardiovascular Diseases.* 2018; 7 (2): 25–36. doi: 10.17802/2306-1278-2018-7-2-25-36.
9. *Smith RJ, Yi T, Nasiri B, Breuer CK, Andreadis ST.* Implantation of VEGF-functionalized cell-free vascular grafts: regenerative and immunological response. *The FASEB Journal.* 2019; 33 (4): 5089–5100. doi: 10.1096/fj.201801856R.
10. *Krilleke D, Ng YS, Shima DT.* The heparin-binding domain confers diverse functions of VEGF-A in development and disease: A structure-function study. *Biochemi-*

cal Society Transactions. 2009; 37 (6): 1201–1206. doi: 10.1530/JOE-15-0342. PMID: 19909247.
11. *Miyazu K, Kawahara D, Ohtake H, Watanabe G, Matsuda T.* Luminal surface design of electrospun small-diameter graft aiming at *in situ* capture of endothelial progenitor cell. *Journal of Biomedical Materials Research Part B: Applied Biomaterials.* 2010; 94 (1): 53–63. doi: 10.1002/jbm.b.31623.
12. *Wang F, Li Y, Shen Y, Wang A, Wang S, Xie T*. The functions and applications of RGD in tumor therapy and tissue engineering. *International Journal of Molecular Sciences*. 2013; 14 (7): 13447–1362. doi: 10.3390/ijms140713447. PMID: 23807504.
13. *Hsu SH, Chu WP, Lin YS, Chiang YL, Chen DC, Tsai CL.* The effect of an RGD-containing fusion protein CBD-RGD in promoting cellular adhesion. *Journal of Biotechnology*. 2004; 111 (2): 143–150. doi: 10.1016/j.jbiotec.2004.03.014. PMID: 15219401.
14. *Sevostianova VV, Mironov AV, Antonova LV, Krivkina EO, Matveeva VG, Velikanova EA et al.* Tissue-engineered patch modified by vascular endothelial growth factor for reconstruction of vascular wall. *Patologiya krovoobrashcheniya i kardiokhirurgiya = Circulation Pathology and Cardiac Surgery*. 2020; 24 (4): 114–128. [In Russ]. doi: 10.21688/1681-3472-2020-4-114-128.
15. *Antonova LV, Silnikov VN, Khanova MYu, Koroleva LS, Serpokrilova IYu, Velikanova EA et al*. Adhesion, proliferation and viability of human umbilical vein endothelial cells cultured on the surface of biodegradable nonwoven matrices modified with RGD peptides. *Russian Journal of Transplantology and Artificial Organs*. 2019; 21 (1): 142–152. [In Russ]. doi: 10.15825/1995-1191-2019-1-142-152.
16. *Sevostianova VV, Antonova LV, Mironov AV, Yuzhalin AE, Silnikov VN, Glushkova TV et al.* Biodegradable patches for arterial reconstruction modified with RGD peptides: results of an experimental study. *ACS Omega*. 2020; 5 (34): 21700–21711. doi: 10.1021/acsomega.0c02593. PMID: 32905385.
17. *Lin HB, Sun W, Mosher DF, Garciaecheverria C, Schaufelberger K, Lelkes PI et al.* Synthesis, Surface, and Cell Adhesion Properties of Polyurethanes Containing Covalently Grafted RGD-peptides. *J Biomed Mater Res.* 1994; 28 (3): 329–342. doi: 10.1002/jbm.820280307. PMID: 8077248.
18. *Sedaghati T, Jell G, Seifalian A.* Investigation of Schwann cell behaviour on RGD-functionalised bioabsorbable nanocomposite for peripheral nerve regeneration. *New Biotechnology*. 2014; 31 (3): 203–213. doi: 10.1016/j.nbt.2014.01.002. PMID: 24503165.
19. *Antonova LV, Mironov AV, Silnikov VN, Glushkova TV, Krivkina EO, Akent'eva TN et al.* Biodegradable vascular patches: comparative characteristics of physical-mechanical and hemocompatible properties. *Yakut Medical Journal*. 2019; 4 (68): 35–39. doi: 10.25789/YMJ.2019.68.08.
20. *Wei K, Li Y, Mugishima H, Teramoto A, Abe K.* Fabrication of core-sheath structured fibers for model drug release and tissue engineering by emulsion electrospinning. *Biotechnology Journal*. 2012; 7 (5): 677–685. doi: 10.1002/biot.201000473. PMID: 22125296.
21. *Spano F, Quarta A, Martelli C, Ottobrini L, Rossi RM, Giglic G et al.* Fibrous scaffolds fabricated by emulsion electrospinning: from hosting capacity to *in vivo* biocompatibility. *Nanoscale*. 2016; 8 (17): 9293–9303. doi: 10.1039/C6NR00782A.
22. *Yarin R.L.* Coaxial electrospinning and emulsion electrospinning of core-shell fibers. *Polymers for Advanced Technologies*. 2011; 22 (3): 310–317. doi: 10.1002/pat.1781.
23. *Ward AS, Cormier JM.* Operative techniques in arterial surgery Dordrecht: Springer Netherlands. 1986.
24. *Hersel U, Dahmen C, Kessler H.* RGD modified polymers: biomaterials for stimulated cell adhesion and beyond. *Biomaterials.* 2003; 24 (24): 4385–4415. doi: 10.1016/S0142-9612(03)00343-0. PMID: 12922151.
25. *Jolee Bartrom BS.* ASTM Hemolysis. *NAMSA*. 2008; 1–12.
26. *Malm CJ, Risberg B, Bodin A, Bäckdahl H, Johansson BR, Gatenholm P et al.* Small calibre biosynthetic bacterial cellulose blood vessels: 13-months patency in a sheep model. *Scand Cardiovasc J*. 2012; 46 (1): 57–62. doi: 10.3109/14017431.2011.623788. PMID: 22029845.
27. *Ahmed M, Hamilton G, Seifalian AM.* The performance of a small-calibre graft for vascular reconstructions in a senescent sheep model. *Biomaterials.* 2014; 35 (33): 9033–9040. doi: 10.1016/j.biomaterials.2014.07.008. PMID: 25106769.
28. *Thomas LV, Lekshmi V, Nair PD.* Tissue engineered vascular grafts – preclinical aspects. Int J Cardiol. 2013; 167 (4): 1091–1100. PMID: 23040078. doi: 10.1016/j.ijcard.2012.09.069.
29. *Swartz DD, Andreadis ST.* Animal models for vascular tissue-engineering. *Curr Opin Biotechnol*. 2013; 24 (5): 916–925. doi: 10.1016/j.copbio.2013.05.005. PMID: 23769861.
30. *Hoerstrup SP, Cummings Mrcs I, Lachat M, Schoen FJ, Jenni R, Leschka S et al.* Functional growth in tissue-engineered living, vascular grafts: follow-up at 100 weeks in a large animal model. *Circulation.* 2006; 114 (1 Suppl): I159–I166. doi: 10.1161/circulationaha.105.001172. PMID: 16820566.
31. *Catto V, Fare S, Freddi G, Tanzi MC*. Vascular tissue engineering: ecent advances in small diameter blood vessel regeneration. *ISRN Vasc Med.* 2014; 923030. doi: 10.1155/2014/923030.
32. *Matsuzaki Yu, Iwaki R, Reinhardt JW, Chang Yu-C, Miyamoto S, Kelly J et al.* The effect of pore diameter on neo-tissue formation in electrospun biodegradable tissue-engineered arterial grafts in a large animal model. *Acta Biomater.* 2020; 115: 176–184. doi: 10.1016/j.actbio.2020.08.011. PMID: 32822820.
33. *Matsuzaki Yu, Miyamoto S, Miyachi H, Iwaki R, Shoji T, Blum K et al.* Improvement of a Novel Small-diameter Tissue-engineered Arterial Graft With Heparin Conjugation. *Ann. Thorac. Surg.* 2021; 111 (4): 1234–1241. doi: 10.1016/j.actbio.2020.08.011. PMID: 32822820.

The article was submitted to the journal on 02.06.2022

DOI: 10.15825/1995-1191-2022-4-109-117

IN VITRO EFFECT OF BIOSCAFFOLDS ON VIABILITY AND INSULIN-PRODUCING FUNCTION OF HUMAN ISLETS OF LANGERHANS

A.S. Ponomareva, N.V. Baranova, I.A. Miloserdov, V.I. Sevastianov

Shumakov National Medical Research Center of Transplantology and Artificial Organs, Moscow, Russian Federation

Introduction. The culture of islets of Langerhans with bioscaffolds – extracellular matrix (ECM) mimetics – can provide a native microenvironment suitable for islets. This is one of the main conditions for creating a pancreatic tissue equivalent. **Objective:** to compare the secretory capacity of viable human pancreatic islets in monoculture (control group) and cultured in the presence of two bioscaffolds: biopolymer collagen-based hydrogel scaffold (experimental group 1) and tissue-specific scaffold from decellularized deceased donor pancreas (experimental group 2). **Materials and methods.** Islets of Langerhans were isolated from the caudal pancreas using a collagenase technique. The viability of cultured islets was accessed by vital fluorescence staining, while secretory capacity was evaluated by enzyme-linked immunosorbent assay (ELISA). **Results.** Pancreatic islets cultured with bioscaffolds showed no signs of degradation and fragmentation, they remained viable throughout the entire period of observation (7 days). The monoculture of islets showed significant destructive changes during this period. Basal insulin levels in experimental groups 1 and 2 increased by 18.8% and 39.5% on day 1 of culture compared to the control group, by 72.8% and 102.7% on day 4 of incubation, and by 146.4% and 174.6% on day 7, respectively. The insulin secretion level of islets with tissue-specific scaffolds was 17.4% higher than that when cultured with biopolymer collagen-based scaffolds. **Conclusion.** Biopolymer and tissue-specific ECM mimetics contribute not only to preservation of the viability of isolated islets of Langerhans but also maintain their insulin secretion capacity for 7 days at a higher level in comparison with monoculture. The experiments revealed that the use of a tissue-specific scaffold for the creation of a pancreatic tissue equivalent has slight potential advantage over biopolymer scaffold.

Keywords: pancreas, culture of the islets of Langerhans, insulin-producing function, tissue-specific scaffold, biopolymer scaffold.

INTRODUCTION

One of the directions of tissue engineering and regenerative medicine technologies includes creation of a tissue equivalent of the endocrine pancreas [1]. The incidence of type 1 diabetes (T1D) in the world is increasing from year to year [2], and improvement in the traditional method of treatment – insulin therapy [3] – does not protect against developing severe complications, such as diabetic angiopathy and neuropathy [4, 5]. Allotransplantation of pancreatic islets is able to provide insulin independence in patients for a certain period of time, without subjecting patients to serious surgical intervention, as in pancreas transplantation [6–8]. However, a significant drawback in this treatment method is the low functional activity of islets due to the action of a number of damaging factors during isolation and culturing procedures.

It is known that the T1D development mechanism is based on autoimmune destruction of insulin-producing pancreatic beta cells of islets of Langerhans, which leads to depletion of the pool of these cells and gradually increasing, progressive loss of endogenous insulin synthesis [9].

During isolation, pancreatic islets are exposed to a number of damaging factors, such as ischemia, oxidative stress, and possible cytotoxic enzyme action. In the process of culturing, islets are fragmented and degraded due to impaired innervation and vascularization provided in the body by ECM [10, 11]. By participating in morphogenesis, differentiation, intracellular signaling, gene expression, adhesion, migration, proliferation, secretion and survival of pancreatic islets [12], ECM contributes to the integrity of islet structure, which is a necessary condition for their functioning.

Previously, we studied the possibility of obtaining viable isolated pancreatic islets from a fragment of the caudal part of donor human pancreas using the collagenase technique [13]. In the post-isolation period, it seems essential to provide the islets with a microenvironment characteristic of native ECM in situ. This problem can be solved by creating a tissue equivalent of the pancreas

Corresponding author: Anna Ponomareva. Address: 1, Shchukinskaya str., Moscow, 123182, Russian Federation. Phone: (499) 196-26-61, (926) 585-23-73. E-mail: a.s.ponomareva@gmail.com

consisting of islet cells and a bioscaffold, which can most of all mimics the structure and composition of ECM to preserve the viability and functional activity of isolated islets in vitro and in vivo [14].

Such bioscaffolds include a commercially available biopolymer-based microheterogeneous collagen-containing hydrogel (BMCH scaffold), registered in Russia for clinical use as a bioimplant – "Composition of microheterogeneous collagen-containing gel Sphero®GEL" (BIOMIR Service, Krasnoznamensk). Sphero®GEL, produced from components of farm animal tissues by acetic acid extraction, contains the main components of ECM: peptides of partially hydrolyzed collagen, glycoproteins, uronic acids and growth factors required for cell life-sustaining activity, synthesis of exogenous uronic acids, proteoglycans and collagen [15].

Tissue-specific bioscaffolds made from decellularized pancreas or its fragments (DP scaffold) appear to be the most promising components of tissue equivalents of pancreas [16–18]. All pancreas decellularization protocols are aimed at preserving the structural, biochemical and biomechanical properties of native ECM with maximum complete removal of cellular material (including antigenic) to minimize immune response to implantation of DP scaffold [19–21]. Presence of the main ECM components in the decellularized pancreatic scaffold, such as structural proteins (type I, III, IV, V and VI collagens, elastin, fibronectin and laminin), glycoproteins and cell adhesion factors, allows creating conditions for prolonged life-sustaining activity of islet cells and maximum imitation of ECM properties [22]. Preservation of ECM architectonics in DP scaffold also affects the survival and secretory function of islets [23, 24]. Scientific literature data and our studies demonstrate increased insulin secretion by porcine pancreatic islets [25] and rat islets [18] cultured in the presence of allogeneic tissue-specific scaffolds compared to monoculture of islets.

The **objective** of our work was to compare the insulin-producing function of viable human pancreatic islets in monoculture and cultured in the presence of two bioscaffolds: biopolymer-based microheterogeneous collagen-containing hydrogel (BMCH) and tissue-specific scaffold from decellularized human pancreas (DP-TSS).

MATERIALS AND METHODS

Baseline

To isolate pancreatic islets and obtain tissue-specific decellularized matrices, we used the caudal part of the pancreas obtained from multiorgan procurement of organs (not suitable for transplantation) from deceased donors.

Isolation and identification of islets of Langerhans

To obtain islets of Langerhans, a small fragment (~2.0 g) of the caudal part of the pancreas was mechanically crushed (1.5 × 1.5 × 1.5 mm) and incubated in collagenase NB1 solution (activity 20 PZ U/g tissue) with neutral protease NP (activity 1.5 DMC U/g tissue) (Serva, Germany) for 10–15 minutes at 37 °C. The action of the enzymes was stopped by adding a threefold volume of cold (4 °C) Hanks' balanced salt solution (PanEco, Russia), followed by filtration through a metal sieve with 0.4–0.6 mm mesh diameter. To purify the islets, a centrifugation mode was selected to avoid using a ficoll density gradient (1 minute at 900 rpm, then 2 minutes at 1300 rpm).

Islets were identified by dithizone staining (Sigma-Aldrich, USA) immediately after isolation. For this purpose, part of the suspension was mixed with a 2 : 1 dithizone solution and incubated for 20–30 minutes at 37 °C. The dithizone selectively stained the pancreatic islets red-orange, while the acinar cells remained unstained. Freshly isolated islets were resuspended in growth medium and used in the experiment no later than 24 hours after isolation.

Biopolymer-based microheterogeneous collagen-containing hydrogel (BMCH scaffold)

One of the bioscaffolds chosen was an injectable form of BMCH (trade name Sphero®GEL, manufactured by Biomir Service, Russia). BMCH scaffold consists of microparticles (145.79 ± 0.09 μm) of scleral collagen type 1, cross-linked by gamma radiation (1.5 Mrad), and a homogeneous hydrogel containing low- and high-molecular ECM components in a 1 : 1 ratio [15]. The heterogeneous component of BMCH scaffold has a porous structure of microparticles with 2–4 μm pore size, which is a positive property in the processes of neovascularization and neoinnervation of tissue-engineered constructs based on it [18].

Tissue-specific matrix from decellularized pancreas (DP scaffold)

As a tissue-specific biomimetic ECM, we used a bioscaffold representing finely dispersed fragments of decellularized human pancreatic tissue. The technique of obtaining DP scaffold (Fig. 1) was developed earlier [21].

The decellularization protocol included three freeze (–80 °C) and thaw (+37 °C) cycles of prostate fragments followed by mechanical grinding of the tissue to a size ≤1 × 1 × 2 mm. The crushed fragments were treated at room temperature in three changes of phosphate-buffered saline (PBS) (pH = 7.4) containing 0.1% sodium dodecyl sulfate and increasing concentration of Triton X100 (1%,

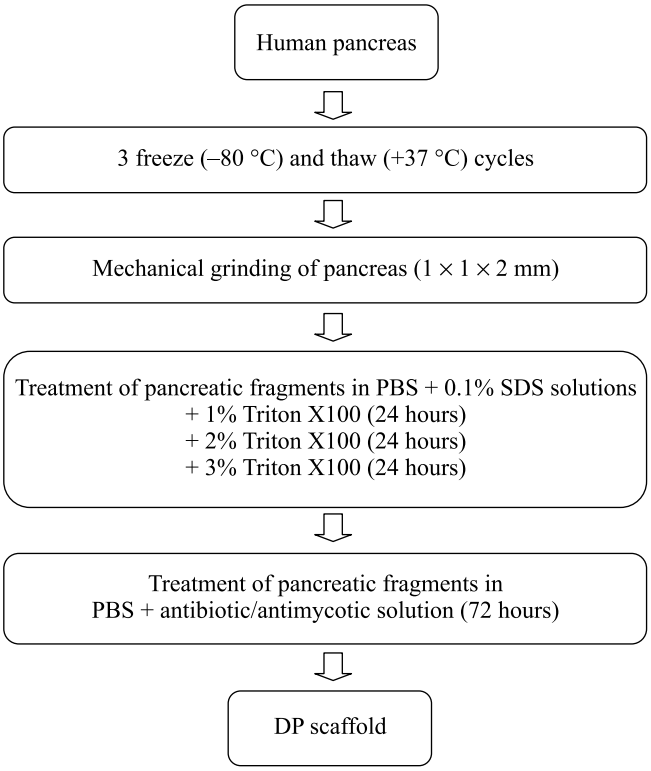

Fig. 1. Schematic representation of the stages for obtaining tissue-specific scaffold from pancreatic tissue

2% and 3%, respectively) (Sigma, USA) under constant stirring for 24 hours. At the final stage of the decellularization process, the fine DP scaffold fragments were thoroughly washed of surfactant residues for 72 hours in three changes of antibiotic-antimycotic solution in PBS.

Fine DP scaffold samples were dehydrated using filter paper, weighed, and added to cryovials at 20.0 ± 0.1 mg each, sterilized with gamma radiation (1.5 Mrad), and frozen at –80 °C. The shelf life of sterile frozen DP scaffold samples with preservation of biochemical and structural properties was not more than 1 year.

DP scaffold contains type I collagen and elastin, has low immunogenicity (no more than 0.1% DNA), is not cytotoxic and retains the morphofunctional properties of native pancreatic tissue ECM regarding adhesion and proliferation of cell cultures [21].

Culture of islets of Langerhans

Equal amounts of isolated islets (~200) were added to three 25 cm^2 culture vials (Greiner bio-one, Germany). No scaffold was added to the first culture vial (control). In the second and third culture vials, 20.0 ± 0.1 mg BMCH scaffold (experimental group 1) and 20.0 ± 0.1 mg DP scaffold (experimental group 2) were added, respectively. All islets were cultured in complete growth medium containing DMEM (1.0 g/L glucose) (PanEco, Russia), 10% fetal calf serum (HyClone, USA), Hepes (Gibco by Life technologies™, USA), 2 mM L-glutamine (PanEco, Russia), and 1% antibiotic/antimycotic (Gibco by Life technologies™, USA). Islets were cultured under standard conditions at 37 °C in a humidified atmosphere containing 5% CO_2. They were subjected to daily visual monitoring and photography using an inverted microscope (Nikon, Japan) equipped with a digital camera. The culture medium was changed at 1, 4, and 7 days to allow sampling for subsequent testing for insulin content.

Viability determination

The viability of freshly isolated islets, as well as islets cultured in control and experimental groups, was assessed on days 1, 4, and 7 using the LIVE/DEAD® Cell Viability/Cytotoxicity Kit (Molecular probes® by Life technologies™, USA). For LIVE/DEAD® staining, a part of islets suspension (monoculture or with matrices) was placed in a Petri dish, mixed with the prepared working dye solution in a 1 : 2 ratio, and incubated in the dark for 15–30 minutes. The results were evaluated using a luminescence microscope (Nikon, Japan).

Determination of insulin-producing function

To determine the insulin-producing function of islets in control and experimental groups, the growth medium was replaced in culture vials on days 1, 4 and 7. After 1 hour of incubation under the same conditions (37 °C, 5% CO_2), samples of growth medium were taken from all vials. The samples were stored frozen (–23 °C) for subsequent ELISA analysis.

Basal concentration of insulin in the culture medium of control and experimental groups was determined using ELISA Kit for insulin human CEA448 Hu-96 (Cloud-Clone Copr., USA) according to the manufacturer's instructions.

This ELISA variant uses the competitive inhibition method. An insulin-specific monoclonal antibody is pre-applied on a microtiter plate. A competitive inhibition reaction is initiated between biotinylated enzyme-labeled insulin and unlabeled insulin (standard and culture medium samples) with the pre-applied insulin-specific antibody. After incubation with all kit reagents, a substrate solution was added that reacted with the complex to produce a signal as a stained product. The intensity of this signal was expressed through optical density, which is inversely proportional to the insulin levels in the samples tested. The inverse correlation between the insulin levels in the sample and the signal intensity is plotted as a standard curve with a logarithmic function.

Results of quantitative ELISA were calculated by measuring the optical density on a Spark 10M microplate reader (TecanTrading AG, Switzerland) with Spark Control™ Magellan V1.2.20 software at 450 nm and 550 nm wavelengths to account for optical defects in the microplate. The data obtained were processed using SPSS26.0 software. The results presented are shown as

mean ± standard deviation. Differences were considered significant at $p < 0.05$.

RESULTS AND DISCUSSION

Freshly isolated islets of Langerhans

Using an inverted microscope, we observed a significant number of freshly isolated islets of various sizes with a predominantly round shape and smooth surface (Fig. 2, a). The remains of exocrine tissue were revealed as follows: acinar cells created a certain roughness on the surface of some islets and were not stained with dithizone. At the same time, dithizone stained pancreatic islets in orange-red color, which made it easy to identify them (Fig. 2, b).

LIVE/DEAD® staining of freshly isolated islets was complicated by the presence of strong background brightness due to the presence of acinar cells around the islets or in the culture medium. Nevertheless, individual living cells in the islet structure were clearly visualized (Fig. 2, c).

Viability of islets of Langerhans

Islet monoculture

Observation under an inverted microscope showed that most islets cultured without bioscaffolds (control group) retained their shape and integrity within the first three days of incubation. Few of them showed signs of fragmentation or were destroyed.

LIVE/DEAD® staining with a fluorescence microscope showed green fluorescence of the islets, confirming their viability (Fig. 3, a). Some dead acinar cells, stained red with ethidium homodimer, were detected in the culture medium surrounding the islets.

After 3 days of culture, the morphology of islets in the control group changed. Some islets showed cavities, signs of fragmentation, the surface of a significant number of islets acquired uneven outlines and became lumpy (Fig. 3, b). Live staining with LIVE/DEAD® at 4–7 days of culture revealed dead cells with red fluorescence in the preserved islets (Fig. 3, c). Thus, by one week of cultivation without bioscaffolds, the islets had undergone significant destructive changes.

Islets of Langerhans in the presence of BMCH scaffold

Islets cultured with BMCH scaffold (experimental group 1) remained intact and underwent no fragmentation or degradation throughout the entire observation period (7 days). On day 2 of incubation, the islets were found to have adhered to the smooth surface of the BMCH scaffold (Fig. 4, a); the unattached islets floated freely in the culture medium. LIVE/DEAD® fluorescence staining performed on days 1, 4, and 7 of incubation confirmed the viability of the islets in the experimental group 1 (Fig. 4, b).

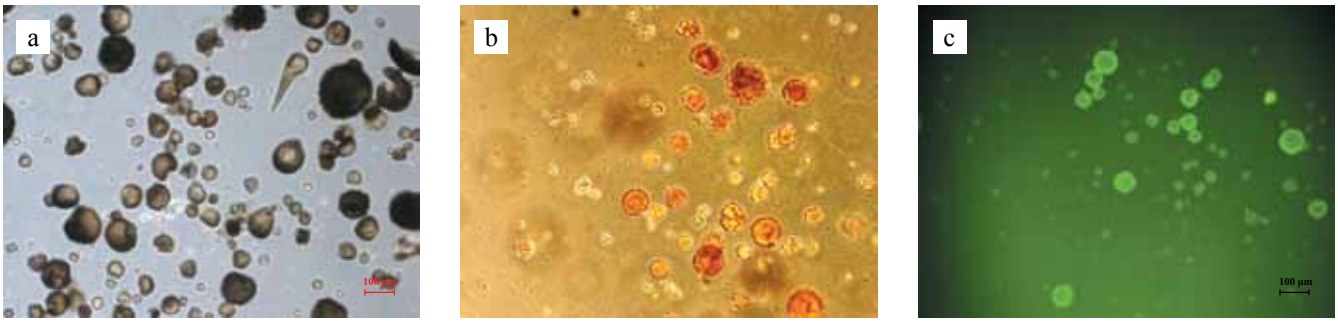

Fig. 2. Freshly isolated human islets of Langerhans. a, inverted phase-contrast microscopy; b, dithizone staining; c, LIVE/DEAD® fluorescence staining. Bar 100 µm

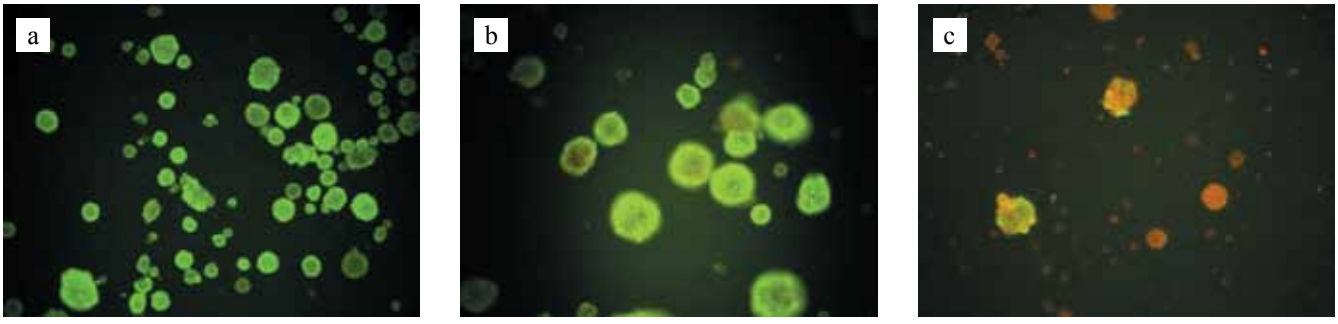

Fig. 3. Monoculture of human islets of Langerhans (control group). LIVE/DEAD® fluorescence staining. a, day 3 of culture. Bar 100 µm; b, day 4 of culture. Bar 200 µm; c, day 7 of culture. Bar 100 µm

Islets of Langerhans in the presence of DP scaffold

Islets cultured with DP scaffold (experimental group 2), just as in experimental group 1, showed no signs of destruction and fragmentation throughout the entire observation period (7 days). On day 2 of incubation with DP scaffold, most of the islets showed adhesive qualities and settled on the fibrous surface of the matrix (Fig. 5, a); the islets remaining in the culture medium continued to float. Live staining of islets in experimental group 2 with LIVE/DEAD® performed at 1, 4, and 7 days of incubation confirmed the viability of the preserved islets (Fig. 5, b).

Insulin-producing function of pancreatic islets

The insulin-producing function of the studied islets was determined at days 1, 4, and 7. Comparative analysis of insulin secretion in experimental groups 1 and 2 was performed in relation to the control group.

After the first day of culture, insulin levels in experimental groups 1 and 2 was 18.8% (46.78 ± 1.29 pg/ml) and 39.5% (54.93 ± 1.58 pg/ml) higher than in the control group (39.37 ± 1.25 pg/ml); on day 4 of incubation, by 72.8% (41.65 ± 0.81 pg/ml) and 102.7% (48.88 ± 1.32 pg/ml), respectively, compared with the control group (24.11 ± 0.58 pg/ml). At day 7, an even more significant difference was observed between the insulin levels in experimental groups 1 (32.9 ± 1.08 pg/ml) and 2 (36.66 ± 1.38 pg/ml) and the control group (13.35 ± 0.55 pg/ml) (Table).

The positive effect of bioscaffolds on the insulin-producing function of islets is manifested by the difference in hormone concentrations in the control and experimental groups at all periods of the study (Fig. 6). A significant difference between the insulin levels

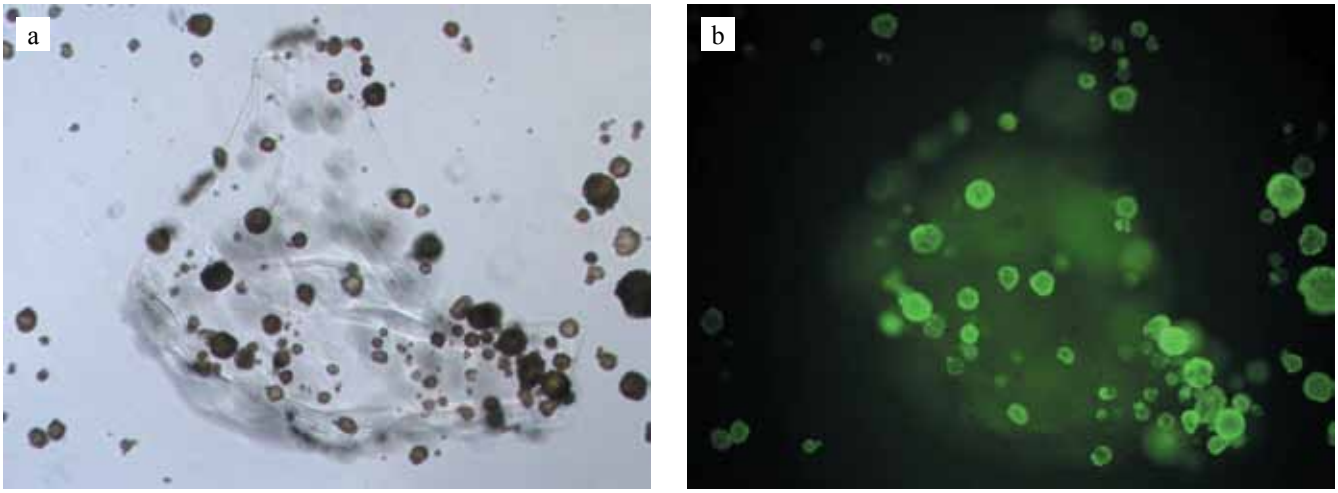

Fig. 4. Human islets of Langerhans cultured with biopolymer collagen-based scaffold (BMCH scaffold). Day 7 of culture: a, inverted phase-contrast microscopy; b, LIVE/DEAD® fluorescence staining. Bar 100 μm

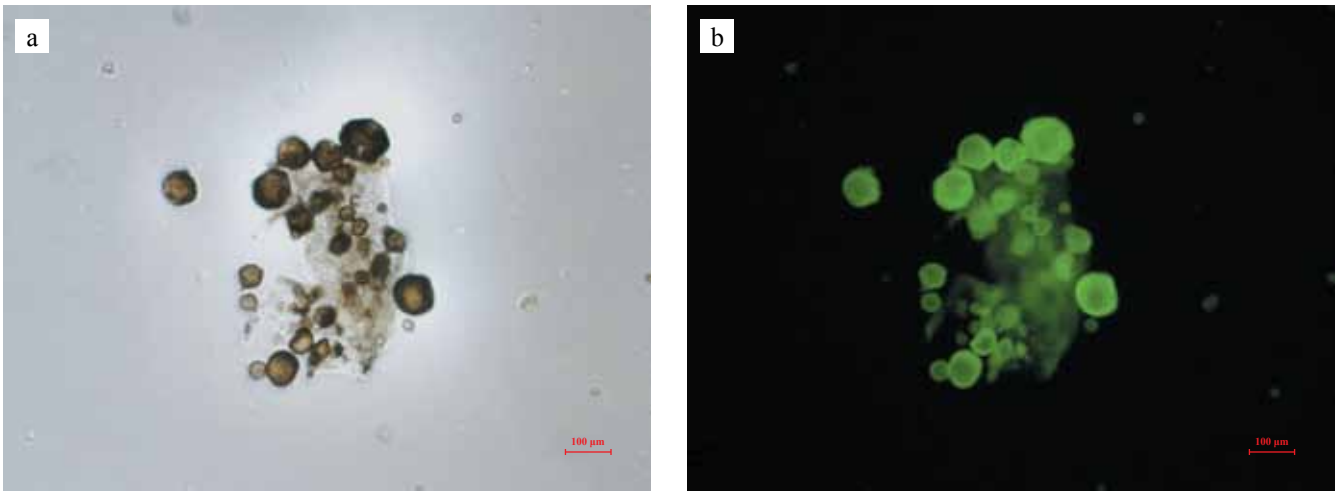

Fig. 5. Human islets of Langerhans cultured with tissue-specific scaffold from decellularized human pancreas (DP scaffold). Day 7 of culture. a, inverted phase-contrast microscopy; b, LIVE/DEAD® fluorescence staining. Bar 100 μm

Table

Comparative analysis of insulin levels (%) in the experimental groups relative to the control group (monoculture of islets)

Day	Islets + BMCH scaffold (experimental group 1), %	Islets + decellularized pancreas scaffold (experimental group 2), %
1	18.8 ± 3.3	39.5 ± 4.0
4	72.8 ± 3.4	102.7 ± 5.5
7	146.4 ± 8.1	174.6 ± 10.3

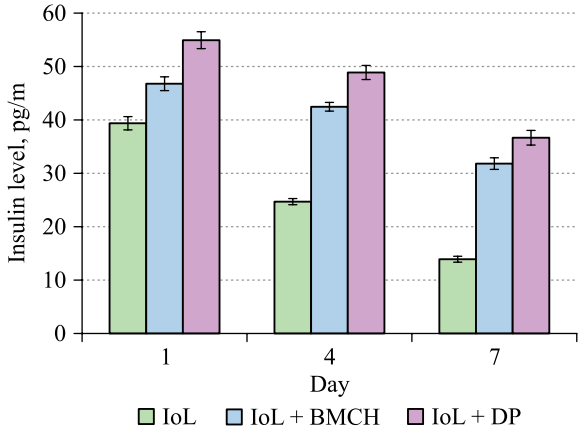

Fig. 6. Insulin-producing function of human islets of Langerhans in control and experimental groups. IoL, islets of Langerhans; BMCH, biopolymer-based microheterogeneous collagen-containing hydrogel; DP, decellularized pancreas. $p < 0.05$

in experimental groups 1 and 2 and the control group may be due to the destructive changes in the monoculture of islets after three days of culture, which is confirmed by fluorescent staining of islets at different time points. The positive trend of the effect of biopolymer and tissue-specific ECM mimetics on the secretory function of islets in percentage terms was maintained throughout the whole period of observation, despite the fact that insulin level, expressed in absolute values, decreased with increasing culture period.

The level of insulin secretion on days 1 and 4 of culture of islets in group 2 was 17.37 ± 0.05% higher than in group 1; 11.43% higher on day 7. Thus, we revealed a slight advantage of using tissue-specific DP scaffold over BMCH scaffold when culturing human pancreatic islets. Earlier we have studied the insulin-producing function of rat islets cultured in the presence of BMCH scaffold and scaffold from decellularized rat prostate [18]. A comparative analysis of insulin secretion showed a more pronounced effect of the studied bioscaffolds on rat islets than on human islets, and the level of insulin secretion in rat islets cultured in DP scaffold was 35.5% higher than that of rat islets cultured in BMCH scaffold.

This study showed that isolated human islets cultured in the presence of bioscaffolds can be preserved for 7 days under standard incubation conditions without significant loss of morphofunctional properties and viability. This method of preserving islet potential in vitro before implantation in patients with T1D is likely to increase the duration of islet function in vivo and in the post-implantation period.

CONCLUSION

Culture of isolated islets of Langerhans with biopolymer and tissue-specific ECM mimetics contributes not only to preservation of islets viability, but also to maintenance of their secretory function at a higher level for 7 days in comparison with the culture of islets without bioscaffolds. The experiments revealed that using tissue-specific DP scaffold has a slight potential advantage over BMCH scaffold when creating a tissue equivalent of the pancreas.

The authors declare no conflict of interest.

REFERENCES

1. *Kumar N, Joisher H, Ganguly A.* Polymeric scaffolds for pancreatic tissue engineering: a review. *Rev Diabet Stud.* 2018; 14 (4): 334–353.
2. *Creusot RJ, Battaglia M, Roncarolo MG et al.* Concise review: cell-based therapies and other non-traditional approacher for type 1 diabetes. *Stem Cells.* 2016; 34 (4): 809–819.
3. *Gururaj Setty S, Crasto W, Jarvis J et al.* New insulins and newer insulin regimens: a review of their role in improving glycaemic control in patients with diabetes. *Postgrad Med J.* 2016; 92 (1085): 152–164.
4. *Gan MJ, Albanese-O'Neill A, Haller MJ.* Type 1 diabetes: current concepts in epidemiology, pathophysiology, clinical care, and research. *Curr Probl Pediatr Adolesc Health Care.* 2012; 42 (10): 269–291.
5. *Mannucci E, Monami M, Dicembrini I et al.* Achieving HbA1c targets in clinical trials and in the real world: a systematic review and meta-analysis. *J Endocrinol Invest.* 2014; 37 (5): 477–495.
6. *Bottino R, Knoll MF, Knoll CA et al.* The future of islet transplantation is now. *Front Med (Lausanne).* 2018; 5: 202.
7. *Shapiro AM, Pokrywczynska M, Ricordi C.* Clinical pancreatic islet transplantation. *Nat Rev Endocrinol.* 2017; 13 (5): 268–277.
8. *Maffi P, Secchi A.* Clinical results of islet transplantation. *Pharmacol Res.* 2015; 98: 86–91.
9. *Ehlers MR.* Strategies for clinical trials in type 1 diabetes. *J Autoimmun.* 2016; 71: 88–96.
10. *Bosco D, Armanet M, Morel P et al.* Unique arrangement of alpha- and beta-cells in human islets of Langerhans. *Diabetes.* 2010; 59 (5): 1202–1210.
11. *Amer LD, Mahoney MJ and Bryant SJ.* Tissue engineering approaches to cell-based type 1 diabetes therapy. *Tissue engineering*. 2014; 20 (5): 455–467.

12. *Riopel M, Wang K.* Collagen matrix support of pancreatic islet survival and function. *Frontiers in Bioscience*. 2014; 19: 77–90. doi: 10.2741/4196.
13. *Ponomareva AS, Kirsanova LA, Baranova NV, Bubentsova GN, Miloserdov IA, Volkova EA, Sevastianov VI.* A technique for separating viable islets of Langerhans from a fragment of human pancreatic tail. *Russian Journal of Transplantology and Artificial Organs*. 2018; 20 (4): 76–82. doi.org/10.15825/1995-1191-2018-4-76-82.
14. *Llacua LA, Faas MM, de Vos P.* Extracellular matrix molecules and their potential contribution to the function of transplanted pancreatic islets. *Diabetologia.* 2018; 61 (6): 1261–1272.
15. *Sevastianov VI. Perova NV.* Injectable heterogeneous biopolymer hydrogel for replacement and regenerative surgery and the method of its preparation. [Patent for invention of the Russian Federation No. 2433828]. 2011.
16. *Goh SK, Bertera S, Olsen P et al.* Perfusion-decellularized pancreas as a natural 3D scaffold for pancreatic tissue and whole organ engineering. *Biomaterials.* 2013; 34 (28): 6760–6772.
17. *Napierala H, Hillebrandt K-H, Haep N, Tang P, Tintemann M, Gassner J et al.* Engineering an endocrine neopancreas by repopulation of a decellularized rat pancreas with islets of Langerhans. *Sci Rep.* 2017; 2 (7): 41777. doi: 10.1038/srep41777.
18. *Sevastianov VI, Baranova NV, Kirsanova LA, Ponomareva AS, Basok YuB, Nemets EA, Gautier SV*. Comparative analysis of the influence of extracellular matrix biomimetics on the viability and insulin-producing function of isolated pancreatic islets. *J Gene Engg Bio Res*. 2021; 3 (2): 17–25.
19. *Rana D, Zreigat H, Benkirane-Jessel N et al.* Development of decellularized scaffolds for stem cell-driven tissue engineering. *J Tissue Eng Regen Med.* 2017; 11 (4): 942–965.
20. *Shirakigawa N, Ijima H.* Decellularized tissue engineering. *Advances in Biomaterials for Biomedical Applications. Springer Nature Singapore Pte Ltd.* 2017; 66: 185–226.
21. *Ponomareva AS, Kirsanova LA, Baranova NV, Surguchenko VA, Bubentsova GN, Basok YuB et al.* Decellularization of donor pancreatic fragment to obtain a tissue-specific matrix scaffold. *Russian Journal of Transplantology and Artificial Organs*. 2020; 22 (1): 123–133. doi: 10.15825/1995-1191-2020-1-123-133.
22. *Sackett SD, Tremmel DM, Ma F et al.* Extracellular matrix scaffold and hydrogel derived from decellularized and delipidized human pancreas. *Sci Rep.* 2018; 8 (1): 10452.
23. *Guruswamy Damodaran R, Vermette P.* Decellularized pancreas as a native extracellular matrix scaffold for pancreatic islet seeding and culture. *J Tissue Eng Regen Med.* 2018; 12 (5): 1230–1237.
24. *Salvatori M, Katari R, Patel T, Peloso A, Mugweru J, Owusu K, Orlando G.* Extracellular matrix scaffold technology for bioartificial pancreas engineering: state of the art and future challenges. *J DiabSci Technol.* 2014; 8 (1): 159–169. doi: 10.1177/1932296813519558.
25. *Mirmalek-Sani S-H, Orlando G, McQuilling J, Pareta R, Mack D, Salvatori M et al.* Porcine pancreas extracellular matrix as a platform endocrine pancreas bioengineering. *Biomaterials.* 2013; 34 (22): 5488–5495. doi: 10.1016/j.biomaterials.2013.03.054.

The article was submitted to the journal on 22.07.2022

DOI: 10.15825/1995-1191-2022-4-118-123

PREDICTORS OF HEPATIC STEATOSIS IN LIVING LIVER DONORS

M.G. Minina[1, 2], D.V. Voronov[1], A.A. Nevredimov[1], E.A. Tenchurina[1]

[1] Botkin City Clinical Hospital, Moscow, Russian Federation

[2] Shumakov National Medical Research Center of Transplantology and Artificial Organs, Moscow, Russian Federation

Fatty liver disease (steatosis) is considered a risk factor in donor liver transplantation (LT). Macrosteatosis (>50%) is associated with primary graft dysfunction and may reduce long-term recipient survival. **Objective:** to identify predictors of macrovesicular steatosis (>50%) by analyzing donor characteristics. **Materials and methods.** The retrospective study included 525 potential liver donors between January 1, 2019 and December 31, 2020. Clinical and morphological characteristics of donors were studied using logistic regression and receiver operating characteristic (ROC) analysis. Threshold values of parameters demonstrating statistical significance in multivariate analysis as predictors of >50% hepatic steatosis were obtained by ROC analysis based on calculation of the optimal cutoff point. **Results.** Diabetes mellitus (DM), cause of donor's death (traumatic brain injury), alanine transaminase (ALT) >90 units/L and aspartate transaminase (AST) >110 units/L were predictors of >50% steatosis, revealed by time-zero biopsy in the donor. Almost identical sensitivity and specificity indicators were determined in ROC analysis for liver enzymes – ALT and AST – which were 69.1 and 80.6; 72.2 and 81.1, respectively. Given the obtained values, we can say that with elevated levels of liver enzymes in the donor's blood, there is a high degree of probability of liver parenchymal damage, but low sensitivity indicates possible multifactoriality of liver damage, and fatty liver disease may be one of the factors, but there may also be no damage to the liver parenchyma. At the same time, the rather high specificity revealed in ROC analysis for liver enzymes is a reliable sign of the absence of fatty liver disease at enzyme values less than the threshold. **Conclusion.** The thresholds established for ALT and AST and their corresponding levels of sensitivity and specificity indicate that these parameters have a relatively low predictive level in the context of the presence of severe fatty liver disease in a donor. This allows, nevertheless, to use models built on their basis as screening models in the primary evaluation of liver donors.

Keywords: steatosis, extended criteria liver donors, metabolic associated fatty liver disease.

INTRODUCTION

Donor hepatic steatosis is an independent risk factor that has some significant impact on post-transplant complications, such as reperfusion injury, early graft dysfunction, and overall recipient survival. According to studies, ≥50% severe macrovesicular steatosis has the greatest negative impact on the effectiveness of LT and development of post-LT complications [1]. About 30–51% of donor liver transplants have some degree of steatosis [2, 3]. Prevalence of hepatic steatosis keeps on increasing to date due to the increasing number of donors with obesity and a history of non-alcoholic fatty liver disease (NAFLD) [4, 5].

The so-called time-zero liver biopsy performed during laparotomy remains the gold standard for diagnosing steatosis in donors [6, 7]. However, even at the stage of initial donor assessment, donor specialists should tentatively predict the level of possible steatosis, based on the donor's available clinical characteristics. Similar studies have been conducted by foreign authors, who established a positive correlation between hepatic steatosis and body mass index (BMI) [10, 11].

Rinella M.E. et al. performed a comparative analysis of the predictive value of BMI, liver chemistry tests, imaging studies in potential living liver donors, as possible indicators of grade of steatosis, confirmed morphologically. For example, the authors showed there was a significant correlation between BMI and overall grade of steatosis [12]. Another study demonstrated that skin folds on the body, ALT levels and serum lipid levels correlate with the severity of fatty hepatosis, although not significantly [13]. Jeong-Hoon Lee et al. developed the liver steatosis index: a multivariate analysis indicated that high serum ALT to serum AST ratio, high BMI, and DM were independent risk factors of NAFLD [14]. At the same time, hepatic steatosis was ruled out at liver steatosis <30, while values >60 reliably indicates the presence of hepatic steatosis.

The approximate level of steatosis in a donor can also be determined by the transplant surgeon during laparotomy by liver visualization and palpation. The advantage of this method lies in its apparent ease

Corresponding author: Elmira Tenchurina. Address: 5, Vtoroy Botkinsky proezd, Moscow, 125284, Russian Federation. Phone: (967) 113-87-64. E-mail: arimle@inbox.ru

of implementation. However, the accuracy of macroscopic assessment directly depends on the severity of steatosis and is 71% for severe, 46% for moderate and only 17% for mild steatosis [7–9]. According to some researchers, the positive predictive score on visual inspection was 65.6% for severe macrovesicular steatosis, while the rate of macrosteatosis overdiagnosis was 10.0% on visual inspection [7].

MATERIALS AND METHODS

The retrospective study included 525 potential liver donors between January 1, 2019, and December 31, 2020. During the study, the pool of potential donors was divided into three groups depending on the severity of morphologically confirmed hepatic steatosis. Clinical and morphological characteristics were assessed by logistic regression and ROC analysis. Borderline values of the indicators demonstrating statistical significance in multivariate analysis as predictors of >50% hepatic steatosis were obtained in ROC analysis based on calculation of the optimal cutoff threshold. In a four-field conjugacy table, sensitivity and specificity scores were calculated for characteristics with variable values.

RESULTS AND DISCUSSION

To analyze the clinical characteristics of donors, the entire pool of effective liver donors included in the study was divided into three groups depending on the degree of fatty liver disease as established by time-zero liver biopsy in the donor: group 1, ≤30% steatosis; group 2, 31–50% steatosis; group 3, >50% steatosis. Donors (58/525 people, 11.1%), who did not undergo morphological examination for one reason or another were excluded from this analysis.

It is noteworthy that in groups 2 and 3, more than half of the donors, 51.3% and 58.6%, respectively, had a BMI <30, while the number of donors in % with BMI ≥30 indicating obesity was almost identical in groups 2 and 3; in group 3, there was even some decrease in obese donors. A more detailed analysis of donors revealed that the difference in BMI in groups 2 and 3 was due to the fact that donors with subtotal and total liver steatosis, presumably of alcoholic genesis, had low BMI, which was a factor in distorting the significance of this index at the level of >50% liver steatosis. Similarly, traumatic brain injury (TBI) as a cause of death prevailed in donors with a history of alcoholic hepatitis, which is confirmed by available data – the proportion of donors with TBI in the group with >50% steatosis was 33.3%, whereas in the group with ≤30% steatosis, it was 17.9%. The mean value of the blood platelets in liver donors in group 3 with >50% steatosis was 183.6×10^9/L, which is lower than in groups 1 and 2. We believe that this fact may be related to reduced production of thrombopoietin (a glycoprotein hormone produced mainly by the liver) in livers with subtotal fatty hepatosis). Markus Peck-Radosavljevic et al. studied thrombocytopenia <50,000/μL in patients with chronic liver disease as a result of decreased production of thrombopoietin in it [16]. Thus, theoretically, thrombocytopenia may serve as a nonspecific indicator of reduced liver function, including against the background of steatosis. In our opinion, this fact requires further study.

ALT and AST, as the best-known markers of liver damage up to and including necrosis, had the highest mean values in group 3 with >50% steatosis, 88.6 units/L and 124.1 units/L, respectively. Incidence of DM in group 3 donors was more than twice as high relative to group 1, 7.6% vs 20.9% (Table 1). The mean value of total bilirubin (TBil) in donors in all donor groups did not exceed reference values; however, there was a slight increase in TBil level in the steatosis groups relative to group 1.

Next, logistic regression analysis was performed to identify reliable predictors of >50% steatosis. Donor characteristics that showed statistical significance of $p < 0.05$ in logistic regression were taken into account. The following factors demonstrated statistical significance in the context of predicting the presence of severe steatosis in liver donors: cause of donor death – TBI, BMI ≥30 kg/m^2, presence of DM in donors, with a rather high OR value of 2.91, increased liver enzymes, TBil, and reduced platelet count. Age is an important factor in the evaluation of donor livers for transplantation, but no proven relationship with the level of hepatic steatosis was found. Various publications have suggested that the ratio of age and sex is the main physiological predictor of developing hepatic steatosis [17], but whereas fatty hepatosis occurs more often in men at a young age [18], when reaching 50 years of age, it is equally common in men and women. The mean age of potential liver donors in group 3 with >50% steatosis was 49.0 years, which is comparable with the above data and confirms our results that there is no relationship between incidence of severe liver steatosis and donor's age and/or gender. Liver steatosis reduces insulin clearance, and has a negative effect on hepatic insulin resistance, leading to increased plasma glucose levels, compensatory hyperinsulinemia, and progression of type 2 DM [19]. In our study, blood glucose levels showed no correlation with severe hepatic steatosis; we tend to associate the elevated blood glucose levels detected in donors with donors' brain death conditions. We considered blood platelets, regardless of the fact that they demonstrated a significant relationship with 50% hepatic steatosis, as highly variable and nonspecific and were excluded from the final predictors (Table 2).

We selected quantitative donor factors for ROC analysis – BMI, ALT, AST, and TBil. Quantitative ROC analysis is characterized by AUC (area under the curve). The higher the AUC, the higher the quality of the classifier (factor), while the value of AUC ≤0.5 demonstrates the low predictive ability of a particular factor. Figure shows ROC curves and AUC values for BMI, ALT, AST and TBil: 0.567, 0.774, 0.750, 0.648, respectively. The greatest prognostic value with respect to >50% macrosteatosis are donor ALT and AST values, whose AUC is 0.774 and 0.750, respectively. Donor BMI and TBil were excluded as predictors of >50% steatosis because of low AUC values. So, we do not consider high TBil and increased body weight as screening predictors of steatosis in the donor (Fig.).

In ROC analysis, optimal cutoff thresholds were obtained by calculations so that the studied models for predicting severe donor steatosis could be used in practice. For ALT and AST values, the cutoff thresholds were 90 U/L and 110 U/L, respectively.

Taking into account the established thresholds, the sensitivity and specificity values for ALT and AST were obtained in the form of a contingency table. See Tables 3–4.

Almost identical indicators of sensitivity and specificity were revealed for liver enzymes ALT and AST – 69.1%, 80.6% and 72.2%, 81.1%, respectively.

Table 1

Comparative analysis of effective liver donor groups depending on steatosis grade

Factors		Group 1	Group 2	Group 3	P
		Steatosis 0–30%, n = 341	Steatosis 31–50%, n = 39	Steatosis >50%, n = 87	
Age, years, avr. (min–max)		48.8 (19–68)	51.2 (29–63)	49.0 (28–67)	0.46
Male / female, n (%)		233 (68.3) / 108 (31.7)	26 (66.7) / 13 (33.3)	64 (73.6) / 23 (26.4)	0.60
Stroke / traumatic brain injury, n (%)		280 (82.1) / 61 (17.9)	33 (84.6) / 6 (15.4)	58 (66.7) / 29 (33.3)	**0.004**
BMI, kg/m^2, n (%)	<30	251 (74.0)	20 (51.3)	51 (58.6)	**0.001**
	≥30	88 (26.0)	19 (48.7)	36 (41.4)	
DM, n (%)		26 (7.6)	4 (10.3)	18 (20.9)	**0.001**
Hypertension, n (%)		166 (48.7)	21 (58.3)	40 (46.0)	0.744
Platelets, ×10^9/L, avr. (min–max)		232.8 (14–567)	200.9 (66–330)	183.6 (18–469)	**<0.0001**
Arterial lactate, mmol/L, avr. (min–max)		2.9 (0.4–17.0)	3.0 (0.7–8.9)	3.4 (0.90–15.0)	0.308
ALT, U/L, avr. (min–max)		41.6 (1.8–783)	58.7 (15.6–459.0)	88.6 (6.60–319.0)	**<0.0001**
AST, U/L, avr. (min–max)		45.5 (1.5–947)	70.2 (7.1–729)	124.1 (16.9–729.6)	**<0.0001**
Total bilirubin, μmol/L, avr. (min–max)		11.8 (2.2–72)	17.2 (3.7–88.5)	16.5 (3.4–58.0)	**<0.0001**
Liver explanted / not explanted, n (%)		284 / 57 (83.3 / 16.7)	17 / 22 (43.6 / 56.4)	15 / 72 (17.2 / 82.8)	**<0.0001**

Note. avr., average value.

Table 2

Logistic regression of donor characteristics and >50% liver steatosis detected by time-zero biopsy in donors

Factors	OR	95% CI, min–max	P
Age, years	1.003	0.984–1.022	0.737
Gender, m/f	1.250	0.786–1.989	0.346
Cause of death, Stroke / TBI	1.903	1.172–3.088	**0.009**
BMI, kg/m^2	1.045	1.008–1.084	0.017
Hypertension	0.972	0.638–1.479	0.893
DM	2.908	1.576–5.364	**0.001**
ALT, U/L	1.009	1.005–1.013	**<0.0001**
AST, U/L	1.011	1.007–1.014	**<0.0001**
TBil, μmol/L,	1.033	1.015–1.052	**<0.0001**
Platelets, ×10^9/L	0.993	0.991–0.996	**<0.0001**
Glucose, mmol/L	1.042	0.991–1.094	0.106

Note. OR, odds ratio; CI, confidence interval.

Given the values obtained, we can say that if the level of liver enzymes reaches and passes the threshold values we have identified, liver parenchyma damage is highly probable, but low sensitivity indicates a possible multifactorial nature of such damage; steatosis may be one of the factors.

CONCLUSION

Predictors of morphologically confirmed >50% steatosis in liver donors were identified. Donor age, sex, and blood glucose levels are not reliable predictors of hepatic >50% steatosis. BMI and TBil have low AUC values (0.56 and 0.645, respectively) in ROC analysis. Therefore, we believe they cannot be used as screening predictors of this pathology. The factor such as thrombocytopenia, although demonstrating a significant correlation with >50% hepatic steatosis, is nonetheless too

variable and nonspecific, and may be associated with various causes that were not considered in this study. TBI, as the cause of donor death, correlates with total and subtotal liver steatosis of alcoholic origin. Among the considered possible predictors of >50% hepatic steatosis, transaminases (ALT, AST) with relatively low sensitivity (69.1% and 72.2%, respectively) showed acceptable specificity (80.6% and 81.1%, respectively), which means that if these parameters are increased (ALT >90 U/L, AST >110 U/L) in a potential liver donor, significant fatty hepatosis can be predicted with a certain degree of probability. A significant association with >50% steatosis

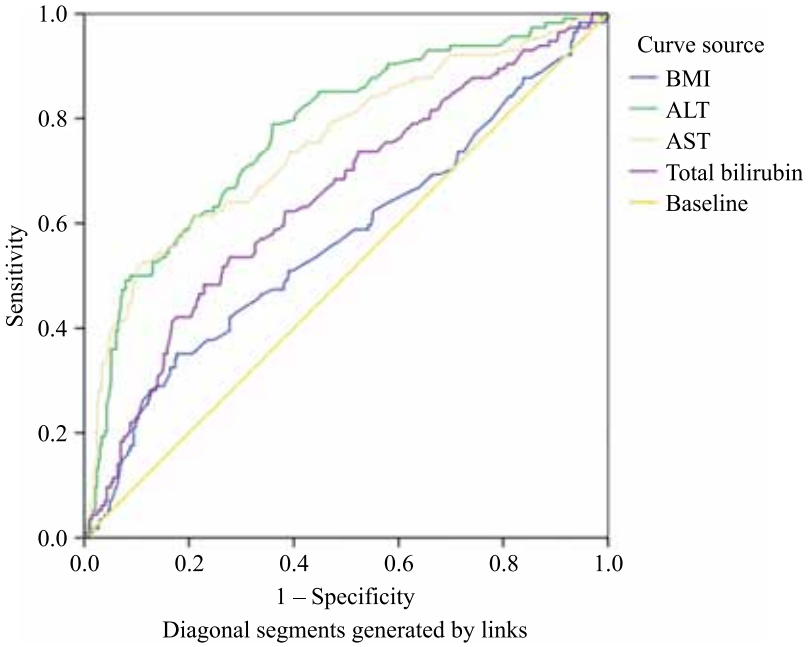

Area under the curve

Validation result variables	Area	Standard error	Asymptotic value	Asymptotic 95% CI	
				Lower bound	Upper bound
BMI	0.567	0.033	0.034	0.503	0.631
ALT	0.774	0.026	0.000	0.723	0.825
AST	0.750	0.028	0.000	0.695	0.805
TBil	0.648	0.030	0.000	0.589	0.708

Fig. ROC curves and AUC for BMI, ALT, AST and TBil

Table 3

Sensitivity and specificity for ALT

	ALT <90	ALT >90	Total:
Steatosis <50	324	17	341
Steatosis >50	78	38	116
Total:	402	55	457
Specificity	324 : (324 + 78) × 100%		**80.6**
Sensitivity		38 : (38 + 17) × 100%	**69.1**

Table 4

Sensitivity and specificity for AST

	ACT <110	ACT >110	Total:
Steatosis <50	327	15	342
Steatosis >50	76	39	115
Total:	403	54	457
Specificity	327 : (327 + 76) × 100%		**81.1**
Sensitivity		39 : (39 + 15) × 100%	**72.2**

was demonstrated by DM in liver donors. Type 2 DM and ALT and AST values above the cutoff point thresholds should raise the concern of specialists during the initial donor evaluation for severe steatosis.

The authors declare no conflict of interest.

REFERENCES

1. *Steggerda JA, Bloom BM, Noureddin M, Brennan TV, Tsuyoshi T, Nissen NN et al.* Higher thresholds for the utilization of steatotic allografts in liver transplantation: Analysis from a U.S. national database. *PLoS ONE.* 2020; 2 (4): 15.
2. *Verran D, Kusyk T, Painter D et al.* Clinical experience gained from the use of 120 steatotic donor livers for orthotopic liver transplantation. *Liver Transpl*. 2003; 9 (5): 500–505.
3. *Halon A, Patrzalek D, Rabczynski J.* Hepatic steatosis in liver transplant donors: rare phenomenon or common feature of donor population? *Transplant Proc*. 2006; 38 (1): 193–195.
4. *Estes C, Razavi H, Loomba R, Younossi Z, Sanyal AJ.* Modeling the epidemic of nonalcoholic fatty liver disease demonstrates an exponential increase in burden of disease. *Hepatology*. 2018; 67 (1): 123–133.
5. *Pais R, Barritt ASt, Calmus Y et al.* NAFLD and liver transplantation: Current burden and expected challenges. *J Hepatol*. 2016; 65 (6):1245–1257.
6. *Durand F, Renz JF, Alkofer B, Burra P, Clavien P-A, Port RJ et al.* Report of the Paris consensus meeting on expanded criteria donors in liver transplantation. *Liver Transpl*. 2008; 14 (12): 1694–1707.
7. *Hubutija MSh, Guljaev VA, Zimina LN, Novruzbekov MS, Minina MG.* Kompleksnaja ocenka sostojanija pecheni posle vypolnenija laparotomii u mul'tiorgannyh donorov. *Vestnik transplantologii i iskusstvennyh organov.* 2012; (14): 1.
8. *Fiorentino M, Vasuri F, Ravaioli M, Ridolfi L, Grigioni WF, Pinna AD, D'Errico-Grigioni A.* Predictive value of frozen-section analysis in the histological assessment of steatosis before liver transplantation. *Liver Transpl*. 2009; 15 (12): 1821–1825.
9. *Brunt EM.* Surgical assessment of significant steatosis in donor livers: The beginning of the end for frozen-section analysis*? Liver Transpl*. 2013; 19 (4): 360–361.
10. *Guzzaloni G, Grugni G, Minocci A, Moro D, Morabito F*. Liver steatosis in juvenile obesity: Correlations with lipid profile, hepatic biochemical parameters and glycemic and insulinemic responses to an oral glucose tolerance test. *Int J Obes Relat Metab Disord.* 2000; (24): 772–776.
11. *Monsour HP Jr, Wood RP, Ozaki C, Katz S, Clark J, Dyer C et al.* Utility of preoperative liver biopsy in live-related donor patients for liver transplantation. *Transplant Proc.* 1994; 26: 138–139.
12. *Rinella ME, Alonso E, Rao S, Whitington P, Fryer J et al.* Body mass index as a predictor of hepatic steatosis in living liver donors. *Liver Transpl*. 2001; 7 (5): 409–414.
13. *Bellentani S, Saccoccio G, Masutti F, Croce LS, Brandi G, Sasso F et al.* Prevalence of and risk factors for hepatic steatosis in Northern Italy. *Ann Intern Med.* 2000; 132: 112–117.
14. *Lee, Jeong-Hoon et al*. Hepatic steatosis index: A simple screening tool reflecting nonalcoholic fatty liver disease. *Digestive and Liver Disease.* 2009; 42 (7): 503–508.
15. *Cesaretti M, Addeo P, Schiavo L, Anty R, Iannelli I.* Assessment of Liver Graft Steatosis: Where Do We Stand? *Liver Transpl.* 2019; 25 (3): 500–509.
16. *Peck-Radosavljevic M.* Thrombocytopenia in chronic liver disease. *Liver Int*. 2017 Jun; 37 (6): 778–793.
17. *Lonardo A, Bellentani S et al.* Epidemiological modifiers of non-alcoholic fatty liver disease: focus on high-risk groups. *Dig Liver Dis.* 2015; 47: 997–1006.
18. *Lonardo A, Carani C, Carulli N et al.* 'Endocrine NAFLD' a hormonocentric perspective of nonalcoholic fatty liver disease pathogenesis. *J Hepatol.* 2006; 44: 1196–1207.
19. *Kotronen A, Juurinen L, Tiikkainen M, Vehkavaara S, Yki-Jarvinen H:* Increased liver fat, impaired insulin clearance, and hepatic and adipose tissue insulin resistance in type 2 diabetes. *Gastroenterology.* 2008; 135 (1): 122–130.
20. *Fernandez-Real JM, Menendez JA, Moreno-Navarrete JM, Bluher M, Vazquez-Martin A, Vazquez MJ, Ortega F, Dieguez C, Fruhbeck G, Ricart W*: Extracellular fatty acid synthase: a possible surrogate biomarker of insulin resistance. *Diabetes*. 2010; 59 (6): 1506–1511.

The article was submitted to the journal on 25.08.2022

DOI: 10.15825/1995-1191-2022-4-124-134

USE OF POLYCLONAL ANTIBODIES IN BRAIN-DEAD DONORS IN KIDNEY TRANSPLANTATION

D.O. Kuzmin[1, 2], V.A. Manukovsky[1], S.F. Bagnenko[2], O.N. Reznik[1, 2, 4], A.N. Ananiev[1, 2], O.A. Vorobyeva[3], S.L. Vorobyev[3], D.V. Gogolev[1, 2], V.S. Daineko[1, 4], A.A. Kutenkov[1, 2], N.A. Chichagova[1, 2], I.V. Uliankina[1, 2]

[1] St. Petersburg Research Institute of Emergency Medicine, St. Petersburg, Russian Federation
[2] Pavlov First St. Petersburg State Medical University, St. Petersburg, Russian Federation
[3] National Center for Clinical Morphological Diagnostics, St. Petersburg, Russian Federation
[4] North-Western State Medical University, St. Petersburg, Russian Federation

Objective. The objective of this study is to develop a therapeutic strategy for protecting grafts in order to improve the efficiency of kidney transplantation (KT) using polyclonal antibodies (pAbs) through elimination of activated forms of neutrophils, chemo- and cytokines from the donor's bloodstream, and a decrease in the level of expression of adhesion molecules on the renal vascular endothelium at the pre-transplant stage. **Materials and methods.** In 2017, we developed and for the first time applied a therapeutic strategy for ischemia-reperfusion injury (IRI) in a brain-dead donor (BDD). Given the limited time interval after brain death has been diagnosed, Timoglobulin (Sanofi Genzyme, France) was administered to the donor at a dose of 8 mg/kg intravenously for 6 hours. Before drug administration and immediately before the start of cold perfusion, a complete blood count and renal transplant biopsy were performed. The study group included 10 BDDs (mean age 39.3 ± 4.4 years) who received anti-thymocyte globulin (ATG). The comparison group included 10 BDDs (mean age 38.5 ± 4.3 years) who did not undergo the new strategy. Donor kidneys were transplanted to 40 recipients (average age 47.5 ± 4.3 years), who were also divided into 2 groups, depending on the graft received (with and without ATG). At the organ donation center, a biobank of specimens from donors of various categories, including those using the IRI therapeutic strategy and recipients for retrospective assessment of the effectiveness of pAbs, was formed. **Results.** Clinical blood test results show that in the ATG group, there was stable leukopenia (neutropenia and lymphopenia) of 1.46 ± 0.18x109/l. Fifteen (75%) recipients of kidneys obtained from donors with ATG had immediate graft function; in the control group – 10 (50%) recipients. **Conclusion.** Data obtained testify to the prospects of implementing the proposed strategy in clinical practice, which will improve the quality of the resulting grafts and their suitability for subsequent transplantation, prolong graft functioning due to elimination of leukocytes as a factor of IRI, prevention of early allograft nephropathy, increase in the donor pool by using expanded criteria donors (ECDs).

Keywords: organ donation and transplantation, ischemia-reperfusion injury, polyclonal antibodies.

INTRODUCTION

KT is a radical surgical intervention for end-stage renal disease. Therefore, it is generally accepted that KT is the treatment of choice and provides a better survival rate compared to long-term dialysis. It is also preferable in terms of quality and life expectancy of the recipient [1]. However, there is a worldwide shortage of suitable donor organs, and this method of treatment remains poorly available. In 2020, only 75,664 kidney transplants were performed worldwide [GODT. Global Observatory on Donation and Transplantation. 2020. http://www.transplant-observatory.org/reports. Accessed August 1, 2021].

For many years, the main source of donor organs was brain-dead donor (BDDs), whose organs were considered ideal. However, donor organ shortage has led to the use of transplants from expanded criteria donors (ECDs). This category of donors used to be regarded as an additional transplant resource, but today they are becoming the main resource [2]. The use of the ECD resource, which includes all donors >60 years old, or ≥50 years old, amidst comorbid conditions such as a history of hypertension, plasma creatinine levels >132 μmol/L just before the explantation procedure, diabetes mellitus, and excessive body weight (body mass index >30) can lead to a high risk of delayed function [3]. Nevertheless, this category of donors is considered an acceptable resource for KT [4].

Delayed graft function and poor long-term transplant outcomes remain a major obstacle to the expansion

Corresponding author: Denis Kuzmin. Address: 3, Budapestkaya str., St. Petersburg, 197345, Russian Federation. Phone: (904) 648-68-38. E-mail: drkuzmindo@gmail.com

of the donor pool. KT from ECDs is characterized by more severe IRI. This is caused by hemodynamics instability in these kinds of donors. As a consequence, a complex set of events develops in such kidneys, which is characterized by more severe acute graft injury [5].

Delayed function occurs due to a pathophysiological complex of events associated with ischemic and hypoxic injury and reperfusion after hypothermic preservation, with a long recovery period after acute tubular necrosis [6]. Some researchers believe that in 23–38% of recipients of a kidney from a deceased donor, who receive hemodialysis within the first week after transplantation, the risk of graft loss increases to 40%. A significant proportion of kidneys obtained from donors over 50 years or from donors with high serum creatinine levels are not used [7].

Systemic inflammatory response, cell adhesion cascade and leukocyte activation are the key pathological mechanisms whose cumulative effect causes a sharp decrease in the functional reserve of the organs or, in the most unfavorable scenario, to irreversible changes leading to unsuitability for transplantation [8]. The most important in this case is the time of hemodynamic instability, warm ischemia, and "leukocyte mobilization" that occurs, having as a target the microcirculatory bed and endothelium of the organs. After triggering blood flow, activated neutrophils become the main source of free radicals and lysis enzymes production [9]. It should be noted that activation of adhesion molecules initiates neutrophil migration into the graft and leukocyte infiltration of tissues in general still at the donor stage, which further potentiates reperfusion kidney injury in the recipient body. So, IRI leads to increased length of hospital stay and reduced graft survival [10].

In turn, activated leukocytes play the leading role in the development of IRI. Mass adhesion of leukocytes to vessel walls and to each other eventually leads to the formation of large leukocyte conglomerates, which clog the vascular lumen and sharply impair venous outflow. In such clusters, individual leukocytes are rather strongly fixed to each other, but conglomerates themselves are of different sizes and sometimes weakly fixed to the vessel wall, so they are washed away by blood a few minutes after formation and carried away into larger vessels. However, during the terminal periods of tissue oxygen starvation, conglomerates persist, and according to Ivanov K.P. (1992), they stop "trains of red blood cell", leukocyte-platelet interactions occur, which leads to occlusion of vessels of increasing diameter and to their deformation. This subsequently explains the difficulty or impossibility of restoring microcirculation after deep hypoxia [11]. After restoration of blood flow, activated neutrophils producing free radicals and lysis enzymes become the main acting factor of IRI [12].

It has been established that at the time when the ischemia-reperfusion process begins, there is activation of neutrophils and further tissue injury through the release of reactive oxygen species (ROS), proteinases and cationic peptides [13]. Under the influence of proinflammatory cytokines and adhesion cascade, nicotinamide adenine dinucleotide phosphate (NADPH) oxidase is activated, which causes production of large amounts of ROS by neutrophils [14]. Neutrophils block the capillary bed, preventing reperfusion, which leads to tissue necrosis and increased immune response [15]. Neutrophils secrete proinflammatory cytokines and chemokines, creating positive feedback [16]. In addition, neutrophil migration causes loss of epithelial barrier integrity and downregulates adhesion molecules [17].

IRI is initiated by an episode of ischemia, when blood supply to a part or whole organ is restricted, causing cell death, which is further exacerbated when blood flow resumes. Ischemia leads to tissue hypoxia, which causes accumulation of metabolites and ROS, namely superoxide, hydrogen peroxide, and hydroxyl radicals. ROS increase the amount of intracellular calcium, causing pH changes and simultaneously depleting adenosine triphosphate acid reserves, which leads to damage of cell organelles and cell necrosis. Prolonged ischemia time lasting from several minutes to half an hour causes irreversible effects, which are aggravated by reperfusion. During reperfusion, the ischemic tissue is filled with oxygen. This activates metabolites and ROS, which leads to an inflammatory response causing IRI [18].

According to Schofield Z.V. et al. (2013), IRI is a complex physiological process, but the undeniable leading role in it is played by neutrophils, which can penetrate the damaged tissue in just a few minutes after activation. Cytokines, ROS and the complement system are also important in the pathogenesis of IRI because they support, activate and enhance the destructive function of neutrophils. However, recent studies have again drawn attention to the role of neutrophils as a key player in the pathophysiology of IRI [12].

With the growing shortage of donor organs and increasing use of suboptimal quality organs, the study of pathophysiological processes developing in the body of a deceased donor has gained particular importance. Understanding the basis of pathological changes in grafts allows for consideration of new possibilities of influencing them, including through the use of new drug therapy techniques at the pre-transplantation stage in the donor's body. This can be an effective means of increasing the longevity of grafts obtained, including those from ECDs [19].

EpCAM (epithelial cell adhesion molecule) proteins are expressed on the membrane of renal epithelial cells, where it is involved in cellular and intercellular inter-

actions. The degree of EpCAM expression increases significantly during renal tissue repair and correlates with the severity of IRI effects. Transplant tissue regeneration requires a very high level of EpCAM expression for the development of cell proliferation, migration and differentiation processes [20]. It is assumed that prolonged and massive expression of EpCAM is associated with its tropism to cell proliferation and adhesion processes, which is observed after IRI. Thus, regulation of EpCAM expression is directly related to the need for renal tissue regeneration [21].

Research is ongoing around the world to find highly specific biomarkers of adverse conditions in transplantation. Creation of transplant biobanks, formed according to the standard methodology, should guarantee reliable statistical and clinical data. Evaluation of this data should result in the introduction of new ways of therapeutic correction of IRI in the donor's body. Collection, processing and storage of different types of samples at all stages of the donor process, during organ transplantation, as well as in the postoperative period, can serve as the basis for the creation of unique biobanks. Such biobanks will represent a matrix for end-to-end prospective longitudinal studies. The use of modern genomic techniques, including next-generation sequencing, will allow for a systematic approach to the study of ischemia-reperfusion and the genetic basis of transplant rejection response, will provide an individual approach to prescription of immunosuppressive drugs based on the genetic profiles of donor and recipient.

In the long term, it will be possible to address more ambitious tasks, such as studying the processes of "dying" with precise determination of the moment of the onset of irreversible changes. This will make it possible to revise the existing criteria for determining the suitability of organs for transplantation, moving away from an empirical approach to a genetically based one [22].

OBJECTIVE

To develop and implement a new method of drug therapy at the pretransplantation stage in BDDs, which can serve as an effective means of increasing the longevity of transplanted organs derived from ECDs, boosting the efficiency of KT through the use of polyclonal antibodies.

MATERIALS AND METHODS

A meeting of the Local Ethics Committee of St. Petersburg Research Institute of Emergency Medicine on March 15, 2017 approved the study "Use of polyclonal antibodies in brain-dead donors in kidney transplantation" and authorized its further development under the St. Petersburg Research Institute of Emergency Medicine. The present study was initiated in March 2017, with its five-year results evaluated in July 2022.

According to the official instructions for polyclonal antibodies thymoglobulin (Sanofi Genzyme, France), the patient develops deep lymphopenia (reduced lymphocyte count by more than 50% compared with the initial value) at day 1 after injection. A new method of therapeutic use of the drug, traditionally used only for the treatment of steroid-resistant rejection crises in recipients, seems to be an effective method of improving the quality of kidney transplants, by "turning off" the IRI leukocyte link, which, according to our hypothesis, will positively affect long-term transplant outcomes.

Given the existing time limitation for administration of the drug in the BDD (corresponding to the time interval required for the brain death diagnosis procedure in the donor), an empirical decision was made to increase the drug dose fourfold in order to achieve maximum reduction in the number of mobilized leukocytes. Thus, a proprietary technique for applying polyclonal antibodies in the BDD during KT was developed.

After the initial examination of the BDD by a team consisting of an anesthesiologist/resuscitator, a surgeon from the organ donation coordination center, and the transplant coordinator of the hospital, and a decision to start the brain death diagnosis procedure and plan kidney explantation, thymoglobulin, manufactured by Genzyme Polyclonals, S.A.S. (France), was administered to the donor within 6 hours at a 4-fold therapeutic dose. The drug dose was 8 mg/kg body weight. The drug was dissolved in 50.0 ml of saline and injected into the central venous catheter using a 0.14 ml/min single-syringe infusion pump.

Before the drug was injected and immediately before the start of cold perfusion, a complete blood count was performed. The study group included 10 BDDs (mean age, 39.3 ± 4.4 years) who received antithymocyte immunoglobulin (ATG); the comparison group consisted of 10 BDDs (mean age, 38.5 ± 4.3 years) without the new protocol; donor kidneys were transplanted to 20 recipients in the study group (mean age, 42.3 ± 3.1 years) and 20 recipients in the control group (mean age, 41.2 ± 3.3 years) depending on the graft received (with and without ATG). The general characteristics of the groups are given in Table 1 and Table 2.

In 2015, a transplant biobank was created for the first time in the Russian Federation under the St. Petersburg Donation Coordination Center. The biobank formed a collection of biological samples from donors and recipients, allowing to perform retrospective immunohistochemistry in kidney transplant biopsies to assess the effectiveness of the use of pAbs for IRI reduction in BDDs at the pre-explantation stage. Qualified specimen collection, processing, characterization and storage are performed for the functioning of the transplant biobank. Work with documentation and databases was standar-

Table 1

General characteristics of donor groups

Characteristics		Control group (no ATG), n = 10	Study group (with ATG), n = 10	P value
Age, years		38.5 ± 4.3	39.3 ± 4.4	0.08
Diagnosis	Stroke	4 (40%)	4 (40%)	
	Brain injury	2 (20%)	1 (10%)	
	Ruptured brain aneurysm	4 (40%)	6 (60%)	
Creatinine, μmol/l		66.5 ± 6.9	68.9 ± 7.3	
Urea, mmol/l		4.9 ± 0.5	5.6 ± 0.6	

Table 2

General characteristics of recipient groups

Characteristics		Control group (no ATG), n = 20	Study group (with ATG), n = 20	P value
Age, years		41.2 ± 3.3	42.3 ± 3.1	0.09
Diagnosis	Chronic glomerulo-nephritis	15 (75%)	15 (75%)	
	Autosomal dominant polycystic kidney disease	3 (15%)	2 (10%)	
	Stage 3 hypertension	2 (10%)	3 (15%)	

dized, algorithms for primary processing and storage of biosamples, and maintenance of proper sample condition were developed.

Incisional biopsies from kidney transplants served as the study material. Histological examination of kidney tissue was carried out at the National Center for Clinical Morphological Diagnostics, St. Petersburg, using the following methods:

1) Light microscopy was performed on paraffin sections using the following stains: H&E and PAS.
2) Immunohistochemistry performed by immunoperoxidase method using anti-EpCAM antibodies.

RESULTS

Immunohistochemistry in kidney transplant biopsies was performed to verify clinical data. In kidney transplant biopsies from BDDs in the comparison group, light microscopy demonstrated preserved histoarchitectonics of the renal parenchyma. The glomeruli had a single-loop capillary wall, with no signs of mesangial and endocapillary hypercellularity, no segmental glomerulosclerosis and crescents. There was artificial vacuolization of the epithelial cell cytoplasm of the proximal convoluted tubules. There were no signs of tubulointerstitial fibrosis. The walls of arterioles and small caliber arteries had no pathological changes. Immunohistochemistry study showed positive expression of EpCAM in the epithelial cell cytoplasm of the proximal convoluted tubules and no expression in other renal tissue structures (Fig. 1).

Histomorphological data indicating the resulting ischemic injury were assessed by the presence of positive expression of EpCAM molecules in the epithelial cytoplasm of the distal convoluted tubules. According to the study of kidney transplant biopsies from BDDs in the study group at the light microscopy level, the histological pattern remained the same. Immunohistochemistry, in turn, demonstrated a change in EpCAM expression – there was complete absence of EpCAM expression in all renal tissue structures, including the epithelial cytoplasm of the distal convoluted tubules.

Evaluation of clinical blood tests results in comparison groups: in the study group, there was stable leukopenia (neutropenia and lymphopenia) of $1.46 \pm 0.18 \times 10^9$/l (Fig. 2).

Also, according to laboratory data, a significantly higher level of Lipocalin-2 (neutrophil gelatinase-associated lipocalin, NGAL) was detected in the urine of BDDs in the control group compared to BDDs in the study group (Fig. 3).

The prognostic and diagnostic value of NGAL in acute kidney injury (AKI) is explained by the fact that it is excreted in the urine after renal parenchymal ischemia injury and is rightfully considered a "kidney troponin".

The high level of NGAL in BDDs in the control group demonstrates tubular lesions that precedes AKI.

Fifteen (75%) patients who got kidneys from donors who received ATG had immediate graft function, whereas there were 10 (50%) recipients in the group without the new protocol (Table 3, Fig. 4).

Five years after transplantation, serum creatinine and urea levels were lower in recipients of kidneys obtained from donors who received ATG (Table 3, Figs. 5 and 6).

Table 3

Assessment of kidney transplant function in two groups of recipients

Characteristics		Control group (no ATG), n = 20	Study group (with ATG), n = 20	P value
Graft function	Immediate	10 (50%)	15 (75%)	0.002
	Delayed	10 (50%)	5 (25%)	
Creatinine, μmol/L (after 5 years)		127.0 ± 6.8	101.0 ± 6.3	0.07
Urea, mmol/L (after 5 years)		8.1 ± 0.9	7.8 ± 1.1	0.08

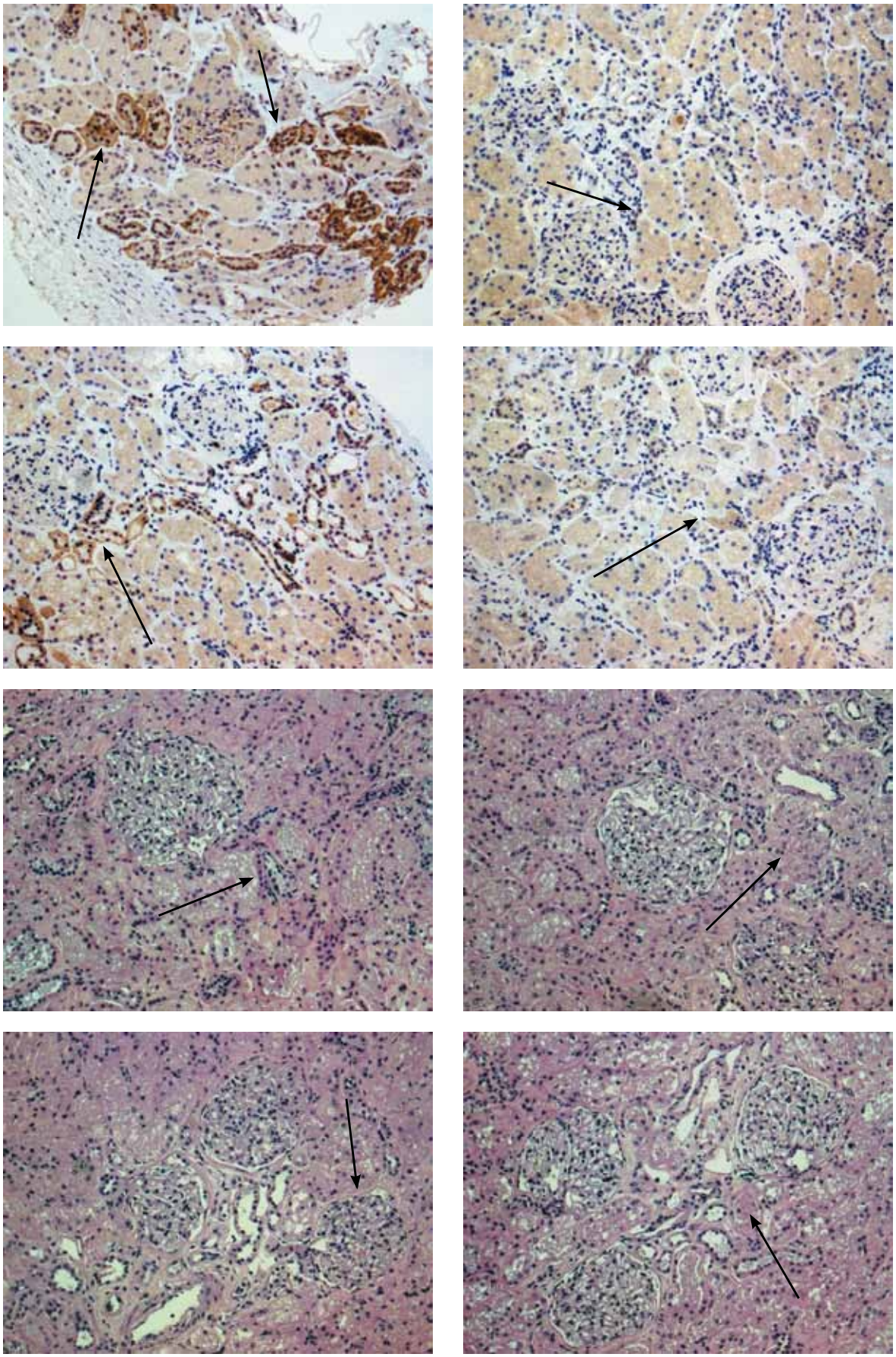

Fig. 1. Immunohistochemistry in null kidney graft biopsies from BDDs in the comparison group and the study group. In the comparison group there is a positive expression of EpCAM in the epithelial cytoplasm of the distal convoluted tubules – indicated by arrows in the figures in the left column. In the study group, there is no EpCAM expression in all renal tissue structures – indicated by arrows in the figures in the right column

Fifteen (75%) patients who received kidneys from donors injected with pAbs were observed to have immediate graft function, compared with 10 (50%) recipients in the comparison group. Five-year graft survival was 100% (n = 20) (pAbs), in contrast to 75% (n = 15). Serum creatinine levels 5 years after transplantation averaged 0.101 mmol/L in patients who received kidneys from BDDs injected with pAbs and 0.127 mmol/L in the comparison group.

Kaplan–Meier curves were plotted to assess the survival of kidney recipients and transplants in the study and comparison groups (Figs. 7 and 8).

ATG administered to donors can prevent IRI effects during KT by reducing the degree of necrosis and apoptosis and improving renal function, which is explained by a decrease in the expression of proinflammatory mediators.

In addition, given the functions and mechanisms of regulation of EpCAM expression, it can be concluded that our immunohistochemical study of kidney transplant biopsies demonstrate the effectiveness of pAbs in BDDs.

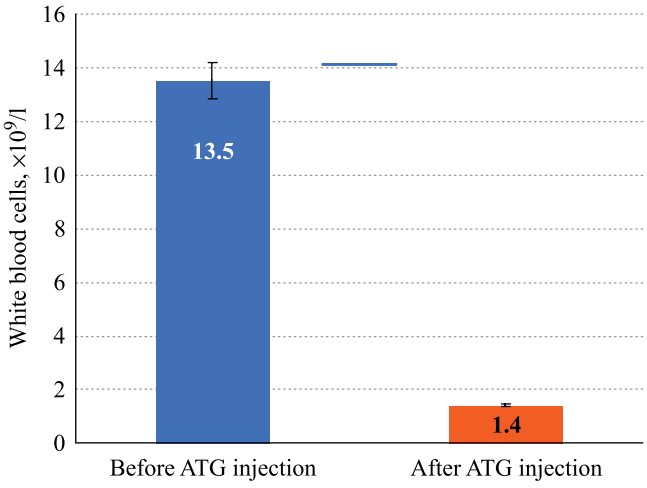

Fig. 2. WBC count in BDDs in the study groups before and 6 hours after ATG injection

DISCUSSION

A significant challenge in transplantation is the ability to use organs from ECDs without compromising immediate graft function and long-term graft survival.

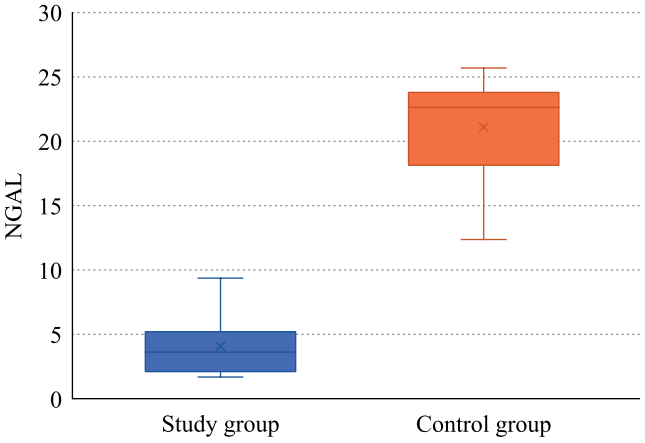

Fig. 3. Urinary NGAL levels in BDDs in the study and control groups

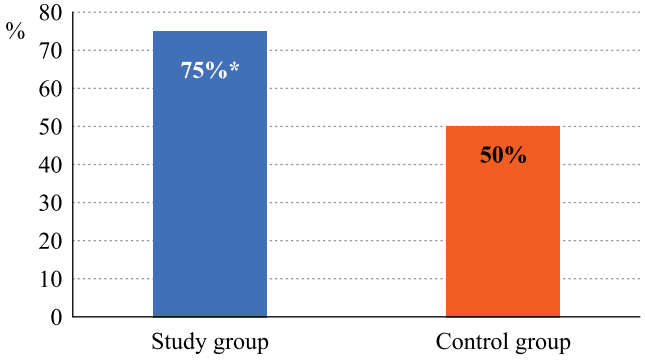

Fig. 4. Immediate function of kidney grafts in recipients in the study groups. * – p = 0.0008 compared to the control group

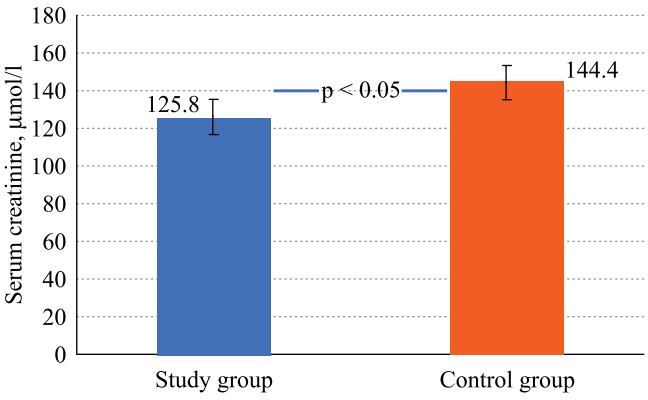

Fig. 5. Serum creatinine levels in recipients 5 years after kidney transplantation in the study groups

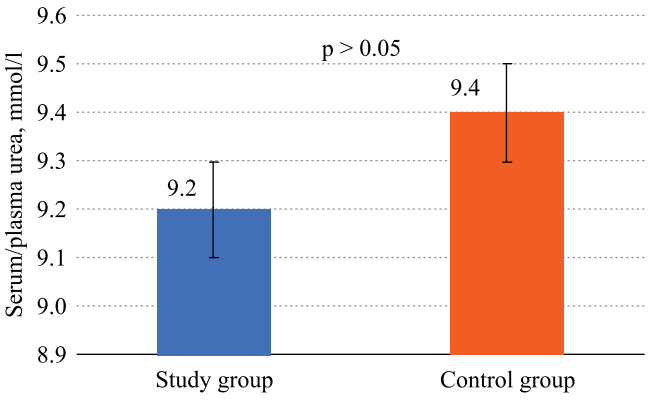

Fig. 6. Serum/plasma urea level in recipients 5 years after transplantation in the compared groups

Therefore, it is crucial to optimize each organ even before transplantation and to minimize additional damage to achieve the best possible function and avoid primary nonfunction, delayed function or acute rejection.

In the last decade, more information on the complex pathophysiology of IRI has emerged, opening the door for new therapeutic tools aimed at reducing the effects of IRI, tissue hypoxia as a result of microcirculatory bed blockage by recruited leukocytes. However, the existing methods for correcting IRI effects involve extracorporeal filtration and a whole arsenal of therapeutic options, which, however, still remain a compromise between desired effect and clinical reality. Despite significant progress in the study of the process underlying the mechanisms of renal graft dysfunction, treatment methods are still insufficient, and the results remain mixed.

For the first time in the clinical practice of KT, we proposed a new original scheme for IRI correction in BDDs. We propose a new way of protecting grafts by eliminating activated neutrophil forms from the donor's

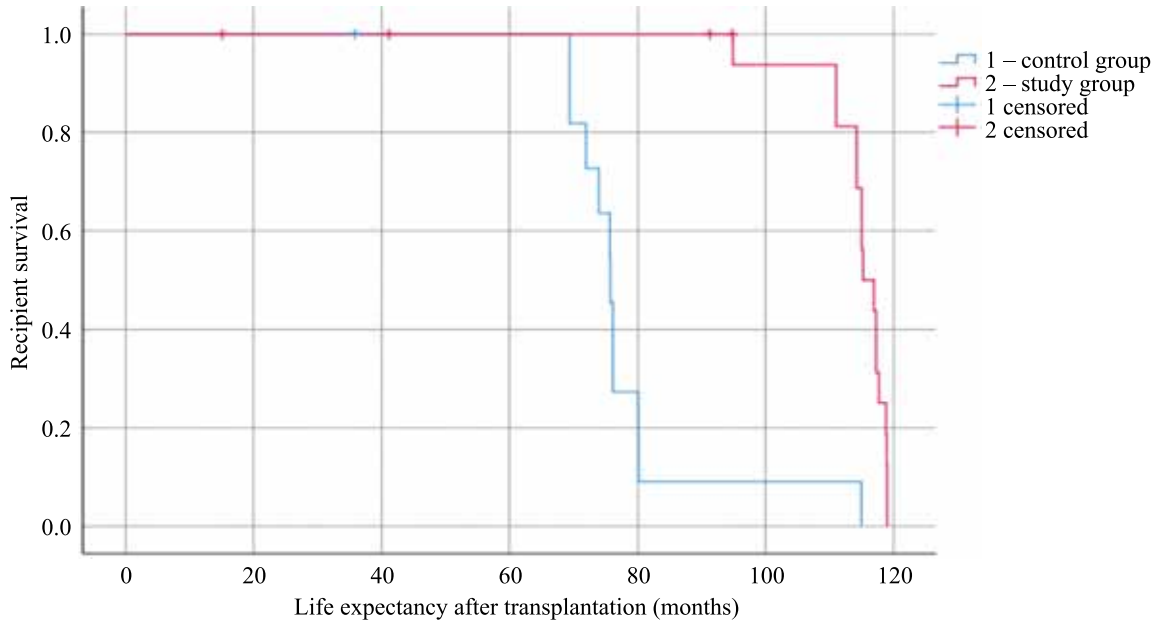

Fig. 7. Assessment of recipient survival

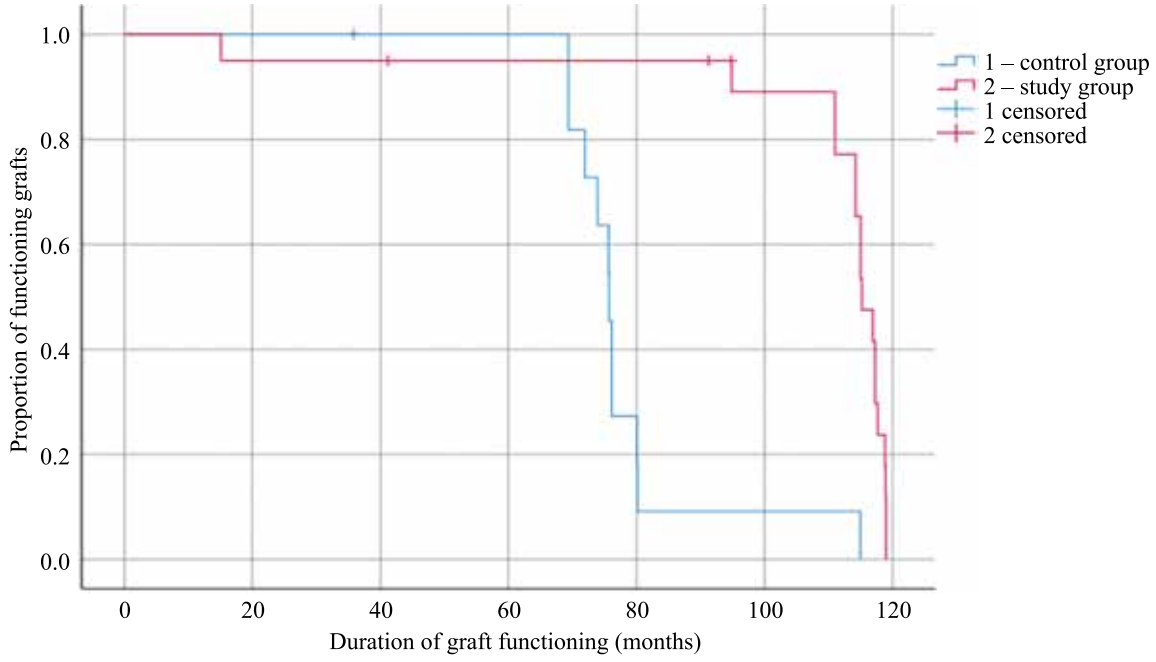

Fig. 8. Assessment of kidney graft survival

blood circulation, reducing the expression of adhesion molecules on the renal vascular endothelium by injecting pAbs into the BDD's body before explantation.

Thymoglobulin is a polyvalent drug, tropic to a variety of target antigens, which can be classified as immune response antigens, adhesion molecules and cellular transport. In this regard, therapeutic use of pAbs in BDDs, previously used only for the treatment of kidney recipients, seems to be an effective method of improving the quality of kidney transplants due to reduction of the IRI leukocyte link, which will positively affect long-term transplant outcomes. However, no reports on the use of pAbs in BDDs to improve the quality of kidney transplants have been found in available literature.

The developed protocol includes the following algorithm of actions when planning kidney explantation: after the BDD has been initially examined by a team consisting of the hospital's transplant coordinator, anesthesiologist/resuscitator and surgeon from the organ donation coordination center, negative serological test results for viral infectious agents has been obtained, and a decision to start a brain death diagnosis procedure has been taken, thymoglobulin was injected into the donor in a dose of 8 mg/kg body weight. Given the existing time limitation for administration of the drug in the BDD (corresponding to the time interval required for brain death diagnosis procedure in the donor), an empirical decision was made to increase the drug dose fourfold in order to achieve maximum reduction in the number of mobilized leukocytes.

Our hypothesis required not only clinical verification but also morphological confirmation, which is difficult to implement "here and now". It was important to preserve biospecimens from BDDs and recipients for future studies. For this purpose, a transplant biobank was created; it is a collection of biospecimens and related information in a form suitable for analysis.

The study results indicate the prospects of implementing the proposed strategy in clinical practice, which will improve the quality of resulting grafts and their suitability for subsequent transplantation, prolong graft functioning by preventing early transplant nephropathy, increase the donor pool by using ECDs, minimize the probability of acute rejection in recipients, reduce the length of hospital stay and, therefore, reduce economic costs. This protocol, using thymoglobulin, demonstrates the need to develop a similar domestic drug aimed at reducing leukocyte aggression in BDDs.

CONCLUSION

The study results indicate the prospects of implementing the proposed strategy in clinical practice, which will improve the quality of resulting grafts and their suitability for subsequent transplantation, prolong graft functioning by eliminating leukocytes as a factor of IRI and preventing early transplant nephropathy, and increase the donor pool by using ECDs. For retro- and prospective evaluation of transplanted organs, it is necessary to create biobanks at donation centers and transplantation departments.

The authors declare no conflict of interest.

REFERENCES

1. *McFarlane PA.* Should patients remain on intensive hemodialysis rather than choosing to receive a kidney transplant? *Seminars in Dialysis.* 2010; 23: 516–519. doi: 10.1111/j.1525-139X.2010.00740.x. PMID: 21039877.
2. *Bahadur MM, Binnani P, Gupta R, Pattewar S.* Marginal donor kidney in a marginal recipient: Five year follow-up. *Indian J Nephrol.* 2010; 20 (2): 100–102. doi: 10.4103/0971-4065.65306. PMID: 20835327.
3. *Barba J, Zudaire J, Robles JE, Rosell D, Berian JM, Pascual I.* Complications of kidney transplantation with grafts from expanded criteria donors. *World J Urol.* 2013; 31: 893–899. doi: 10.1007/s00345-012-0831-3. PMID: 22290479.
4. *Ojo AO, Wolfe RA, Held PJ, Port FK, Schmouder RL.* Delayed graft function: risk factors and implications for renal allograft survival. *Transplantation.* 1997; 63: 968–974. doi: 10.1097/00007890-199704150-00011. PMID: 9112349.
5. *Perico N, Gaspari F, Remuzzi G.* Assessing Renal Function by GFR Prediction Equations in Kidney Transplantation. *American Journal of Transplantation.* 2005; 5: 1175–1176. doi: 10.1111/j.1600-6143.2005.00939.x. PMID: 15888019.
6. *De Vries DK, Lindeman JHN, Ringers J, Reinders MEJ, Rabelink TJ, Schaapherder AFM.* Donor brain death predisposes human kidney grafts to a proinflammatory reaction after transplantation. *American Journal of Transplantation*. 2011; 11 (5): 1064–1070. doi: 10.1111/j.1600-6143.2011.03466.x. PMID: 21449948.
7. *Yarlagadda SG, Coca SG, Formica Jr RN, Poggio ED, Parikh CR.* Association between delayed graft function and allograft and patient survival: a systematic review and meta-analysis. *Nephrology Dialysis Transplantation.* 2009; 24 (3): 1039–1047. doi: 10.1093/ndt/gfn667. PMID: 19103734.
8. *Hashemi P et al.* NETosis in ischemic/reperfusion injuries: An organ-based review. *Life Sci.* 2022; 290: 120158. doi: 10.1016/j.lfs.2021.120158. PMID: 34822798.
9. *Cahilog Z et al.* The Role of Neutrophil NETosis in Organ Injury: Novel Inflammatory Cell Death Mechanisms. *Inflammation.* 2020; 43 (6): 2021–2032. doi: 10.1007/s10753-020-01294-x. PMID: 32830308.
10. *Nakamura K, Kageyama S, Kupiec-Weglinski JW.* Innate immunity in ischemia-reperfusion injury and graft rejection. *Curr Opin Organ Transplant.* 2019; 24 (6): 687–693. doi: 10.1097/MOT.0000000000000709. PMID: 31592839.

11. *Ivanov KP, Levkovich JI.* Izmenenie mikrocirkuljacii pri lejkocitoze. *Fiziol zhurn.* 1992; 76: 321–326.
12. *Schofield ZV, Woodruff TM, Halai R, Wu MC, Cooper MA.* Neutrophils – a key component of ischemia-reperfusion injury. *Shock.* 2013; 40 (6): 463–70. doi: 10.1097/SHK.0000000000000044. PMID: 24088997.
13. *Liew PX, Kubes P.* The neutrophil's role during health and disease. *Physiological reviews.* 2019: 99 (2): 1223–1248. doi: 10.1152/physrev.00012.2018.
14. *Carbone F, Bonaventura A, Montecucco F.* Neutrophil-Related Oxidants Drive Heart and Brain Remodeling After Ischemia/Reperfusion Injury. *Front Physiol.* 2020; 10: 1587. doi: 10.3389/fphys.2019.01587. PMID: 32116732.
15. *Tejchman K et al.* The Role of Endothelins, IL-18, and NGAL in Kidney Hypothermic Machine Perfusion. *Biomedicines.* 2021; 9 (4): 417. doi: 10.3390/biomedicines9040417. PMID: 33924469.
16. *Qi H, Yang S, Zhang L.* Neutrophil Extracellular Traps and Endothelial Dysfunction in Atherosclerosis and Thrombosis. *Front Immunol.* 2017; 8: 928. doi: 10.3389/fimmu.2017.00928. PMID: 28824648.
17. *Mittal M et al.* Neutrophil Activation of Endothelial Cell-Expressed TRPM2 Mediates Transendothelial Neutrophil Migration and Vascular Injury. *Circ Res.* 2017; 121 (9): 1081–1091. doi: 10.1161/circresaha.117.311747. PMID: 28790198.
18. *Urisono Y et al.* Von Willebrand Factor Aggravates Hepatic Ischemia-Reperfusion Injury by Promoting Neutrophil Recruitment in Mice. *Thromb Haemost.* 2018; 118 (4): 700–708. doi: 10.1055/s-0038-1636529. PMID: 29618155.
19. *Fernández AR, Sánchez-Tarjuelo R, Cravedi P, Ochando J, López-Hoyos M.* Review: Ischemia Reperfusion Injury-A Translational Perspective in Organ Transplantation. *Int J Mol Sci.* 2020; 21 (22): 8549. doi: 10.3390/ijms21228549. PMID: 33202744.
20. *Trzpis M et al.* Expression of EpCAM is up-regulated during regeneration of renal epithelia. *J Pathol.* 2008; 216 (2): 201–208. doi: 10.1002/path.2396. PMID: 18702175.
21. *Akhtar AM et al.* In vivo quantification of VCAM-1 expression in renal ischemia reperfusion injury using non-invasive magnetic resonance molecular imaging. *PLoS One*. 2010; 5 (9): 34–35. doi: 10.1371/journal.pone.0012800. PMID: 20877722.
22. *Hanif Z et al.* Role of biobanks in transplantation. *Annals of medicine and surgery*. 2018; 28: 30–33. doi: 10.1016/j.amsu.2018.02.007.

The article was submitted to the journal on 05.07.2022

DOI: 10.15825/1995-1191-2022-4-135-144

HYPOPHARYNGEAL RECONSTRUCTION USING PRELAMINATED AUTOLOGOUS BIO-ENGINEERED PECTORALIS MAJOR FLAPS

I.V. Rebrikova[1, 2], E.A. Vorotelyak[3], O.S. Rogovaya[3], A.P. Polyakov[1, 2], A.V. Mordovskiy[1], M.V. Ratushnyy[1], A.D. Kaprin[1], A.V. Vasiliev[3]

[1] National Medical Research Radiological Centre, Moscow, Russian Federation
[2] RUDN University, Moscow, Russian Federation
[3] Koltzov Institute of Developmental Biology, Moscow, Russian Federation

After removal of metastatic malignant tumors of the hypopharynx and larynx, hypopharyngeal defects are formed. To restore the hypopharynx, a mucosa and a muscular component are needed. The **objective** of this study is to develop a hypopharyngeal reconstruction technique using prelaminated pectoralis major flap with mucosal epithelium analogue from autologous epithelial layers. **Materials and methods.** Nine patients underwent reconstruction of the hypopharynx using bioengineered prelaminated pectoralis major flaps. The mucosa was restored by tissue-engineered autologous epithelial cell layers that were obtained by culturing in vitro cells isolated from skin biopsies that were previously obtained from patients. **Results.** Oral nutrition was restored in all cases. Pharyngeal stenosis was detected in one (11%) patient. A stratified squamous epithelium on the pectoral fascia was revealed in 67% of cases at week 2 after prelamination, in 89% of cases at week 4 after reconstruction and in 100% of cases at month 3, 6, 12 and 24 after reconstruction. **Conclusion.** Reconstruction using prelaminated bioengineered flaps allows recreating the anatomical integrity and function of the hypopharynx.

Keywords: hypopharyngeal defects, reconstruction, prelaminated pectoralis major flap, tissue engineering, epithelial layers, keratinocytes.

INTRODUCTION

Patients with advanced hypopharyngeal and laryngeal cancers (stages III and IV) are most often candidates for combined oncologic treatment, combining extensive surgical resection and reconstruction with adjuvant radiotherapy (RT) or chemoradiotherapy (CRT). Sometimes the surgery is limited to tumor removal without a reconstructive phase due to the presence of severe comorbidities or treatment in non-specialist hospitals.

Different variants of flaps are used for hypopharyngeal reconstruction, including local flaps from the neck area, displaced regional flaps from the chest area, displaced visceral flaps, microsurgical free fasciocutaneous flaps, musculocutaneous flaps, visceral flaps, etc. [1, 2]. The main disadvantage of skin flaps is hair growth in the pharyngeal lumen. Visceral flaps are inapplicable in somatically burdened patients; their use is limited by concomitant abdominal conditions and previous interventions on the abdominal cavity.

The ideal material for reconstruction is autologous identical tissue, whose formation involves minimally invasive procedures on the donor site. There are known attempts to solve these issues by tissue engineering. Mucosal epithelial fragments have been cultured for use as biomaterials [1]. The use of cultured epithelial cells to restore the mucosa of the upper GI tract has been described. After oral tumor resection and endoscopic resection of the esophagus, surgeons implanted tissue-engineered epithelial cell layers on the underlying tissue [3, 4, 5]. It is important to note that epithelial-stromal interaction is a key determinant of the phenotypic dynamics of the epithelium in homeostasis and injury. The epithelium and the direction of epithelial stem cell differentiation are influenced by the underlying stromal cells producing a complex of signaling molecules [6, 7].

Prelamination transforms a native axial flap into a stratified one by adding appropriate structures for composite reconstruction [8]. It is a process involving the implantation of tissues or structures into the blood supplying microenvironment before they are transferred directly to the defect area [8, 9, 10].

The objective of the present study is to develop a technique for hypopharyngeal reconstruction by prelaminated flaps with mucosal restoration with tissue-engineered autologous epithelial cell sheets.

MATERIALS AND METHODS

Ethics statement

A prospective study was carried out from January 2018 to December 2019 at the National Medical Re-

Corresponding author: Olga Rogovaya. Address: 26, Vavilova str., Moscow, 119334, Russian Federation.
Phone: (499) 135-40-81. E-mail: Rogovaya26f@gmail.com

search Radiological Centre, Moscow. The study was reviewed and approved by the local ethics committee. All patients signed an informed consent.

Patients

Nine patients with hypopharyngeal defects after surgical treatment for malignant laryngeal tumors were included in the study. They were not candidates for microsurgical reconstruction due to comorbidities. In all cases, the reconstruction was delayed.

Characteristics of the patients are shown in Table. There were 8 males and 1 female; their ages ranged from 57 to 82 years (median: 69.5). Histological examination revealed squamous cell carcinoma in all cases. Six patients had stage III and IVA primary tumors. Six patients with primary laryngeal tumors had postoperative staging according to the 8th edition of TNM classification (developed and adopted by the American Joint Committee on Cancer (AJCC) and the Union for International Cancer Control (UICC). The tumor process in these patients corresponded to the following indicators: T4a (n = 4), T3 (n = 2), N0 (n = 5), N2c (n = 1). Three patients had recurrent tumors after previous CRT. All patients underwent laryngectomy, hypopharyngeal resection, and unilateral and/or bilateral lymphadenectomy depending on the condition of the cervical nodes. Eight patients underwent RT or CRT according to the stages of antitumor treatment prior to the reconstructive phase. Most patients had comorbidities according to the adult comorbidity evaluation 27 (ACE-27) scoring system. Hypopharyngeal defect after tumor removal was partial with preservation of a fragment of the posterior pharyngeal wall in all cases (Fig. 1, a).

Fabrication of autologous cell sheets

To isolate autologous epithelial cells, a skin biopsy from the patient's scalp was used. The skin fragment was resected under local anesthesia; the wound was sutured with Vicryl® 3.0 sutures. After the biopsy was taken, it was placed in a special container with a transport medium (DMEM with 0.4 mg/ml gentamicin) and transported to the Koltzov Institute of Developmental Biology, Moscow. Epithelial cell isolation was performed on the day the biopsy was taken. All procedures for isolating, cultivating, and transferring cell cultures to biopolymer

Table

Demographic data, treatment modality, and follow-up periods

Patient	Age	Gender	Tumor location	Stage	TNM	Primary or recurrent	RT/ChRT (Gr)	Preoperative comorbidity (ACE-27)	Follow-up period (months)
1	65	M	Larynx	IVA	T4aN0M0	Primary	RT (40)	Severe	27
2	59	F	Larynx	IVA	T3N2cM0	Primary	RT (50)	Severe	25
3	57	M	Larynx	IVA	T4aN0M0	Primary	RT (46)	Moderate	24
4	61	M	Larynx	IVA	T4aN0M0	Primary	CRT (59, 6)	Severe	20
5	60	M	Larynx	IVA	T4aN0M0	Primary	RT (50)	Severe	27
6	65	M	Larynx	III	T3N0M0	Primary		Severe	22
7	63	M	Larynx		rT4aN0M0	Recurrent	CRT (66)	Moderate	27
8	70	M	Larynx		rT4aN0M0	Recurrent	RT (50)	Moderate	24
9	82	M	Larynx		rT4aN0M0	Recurrent	CRT (70)	Severe	10

Abbreviations: RT, radiation therapy; CRT, CRT; Gr, Gray.

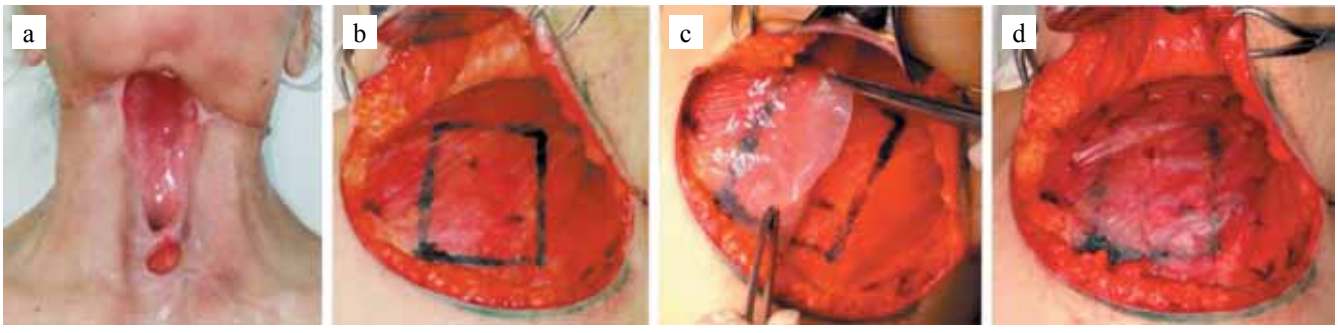

Fig. 1. The first stage of reconstructive surgery: (a) Patient with pharyngostomy after combined treatment of stage IVA laryngeal cancer; (b) surgical access for prelamination; (c) implantation of epithelial cell layer on the pectoral fascia; (d) isolation of epithelial cell sheet with film

matrices were performed strictly under aseptic conditions in the laboratory.

Isolation of epidermal keratinocytes

Skin biopsies obtained from the donor were cut into 3 × 10 mm wide strips, washed with phosphate-buffered saline (PBS) solution, placed in 0.2% dyspase solution (Sigma), and incubated at 4 °C for 18 hours. After fermentation, the epidermis was separated from the dermis along the basement membrane line, washed with PBS solution, and additional fermentation was performed with trypsin solution for 10 minutes to obtain a single-cell suspension. The suspension was centrifuged at 1000 rpm for 6 minutes, the supernatant was removed, and the precipitate was suspended in keratinocyte culture medium.

Cultivation of epidermal keratinocytes

A suspension of keratinocytes was seeded into 75 cm^2 cell culture vials (Costar) at a 2×10^5 cells/ml concentration, 15 ml each. Cells were cultured in a CO_2 incubator at 37 °C and saturation humidity in Keratinocyte-SFM medium (Gibco). The cells were grown with regular medium changes (every 2 days) for 3–6 weeks until the formation of a subconfluent layer. The date of pharyngoplasty was assigned depending on the growth rate of the patient's cells.

Immunohistochemistry and immunofluorescence

Cells were fixed with 4% paraformaldehyde for 15 minutes, followed by immunofluorescence staining for keratinocyte-specific marker using Abcam's first anti-cytokeratin 14 antibody (CK 14) (ab181595) and epithelial stem cell and early epidermal progenitor marker p63 (ab124762), using the method recommended by the manufacturer. After incubation, the preparations were washed with PBS, and then a solution of second antibodies conjugated with Alexa Fluor 555 and Alexa Fluor 488 (ThermoFisher) was added for visualization.

Immunohistochemical detection of keratinocyte-specific markers on the surface of the muscle flap was performed on histological preparations that were stained for total cytokeratin markers – PanCk (ab7753) and p63 (ab124762). Primary antibodies from Abcam were used according to the manufacturer's recommended technique; peroxisome method and second antibodies with streptovidin-DAB complex, followed by H&E staining, were used to visualize reaction products.

Planting and growing cell cultures on matrix

To form a cell layer, cultured keratinocytes were seeded on the surface of the matrix, which is a 0.3–0.5 mm thick plate consisting of hyaluronic acid and collagen. Epidermal keratinocytes were separated from the culture vial using a mixture of trypsin and Versene solutions (1 : 1). An epidermal keratinocyte suspension was seeded into a Petri dish with a 4×10^5 cell/cm^2 density matrix placed in it. The resulting stratum with keratinocytes was then incubated under standard conditions, at 37 °C, 5% CO_2. The bioengineered autologous stratum was ready for use after about 5–7 days, during which time the epidermal colonies formed a confluent layer on the matrix surface. The number of cells at the end of this period should be $80 \pm 20 \times 10^5$ cells/cm^2. The prepared epithelial layers on the matrix were packed in sterile packaging and used within 12 hours.

Assessment of cell viability on the surface of epithelial cell sheets

A fragment of the prepared cell layer was placed in a well of a 48-well plate, and 0.5 ml of Calcein AM working solution (BD Pharmingen) was added. After a 30-minute incubation, the cell sheet was visualized under an Olympus IX73 fluorescence microscope (CKP equipment, Koltzov Institute of Developmental Biology). The obtained micrographs made it possible to assess the morphology of viable cells and their distribution on the matrix surface.

Reconstructive stages

At the first stage, prelamination of the bioengineered muscle and epithelial flap was performed.

A graft grown from the patient's autologous epithelial cells on the matrix was implanted into the pectoral fascia and fixed with Vicryl 5.0 suture (Fig. 1, c). It was covered with a latex film and fixed with a Prolen 3.0 Prolen 3.0 suture (Fig. 1, d). The epithelial cell sheets were thus left to take root for 3 weeks.

At the second stage, the laryngopharynx was reconstructed. First, pharyngostoma edges were mobilized (Fig. 2, a). During the formation of the prelaminated pectoralis major epithelial flaps, the pectoralis major was mobilized from the chest wall and moved to the area of the defect, as in the traditional surgical technique (Fig. 2, b). The size of the muscle fragment of the pectoralis major and epithelial flap was determined according to the size of the soft tissue defect in the neck. The surface of the pectoralis major with a prelaminated cellular layer (bioengineered muscle and epithelial flap) was oriented such that it was directed into the hypopharyngeal lumen (Fig. 2, c). The bioengineered fragment was modeled according to the size of the defect in the hypopharyngeal mucosa and fixed using a Vicryl 2.0 suture to the mobilized edges of the hypopharyngeal mucosa along

the pharyngostoma perimeter (Fig. 2, d). The soft tissues were restored with the muscular part of the flap.

Postoperative period

Before starting oral feeding, all patients underwent imaging of the larynx, hypopharynx and cervical esophagus to determine the condition and patency of the newly formed organ and assess swallowing function. In the absence of signs that the contrast agent had exited the contours of the upper GI tract, the nasogastric tube was removed, and the patients began feeding by mouth. Results were assessed at weeks 2 and 4, and months 3, 6, 12, and 24 after pharyngoplasty. X-rays of the pharynx and esophagus with contrast agent and videolaryngoscopy with biopsy were performed. Biopsy of the bioengineered fragment of prelaminated flap with histological examination was performed at week 3 after prelamination, and week 2 and 4, month 3, 6, 12, and 24 after pharyngoplasty.

Statistical analysis

Only descriptive statistics were used to analyze treatment and outcomes. The authors had access to the data and reviewed and approved the final version of the manuscript.

RESULTS

All patients underwent hypopharyngeal reconstruction using a bioengineered prelaminated pectoralis major and epithelial flap as described above.

Cells obtained from patients undergoing antitumor therapy show low growth rate and high sensitivity to culture conditions in the first few days after isolation. Therefore, to increase the required cell mass, they were grown in culture vials on special low-calcium, proliferation-stimulating culture medium (Fig. 3, a, b). Immunofluorescence study at the stage of formation of stable monolayer culture cells revealed the presence of typical epithelial cells expressing ck14, a keratinocyte-specific marker, and a large number of cells positive for p63, the epithelial stem cell and early epidermal progenitor marker (Fig. 3, b). After the cells formed a normal epithelial layer, they were transferred to a biocompatible matrix. The base of the matrix used was collagens and hyaluronic acid, 0.5 mm thick. Thus, an epithelial tissue autograft of 60 to 80 cm^2 in area was created for each patient (Fig. 3, c). The presence of living cells in the graft was monitored using a fluorescent microscope, after staining a small area of the graft with viability dye Calcein AM (Fig. 3, d).

Histological examination at week 3 after prelamination revealed areas with keratinocyte colonies on the muscle flap surface (Fig. 4, a, b, c, d). Positive expression of cytokeratins (Fig. 4, b) and specific protein p63 characteristic of keratinocytes of basal skin layer (Fig. 4, d) indicates that these cells belong to epithelial tissue cells. This confirms that keratinocytes were present on the pectoralis major for 3 weeks after transplantation. Thus, after 3 weeks of preliminary preparation of the muscle and epithelial flap, we considered it ready for the reconstructive stage of surgery.

The median postoperative follow-up period was 23.1 months (range 10–27 months). Videolaryngoscopy of the pharynx and esophagus in the patients showed that the area of epithelial-cellular flap implantation at month 3, 6, 12 and 24 was macroscopically indistinguishable from the surrounding mucosa (Fig. 5, a, c).

In histological studies, we observed a stratified squamous epithelium on the pectoral fascia at week 2 after pharyngoplasty in 78% of cases, week 4 after pharyngoplasty in 89% of cases (Fig. 5, b), month 3, 6, 12 and 24 after pharyngoplasty in 100% of cases (Fig. 5, d).

Oral feeding was restored in all cases. The overall median time to resumption of feeding was 18 days after surgery (range, 14–22 days). The mean postoperative

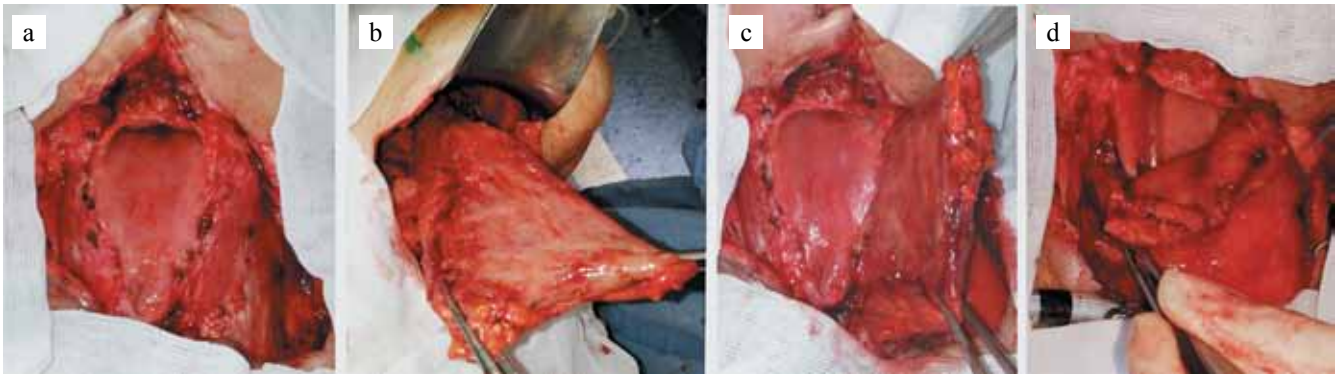

Fig. 2. Pharyngeal reconstruction using a prelaminated bioengineered pectoral flap: (a) mobilized edges of the pharyngostoma; (b) prelaminated bioengineered pectoral flap; (c) movement of the bioengineered pectoral flap to the neck; (d) fixation of the prelaminated flap section to the mobilized mucosa edges along the perimeter of the pharyngostoma

hospital stay was 17.5 days (range, 16 to 19 days). Voice function was restored by voice prosthesis implantation in 78% of cases.

No flap necrosis was noted. Fistula was observed in 4 patients (44%). The cause of delayed wound healing and formation of suture failure in the pharyngeal suture area could be RT/CRT performed before pharyngoplasty and nutritional deficiency. In all patients, fistulas were formed in the area of anastomosis between the upper edge of the flap and the base of the tongue, and were closed within 7–10 days after conservative therapy and dressings without the need for additional surgical intervention. One patient had hypopharyngeal stenosis in the lower edge of flap fixation. The stenosis area was subjected to bougienage dilation, and as a result, the hypopharyngeal lumen reached a diameter of 1 cm. This patient had difficulty swallowing only solid food. Suppuration of the donor area was observed in one patient; the wound healed after conservative therapy and dressings.

DISCUSSION

Reconstruction of the upper GI tract after laryngectomy with hypopharyngeal resection remains a major challenge for head and neck cancer surgeons, as in most cases it is performed after RT/CRT in somatically burdened patients [11]. Various reconstruction options are used to repair extensive defects after surgical treatment [12]. The reconstruction technique depends on the patient's health status, clinic options, size and composition of the defect, radiation history, and previous surgeries. Somatically burdened patients with a high risk of postoperative complications are rarely acceptable candidates for microsurgery. Because of these limiting factors, advanced flaps remain the preferred method [13].

In some cases, a bioengineered flap can be a good alternative to standard skin and muscle flaps. Bioengineering technologies facilitate the creation of tissue analogues of the mucosa used for restoration of the mucosa of the upper GI tract, oral cavity, urethra, bladder, vagina

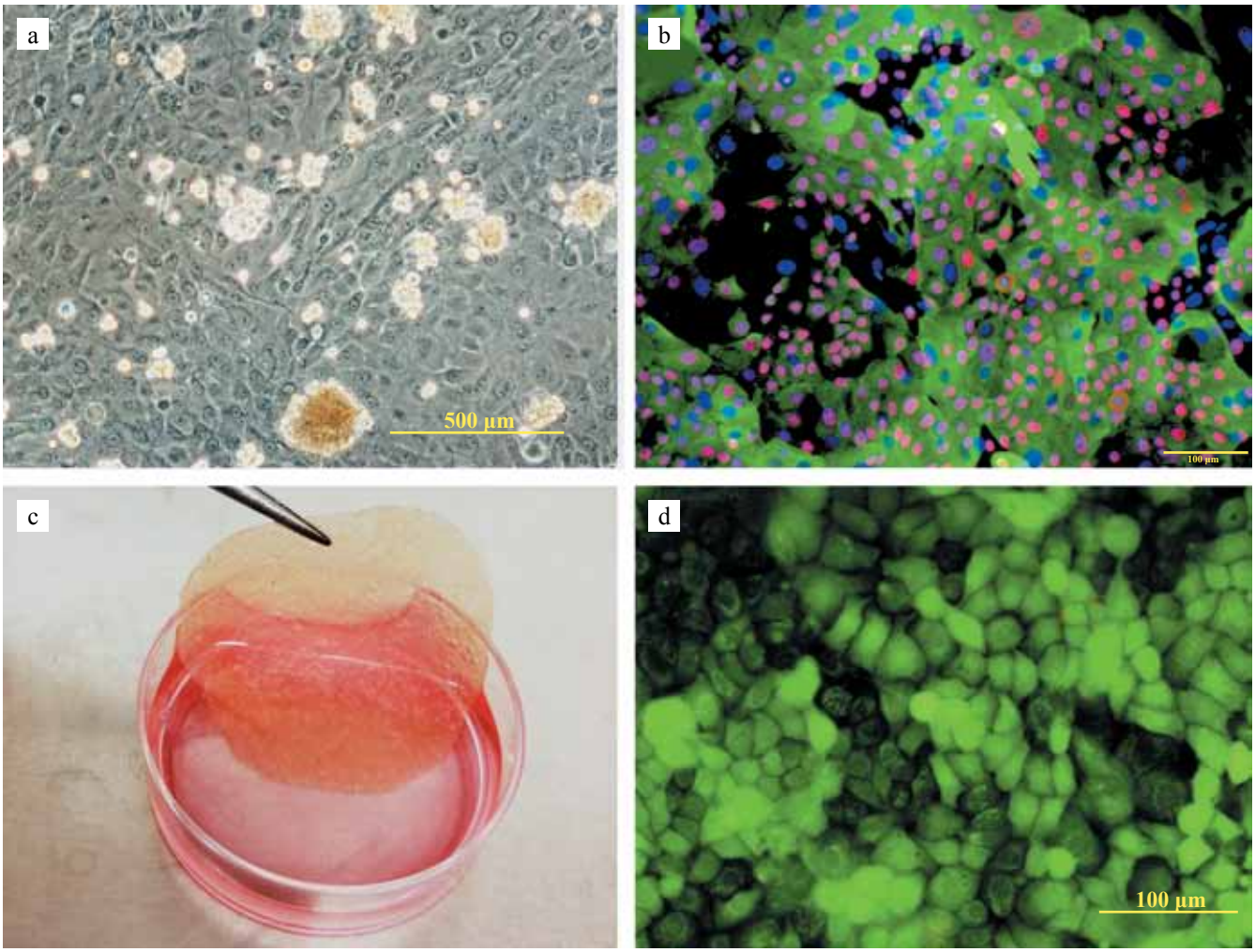

Fig. 3. Cell graft preparation: culture of patient's autologous keratinocytes at week 4 of cultivation: (a) phase-contrast; (b) immunofluorescence identification of keratinocyte-specific marker ck14 (green staining); specific epidermal transcription factor p63 (red staining), nuclei stained with DAPI (blue staining). Ready-to-use graft, appearance (c) Micrograph of human keratinocytes grown on matrix surface, detection of viable cells using viability dye Calcein AM (green staining) (d)

and cornea. Restoration of damaged epithelial tissue in this case occurs due to the fact that the graft contains autologous poorly differentiated cells of the basal layer of the epidermis, which can proliferate and integrate into the defect site. At the same time, the tissues surrounding the bioengineered construct influence the cells included in it. For instance, it was found that corneal cells can transdifferentiate into epidermal cells under the influence of signals from the embryonic dermis [14].

The plasticity of epidermal keratinocytes was also observed in experiments on cell transplantation into the urethra. It was shown that three weeks after transplantation of autologous EGFP-expressing rabbit skin keratinocytes into the urethra, they restored the urothelium, showing signs of specific marker expression [15].

Recently, the ability of esophageal cells to differentiate in the cutaneous direction under the influence of adult skin stroma has been demonstrated [16]. Since the hypopharynx itself is lined with non-keratinized, stratified squamous epithelium, it was reasonable to assume that the epidermis is highly suitable for its replacement. In the humidified microenvironment, epidermal keratinocytes lose their ability to keratinize as they do in culture conditions. Thus, they may well perform the functions of the pharyngeal epithelium. Previously, a study was published in which a displaced muscle graft consisting of the pectoralis major with a pre-implanted mucosal tissue equivalent, created on the basis of cultured donor keratinocytes, was used for hypopharyngeal reconstruction. Donor cells used as an epithelial layer in such constructions can temporarily act as a barrier epithelium, ensuring reliable engraftment of the graft in the recipient tissue area, and also modify the wound surface, stimulating the wound's own epithelization [5].

When eliminating hypopharyngeal defects after removal of locally advanced tumors, comprehensive restoration of soft tissues and mucosa, as well as normal functioning of the digestive tract and vocal function is necessary. Prelaminating the cultured cells onto a well-

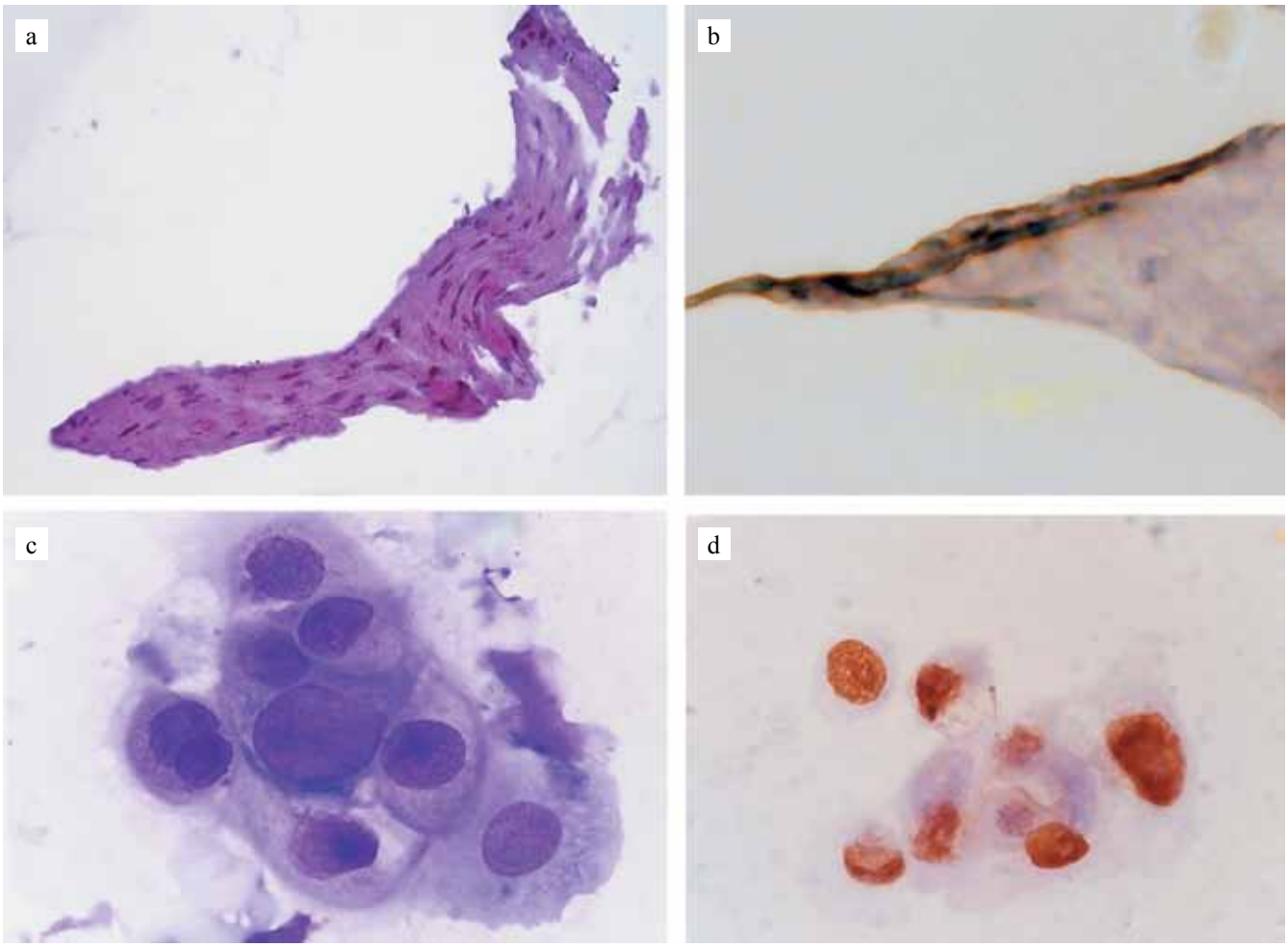

Fig. 4. Biopsy of muscle slice at week 3 of prelamination with epithelial tissue equivalent: a fragment of muscle tissue from the transplantation area (a) H&E staining (100× magnification); Immunohistochemistry. Expression of common cytokeratins (DAB staining, magnification ×100) (b). Cytological study of muscle flap surface with a ready-made analog: H&E staining (1000× magnification) (c); Immunohistochemical detection of epidermal transcription factor p63 (DAB, 1000× magnification) in cell nuclei (d)

perfused tissue of the pectoralis major allows creating flaps with the required properties: a layer of epithelial cells has time to form on the muscle surface, which together with the muscle tissue can be formed according to the size of the existing defect.

We used bioengineered prelaminated flaps to reconstruct extensive hypopharyngeal defects. The use of an epithelial layer grown from the patient's skin instead of a full-layer autodermal flap avoids such complications as hair ingrowth into the laryngeal lumen, stenosis of the upper GI tract lumen in the postoperative period. The percentage of fistula complications observed in patients in our study is 44%, which is comparable to the known rate of fistula in patients who received preoperative RT, which ranges from 13% to 50% [17]. After reconstructive surgery using skin and muscle flaps, 56.5% of patients mentioned difficulty swallowing only solid foods and 21.7% reported difficulty swallowing both solid and liquid food [17].

In our study, 1 (11%) patient had pharyngeal stenosis, which, after bougienage, caused problems with swallowing only solid food. Based on our postoperative follow-up, we can conclude that the technique we developed is able to restore the anatomy and functions of the laryngopharynx with identical tissues.

CONCLUSION

Hypopharyngeal reconstruction with a prelaminated bioengineered flap can was able to recreate the anatomical integrity and function of the hypopharynx in all the 9 clinical cases described.

This work was completed within the framework of the section of the State Assignment No. 0088-2021-0016 of Koltzov Institute of Developmental Biology and Grant MK-4667.2018.7 of the President of the Russian Federation for state support of young Russian scientists.

The authors declare no conflict of interest.

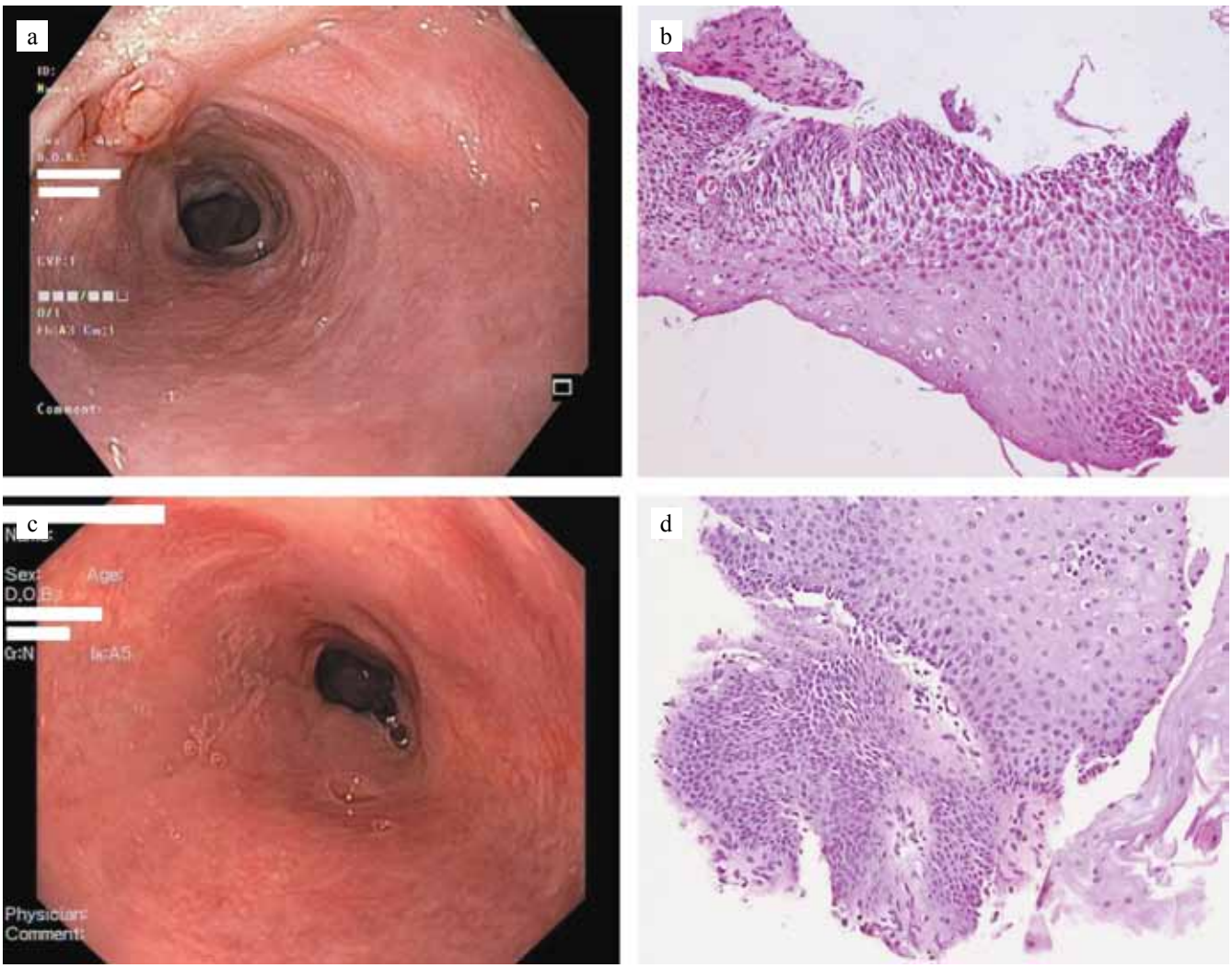

Fig. 5. Postoperative data: (a) Videolaryngoscopy at week 4 after pharyngoplasty; (b) H&E, at 100× magnification shows stratified squamous epithelium; (c) Videolaryngoscopy at month 24 after pharyngoplasty; (d) H&E, at 100× magnification shows stratified squamous epithelium with basal layer proliferation

REFERENCES

1. *Kim Evans KF, Mardini S, Salgado CJ, Chen HC*. Esophagus and hypopharyngeal reconstruction. *SeminPlast Surg*. 2010; 24 (2): 219–226. doi: 10.1055/s-0030-1255339.
2. *Rauchenwald T, Dejaco D, Morandi EM et al.* The Pectoralis Major Island Flap: Short Scar Modified Muscle-Sparing Harvesting Technique Improves Aesthetic Outcome in Reconstructive Head and Neck Surgery. *ORL J Otorhinolaryngol Relat Spec*. 2019; 81 (5–6): 327–337. doi: 10.1159/000503008.
3. *Jonas E, Sjöqvist S, Elbe P et al.* Transplantation of tissue-engineered cell sheets for stricture prevention after endoscopic submucosal dissection of the oesophagus. *United European Gastroenterol J*. 2016; 4 (6): 741–753. doi: 10.1177/2050640616631205.
4. *Amemiya T, Nakamura T, Yamamoto T, Kinoshita S, Kanamura N*. Autologous transplantation of oral mucosal epithelial cell sheets cultured on an amniotic membrane substrate for intraoral mucosal defects. *PLoS One*. 2015; 10 (4): e0125391. doi: 10.1371/journal.pone.0125391.
5. *Chissov VI, Reshetov IV, Vasil'ev AV, Kravtsov SA, Terskikh VV, Batukhtina EV i dr.* Klinicheskie aspekty bioinzhenernoy rekonstruktsii glotki u onkologicheskikh bol'nykh. *Onkokhirurgiya*. 2012; 4 (3): 29–33.
6. *Pereira D, Sequeira I.* A Scarless Healing Tale: Comparing Homeostasis and Wound Healing of Oral Mucosa With Skin and Oesophagus. *Front Cell Dev Biol*. 2021; 9: 682143. doi: 10.3389/fcell. 2021.682143.
7. *Wang J, He J, Zhu M et al*. Cellular Heterogeneity and Plasticity of Skin Epithelial Cells in Wound Healing and Tumorigenesis. *Stem Cell Rev and Rep*. 2022; doi: 10.1007/s12015-021-10295-8.
8. *Pribaz JJ, Fine NA*. Prelamination: defining the prefabricated flap – a case report and review. *Microsurgery*. 1994; 15 (9): 618–623. doi: 10.1002/micr.1920150903.
9. *Pribaz JJ, Fine NA*. Prefabricated and prelaminated flaps for head and neck reconstruction. *Clin Plast Surg*. 2001; 28 (2): 261–272.
10. *Pribaz JJ, Maitz PK, Fine NA*. Flap prefabrication using the "vascular crane" principle: an experimental study and clinical application. *Br J Plast Surg*. 1994; Jun, 47 (4): 250–256. doi: 10.1016/0007-1226(94)90007-8.
11. *Pribaz JJ, Fine N, Orgill DP*. Flap prefabrication in the head and neck: a 10-year experience. *Plast Reconstr Surg*. 1999; 103 (3): 808–820. doi: 10.1097/00006534-199903000-00006.
12. *Wang Q, Chen R, Zhou S*. Successful management of the supraclavicular artery island flap combined with a sternohyoid muscle flap for hypopharyngeal and laryngeal reconstruction. *Medicine (Baltimore)*. 2019; 98 (41): e17499. doi: 10.1097/MD.0000000000017499.
13. *Ki SH, Choi JH, Sim SH*. Reconstructive Trends in Post-Ablation Patients with Esophagus and Hypopharynx Defect. *Arch Craniofac Surg*. 2015; 16 (3): 105–113. doi: 10.7181/acfs.2015.16.3.105.
14. *Pearton DJ, Yang Y, Dhouailly D*. Transdifferentiation of corneal epithelium into epidermis occurs by means of a multistep process triggered by dermal developmental signals. *Proc Natl Acad Sci USA*. 2005; 102 (10): 3714–3719.
15. *Rogovaya OS, Fayzulin AK, Vasiliev AV, Kononov AV, Terskikh VV*. Reconstruction of Rabbit Urethral Epithelium with Skin Keratinocytes. *Acta Naturae*. 2015; 7 (1): 70–77.
16. *Bejar MT, Jimenez-gomez P, Moutsopoulos I, Colom B, Han S*. Defining the transcriptional signature of esophageal-to-skin lineage conversion. 2021; bioRxiv [Preprint]. doi: 10.1101/2021.02.19.431899.
17. *Somuk BT, Çiftçi O, Aygenç E*. Evaluation of Cases Who Underwent Reconstruction Through Pectoralis Major Myocutaneous Flap after Laryngopharyngectomy. *Turk Arch Otorhinolaryngol*. 2016; 54 (2): 58–62. doi: 10.5152/tao.2016.1603.

The article was submitted to the journal on 05.07.2022

DOI: 10.15825/1995-1191-2022-4-145-151

CORONARY PARADOX

V.V. Chestukhin[1], F.A. Blyakhman[2, 3]

[1] Sklifosovsky Research Institute of Emergency Care, Moscow, Russian Federation
[2] Ural State Medical University, Ekaterinburg, Russian Federation
[3] Ural Federal University, Ekaterinburg, Russian Federation

This work is a scientific and educational analytical review intended for practicing cardiologists. The purpose of the review is to draw physicians' attention to the role of myocardial contractility in the regulation of coronary circulation. We consider the fundamental phenomenon of arterial compression (squeezing) in the left ventricular (LV) wall, creating an obstruction to blood flow during cardiac systole. This phenomenon formally resembles functional coronary artery stenosis. Based on a review of the literature, the positive role of arterial compression in coronary hemodynamics is interpreted. Understanding the mechanical relationship between the contractile and coronary systems in the cardiac wall may be useful for practicing physicians when choosing treatment tactics for patients, optimizing LV bypass during heart surgeries, and improving the efficiency of adaptation of the transplanted heart.

Keywords: heart, left ventricle, coronary arteries, myocardial contractility, arterial compression, coronary circulation.

INTRODUCTION

The heart is a biological pump that circulates blood to all tissues of the body. Unlike the other organs, the heart participates in its own blood supply to realize the mechanical function of the myocardium. Thus, the contractile system of the heart and the myocardial life-support system, which contains an extensive network of blood vessels, are structurally concentrated in the heart wall, and are closely connected with each other.

Hemodynamics in proximal coronary arteries is fundamentally different from blood flow in other arteries of the body, where circulation is directly related to cardiac systole; more precisely, to the LV blood ejection phase, during which pressure gradient occurs in the vascular system, which determines the driving force in blood flow.

It is generally accepted that in the coronary system, systolic blood flow is limited and the main hemodynamic events occur during cardiac diastole. Such peculiarity of coronary blood flow was drawn attention to as early as 1695 [1]. The author noted that during cardiac relaxation, the coronary vessels are filled, and when they contract, they are emptied. In the first half of the last century, it was experimentally confirmed that during heart contraction, coronary arterial inflow is obstructed and venous outflow increases [2, 3].

It can be considered proven that the noted features of coronary hemodynamics are the consequence of mechanical function of the cardiac wall leading to compression of a certain part of coronary arteries and reduction of coronary blood flow [4–7]. This phenomenon seems paradoxical at first sight, since myocardial contractile function prevents coronary blood flow.

This work is intended to draw the attention of cardiologists to the above contradiction, which we have conventionally termed "coronary paradox". On the basis of literature analysis, we will attempt to give a reasonable interpretation to the presence of a nontrivial connection between mechanical phenomena in the cardiac wall and hemodynamic events in LV coronary arteries. This issue has been the subject of long-standing discussions among specialists in circulatory physiology; but it remains out of the focus of practicing physicians.

THE PHENOMENON OF CORONARY PARADOX

Fig. 1 shows a synchronous recording of pressure measurements in the aorta, right and left ventricles; volumetric blood flow velocity (VBFV) in the proximal right coronary artery and left anterior descending artery (LAD) off the left coronary artery, and VBFV in the great cardiac vein.

The figure clearly illustrates that with the beginning of the LV mechanical cycle, the VBFV in LAD sharply decreases, and during LV blood ejection (increase in aortic pressure), it increases slightly. However, with the onset of LV isovolumetric relaxation phase (the moment of aortic valve closure) there is a significant increase in coronary blood flow velocity.

Coronary blood flow limitation in LV systole can be observed in clinically healthy individuals with abnormal passage of part of the epicardial artery in myocardium. In such cases, pronounced systolic stenosis is visualized on coronarogram, disappearing with the beginning of diastole. This phenomenon is called "muscular bridges"

Corresponding author: Felix Blyakhman. Address: 3, Repina str., Ekaterinburg, 620028, Russian Federation.
Phone: (343) 214-86-96. E-mail: feliks.blyakhman@urfu.ru

and, as a rule, is not accompanied by symptoms of coronary heart disease [9].

Fig. 2 shows two angiogram frames recorded in LV systole and diastole in a patient with suspected myocardial ischemia as an example. We can clearly see that the LAD lumen of the left coronary artery sharply narrows in systole and recovers at the beginning of diastole. Muscle bridges clearly demonstrate the effect of arterial constriction during LV contraction.

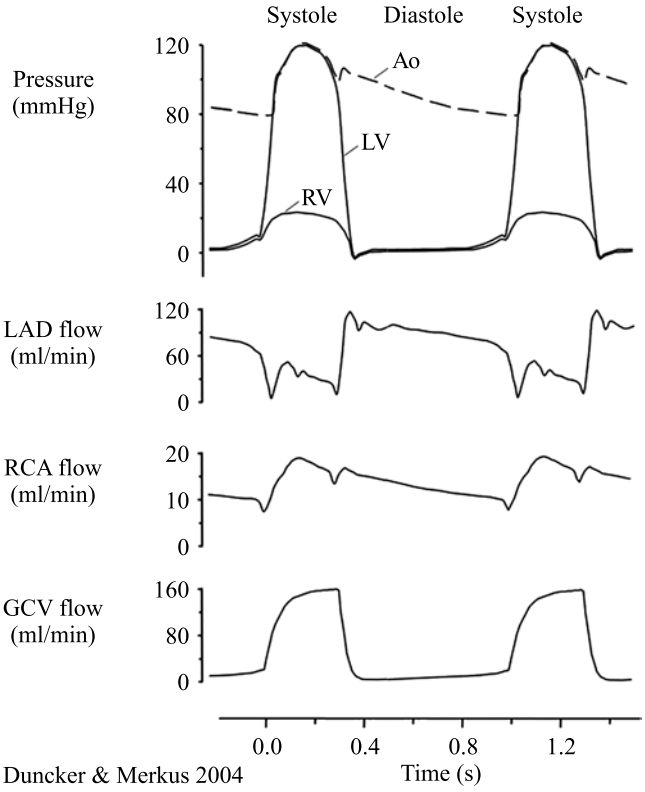

Fig. 1. Dynamics of pressure (upper panel) and Volumetric blood flow velocity in different parts of the heart. Ao, aorta; LV, left ventricle; RV, right ventricle; LAD, left anterior descending artery; RCA, right coronary artery; GCV, great cardiac vein. The diagram is borrowed from a presentation by Dirk J. Duncker (2014) in open access [8]

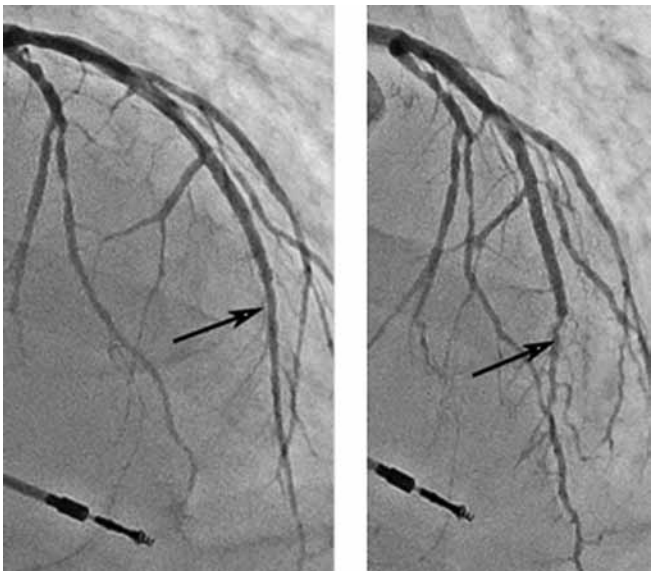

Fig. 2. An example of left coronary artery imaging with myocardial bridge (location indicated by arrow) at the end of diastole (left) and at the end of LV systole (right)

Meanwhile, in the normal heart, mechanical obstruction of blood flow in LV systole occurs at the level of blood macrocirculation system in the cardiac wall, in particular, in intramural (perforating myocardium) arteries with diameter less than 500 μm and arterioles with diameter of at least 100 μm [10]. These vessels are located in connective-tissue interlayers between bundles of muscle fibers, extend from the epicardium to the subendocardial plexus in the LV wall [6].

On the contrary, at the level of blood microcirculation in vessels with diameter <100 μm, cardiac muscle contraction has practically no effect on arterial lumen [11, 12]. Compression of arterial vessels in the microcirculatory system during LV systole is prevented by two factors. Firstly, small caliber arterioles are located parallel to cardiomyocytes and secondly, each arterial vessel is surrounded by two venules. In fact, these vessels dampen the compression of the arterioles by contracting myocytes, and the diameter of the venules changes significantly, from 48 μm in LV diastole to 31 μm in systole. Due to these two factors, a protective effect is provided, allowing to keep the lumen of arterioles of the microcirculation system almost unchanged: 38 μm in LV systole and 39 μm in diastole [13].

Thus, the **coronary paradox** is a phenomenon of hemodynamically significant compression of the perforating vessels of the LV coronary blood flow macrocirculation system during cardiac systole. It is based on the mechanical relationship between myocardium and coronary arteries, which is predetermined by peculiarities of the heart structure and left ventricle in particular.

MECHANISMS OF ARTERIAL COMPRESSION IN LV SYSTOLE

A number of hypotheses are known to explain the mechanism of coronary blood flow obstruction in LV systole. In general, these hypotheses are to some extent supported by evidence, and they can be divided into two main groups. The first includes functional models explaining myocardial mediated action on coronary artery lumen due to increased intramyocardial pressure in the cardiac wall during systole. The second group of assumptions considers the direct mechanical action of the myocardium on coronary arteries.

The mediated mechanism of arterial compression is represented by two basic models: waterfall [14] and intramyocardial pump [15]. Both models are based on the assumption that myocardial contraction increases intramyocardial pressure in the cardiac wall, which acts

on the outer surface of the artery. In this case, the vessel lumen decreases and resistance to blood flow increases.

The waterfall model states that the rate of blood flow in the coronary system in LV systole will be determined by the difference between the pressure in the area of arterial compression and venous pressure, divided by peripheral vascular resistance. Additionally, the intramyocardial pump model suggests that in LV systole, arterial compression moves blood in mutually opposite directions like a pump [16]. The advantage of the intramyocardial pump model over the waterfall model is that it can explain retrograde blood flow in arteries and the increase in venous outflow in cardiac systole.

The existence of direct (mechanical) myocardial action on coronary blood flow has been convincingly demonstrated on isolated cat hearts [17] and dog hearts in situ [18]. In these experiments, conditions for isovolumetric and isobaric LV contractions were created. In the first case, ventricular pressure increased with unchanged chamber volume, i.e. there was no cardiac output. In the case of isobaric contraction, pressure in the chamber was maintained constant from the moment of myocardial excitation, while the LV volume decreased, that is, blood ejection began immediately with the beginning of the mechanical cardiac cycle. The authors found that irrespective of fundamentally different pressure dynamics in the LV, the same effect of coronary blood flow reduction in systole was observed.

To explain the mechanism of direct action of cardiac muscle on coronary blood flow, several basic models have been proposed, three of which seem to be the most realistic. They are varying elastance, muscle shortening and thickening, and vascular deformation. All models imply a direct mechanical connection between coronary vessels and myocardium in the heart wall.

The variable elastance model is based on the concept of changing myocardial elasticity in LV systole [19]. At the subcellular level, an increase in cardiomyocyte rigidity is associated with the interaction among major sarcomeric proteins (myosin with actin). After cardiac cell excitation, myocardial elasticity increases significantly, and the higher the cell contractility, the greater the active stiffness of the muscle, and the greater the elastance. Elastic force in the myocardium exerts pressure on the arterial walls, due to which the lumen and blood volume in the vessels decrease in places where they are compressed [20].

The muscle shortening and thickening model is based on the position about the constancy of cardiomyocyte volume in all phases of the cardiac cycle. Therefore, cardiac cell shortening in LV systole is accompanied by increased transverse size, which puts pressure on the vessels [21]. The proposed arterial compression mechanism can be realized in both early and late LV systole, where myocardial shortening and thickening take place to a greater or lesser degree due to a high degree of structural heterogeneity in the LV wall [5].

The vascular deformation model relates myocardial contraction to coronary blood flow not only due to changes in arterial lumen, but also due to the influence of cardiac muscle mechanics on arterial tortuosity, branching angles at their bifurcation sites [22]. It is believed that the proposed mechanism can manifest itself predominantly in the microcirculatory system of coronary blood flow.

It should be noted that all considered mechanisms of mediated and direct influence of myocardial contractile function on blood dynamics in coronary arteries are sufficiently reasonable but not universal. Probably, one or another phenomenon of blood circulation in LV systole can be explained by the combined action of mechanisms depending on specific conditions. At the same time, it is important to emphasize that, in the context of the topic of the present presentation, any of the mechanisms considered explains the limiting effect of myocardial contraction on blood flow in the heart vessels in LV systole.

ROLE OF CORONARY ARTERY COMPRESSION IN MYOCARDIAL CIRCULATION

The systolic role of LV in coronary blood flow is about 20–25% of the total per mechanical cardiac cycle [6, 23]. This circumstance was the basis for talking about the limiting effect of myocardial contractile function on coronary blood flow. There is an opinion that systolic compression (squeezing) of cardiac arteries is a "forced situation" negatively influencing coronary circulation. Below, we will try to formulate possible mechanisms to support the hypothesis about the positive contribution of coronary paradox to blood circulation in heart vessels.

So, cardiac systole occurs immediately after electrical excitation of the myocardium and begins with LV isovolumetric contraction phase, which proceeds with closed valves, and takes a short time interval (50–70 ms). During this period, cardiomyocytes generate force, active cell stiffness rapidly increases, which leads to increased mechanical tension in the LV wall, intraventricular and intramyocardial pressures.

Ultimately, a combination of the above events leads to compression of the perforating arteries, resulting in a rapid decrease in VBFV in the proximal parts of the coronary bed to almost zero (see Fig. 1). In some cases, during this period of the cardiac cycle, one can observe retrograde blood flow, i.e. in the direction towards the aorta [3, 24]. It means that in the places of compression of perforating arteries, there is not only blood flow limitation but also the driving force (pressure on vessels) that ensures blood flow. The mechanism of such myocardial action on the arteries is well described within the concepts of intramyocardial pump [15] and/or variable elastance [19, 20] (see above). The contribution of LV isovolumetric contraction phase to myocardial blood

supply is usually not taken into account due to the lack of the possibility of quantifying it.

The isovolumetric phase of LV systole passes into the phase of blood ejection into the aorta. Cardiomyocytes during this period are significantly shortened, active cell stiffness continues to increase to the maximum value. The pressure in the aorta increases up to the value of the LV end-systolic pressure. In relation to systemic hemodynamics, where blood flow is determined by arteriovenous pressure difference, coronary circulation is critically different due to prior compression of perforating arteries during isovolumetric LV contraction phase. Similar to hemodynamic changes in arterial stenosis, increased resistance to blood flow in early systole leads to a decrease in its volumetric characteristics, systolic and pulse pressure values, and the emergence of a pressure gradient in the arteries at their narrowing level.

In LV coronary macrocirculation system, blood flow during the ejection phase is determined by pressure difference in the aorta and perforating arteries. Compression of perforating arteries during this cardiac cycle phase continues to increase and, therefore, makes additional pumping contributions to antegrade blood flow below the level of arterial compression. The systolic contribution of arterial compression to coronary blood flow can be explained within any or all of the known concepts discussed above.

Noteworthy are the few studies that have investigated functional differences in myocardial and circulation mechanics in the layers of the cardiac wall. In particular, significant axial differences in both regional myocardial function and perfusion density by wall thickness have been shown. The relationship between these characteristics has also been demonstrated [25, 26].

Evidence suggests that in LV systole, there is not just compression of perforating coronary arteries, but sequential compression of vessel sections along its axis, coordinated in space and time. In terms of the intramyocardial pump and/or variable elastance concepts, this circumstance increases blood pumping capacity in the corresponding direction. It is similar to the principle of peristaltic pump operation, where volumetric liquid flow velocity directly depends on the number of rollers squeezing the tube.

It should be added that in the system of precapillary arterioles of coronary microcirculation, there is also a myocardial compression role, but on the venules surrounding arterioles [13]. This fact gives grounds to speak about the presence of the pumping role of cardiac muscle in venous outflow in LV systole.

Thus, mechanical (contractile) function of the myocardium in LV systole determines coronary blood flow due to two factors: 1) compression of the perforating arteries, which begins even before an increase in arterial pressure and, 2) increase in aortic pressure. In the context of the coronary paradox, LV can be formally considered as a dual-purpose mechanical pump – providing global hemodynamics for the body as a whole on one hand, and a pump for coronary blood circulation, in particular, on the other hand.

Cardiac diastole begins with the LV isovolumetric relaxation phase, when actin-myosin interaction in cardiomyocyte sarcomeres rapidly subsides. At the same time, myocardial stiffness, intramyocardial pressure and LV pressure rapidly decrease at a constant chamber volume. Fig. 1 clearly shows that during a short period of time (~50 ms), VBFV in the LAD, off the left coronary artery, increases sharply and reaches its maximum value by the beginning of the LV diastolic filling phase.

This hemodynamic phenomenon is commonly referred to as "suctioning" or decompression effect in coronary arteries [27, 28]. It is based on rapid reduction of elasticity in the cardiac wall during myocardial relaxation, which leads to restoration of perforating arterial lumen within a short period of time. A sharp decrease in arterial hydrodynamic resistance is accompanied by increased gradient between the pressure in the proximal and distal parts of the coronary system, leading to rapid filling of the arteries with blood below the vessel compression places in LV systole. Further, blood flow in LV diastole is determined by arteriovenous pressure difference and peripheral resistance in the coronary system.

Thus, arterial compression realizes its effect on coronary hemodynamics in all phases of the cardiac cycle, from the moment of myocardial excitation. Coronary artery compression provides not only systolic contribution to coronary circulation, e.g., by the intramyocardial pump principle, but also sets the conditions for blood flow through the heart vessels in LV diastole. The ratio of the systolic and diastolic contributions of the "coronary paradox" to cardiac hemodynamics depends on the inotropic state of the myocardium. This plays an important role in the adaptation of the heart to increasing load, regardless of whether the load is physical or related to the development of pathological processes in the heart [5, 7, 29].

THE ROLE OF CORONARY ARTERY COMPRESSION IN THE HEART

The history of coronary blood flow studies dates back more than three centuries. Centuries-old scientific ideas about blood flow regulation in heart vessels were based on the study of hemodynamics in large coronary arteries. Development of modern medical diagnostic technologies in the last few decades has allowed a new perspective on many aspects of coronary blood flow regulation due to the possibility of assessing blood flow in the microcirculatory system. In particular, it became clear that normal blood flow in branched capillary networks is nonpulsating and has ~0.5 mm/s velocity at 25–35 mmHg pressure [30]. It can be considered that such hemody-

namic parameters are optimal for blood-cardiomyocyte metabolic processes. However, how this optimality is achieved is still not completely clear.

At rest, myocardial contractile activity provides a systolic pressure of about 110–120 mmHg in the aorta, with a pulse pressure of about 40 mmHg. The coronary system, being in close proximity to the heart, experiences approximately the same hemodynamic loads in the large subepicardial arteries. Taking into account the small length of the coronary system compared to the large circulatory circle, it can be assumed that pressure boundary conditions at the inlet of the coronary system are excessive to provide the necessary parameters in the blood microcirculation system in the heart.

Compression of perforating arteries in LV systole increases resistance to blood flow, reduces arteriovenous pressure difference in the system and, therefore, prevents hydrodynamic stroke in the distal parts of the coronary bed. In its essence, the "coronary paradox" is a kind of "systolic barrier" to blood flow at the inlet of the coronary hemodynamic system.

Let us pay attention to the fact that the systolic barrier principle is also realized in the cerebral circulation system, where straightening siphons (S-shaped bends) of main arteries play the damping role of blood flow in LV systole [31]. Curiously, the organs more distant from the aortic orifice do not have such protection.

A priori, obstruction of blood flow in the large coronary arteries is likely to reduce LV efficiency. However, as noted above, nature has been able to "turn" what seems to be disadvantages in heart design into advantages of its functioning. Indeed, the presence of arterial vessel compression is able to optimize coronary hemodynamics in all phases of the cardiac cycle, thus providing blood flow conditions necessary for metabolic processes in cardiomyocytes. Hence, the "coronary paradox" can be considered as an integral determinant in coronary circulation regulation.

In conclusion, it should be said that the issues raised are the subject of ongoing discussions [6, 7]. This is due to the extraordinary complexity of studying the coronary system, in which all regulatory links are closely interconnected with each other. It concerns not only mutual humoral influences between the myocardium and smooth muscle of coronary vessels, but also mechanical interactions caused by structural heterogeneity of the heart and left ventricle in particular [32].

In this work, we have tried to convince the interested reader that systolic arterial compression is not a "forced" but a strictly "grounded" natural phenomenon. A phenomenon aimed at solving the problem of optimization of the joint activity of contractile and coronary systems in biological pump design. We hope that interpretation of the facts proposed in the paper gives grounds to suggest that LV systolic contribution to coronary blood flow is clearly underestimated. Understanding the role of the "coronary paradox" in the heart can be useful for practicing physicians when choosing treatment tactics for patients, optimizing left ventricular bypass during heart surgeries, as well as improving the efficiency of adaptation of the transplanted heart.

Felix Blyakhman would like to thank the Russian Science Foundation for financial support in the preparation of this work (Grant No. 22-71-10071 of the Russian Science Foundation "Hemorheological Modeling of Coronary Artery Flow for the Needs of Personalized Diagnosis and Treatment of Coronary Heart Disease").

The authors declare no conflict of interest.

REFERENCES

1. *Scaramucci J.* De motu cordis, theorema sextum. *Theoremata familiaria de physico-medicis lucubrationibus iucta leges mecanicas*. 1695: 70–81.
2. *Anrep GV, Cruickshank EW, Downing AC, Subba RA*. The coronary circulation in relation to the cardiac cycle. *Heart*. 1927; 14: 111–133.
3. *Gregg DE, Green HD.* Registration and interpretation of normal phasic inflow into the left coronary artery by an improved differential manometric method. *Am J Physiol.* 1940; 130: 114–125.
4. *Gregg DE, Sabiston DC.* Effect of cardiac contraction on coronary blood flow. *Circulation.* 1957; 15: 14–20.
5. *Westerhof N, Boer C, Lamberts RR, Sipkema P.* Cross-talk between cardiac muscle and coronary vasculature. *Physiol Rev.* 2006; 86: 1263–1308. doi: 10.1152/physrev.00029.2005.
6. *Duncer DJ, Koller A, Mercus D, Canty Jr JM*. Regulation of coronary blood flow in health and ischemic heart disease. *Progress in Cardiovascular Disease*. 2015; 57 (5): 409–422. doi: 10.1016/j.pcad.2014.12.002.
7. *Goodwill AG, Dick GM, Kiel AM, Tune JD*. Regulation of coronary blood flow. *Compr Physiol*. 2017; 7: 321–382. doi: 10.1002/cphy.c160016.
8. *Duncker DJ.* Regulation of Coronary Blood Flow. ETP. https://www.escardio.org/static-file/Escardio/education/live-events/courses/education-resource/101-Duncker.pdf.
9. *Murtaza G, Mukherjee D, Gharacholou SM, Nanjundappa A, Lavie CJ, Khan AA et al.* An updated review on myocardial bridging. *Cardiovascular Revascularization Medicine.* 2020; 21 (9): 1169–1179. https://doi.org/10.1016/j.carrev.2020.02.014.
10. *Rizzoni D, De Ciuceis C, Salvetti M, Paini A, Rossini C, Agabiti-Rosei C, Muiesan ML.* Interactions between macro- and micro-circulation: are they relevant? *High Blood Press. Cardiovasc Prev*. 2015; 22: 119–128. doi: 10.1007/s40292-015-0086-3.
11. *Motwani M, Kidambi A, Uddin A, Sourbron S, Greenwood JP, Plein S.* Quantification of myocardial blood with cardiovascular magnetic resonance throughout the cardiac cycle. *Journal of Cardiovascular Magnetic Resonance*. 2015; 17 (1): 4. doi: 10.1186/s12968-015-0107-3.

12. *Kuhl JT, George RT, Merha VC, Lind JJ, Chen M, Arai AE et al.* Endocardial – epicardial distribution of myocardial perfusion reserve assessed by multidetector computer tomography in symptomatic patients without significant coronary artery disease: insights from the CORES320 multicentre study. *European Heart Journal Cardivascular Imaging*. 2016; 17 (7): 779–787. doi: 10.1093/ehjci/jev206.
13. *Westerhof N, Sipkema P, Vist M.* How cardiac contraction affects the coronary vasculature. *Adv Exp Med Biol*. 1997; 430: 111–121. doi: 10.1007/978-1-4615-5959-7_10.
14. *Downey JM, Kirk ES.* Inhibition of coronary blood flow by a vascular waterfall mechanism. *Circ Res*. 1975; 36: 753–760. doi: 10.1161/01.res.36.6.753.
15. *Spaan JA, Breuls NP, Laird JD*. Diastolic-systolic coronary flow differences are caused by intramyocardial pump action in the anesthetized dog. *Circ Res*. 1981; 49: 584–593. doi: 10.1161/01.res.49.3.584.
16. *Spaan JA, Breuls NP, Laird JD.* Forward coronary flow normally seen in systole is the result of both forward and concealed back flow. *Basic Res Cardiol*. 1981; 76: 582–586. doi: 10.1007/BF01908365.
17. *Krams R, van Haelst AC, Sipkema P, Westerhof N*. Can coronary systolic-diastolic flow differences be predicted by left ventricular pressure or time-varying intramyocardial elastanse? *Basic Res Cardiol*. 1989; 84: 149–159. doi: 10.1007/BF01907924.
18. *Van Winkle DM, Swafford Jr AN, Downey JM*. Subendocardial coronary compression in beating dog hearts is independent of pressure in the ventricular lumen. *Am J Physiol Heart Circ Physiol*. 1991; 261 (2 Pt 2): H500–H505. doi: 10.1152/ajpheart.1991.261.2.H500.
19. *Suga H, Sagawa K, Shoukas AA*. Load independence of the instantaneous pressure-volume ratio of the canine left ventricle and effects of epinephrine and heart rate on the ratio. *Circ Res.* 1973; 32: 314–322. https://doi.org/10.1161/01.res.32.3.314.
20. *Krams R, Sipkema P, Zegers J, Westerhof N*. Contractility is the main determinant of coronary systolic flow impediment. *Am J Physiol Heart Circ Physiol.* 1989; 257: H1936–H1944. https://doi.org/10.1152/ajpheart.1989.257.6.H1936.
21. *Willemsen MJ, Duncker DJ, Krams R, Dijkman MA, Lamberts RR, Sipkema P, Westerhof N*. Decrease in coronary vasculare volume in systole augments cardiac contraction. *Am J Physiol Heart Circ Physiol*. 2001; 281: 731–737. doi: 10.1152/ajpheart.2001.281.2.H731.
22. *Fibich G, Lanir Y, Liron N, Abovsky M*. Modeling of coronary capillary flow. *Adv Exp Ved Biol*. 1993; 346: 137–150. doi: 10.1007/978-1-4615-2946-0_13.
23. *Chilian WM, Eastham CL, Marcus ML*. Microvascular distribution of coronary vascular resistance in beating left ventricle. *Am J Physiol*. 1986; 251 (4): H779–H788. https://doi.org/10.1152/ajpheart.1986.251.4.H779.
24. *Starodumov IO, Sokolov SY, Alexandrov DV, Zubarev AY, Bessonov IS, Chestukhin VV, Blyakhman FA*. Modelling of hemodynamics in bifurcation lesions of coronary arteries before and after myocardial revascularization. *Phil Trans R Soc A*. 2022; 380: 20200303. https://doi.org/10.1098/rsta.2020.0303.
25. *Forte E, Punzo B, Gentile F, Salvatore M, Cavaliere C, Cademartiri F.* Normal patterns of left ventricle rest myocardial perfusion assessed by third-generation cardiac computed tomography. *Clin Physiol Funct Imaging*, 2020; 40: 30–36. doi: 10.1111/cpf.12598.
26. *Namani R, Lee LC, Lanir Y, Kaimovitz B, Shavik SM, Kassab GS.* Effects of myocardial function and systemic circulation on regional coronary perfusion. *J Appl Physiol*. 2020; 128: 1106–1122. doi: 10.1152/japplphysiol.00450.2019.
27. *Davies JE, Whinnett ZI, Francis DP, Manisty CH, Aguado-Sierra J, Willson K et al.* Evidence of a dominant backward-propagating "Suction" wave responsible for diastolic coronary filling in humans, attenuated in left ventricular hypertrophy. *Circulation.* 2006; 113: 1768–1778. https://doi.org/10.1161/circulationaha.105.603050.
28. *Ladwiniec A, White PA, Sukhjinder S.* Diastolic backward-traveling decompression (Suction) wave correlates with simultaneously acquired indices of diastolic function and is reduced in left ventricular stunning. *Circ Cardiovasc Interv*. 2016; 9 (9): 1–9. doi: 10.1161/circinterventions.116.003779.
29. *Sabbah HN, Marzzilli M, Liu ZL, Stein PD.* Coronary extravascular compression influence systolic coronary blood flow. *Heart Vessels*. 1986; 2: 140–146. doi: 10.1007/BF02128139.
30. *Jacob M, Chahhell D, Becker BF*. Regulation of blood flow and volume exchange across the microcirculation. *Crit Care*. 2016; 20 (1): 319. https://doi.org/10.1186/s13054-016-1485-0.
31. *Schubert T, Santini F, Stalder AF, Bock J, Meckel S, Bonati L et al.* Dampening of blood-flow pulsatility along the carotid siphon: does form follow function? AJNR Am J Neuroradiol. 2011; 32 (6): 1107–1112. doi: 10.3174/ajnr.A2426.
32. *Blyakhman F.* Left ventricular inhomogeneity and the heart's functional reserve. *The cardiac pumping and perfusion engineering*. Ghista D, Ng E, eds. Singapore: World Scientific Press, 2007: 17–56. doi: 10.1142/9789812775597_0002.

The article was submitted to the journal on 04.08.2022

INSTRUCTIONS TO AUTHORS

Articles should contain original information that has not been previously published and is not considered for publication in other editions. Fee for publication of manuscripts will not be charged.

The manuscript should be presented in Microsoft Word format A4, 1.5 spacing, and Times New Roman font size 12. Submit your article to the online submission system in accordance with the instructions on the journal's website https://journal.transpl.ru.

Structure of the article

The Title page should include:

- Initials (first name and patronymic) of the authors of the article should be specified before their respective last names.
- Full official name of the institution, city and country.
- If authors from different institutions participated in writing of the manuscript, it is necessary to correlate those with the names of the authors by adding a digital index uppercase after last name, and right before the name of the institution.

Information about the authors

For each author fully specify the last and the first name, patronymic and position in the relevant department/institution.

For correspondence

Fully specify the last and the first name, patronymic of the author, who will be holding correspondence, address (including postal code), telephone, fax number, e-mail.

Abstract

Each article must be accompanied by an abstract. The amount of text for the abstract of the original article should be of no more than 300 words, for a literature review, clinical observation – no more than 200 words. The abstract must fully comply with the content of the work. The abstract should not use abbreviations without prior expansion.

Abstract of ***the original article*** should contain the following sections: ***Objective***, ***Materials and methods***, ***Results***, ***Conclusion***. The abstract should present the most important results of the research.

Do not write: "*A comparative analysis of the sensitivity and specificity was conducted …*"

Should write: "*The sensitivity was ... % and ...%, p = , specificity, respectively ...% and ...%, p =* ".

Keywords

At the end of the abstract keywords must be given. To select the keywords a thesaurus of U.S. National Library of Medicine should be used – Medical Subject Headings (MeSH) at http://www.ncbi.nlm.nih.gov/mesh.

Conflict of interest

The author should inform the editor about the factual or potential conflict of interest have included the information about such conflict into the respective section of an article.

If there is no conflict of interest, the author should say so in the form like the following: "Author declares unawareness of the conflict of interest".

This information is supposed to be placed before the article text.

Text of article

Original article should include the following sections:

- Introduction
- Materials and methods
- Results
- Discussion
- Conclusion
- References

Review article should include an analysis of the literature with the presentation of modern sources (mainly in the last 5 years).

Clinical observation should be well illustrated (to reflect the essence of the problem) and include discussion with the use of literature data.

References in the text are indicated by number in square brackets: [1], [2, 5], [14–18] and ***in the references section are presented in order of their appearance in the text.*** All values given in the article should be expressed or duplicated in **SI** units.

References

The author is solely responsible for the accuracy of the data included in the references section of the article. References to unpublished papers or papers in print works are not allowed.

References are presented on a separate page.

The names of journals can be contracted in accordance with an embodiment of reduction adopted by the specific journal.

If the article quoted has DOI (a digital object identifier) or/and PMID (Pub Med identifier) they must be specified after the description of the article. To compile descriptions in References section NLM bibliographic reference citation standard is used – U.S. National Lib-

rary of Medicine (http://www.nlm.nih.gov/bsd/uniform_requirements.html). If the number of authors does not exceed 6, the bibliographic description includes all the authors. If the number of authors is more, only the first six authors should be indicated and then add et al.

Requirements for tables and figures

Tables should be placed into the text; they should have numbered heading and clearly labeled graphs, convenient and simple to read. Table's data must comply with the numbers in the text, but should not duplicate the information therein. Table references in the text are required.

Illustrations and drawings should be submitted in electronic format (JPEG or TIFF format with a resolution of at least 300 dpi and no smaller than 6 × 9 cm), in a volume of close to 1 MB. Drawings must include all copyright symbols – arrows, numbers, signs, etc. Figure captions should be submitted in a separate file with the extension *.doc. First, the name is given, then all arithmetic and alphabetical symbols (lettering) are explained.

Articles should be addressed to the Editor at:
Russian Journal of Transplantology and Artificial Organs
Shumakov National Medical Research Center of Transplantology and Artificial Organs
1, Shchukinskaya ul., Moscow 123182, Russian Federation
E-mail: **vestniktranspl@gmail.com**

Издание зарегистрировано в Госкомпечати РФ, № 018616 от 23.03.99 г.

Подписано к печати 5.12.22.

Тираж 1000 экз.

ООО «Издательство «Триада».
ИД № 06059 от 16.10.01 г.
170034, г. Тверь, пр. Чайковского, 9, оф. 514,
тел./факс: (4822) 42-90-22, 35-41-30
E-mail: triadatver@yandex.ru
http://www.triada.tver.ru

Отпечатано в ООО «Тверская фабрика печати».
170006, г. Тверь, Беляковский пер., 46.

Заказ ___